

“A RAPID FABRICATED DERMAL EQUIVALENT”

Michaël Ananta, M.D.

A dissertation submitted in partial fulfilment of the requirements for the degree of
Doctor of Philosophy in Tissue Engineering

University College London

2010

I, Michaël Ananta, confirm that the work presented in this thesis is my own. Where information has been derived from other sources, I confirm that this has been indicated in the thesis.

Acknowledgements

First and foremost, I would like to express my utmost gratitude to God, the most Gracious and most Merciful.

I am very grateful to my primary supervisor Dr Vivek Mudera, Ph.D. He has been a source of practical council and support throughout. He provided me with invaluable guidance and inspiration. I am indebted to him for his time and patience. I would like to thank Professor Robert A. Brown, my secondary supervisor, for his guidance and academic support throughout my project. I am deeply grateful to Erik Walbeehm for his referral which provided me with the opportunity to step into the world of science.

During this work I have had the good fortune to collaborate with a great many colleagues for whom I have the utmost regard, and I wish to extend my sincerest gratitude for their invaluable support, both professionally and personally. From the Institute of Orthopaedics: Ektoras (Hector) Hadjipanayi, Umber Cheema, Jennifer Verhoekx, Rebecca A. Porter, Sally Brown, Michelle Korda, Hedeer Jawad, Chavaunne Thorpe, Kevin Ho, Elena Garcia, Carolina Arevalo, Jasmine Ho, Mariea Brady, Tijna Alekseeva, Sorousheh Samizadeh, Alvena Kureshi, Farhad Foroughi, Alla Alovskaya, Shweta Aggarwal, Mrs. Anita Onsworth, Mrs. Michele Panaman, Mrs. Julie Cheek, Mr. Suhel Miah; from the Eastman Dental Institute: Batool Kazmi, Mrs. Nicky Mordan; from the Department of Histopathology (Royal National Orthopaedic Hospital, RNOH): Mrs. Margaret Byers, Mr. Steve Crane, Ms. Francesca Maggiani, Mr. Hongtao Ye, Mr. Fitim Berisha, Mrs. Thama Kugan, Mrs. Madeline Guntrip; from Northwick Park Institute for Medical Research: Lisandra E. de Castro Brás, Mrs. Cathy Gray, Mrs. Lindsey C. Fletcher, Neelam Gurav, Dr. Paul Sibbons, Dave; from the 3G-SCAFF collaboration: Cecilia Aulin, Jöns Hilborn, Stéphanie Houis, Dilibaier Aibibu, Camilla Frederiksson, Lionel Micol and Eva-Maria Engelhardt. Special thanks go out to Tim Morris for his statistical advice and I gratefully acknowledge funding from the EU Framework VI program (3G-Scaff reference: 013603-3G SCAFF), EPSRC, BBSRC, and RNOH Special Trustees.

Most of all, I wish to extend my endless gratitude and appreciation to my family: Mother, Father, Maya, Mira and Paul for their help, inspiration and support.

Publications

(Resulting in part from the work presented in this thesis)

I. Research papers

1. A Rapidly Fabricated Dermal Equivalent

Michaël Ananta, Robert A. Brown, Vivek Mudera (submitted for publication).

2. High Density Collagen Gel Tubes: A matrix for Primary Human Bladder Smooth Muscle Cells

Lionel A. Micol, Michaël Ananta, Eva-Maria Engelhardt, Vivek Mudera, Robert A. Brown, Jeffrey A. Hubbell, Peter Frey (submitted for publication).

3. Mechanisms of structure generation during plastic compression of nanofibrillar collagen hydrogel scaffolds: towards engineering of collagen

*Ektoras Hadjipanayi, Michaël Ananta, Marcin Binkowski, Ian Streeter, Zhan Feng Cui, Robert A. Brown and Vivek Mudera. *Journal of Tissue Engineering and Regenerative Medicine* (2010) 4.*

4. A Poly(Lactic Acid-Co-Caprolactone)-Collagen Hybrid for Tissue Engineering Applications

*Michaël Ananta, Jöns Hilborn, Dilibaier Aibibu, Robert A. Brown, Vivek Mudera. *Tissue Engineering Part A* (2009) 15, 1667-75.*

II. Oral presentations

1. A Co-Culture Dressing with a Rapidly Tissue Engineered Dermal Component Tested in Acute Full Thickness Skin Defects: A Lapine Study

*Michaël Ananta, Robert A. Brown, Vivek Mudera. *TERMIS-eu 2010, Galway, Ireland**

2. Complex Tissue Engineering with a Novel Poly(Lactic Acid-Co-Caprolactone)-Collagen Hybrid

*Michaël Ananta, Cecilia Aulin, Jöns Hilborn, Stéphanie Houis, Robert A. Brown, Vivek Mudera. *TERMIS-eu 2008, Porto, Portugal**

3. A Novel Poly(L-Lactide-co-e-Caprolactone)-Collagen Hybrid Construct for Application in Tissue Engineering

*Michaël Ananta, Jöns Hilborn, Dilibaier Aibibu, Robert A. Brown, Vivek Mudera. *TERMIS-eu 2007, London, United Kingdom**

Abstract

Cell encapsulation in collagen hydrogels affords the ability to rapidly create living yet mechanically weak tissue equivalents. A previously developed compression technique that removes the interstitial fluid from these hydrogels allows for a rapid improvement of the mechanical strength with adequate cell survival. However, although the UTS of the resulting compressed collagen-rich tissue sheets approach those found *in vivo*, the break strength, due to the small size of these sheets, does not allow for appropriate handling properties such as suturing.

In the present study it was found that both the thickness and the break strength of the compressed sheets could be improved by increasing the (pre-compression) collagen hydrogel volume. It was found here, however, that the previously described anisotropic increase of the collagen density in the hydrogel at the surface through which the interstitial fluid content is removed forms a mass transfer dependent resistance to the outflow of fluid through this surface which indicates that there is a limit to the size and strength of living tissue that can be achieved with this technique.

It was found here that the suturability of the compressed sheets could also be enhanced by the hybridisation with a synthetic degradable mesh without compromising cell survival or the speed of construction.

Fibroblast seeded hybrid constructs featuring a near confluent epithelial monolayer and with a stratified epithelium, created within 5 hours and 2 weeks respectively, were tested in a lapine model of an acute full thickness skin defect to test for their safety and efficacy in wound healing. Only constructs with a stratified epidermis showed a significant increase in wound closure and neo-vascularisation of the wound bed compared to untreated wounds.

Comparison of the present findings with currently available living biological dressings for the treatment of chronic wounds suggests the utility and possible cost-effectiveness of this rapid tissue engineering technique.

Contents

Acknowledgements.....	3
Publications	4
Abstract	5
List of figures	9
List of tables	21
1. Introduction	24
1.1 Acute wound healing.....	25
1.1.1 Haemostasis	25
1.1.2 Inflammatory phase	25
1.1.3 Proliferative phase.....	27
1.1.3.1 Re-epithelialisation	27
1.1.3.1.1 Normal keratinocyte biology	27
1.1.3.1.2 Keratinocytes in wound healing	29
1.1.3.2 Angiogenesis	30
1.1.3.3 Granulation tissue formation.....	30
1.1.4 Remodelling phase	31
1.1.4.1 Hypertrophic scarring, keloids and scar contracture	33
1.2 Chronic wound healing.....	34
1.2.1 Molecular pathogenesis of chronic wounds.....	34
1.2.2 Venous leg ulcers	34
1.2.3 Diabetic foot ulcers.....	35
1.3 Tissue Engineering.....	36
1.3.1 Basic principles of tissue engineering	36
1.3.2 Cell sources for tissue engineering.....	37
1.3.3 Tissue engineering scaffolds	39
1.3.3.1 Prefabricated scaffolds.....	39
1.3.3.2 Cell encapsulating scaffolds.....	40
1.4 Collagen as a scaffolding material	40
1.4.1 ‘In vitro’ self-assembly of collagen fibrils	42
1.4.2 Cell encapsulation in collagen hydrogels	42
1.4.2.1 Mechanical instability of collagen hydrogels.....	43
1.4.2.2 Self-compaction.....	43
1.4.2.3 Cell-mediated compaction	43
1.4.2.4 Mechanical compaction	43
1.5 Thesis overview	45
1.5.1 Hypothesis under test.....	45
1.5.2 Aims and objectives	46
2. Materials and Methods.....	47
2.1 Collagen hydrogels.....	47
2.1.1 Formation.....	47
2.1.2 Unconfined compression	48

2.1.3	Confined compression	49
2.1.4	Compaction assay	50
2.1.5	Scanning Electron Microscopy	50
2.1.6	Double fluid leaving surface compression.....	50
2.1.6.1	Physical characterisation.....	50
2.1.6.2	Dynamic mechanical analysis	51
2.2	Hybrid constructs	52
2.2.1	PLACL mesh fabrication	52
2.2.2	Hybridisation of collagen hydrogels	53
2.2.3	Physical characterisation of compression.....	54
2.2.4	Cell culture	54
2.2.4.1	Fibroblast maintenance	54
2.2.4.2	Passaging of fibroblasts	55
2.2.5	Fabrication of living dermal equivalents	56
2.2.6	Morphometric measurements.....	56
2.2.7	Alamar Blue reduction assay	57
2.2.8	Confocal microscopy.....	58
2.3	Skin equivalents	59
2.3.1	Cell culture.....	59
2.3.1.1	Keratinocyte isolation	59
2.3.1.2	Keratinocyte passage	61
2.3.1.3	Fibroblast explant culture.....	62
2.3.2	Fabrication of living skin equivalents	63
2.4	Implantation study.....	65
2.4.1	Study design.....	65
2.4.2	Preparation	66
2.4.3	Surgical procedure.....	68
2.4.4	Tissue harvest and handling.....	69
2.4.5	Histology.....	70
2.4.5.1	Hematoxylin & eosin	70
2.4.5.1.1	Epidermal regeneration	70
2.4.5.1.2	Wound contraction.....	71
2.4.5.1.3	Wound composition	71
2.4.5.2	Collagen birefringence	72
2.4.5.2.1	Picrosirius red staining	72
2.4.5.2.2	Polarised light microscopy	73
2.4.5.2.3	Image analysis	74
2.4.6	Immunostaining	75
2.4.6.1	Immunofluorescence.....	75
2.4.6.2	Immunohistochemistry	77
2.4.6.3	Image Analysis	79
2.4.6.3.1	Angiogenic response	79
2.4.6.3.2	Inflammatory response.....	79
2.5	Statistical analysis	80
3.	Results	82
3.1	Collagen hydrogel compression.....	82
3.1.1	Compression of large volume hydrogels	82
3.1.2	Non-linear relationship of hydrogel volume to fluid loss.....	84
3.1.3	Fluid saturation of blotting elements and fluid outflow	86

3.1.4 Anisotropic collagen compaction.....	88
3.1.5 Sequential fluid expulsion through two fluid leaving surfaces.....	91
3.1.6 Characterisation of compressed large volume hydrogels	92
3.2 Hybrid constructs	95
3.2.1 Hybridisation of compressed collagen hydrogels	95
3.2.2 Fluid removal from a PLACL-CCHH	95
3.2.3 Physical characterisation of PLACL- and PLGA-CCHHs	98
3.2.4 Post-compression cell viability and proliferation.....	100
3.2.5 In vitro analysis of short term biocompatibility of PLACL.....	103
3.2.6 Effect of an aqueous medium on the PLACL and PLGA mesh	105
3.2.7 Keratinocyte-fibroblast co-culture in PLGA-CCHHs	108
3.3 Implantation study.....	111
3.3.1 Engraftment.....	112
3.3.2 Wound contraction	117
3.3.3 Inflammatory response to allogeneic cell therapy.....	120
3.3.4 New connective tissue formation	123
3.3.5 Collagen content of the newly formed connective tissue	127
3.3.6 Collagen maturation	132
3.3.7 Panniculus carnosus.....	135
3.3.8 Epidermal regeneration.....	137
3.3.9 Angiogenic response.....	140
4. Discussion.....	145
4.1 Collagen hydrogel compression.....	145
4.2 Hybrid constructs	152
4.3 Implantation study.....	157
4.3.1 Epidermal closure.....	158
4.3.2 Inflammatory response	159
4.3.3 Angiogenesis	160
4.3.4 Wound contraction	161
4.3.5 Engraftment.....	162
4.3.6 Granulation tissue formation.....	163
4.3.7 Comparison with commercially available skin equivalents.....	164
5. Conclusions and future work.....	169
5.1 Conclusions.....	169
5.2 Future work.....	170
6. References	171

List of figures

- Figure 1 - Illustration of the progression of the normal wound healing response in adult humans which following a haemostatic phase is characterised by (1) an inflammatory phase, (2) a proliferative phase, and (3) remodelling phase..... 26
- Figure 2 – Illustration highlighting the characteristics of keratinocyte biology (Mitev and Miteva, 1997): cell anatomy, differentiation and stratification (see text for detailed description)..... 28
- Figure 3 - In the acute wound (left) keratinocytes are activated in response to pro-inflammatory cytokines and growth factors and proliferate and migrate into the wound bed. The chronic wound (right) is characterised by mitotically active cells located in the suprabasal (differentiated) layers. Furthermore, the cornified layer is hyperkeratotic and parakeratotic suggesting a derangement in the completion of either activation or differentiation (Morasso and Tomic-Canic, 2005). 29
- Figure 4 – Fibroblasts exposed to mechanical stress will differentiate into myofibroblasts which feature a contractile microfilamentous apparatus. Fibroblasts *in vivo* are normally stress shielded and their cytoplasmic actin (CA) filaments are mainly organised into a cortical network. When exposed to an extracellular mechanical load, fibroblasts transition into proto-myofibroblasts forming stress fibres initially composed of CA and anchored at sites of focal adhesion. Further increases in matrix tension and the action of TGF- β stimulate the formation of super-mature FAs and assembly of the contractile apparatus hallmarking the differentiation into myofibroblasts. The contractile stress fibres in these cells contain bundles of actin microfilaments associated with α -smooth actin (α -SMA) (Tomasek *et al.*, 2002; Gabbiani, 2003)..... 31
- Figure 5 – Illustration of the hypothesis that myofibroblasts contract the matrix in a lock-step mechanism (Tomasek *et al.*, 2002; Castella *et al.*, 2010). It has previously been shown that the cellular contraction of the collagen network by the myofibroblast is eventually stabilised into the matrix. The exact mechanism, however, is unknown but it is proposed by Castella *et al.* (2010) that the contraction induced laxity of the collagen network is removed through proteolysis. 32

Figure 6 – Illustration of the basic principles of tissue engineering. Cells obtained from a tissue biopsy, taken from a patient or a donor, are expanded through serial passages. Once a sufficient cell number has been obtained, cells are seeded (1) inside or (2) on a polymeric scaffold material, and cultured *in vitro* in a bioreactor or incubator. When the construct is sufficiently matured it can be implanted in or applied to an area of interest.

..... 37

Figure 7 – A type I collagen fibre is composed of smaller collagen fibrils which themselves comprise of microfibrils. These in turn are assembled from tropocollagen molecules in a regular staggered array which give rise to their striated appearance when viewed under an electron microscope..... 41

Figure 8 – (a) Neutralised collagen hydrogels (pink) cast in pockets of a stainless steel mould (arrow head) which is seated on a glass slide (arrow). (b) Collagen hydrogel after a 30 minute setting period transferred onto a standard setup of blotting elements (BE). Scale bars are shown at the bottom right corners. 47

Figure 9 – (a) Illustration of the standard assembly in which the fluid content (grey arrow) of collagen hydrogels is removed through the basal surface by the negative capillary action exerted by a standard setup of blotting elements (three sheets of filtration paper, a metal and a nylon mesh) and the gravitational force from the application (in an unconfined configuration and in the direction of the black arrow) of a load on the apical surface. (b) The resulting (i) compressed collagen sheet (after a 5 minute compression) could be rolled along the long axis (ii) into spiralled constructs. 48

Figure 10 – (a) Photograph (scale bar shown at bottom right) and (b) cutaway illustration of the custom built compression chamber (i, front and, ii, side view) in which collagen hydrogels are compressed on the standard setup of blotting elements (BE) and through the application of a free gliding stainless steel plunger (white and black arrow)..... 49

Figure 11 – (a) Photograph of spiralled, compressed collagen hydrogel clamped at either end with strips of metal mesh reinforced with super glue to facilitate gripping. (b) Specimen (insert, c) mounted in the tension clamps of a dynamic mechanical analyser.

..... 51

Figure 12 – Typical tensile test stress-strain curve showing the toe and elastic region, yield point and ultimate tensile (break) stress..... 52

Figure 13 – (a) Scanning electron micrograph of the filament structure of the PLACL yarn (scale bar is shown at the bottom right corner). (b) Light micrograph of the PLACL mesh showing the weft-knit pattern (scale bar shown at bottom right). (c) Illustration of a weft knit pattern which consists of a single yarn looped horizontally to form a row with each row building on the previous one..... 53

Figure 14 – (a) Photograph showing seated on a glass slide (white arrow) the stainless steel mould (arrow head) of increased height in which the two volumes (10 ml) of collagen are set around a synthetic degradable mesh. Scale bar shown at bottom right corner. (b) Illustration of the unconfined compression setup of the set collagen hydrogel with encapsulated synthetic degradable mesh..... 54

Figure 15 – (a) Illustration of a haemocytometer used to count cells suspended in a known volume trapped in two counting chambers (with a depth of 0.1 mm) underneath a cover slip and over ruled counting areas (b) Cells in either chamber were counted in four (i, - iv) ruled (1 mm²) counting areas (insert, c)..... 56

Figure 16 – AB reduction (expressed as relative fluorescent units, RFU) as a function of cell number. (a) Human fibroblasts and (b) rabbit fibroblasts were incubated on tissue culture plastic with AB as previously described. For both panels, values were deducted from the autofluorescence of AB without cells. For rabbit fibroblasts it was found that over 1 million cells the linear relationship between the RFU and cell number changed (arrow)..... 57

Figure 17 – (a) Photograph showing the harvest of skin (arrow head) from rabbit ear lobes ventral to the cartilage (C). (b) Histological section showing the difference in number of hair follicles between skin ventral and dorsal to the cartilage (dashed line shows the plane of dissection)..... 59

Figure 18 – (a) Histological section showing the basal keratinocytes (black arrow heads) in the epidermis (E) that were separated enzymatically from the dermis (D) and mechanically from the stratum corneum (SC). (b) Phase contrast micrograph showing

the typical cobble stone morphology of basal keratinocytes. Scale bars are shown at the bottom right corner. 60

Figure 19 – (a) Illustration of the top view of a skin explant culture showing a glass cover slip placed over dermal fragments in a 6-well plate. (b) Side view of skin explant culture showing a stainless steel weight on top of the cover slip to physically attach the dermal fragments to the plate to allow for the outgrowth of fibroblasts..... 62

Figure 20 – (a) Micrograph showing a fibroblast explant culture, day 5, established from a dermal fragment (EX) using the skin explant culture system described in Figure 19. (b) Fibroblast explant culture, at day 14. Scale bar shown at bottom right corner..... 63

Figure 21 – Illustration of the keratinocyte / fibroblast co-culture setup. (a) Keratinocytes were statically seeded on the apical surface of living dermal equivalents (*i.e.* fibroblast seeded PLGA-compressed collagen hybrid constructs) (a1) placed on stainless steel meshes in 6-well plates. (a2) The subconfluent epidermis was cultured to confluence submerged in growth medium. (b1) At confluence the skin equivalents were raised to the air-liquid interface by lowering the volume of growth medium to allow for the formation of a (b2) stratified epidermis. 64

Figure 22 – Schematic diagram of the experimental design. Six full thickness skin defects were created on the dorsum of rabbits which were either left untreated (NT) or treated with full thickness skin grafts (FTSG), acellular constructs (AC), uncultured (UC) and cultured (CC) cell seeded constructs. Wound healing was evaluated in histological sections 1, 3 and 5 weeks after injury. 65

Figure 23 – (a) Pre-operative preparation of a rabbit subject. Anaesthetics and fluids were administered peri-operatively through a cannula inserted in a marginal ear vein (black arrow). The dorsum between the scapulae and the iliac crests was depilated and squares of 2x2 cm² (white arrows) were marked out with indelible ink and tattooed. (b) A three character code was tattooed inside the ear to identify the individual animals. (c) Oxygen was supplied during surgery at a flow rate of 1 L/min through a face mask (white arrow, d) and supplemental doses of anaesthetic (black arrow) were administered throughout the operation. 67

Figure 24 – Detailed photograph of the surgical procedure. (a) A 2x2 cm² square was tattooed and (b) a full thickness defect was created along the inner margins of the outline. (c) Constructs were implanted into the defect by the placement of corner and midway sutures (arrow heads) and a single central quilting suture (arrow). (d) Photograph showing the anatomy of the relevant tissue layers: integument (IN), panniculus carnosus (PC) and latissimus dorsi muscle (LD). (e) Histological transverse cross-section showing the intact integument (IN) and the skin equivalent (SE) implanted in the defect over the panniculus carnosus (PC). (f) After implantation the wounds were covered with an adhesive occlusive dressing. 68

Figure 25 – (a) Rabbits were individually caged and had free access to water and food. (b) Post-surgery rabbits were fitted with a plastic cone collar (arrow) for the further duration of the study to prevent interference of the wounds by grooming. 69

Figure 26 – Illustration of the histomorphometric evaluation of the excised wound. See text for details (D, dermis; WL, wound length; GT, granulation tissue; PC, panniculus carnosus; ER, epidermal regenerate). 71

Figure 27 – Illustration of the principal behind polarised light microscopy. (a) Natural light is polarised by a linearly polarising filter (*i.e.* polariser) parallel to the transmission axis. (b) This linearly polarised light beam is then transmitted through the specimen (Sirius red stained collagen) and is refracted in an ordinary and an extra-ordinary ray which move out of phase depending on the degree of birefringence and the thickness of the specimen. As they pass through the second polariser (*i.e.* analyser) they interfere either destructively or constructively depending on the phase difference and an image is created resulting from the unequal transmission of the components of the polychromatic light. 73

Figure 28 – Analysis of birefringence within tissue samples using image analysis software. (a, b) The RGB (red, green, and blue) colour space (16.7 million colours) in which the micrographs were photographed was converted into a (a, c) HSB (hue, saturation and brightness) colour space (8-bit; 256 colours). The (birefringent) colours of interest (*i.e.* red, orange, green and yellow) were numerically defined (see ‘a’) and measured in the HSB channel (d, an example is given for the colour green). 75

Figure 29 – Illustration showing the main principle behind immunofluorescence (IF) and immunohistochemistry (IHC). In both IF and IHC a primary antibody (monoclonal) attaches to an antigen of interest after which a secondary antibody (polyclonal) conjugated with a visualising system is attached to the primary antibody to visualise the location of the antigen. In IF the secondary antibody is conjugated to a fluorescent molecule whereas in IHC it is conjugated with biotin which binds to a preformed biotinylated avidin-horseradish peroxidase (HRP) complex which converts the colourless substrate into a coloured reaction product. As avidin binds to four biotin molecules the reaction is enhanced by the localised complex of an accumulated ‘cloud’ of HRP enzyme..... 76

Figure 30 –Tissue sections stained for CD31 positive endothelial cells (with DAB) were (a) photographed and, using image analysis software, the staining was converted, in three steps (see text for details), into (b) black areas representing blood vessel cross sections comprising an endothelial cell mass and (when present) a lumen. (c) The number and the total area of the blood vessel cross sections per area were then calculated..... 79

Figure 31 - Figure 30 – (a) Immuno-histochemical detection of CD45-positive leukocytes using DAB visualisation. (b) Visual output of the ‘cell counter’ plugin showing the stained cells that were manually marked for inclusion in the total count. (c) The visual output for haematoxylin stained nuclei..... 80

Figure 32 – (a) Rabbit model of a full thickness skin defect. (b) Compressed collagen sheet placed onto the defect and sutured in place. (c) Manually applied strain of 20% tears the collagen sheet away from the stitches (arrow heads)..... 83

Figure 33 – A non-linear increase of compression time (t^{1-3}) of collagen hydrogels is required for every unit (here 0.65 ml/cm²) increase in collagen volume (per fluid leaving surface area; ml/cm²) to achieve the same percentage (*e.g.* 75%) fluid loss. Values are means \pm SD for 3 hydrogels for each volume. 85

Figure 34 – Representative plots of fluid expulsion from collagen hydrogels under confined compression on two different types of blotting elements. Fluid saturation of the blotting elements does not influence the logarithmic relationship between fluid loss and time. 87

Figure 35 – (a) Photograph of a collagen hydrogel marked with charcoal particles (white arrow heads) (FLS, fluid leaving surface) (b) Binarised photographs showing the change in distance ($\delta y_{1,2}$) between markers trapped inside a collagen gel at various time points of confined compression (white arrows show the direction of compression). 88

Figure 36 – (a) A vertical bar graph. Each bar represents the height of a collagen hydrogel at different times during confined compression. The two horizontal lines with the bars represent the position of two arbitrarily selected markers within the gel. Collagen above these markers does not compact until the markers reach the basal fluid leaving surface..... 89

Figure 37 – (a) Scanning electron micrograph of a transverse cross-section of a 3.25 ml/cm² collagen hydrogel sequentially compressed on its basal and apical horizontal surface to achieve a near 100% strain level. Scale bar measures 50 μ m. (b) At higher magnification the lamellar structure formed by the compression process can be observed within the hydrogel. Scale bar measures 10 μ m..... 90

Figure 38 – Representative stress-strain curves for (a) compressed 0.7 ml/cm² (spiralled) and (b) 3.33 ml/cm² (thick) collagen hydrogel showing the toe region, the yield and break point. (c, d) Box and whisker plots showing the spiralled collagen gels had better mechanical tensile properties than thick collagen constructs. The boxes indicate the 75th and 25th percentiles, the whiskers indicate the minimum and maximum values, the lines show the median values. Values are derived from 7 samples for spiralled constructs and 5 samples for thick constructs. Asterisks above graphs indicate significance level (*, $p < 0.05$; ** $p < 0.01$)..... 93

Figure 39 – Bar graphs showing the amount of fluid removed from PLACL hybridised collagen gels (1.4 ml/cm²) expressed as the percentage weight loss resulting from an unconfined compression with a gravitational load of 1.8 or 3.6 kN/m² for 5 or 10 minutes. Values are means \pm SD for 3 samples. Asterisks show a significant main effect of time on weight loss (*, $p < 0.001$)..... 97

Figure 40 – Scanning electron micrographs of meshes made of (a, c, e) poly-[lactic acid-co-caprolactone] (PLACL) and (b, d, f) poly-[lactide-co-glycolide] (PLGA): (a, b) Mesh structure. (c, d) Transverse cross sections of collagen hydrogels hybridised with either of the meshes. The compressed collagen component (arrow heads) can be seen as flat

sheets above and below the mesh. (e) In PLACL-collagen hybrid constructs the collagen (left from dotted line) does not extend deeply into the pores (right from dotted line) and superficial shards (arrow heads) can be seen at the interface with the mesh, suggesting that there is no physical contact between the apical and basal collagen components. (f) The collagen in the PLGA-collagen gel hybrid construct can be seen protruding through the pores and extending towards the other side (arrow heads). Scale bars are shown in the bottom right corners. 99

Figure 41 – Photographs of the cell-seeded (a) PLACL- and (b) PLGA-collagen hybrid construct after 7 days of static culture. (c) Box-and-whisker plots showing the amount of fluorescence (from the Alamar Blue reduction assay expressed as relative fluorescence units) produced by $5 \cdot 10^5$ cells (human and rabbit dermal fibroblasts) not exposed to the compression process (non-PC; plated on tissue culture plastic) and by the same number of cells directly (PC, day 0) and seven days (PC, day 7) after being exposed to the compression process while seeded inside the (d) PLACL- and (b) PLGA-collagen hybrid constructs (*NS*, not significant; Tukey’s HSD *post hoc* analysis; ***, $p < 0.001$; values are for 6 samples). 101

Figure 42 – (a) Illustration of a transverse cross section through the PLACL based dermal equivalent showing the apical and basal collagen component and the PLACL-mesh in between. (b) Detailed illustration of the box shows the proposed direction of the release of degradation products (DP). To study possible cytotoxic effects regions (45 m thick) proximal and distal to the mesh were studied for differences in percentage viable cells and in cell number to establish if cells died with the proximal region or moved out of this region. 103

Figure 43 - Confocal fluorescence micrograph of CMFDA (live cells staining in green) and EH-1 (dead cell staining in red; white arrow heads) stained human dermal (foreskin) fibroblasts seeded within the bottom collagen component of a PLACL-based dermal equivalent. Image obtained 7 days after fabrication and static culture Scale bar is shown at bottom right. 104

Figure 44 – Box-and-whisker plots. PLACL-collagen hybrid constructs, after seven days of static culture, showed no differences in (a) cell viability and (b) cell distribution between the collagen region at the collagen-PLACL interface (proximal) and the

collagen region at the free interface (distal) (NS, not significant; values are for 6 samples)..... 105

Figure 45 – Photograph. Contraction and rolling of the cell-seeded PLACL-compressed collagen hybrid construct under static *in vitro* culture conditions. Scale bar is shown at the bottom right corner..... 106

Figure 46 – (a, d) Photographs, (b, e) light micrographs, and (c, f) scanning electron micrographs showing the PLACL mesh before (a, b, c) and after (d, e, f) 3 hours of incubation in a buffer solution at 37°C and neutral pH. Macroscopically (a, d) contraction and deformation (curling) was observed, and at a microscopic level (b, c, e, f) a decrease in pore size and a tightening of the fibres was found (c, f)..... 107

Figure 47 – Box-and-whisker plots. (a) The decrease in porosity and (b) mesh size of the PLACL mesh after exposure to an aqueous medium (NS, not significant; ***, $p < 0.001$; values are for 6 samples). 108

Figure 48 - Micrographs of haematoxylin-eosin stained reconstructed skin showing the PLGA-compressed collagen gel hybrid constructs with rabbit keratinocytes (white arrow heads) seeded on the surface of the apical collagen component (CG) (a) directly after cell seeding and (b) after 2 weeks of culture (PG, poly(lactide-co-glycolide) mesh). The region in the box is magnified (x2) in (c) showing that the rabbit dermal keratinocytes form a continuous and stratified epidermis with (1) cuboidal basal cells attached to the apical collagen component, (2) flattened suprabasal cells and (3) a stratum corneum. (d) Immunofluorescent staining of cytokeratins showing the epithelial origin of the formed epidermal tissue (arrow points to the stratum corneum)..... 109

Figure 49 – Weekly, post-operative photographs of full thickness wound defects on the dorsum of a rabbit treated with full thickness skin grafts (FTSG), untreated, treated with acellular skin equivalents and uncultured and (2 week) cultured (cell seeded) skin equivalents (white arrow heads indicate the margins of the closed wound)..... 113

Figure 50 – Micrographs (magnification bar measures 1 mm) of haematoxylin and eosin stained tissue cross sections of rabbit, dorsal, full thickness wounds (1, 3 and 5 week post-injury) treated with full thickness skin grafts (FTSG), untreated, treated with acellular skin equivalents and uncultured and (2 week) cultured (cell seeded) skin

equivalents (IM, implant; PC, panniculus carnosus muscle; NT, newly formed connective tissue; white arrow head shows epidermal regeneration)..... 116

Figure 51 – Micrographs of the interface between the implant and the wound bed in full thickness skin defects one week after implantation (staining with CD31 antibody for endothelial cells and haematoxylin counterstaining). Full thickness defect treated with acellular skin equivalents show partial integration of (a) the basal collagen component (bc) and (b) PLGA-mesh (PG) (of the PLGA-compressed collagen hybrid material) into the underlying granulation tissue. The inflammatory infiltration (INF) was more marked in wounds treated with (c) uncultured and (d) cultured (cell seeded) skin equivalents than in wounds treated with the acellular constructs (ac, apical collagen component; black arrow heads point to CD31+ blood vessels; white arrow heads point to the *in vitro* formed epidermal layer on top of the apical collagen component of the skin equivalent). 116

Figure 52 – Polarised light micrographs of picrosirius stained tissue sections showing the wound length of full thickness skin defects at five weeks after implantation of (a) full thickness skin graft (FT; scale bar is shown at the bottom right corner), and (b) a skin equivalent (here no longer *in situ*) and after (c) no treatment (white arrow heads point to unwounded skin; NT, newly formed connective tissue). 117

Figure 53 – Box and whisker plots showing the effect of full thickness skin grafts (FTSG), (acellular and cell seeded) hybrid constructs (HC) and ‘no treatment’ (NT) on post-operative wound size after 1, 3 and 5 weeks (*NS*, not significant; *, $p < 0.05$).... 119

Figure 54 – Immunohistochemical detection of CD45+ cells (black arrows) within the newly formed connective tissue for the different treatment groups at weeks 1, 3 and 5 (DAB visualisation and haematoxylin counterstain; magnification bar measures 100 μm). 120

Figure 55 - Box and whisker plots for the percentage CD45+ cells at each time point for each treatment condition. (c) Box and whisker plots for the percentage CD45+ cells comparing the effect of the presence (+) or absence (-) of (allogeneic) cells in the defects at each time point (***, $p < 0.001$; *, $p < 0.05$; *NS*, not significant). 121

Figure 56 – Box and whisker plots for the average thickness of newly formed connective tissue in full thickness wounds untreated (open defects, ‘no treatment’) and treated with acellular and uncultured and cultured cell seeded skin equivalents for three time points post-wounding.	123
Figure 57 – The effect of wound grafting of full thickness skin defects with the PLGA-collagen hybrid construct on (a) the cross sectional area and (b) thickness of the newly formed connective tissue compared to open defects or no treatment (*, $p < 0.05$).	124
Figure 58 – Correlation between cross sectional area of the connective tissue newly formed in full-thickness skin defects and the wound size (*, $p < 0.002$).	126
Figure 59 – Micrograph visualising the birefringence of a picrosirius stained tissue section of a full thickness skin defect 3 weeks after injury. Central, the full thickness defect (d) can be seen bordered by hair follicles (white arrow heads) and extending from the epidermis to the original wound bed (wb) (between white arrows). Within the defect a new connective tissue has been deposited in which two distinct regions can be seen; an apical region (a) and a basal region (b). (pc, panniculus carnosus muscle).	127
Figure 60 – Picrosirius red stained, newly formed connective tissue in full thickness wounds viewed under a linearly polarising light microscope showing the change in amount of collagen and their interference colours over time and between treatment groups. The colour chart indicates the hues for immature to mature collagen fibrils, scale bar is shown at the bottom right corner.	128
Figure 61 - Box and whisker plot for the collagen content (from the percentage birefringent material per tissue area) in the basal region of the newly formed connective tissue showing the effect of cell therapy on the amount of collagen in the apical regions of the newly formed tissue.	129
Figure 62 - Box and whisker plot for the collagen content (measured by the percentage increase of birefringent material per field of view) showing the effect of cell therapy on the amount of collagen in the apical regions of the newly formed tissue.	130
Figure 63 – Collagen maturation in the basal regions of the newly formed connective tissue. (a) Post-injury changes (at three time points) in proportion of birefringence	

interference colours of collagen fibres in full thickness wounds treated without cells (no cells; groups consist of untreated wounds and those treated with acellular skin equivalents) and with uncultured and cultured (cell seeded) skin equivalents. (b) Box and whisker plot of the ratio in the proportion of thick (represented by red and orange colours) to thin (represented by green and yellow colours) collagen fibres as presented in (a). 133

Figure 64 – Collagen maturation in the apical regions of the newly formed connective tissue. (a) Post-injury changes (at three time points) in proportion of birefringence interference colours of collagen fibres in full thickness wounds treated without cells (no cells; groups consist of untreated wounds and those treated with acellular skin equivalents) and with uncultured and cultured (cell seeded) skin equivalents. (b) Box and whisker plot of the ratio in the proportion of thick (represented by red and orange colours) to thin (represented by green and yellow colours) collagen fibres as presented in (a) (NS, not significant)..... 134

Figure 65 – Correlation between the thickness of the panniculus carnosus muscle and the wound length (*, $p < 0.002$)..... 135

Figure 66 - Box and whisker plots for the average thickness of the subcutaneous panniculus carnosus muscle in full thickness wounds untreated ('no treatment') and treated with acellular and uncultured and cultured cell seeded skin equivalents for three time points post-wounding. 136

Figure 67 – Micrographs of wound edges, one week after injury, showing the difference in the length of epidermal regenerates (ER) in full-thickness skin defects receiving (A) no treatment or (B) treatment with cultured (cell seeded) skin equivalents (SE). Black arrows indicate the wound bed and white arrow heads point to the normal epidermis. Scale bar at the bottom right measures 1 mm. 137

Figure 68 – (a) Box and whisker plots for percentage wound coverage of full-thickness skin defects by epidermal regeneration at week 1 showing that the percentage closure increased with the number of cells used to treat the wound. (b) The epidermis had completely regenerated in all wounds at weeks 3 and 5 and the regenerated epidermis was 4 times thicker than that of normal (unwounded) skin (**, $p < 0.01$). 138

Figure 69 – Immunohistochemical detection of CD31+ endothelial cells visualising angiogenesis at three points in the connective tissue newly formed in healing full thickness skin defects, untreated, treated with acellular, uncultured and cultured skin equivalents (DAB chromogen, haematoxylin counterstain; scale bar is shown at the bottom right corner).....	140
Figure 70 - Box and whisker plots for the number of CD31+ blood vessel cross sections per area newly formed connective tissue in wounds treated without cells (no cells; groups consist of untreated wounds and those treated with acellular skin equivalents) and with uncultured and cultured (cell seeded) skin equivalents for three time points post-surgery (*, $p < 0.05$; <i>post hoc</i> analysis for the interaction between treatment and time). Values are for 6 samples, except ‘no cells’ = 12 samples.....	141
Figure 71 - Box and whisker plots for the size percentage of the blood vessel cross sectional area per area newly formed connective tissue in wounds treated without cells (no cells; groups consist of untreated wounds and those treated with acellular skin equivalents) and with uncultured and cultured (cell seeded) skin equivalents for three time points post-surgery (*, $p < 0.05$; <i>post hoc</i> analysis for the interaction between treatment and time). Values are for 6 samples, except ‘no cells’ = 12 samples.....	143

List of tables

Table 1 - Poly-[lactic acid-co-caprolactone] (PACL) and poly-[lactide-co-glycolide] (PLGA) meshes and compressed collagen components in respective hybrid constructs. Values are means \pm <i>SD</i> for 6 samples (*, $p < 0.05$; ***, $p < 0.001$).	98
Table 2 - Number of grafts out of the initial number of grafts that were still found <i>in situ</i> at each time point (post-operatively). (FTSG, full thickness skin graft; acellular skin equivalents and cell-seeded uncultured and cultured skin equivalents).	114
Table 3 – Comparison of the fabrication times for the experimental skin equivalents (UC, uncultured constructs; CC, cultured constructs) and currently, commercially available, living, biological dressings (Dermagraft, OrCel, Apligraf).	168

Table of abbreviations

AB	– Alamar Blue
ABC	– avidin biotin complex
AC	– acellular construct
ANOVA	– analysis of variance
CC	– cultured constructs
CCHH	– compressed collagen hydrogel hybrid
CD	– cluster of differentiation
CMFDA	– 5-chloromethylfluorescein diacetate
DAB	– 3,3'-diaminobenzidine
DAPI	– 4',6-diamidino-2-phenylindole
DMA	– dynamic mechanical analysis
DMEM	– Dulbecco's modified Eagle medium
ECM	– extracellular matrix
EDTA	– ethylenediaminetetraacetic acid
EGF	– epidermal growth factor
EH-1	– ethidium homodimer-1
F_{break}	– break force
FCS	– fetal calf serum
FGF	– fibroblast growth factor
FITC	– fluorescein isothiocyanate
FLS	– fluid leaving surface
FTSG	– full thickness skin graft
Gly	– glycine
H&E	– haematoxylin & eosin
hNNF	– human neonatal foreskin fibroblasts
HRP	– horseradish peroxidase
HSB	– hue, saturation, brightness
HSD	– honestly significant difference
IFN	– interferon
IgG	– immunoglobulin G
IL	– interleukin
IMS	– industrial methylated spirits
KGF	– derived keratinocyte growth factor

KGM – keratinocyte growth medium
LSD - least significant difference
M – mean
MEM – minimal essential medium
MMP – matrix metalloproteinase
MP – megapixel
NaOH – sodium hydroxide
NS – not significant
NT – no treatment
P/S – penicillin/streptomycin
PBS – phosphate buffered saline
PDGF – platelet derived growth factor
PLACL – poly-[lactic acid-co-caprolactone]
PLGA – poly-[lactide-co-glycolide]
PMN – polymorphonuclear leukocytes
rDEF – rabbit dermal ear fibroblasts
RFU – relative fluorescence units
RGB – red, green, and blue
RM-ANOVA – repeated measures ANOVA
ROS – reactive oxygen species
RPM – revolutions per minute
SD – standard deviation
SEM – scanning electron microscope
TBS – tris-buffered saline
TE – tissue engineering
TGF – transforming growth factor
TNF – tumor necrosis factor
UC – uncultured constructs
UTS – ultimate tensile strength
VEGF – vascular endothelial growth factor
SMA – smooth actin

1. Introduction

Cutaneous wounds extend the range of epidermal wounds to full thickness skin defects (*i.e.* those extending through the full thickness of the dermis). In adult humans, full thickness dermal wounds close or heal in small part by wound contraction but in most part by the formation of a dense collagen type I rich connective (scar) tissue replacing the void left by the original tissue architecture (Martin, 1997; Li *et al.*, 2007).

Although, normal scar tissue supports the restoration of the barrier function of the skin it lacks normal skin appendages (*e.g.* hair follicles, sweat glands) and is mechanically inferior to normal dermal tissue ultimately regaining only 80% of the original tensile strength (Martin, 1997). Additionally, this newly formed connective tissue is prone to contracture (Brissett and Sherris, 2001) which depending on the anatomical location and severity can lead to cosmetic and functional problems.

The aetiology of wounds spans an array of acute (unintentional and intentional, *i.e.* surgery) insults and chronic conditions. Acute injuries comprise a group of mechanical (*e.g.* blunt or sharp force), thermal (Monstrey *et al.*, 2008), chemical, electrical injuries (Choi *et al.*, 2009). Chronic wounds (or ulcers) are those that do not heal within a period of time in which normal wound closure can be expected (Stadelmann *et al.*, 1998). The vast majority of chronic wounds (or ulcers) develop in the context of chronic venous insufficiency, neuropathy and diabetes mellitus, or unrelieved pressure and are in a minority of cases caused by peripheral vascular disease.

There are three general techniques of wound treatment (Mulder *et al.*, 2002): (i) primary intention (*i.e.* immediate wound closure through surgical means), (ii) secondary intention (*i.e.* the wound is left open and allowed to close by natural wound healing), or (iii) third intention (*i.e.* delayed surgical wound closure after a period of natural wound healing). Of these techniques healing by primary intention is preferred as it is generally associated with the least formation of scar tissue when performed with minimal wound tension. It involves the immediate closure of the wound by opposing the wound edges through some form of fixation (*e.g.* sutures, staples, or adhesive materials) with or without surgical debridement of foreign contaminants or devitalised tissues.

Chronic wounds generally heal by secondary intention (with the aid of wound dressings) with the added attention to the underlying aetiology, although in certain cases

these wounds can be excised and converted to a surgical wound with or without the transplantation of distant skin tissue or transposition of local skin tissue.

1.1 Acute wound healing

1.1.1 Haemostasis

A physical insult of the skin involving the dermis generally results in injury of blood vessels with the subsequent leakage of blood into the wound. In the primary hemostasis process, activated platelets aggregate and adhere at the site of injury forming a platelet plug. A secondary hemostasis process, the coagulation cascade, occurs in parallel and involves the thrombin mediated conversion of fibrinogen in fibrin which subsequently polymerises, forming a network to which activated platelets adhere (Laurens *et al.*, 2006).

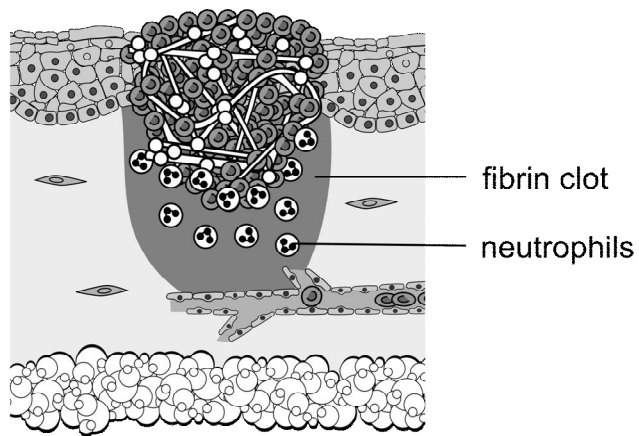
This plug prevents further blood loss (Figure 1), forms a reservoir of growth factors derived from encapsulated cells (*e.g.* platelet derived growth factor, PDGF; transforming growth factor β , TGF- β), plasma protein (fibronectin, vitronectin) and cytokines that stimulate wound healing and acts as a temporary scaffold for new tissue formation.

1.1.2 Inflammatory phase

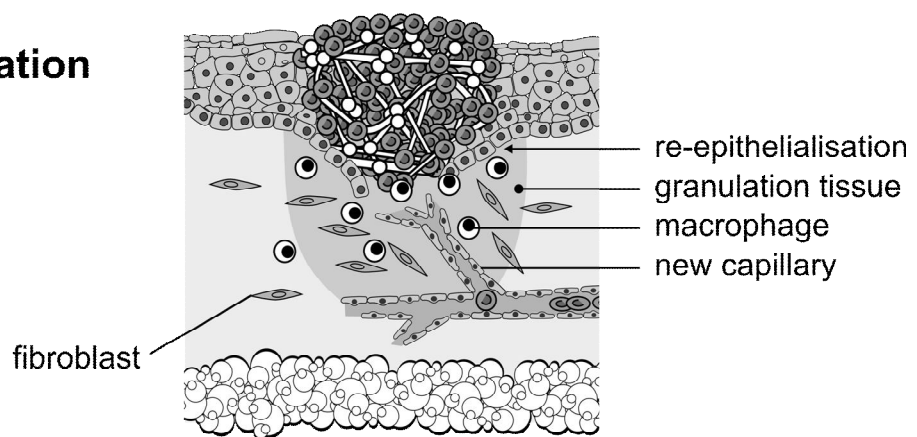
Within minutes of injury, blood-borne polymorphonuclear leukocytes (neutrophils, PMN) extravasate in venous capillaries (activated by macrophage derived interleukin- 1β , IL- 1β ; tumor necrosis factor- α , TNF- α ; interferon- γ , IFN- γ) and collect at the wound site (Figure 1) to debride devitalised tissue and reduce the bacterial load through phagocytosis (Eming *et al.*, 2007).

Neutrophil recruitment to the wound site ceases as the stimulus is removed. Chemo-attractants from platelets encapsulated in the fibrin clot, keratinocytes at the wound margins, and fibroblasts attract monocytes from the systemic circulation which subsequently become activated and differentiate into mature tissue macrophages adding to the resident macrophage population (Figure 1).

Inflammation



Proliferation



Remodeling

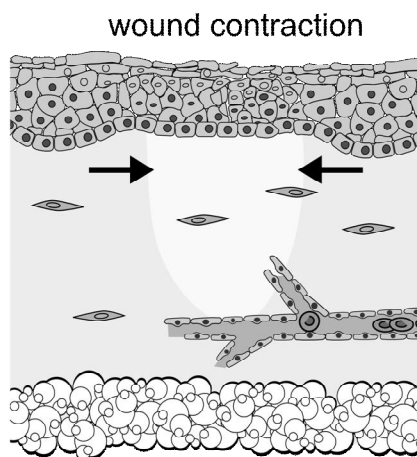


Figure 1 - Illustration of the progression of the normal wound healing response in adult humans which following a haemostatic phase is characterised by (1) an inflammatory phase, (2) a proliferative phase, and (3) remodelling phase.

These professional antigen presenting cells not only serve an immunological role but are also essential for a normal wound healing response by activating local fibroblasts, keratinocytes and endothelial cells through the secretion of growth factors such as TGF- β , TGF- α , basic fibroblast growth factor (FGF), PDGF and vascular endothelial growth factor (VEGF) (Barrientos *et al.*, 2008).

1.1.3 Proliferative phase

The proliferative phase overlaps the end of the inflammatory phase and is characterised by angiogenesis and collagen deposition (*i.e.* granulation or new connective tissue formation), re-epithelialisation, and wound contraction (Martin, 1997).

1.1.3.1 Re-epithelialisation

The epidermis, a stratified squamous epithelium, has an important barrier function protecting the body against infection and dehydration. Both the epidermis and basement membrane can regenerate provided that sufficient dermal tissue remains within the wound bed (Suter *et al.*, 2009).

1.1.3.1.1 Normal keratinocyte biology

The epidermis, in uninjured conditions, is renewed by a basal population of progenitor cells (*i.e.* basal cells or transit amplifying cells) through proliferation and differentiation. The stem cell population within the hair follicle bulge rarely divide under normal circumstances but can reconstitute the epidermis if the basal progenitor population is eradicated through injury (Morasso and Tomic-Canic, 2005).

In the normal epidermis, keratinocytes committed to differentiate progressively move towards the periphery of the epidermis, from the basal to the suprabasal layers, transitioning from basal cells to spinous cells, then to granular cells and ultimately into a keratinised (or cornified) anucleated cells (*i.e.* squame) (Figure 2) (Maja *et al.*, 1997; Mitev and Miteva, 1997).

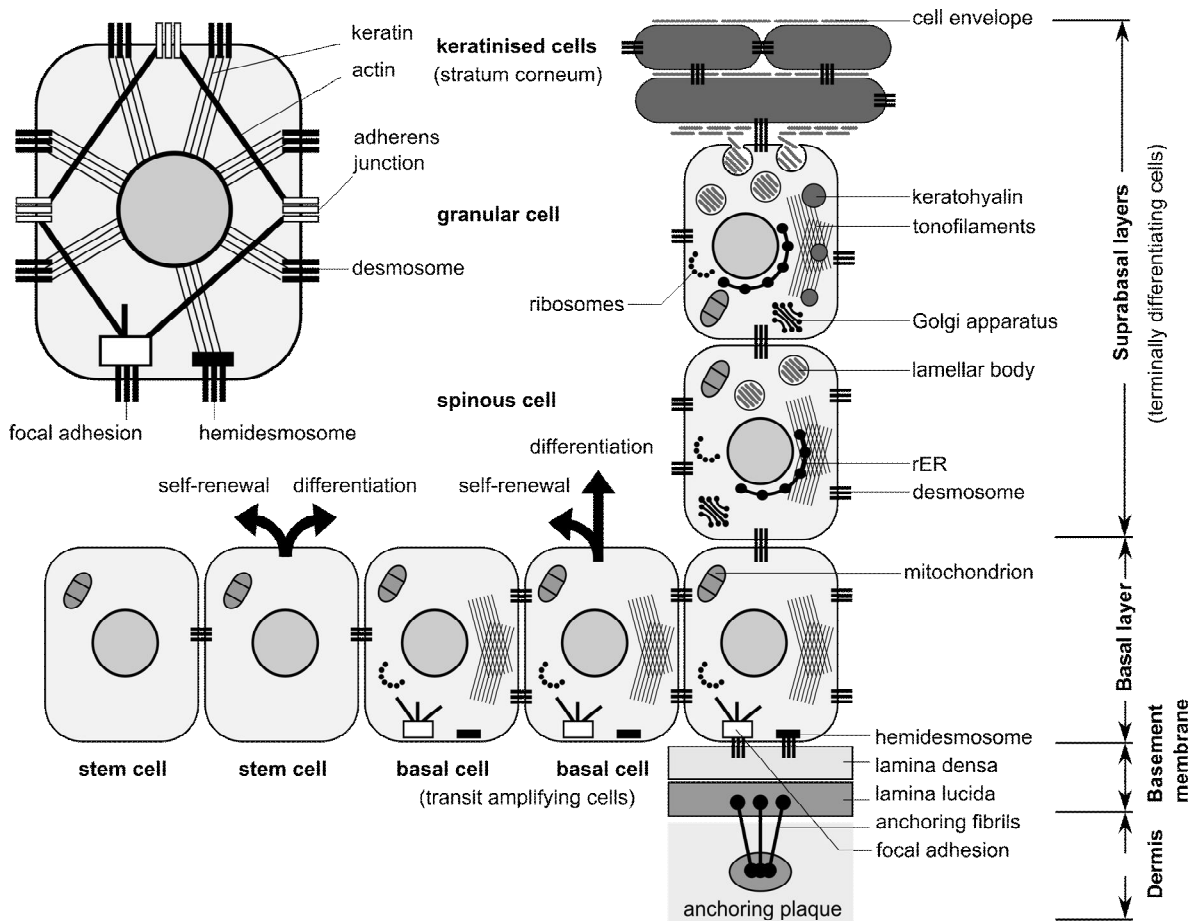


Figure 2 – Illustration highlighting the characteristics of keratinocyte biology (Mitev and Miteva, 1997): cell anatomy, differentiation and stratification (see text for detailed description).

As spinous cells transform to granular cells, the keratin filaments (a cytoskeletal element) are organised and cross-linked into large macrofilaments by filaggrin (stored in keratohyalin granules as profilaggrin) to provide the cells with mechanical strength. In the transition zone between the stratum granulosum and stratum corneum, precursor proteins such as loricrin and involucrin in the granular cells are cross-linked at the inner surface of the cell membrane by transglutaminases forming a cornified envelope which replaces the cytoplasmic membrane of the differentiating keratinocyte. Additionally, submembranous lamellar bodies within the granular cells secrete lipids (*e.g.* ceramides) into the extracellular space forming intercellular lamellae which make up the lipid envelope.

1.1.3.1.2 Keratinocytes in wound healing

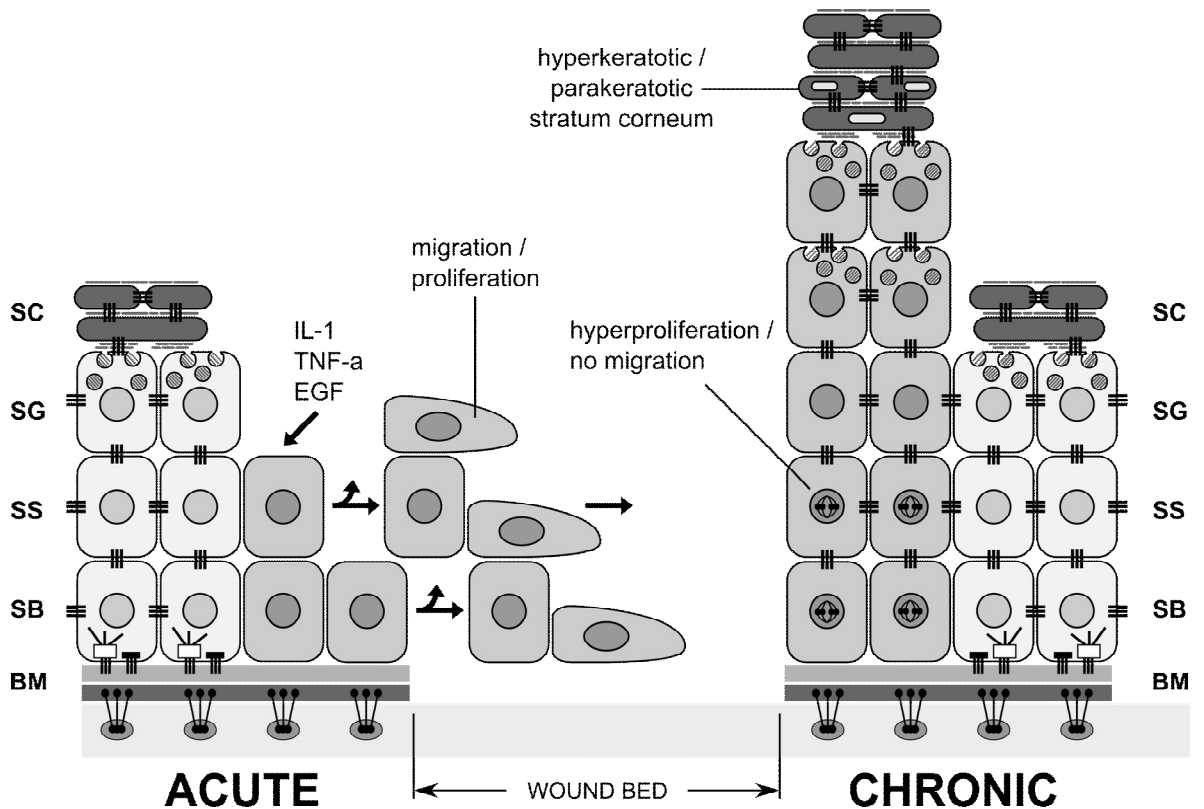


Figure 3 - In the acute wound (left) keratinocytes are activated in response to pro-inflammatory cytokines and growth factors and proliferate and migrate into the wound bed. The chronic wound (right) is characterised by mitotically active cells located in the suprabasal (differentiated) layers. Furthermore, the cornified layer is hyperkeratotic and parakeratotic suggesting a derangement in the completion of either activation or differentiation (Morasso and Tomic-Canic, 2005).

Basal keratinocytes during wound healing are activated by growth factors and pro-inflammatory cytokines (*i.e.* keratinocyte derived epidermal growth factor, EGF, heparin-binding EGF, transforming growth factor- α , TGF- α , and fibroblast derived keratinocyte growth factor, KGF or FGF7, TGF- β 1), resulting in increased proliferation and in migration mediated by the dissolution of cell-cell adhesion molecules, down-regulation of hemidesmosomes that attach to laminin (present in uninjured basal membrane), and up-regulation of those that recognise fibronectin (integrin α 5 β 1), vitronectin (integrin α v β 5), collagen (integrin α 2 β 1) of the provisional extracellular matrix (ECM) present in the wound bed (Mitev and Miteva, 1997; Werner *et al.*, 2007).

Essential for the migrating phenotype are the production of (urokinase-type and tissue-type) plasminogen activator that can degrade the fibrin barrier by activating plasmin within the fibrin clot and the production of matrix metalloproteinases (MMPs) that can release keratinocytes from their attachments to the basal lamina (collagen type VII of anchoring fibrils and collagen type IV present within the lamina densa of the basement membrane) and digest focal adhesion attachments to the dermal substrate (collagens I and III) within the wound (Coulombe, 2003).

Basal and suprabasal keratinocytes return to their normal differentiation program once the wound surface is covered with a monolayer of keratinocytes resulting in the re-establishment of a stratified epidermis and underlying basal lamina.

The failure of chronic wounds to epithelialise is characterised by hyperproliferation and a hyperkeratotic and parakeratotic (*i.e.* presence of nuclei) cornified layer, suggesting an inability of keratinocytes to migrate into the wound (Morasso and Tomic-Canic, 2005).

1.1.3.2 Angiogenesis

At day 4 post-injury, new blood vessels (sprouting) from preexisting vessels invade the wound clot and it is these capillaries that give the granulation tissue its granular appearance and name (Tonnesen *et al.*, 2000; Li *et al.*, 2003a). Basic FGF (also known as FGF-2) and vascular endothelial growth factor (VEGF) promote angiogenesis. FGF-2 is membrane bound in endothelial cells but released when cells are damaged (through injury) and is also secreted by macrophages. VEGF is produced by keratinocytes, endothelial cells and fibroblasts (Cheema *et al.*, 2008) under hypoxic conditions.

1.1.3.3 Granulation tissue formation

Fibroblasts form a heterogeneous group of mesenchymal connective tissue cells responsible for ECM synthesis and re-modelling. These cells are recruited to the site of injury from proliferating populations within the wound margins and from differentiating pericytes/vascular smooth muscle cells associated with the micro-vasculature and fibrocytes (*i.e.* bone marrow derived fibroblast-like leukocytes) (Hinz, 2007).

After 3 to 4 days post-injury, activated fibroblasts migrate into the fibrin matrix by the action of motogens and mitogens (*i.e.* PDGF and TGF- β) derived from activated

platelets, leukocytes and resident cells, where they deposit collagen-rich matrix. Like keratinocytes fibroblasts also need to change their integrin profile to migrate, down-regulating collagen receptors and up-regulating integrins binding fibrin, fibronectin and vitronectin.

1.1.4 Remodelling phase

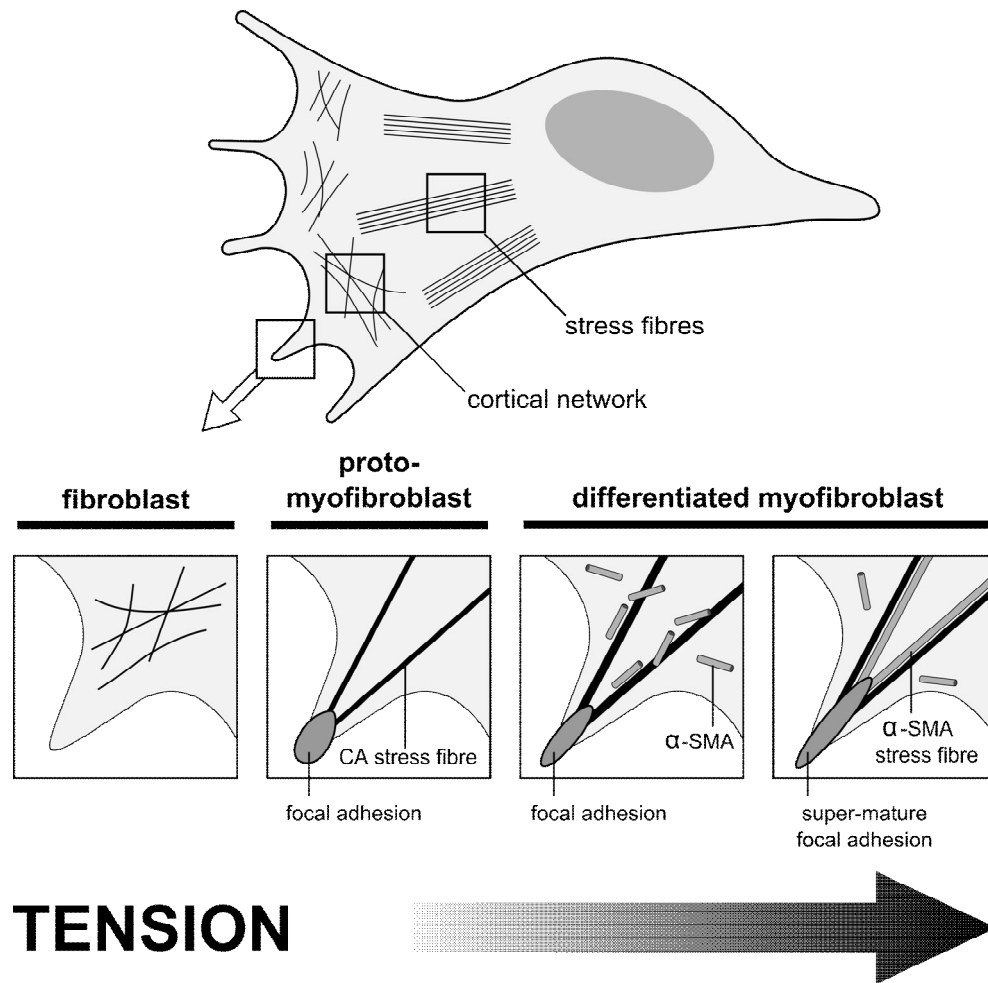


Figure 4 – Fibroblasts exposed to mechanical stress will differentiate into myofibroblasts which feature a contractile microfilamentous apparatus. Fibroblasts *in vivo* are normally stress shielded and their cytoplasmic actin (CA) filaments are mainly organised into a cortical network. When exposed to an extracellular mechanical load, fibroblasts transition into proto-myofibroblasts forming stress fibres initially composed of CA and anchored at sites of focal adhesion. Further increases in matrix tension and the action of TGF- β stimulate the formation of super-mature FAs and assembly of the contractile apparatus hallmarking the differentiation into myofibroblasts. The contractile stress fibres in

these cells contain bundles of actin microfilaments associated with α -smooth actin (α -SMA) (Tomasek *et al.*, 2002; Gabbiani, 2003).

Exposure to TGF- β 1 in the context of a change of in mechanical microenvironment, from an intact, stress-shielded, protective environment to the stressed condition in the wound bed, results in a proportion of fibroblasts in the acquisition of contractile stress fibres composed of β -cytoplasmic actins and focal adhesions hallmarking the proto-myfibroblast (Figure 4) (Tomasek *et al.*, 2002).

In fibroblasts, cytoplasmic actin filaments are anchored to focal complexes at sites of integrin clustering. Upon increase in intra- and/or extracellular tension these focal complexes mature into focal adhesions (Goffin *et al.*, 2006) (Figure 4).

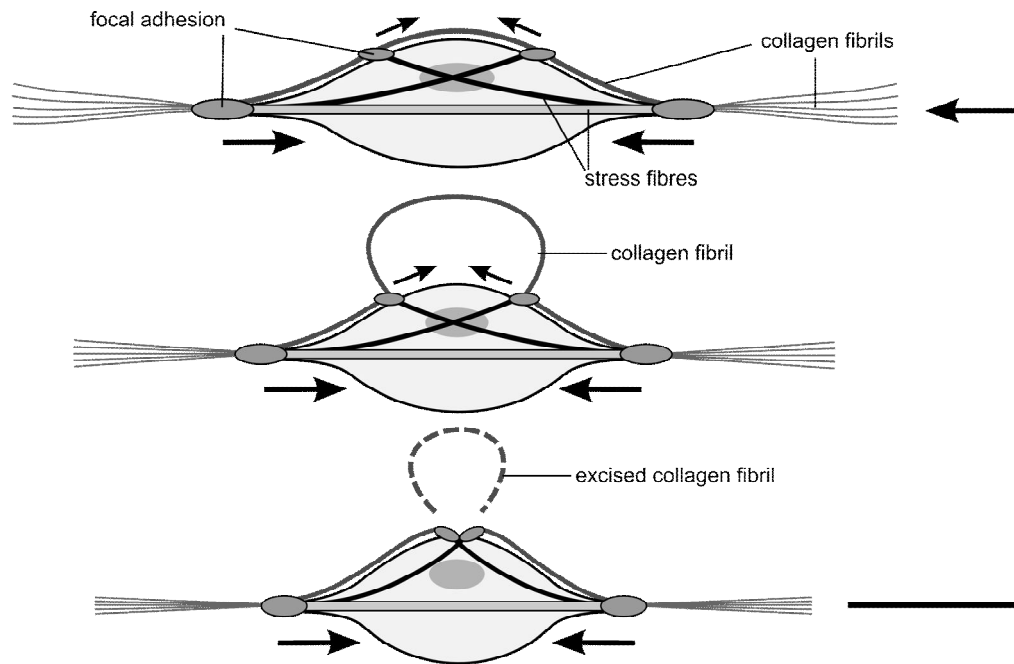


Figure 5 – Illustration of the hypothesis that myofibroblasts contract the matrix in a lock-step mechanism (Tomasek *et al.*, 2002; Castella *et al.*, 2010). It has previously been shown that the cellular contraction of the collagen network by the myofibroblast is eventually stabilised into the matrix. The exact mechanism, however, is unknown but it is proposed by Castella *et al.* (2010) that the contraction induced laxity of the collagen network is removed through proteolysis.

Further stimulation (*i.e.* TGF- β 1 and mechanical stress) transforms the proto-myfibroblasts into differentiated myofibroblasts which feature supermature (*i.e.* more

complex) focal adhesions and the *de novo* expression of α -smooth muscle actin incorporated in preformed β -cytoplasmic actin stress fibres (Figure 4) (Gabbiani, 2003). These contractile and secretory myofibroblasts contribute to wound closure through the deposition of ECM and through tissue contraction.

The exact mechanism by which the cell mediated contraction is permanently built into the matrix is still unclear (Marenzana *et al.*, 2006), but the following hypothesis is proposed (Castella *et al.*, 2010). Global cell contraction shortens the bulk ECM network generating slack in individual ECM fibrils (Figure 5). These locally relaxed fibrils can be tensed by (Ca^{2+} -dependent) subcellular contractions followed by proteolyses and subsequent stabilisation of the fibrils through new collagen secretion and/or cross-linking. The cell then re-spreads and the process is repeated. A further refinement of this hypothesis is that the collagen fibrils relaxed by cellular contraction are unilaterally cleaved and the freed ends are incorporated into the same or an adjacent fibrils at the shortened length (Cheema *et al.*, 2007).

The contractile activity is terminated as α -SMA expression decreases and myofibroblasts apoptose when the tissue is repaired and tensional homeostasis is restored.

1.1.4.1 Hypertrophic scarring, keloids and scar contracture

In pathological wound healing myofibroblast activity persists even after the wound has re-epithelialised and healed leading to hypertrophic scars which are characterised by a high cell, collagen density and contracture. The development of this long term complication is linked to delayed epithelialisation and to mechanical tension exerted on the wound (Brissett and Sherris, 2001; Kose and Waseem, 2008). Depending on the extent and the anatomical location, scar contracture can lead to debilitating functional impairment.

1.2 Chronic wound healing

A wound is considered chronic, if it does not heal in an orderly or timely fashion, or if the healing process does not result in structural integrity (Stadelmann *et al.*, 1998).

1.2.1 Molecular pathogenesis of chronic wounds

In chronic wounds, healing is compromised by a persistent inflammatory phase resulting in high levels of MMPs and ROSs in the wound (Harding *et al.*, 2005).

The MMPs are thought to contribute to the impairment of wound healing by the proteolysis and inactivation of growth factors, chemotactic agents and pro-inflammatory cytokines. In acute, partial thickness burns in humans increased levels of proteases are associated with a decreased angiogenic response and epidermal regeneration (Caulfield *et al.*, 2008). Further, the excessive proteolytic break-down of the ECM negatively affects the balance between tissue synthesis and degradation (Rayment and Upton, 2009).

Endogenously produced ROSs might induce premature and telomere-independent (*i.e.* independent of population doublings) senescence of fibroblasts and keratinocytes decreasing the expression of pro-inflammatory cytokines and chemokines (Harding *et al.*, 2005). The net result is suppression of cell proliferation and migration which leads to the reduced accumulation of leukocytes, keratinocytes, fibroblasts and endothelial cells at the site of injury.

1.2.2 Venous leg ulcers

Venous skin ulceration (*i.e.* loss of skin that takes more than 6 weeks to heal) forms one end of the spectrum of chronic venous disease consisting of varicose veins, leg edema, hyperpigmentation, eczema and lipodermatosclerosis (Schmid-Schonbein *et al.*, 2001; Bergan *et al.*, 2006). These ulcers are associated with primary venous hypertension or secondary to venous valve dysfunction or venous thrombosis.

Although the exact temporal and causal sequences of events have not yet fully been elucidated, the current hypothesis is that venous flow disturbances causes leukocyte

pooling in the capillary microcirculation (Raffetto, 2009). The concomitant fluid shear stress causes the activation of endothelial cells and leukocytes resulting in the extravasation of activated leukocytes and plasma proteins in the extra-vascular compartment.

The chronic inflammation is characterised by the accumulation in the dermis of macrophages and mast cells which produce TGF- β 1, MMPs (Rayment and Upton, 2009) and reactive oxygen species (ROSs) (Harding *et al.*, 2005). It is thought these inflammatory agents underlie the formation of ulcers, dermal fibrosis, and the impairment of the normal wound healing capacity.

Venous leg ulcers have been estimated to affect 0.2-1% of the population in developed countries (Simka and Majewski, 2003) and, although generally not limb threatening, are associated with a loss in quality of life due to pain and functional limitations (Koupidis *et al.*, 2008).

1.2.3 Diabetic foot ulcers

The aetiology of diabetic foot ulcers can largely be attributed to the clinical triad of peripheral sensory neuropathy, trauma, and ischemia (Falanga, 2005). Peripheral sensory neuropathy (often secondary to diabetes) is associated with reduced sensory guarding against pressure and heat making diabetic patients more prone to traumatic injury. Additionally, neuropathy can cause a maldistribution of blood flow which in combination with any associated macro-vascular disease can lead to ischemia and ulceration of the skin.

The World Health Organisation estimated that 2.8% of the world population (or 171 million) was suffering from diabetes in 2000. This number is expected to rise to 4.4% (or 366 million) in 2030 (Wild *et al.*, 2004). Fifteen percent of patients with diabetes will develop a foot ulcer in their lifetime. Of those with foot ulcers 15-24% require minor or major amputations because of limb or life threatening infections (Cheer *et al.*, 2009).

1.3 Tissue Engineering

The treatment of acute and chronic cutaneous wounds and their long term sequelae extends a whole range of surgical and non-surgical treatments. An important treatment modality is the use of native skin tissue from the patient self (*i.e.* autologous) or from an allogeneic source (Valencia *et al.*, 2000). Full thickness skin grafts are the gold standard for acute full thickness skin defects as it is effective in preventing long term complications such as scar contracture and associated functional deformities (Frame *et al.*, 2004). The use of skin grafting has also been found effective in increasing closure of chronic wounds over non-surgical treatments (Jankunas *et al.*, 2007; Mahmoud *et al.*, 2008).

Limiting factors in the application of this therapeutic option is the restricted supply of skin tissue, donor site morbidity after harvest, and acceptor site morbidity due to general and/or immunological issues (in the case of allogeneic grafts). An alternative approach to repair and reconstruction aiming to meet the requirements of human anatomy and physiology is tissue engineering (TE) (Langer and Vacanti, 1993), also known under the synonyms “reparative medicine” (Sipe, 2002) and “regenerative medicine” (Suh, 2000).

1.3.1 Basic principles of tissue engineering

TE, as viewed today, is ‘an interdisciplinary field that applies the principles of engineering and life sciences toward the development of biological substitutes that restore, maintain, or improve tissue function or a whole organ’ (Langer and Vacanti, 1993).

The basic components of TE are cells, signals and scaffolds (Langer and Vacanti, 1993). The first two components are transplanted directly or within a protective (often degradable, porous) framework (*i.e.* scaffold) to induce tissue repair (Figure 6). From this three general strategies are employed in TE:

1. Transplantation of culture-expanded or modified cells or cell substitutes to augment the (diseased or normal) local cell population (*i.e.* cell-based TE) (Fodor, 2003).
2. Use of tissue-inducing substances for local targeting of cells where new tissue is needed (genes and/or local or systemic growth factors) (Bleiziffer *et al.*, 2007; Chen *et al.*, 2010).

3. Use of matrices, with or without cells placed on or within, to conduct or induce tissue formation (Cima *et al.*, 1991).

1.3.2 Cell sources for tissue engineering

Part of the TE strategy for tissue repair is the expansion and engraftment of cells. Tissue engineers have experimented with different cell types from different sources over the past two decades to try to determine the best substrate for each particular tissue to be constructed.

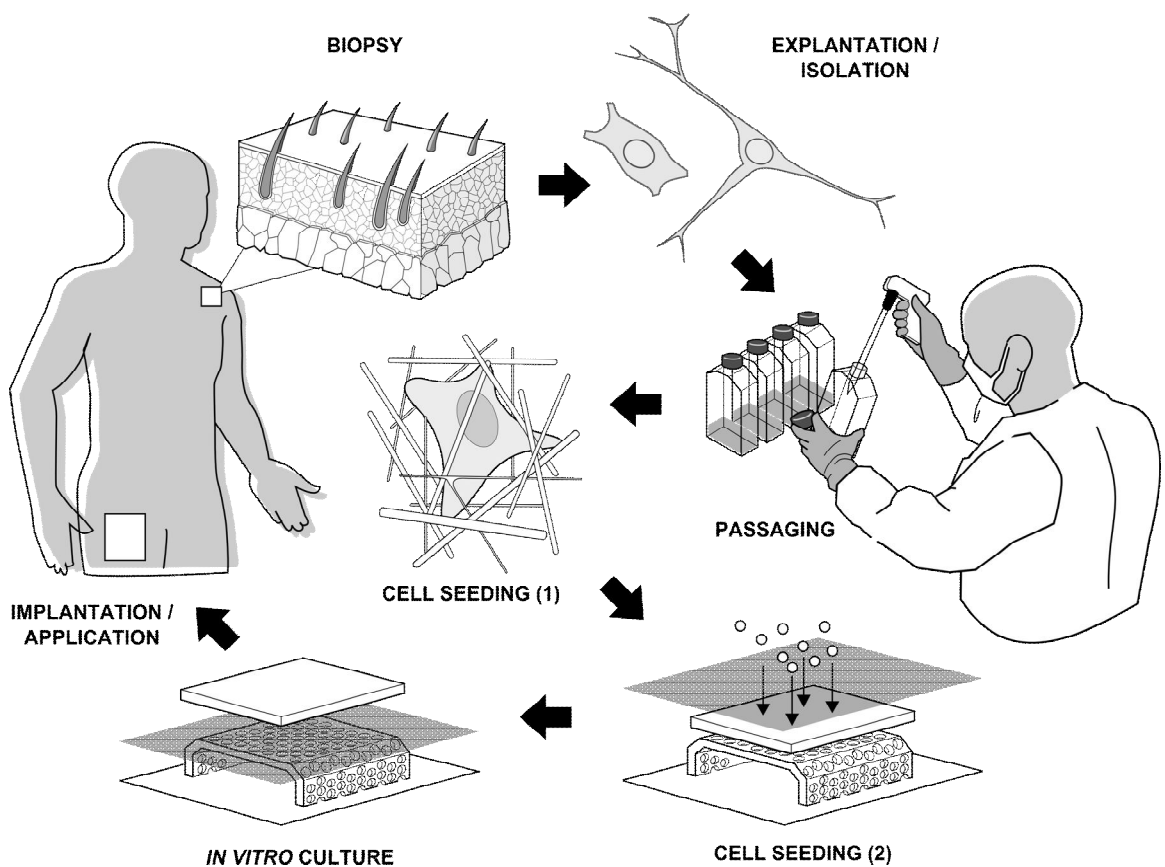


Figure 6 – Illustration of the basic principles of tissue engineering. Cells obtained from a tissue biopsy, taken from a patient or a donor, are expanded through serial passages. Once a sufficient cell number has been obtained, cells are seeded (1) inside or (2) on a polymeric scaffold material, and cultured *in vitro* in a bioreactor or incubator. When the construct is sufficiently matured it can be implanted in or applied to an area of interest.

Cell sources are either autologous (from the same organism), allogenic (from a different organism within the same species) or xenogeneic (from an organism of a different species). Potential limitations specific to each of these therapies are: donor site morbidity associated with autologous cell therapy, the immunogenicity of allogenic cell therapy, the immunogenicity and risk of xenozoonosis (cross-species pathogen infectivity) associated with xenotransplantation.

The specific cell types used for transplantation are categorised as follows (Fodor, 2003):

1. tissue specific differentiated (or primary) cells
2. postnatal stem or progenitor cells
3. embryonic stem cells

Primary mature cells are tissue specific differentiated cells released from explanted tissue, cultivated for *ex vivo* expansion to acquire sufficient cell numbers, and then implanted. These cells are ideal in that they already express the desired phenotype. However, the success of primary cell culture is limited due to, senescence or dedifferentiation during *in vitro* cultivation, expression of inappropriate phenotypes, and low proliferation rates. An additional limitation is that harvest of certain phenotypes can only be performed on tissues that can sustain surgical harvesting.

Progenitor cells are early descendants of stem cells that still have limited differentiation capabilities (*i.e.* are oligopotent), but have lost the ability for self-renewal like stem cells, and thus proliferate indefinitely (Polak and Bishop, 2006).

Adult (or postnatal somatic) stem cells have the ability of self-renew and they can differentiate to all the cell types of the tissue they came from (*i.e.* are multipotent) (Young *et al.*, 2004). Stem cells have been found in a variety of tissues including bone marrow, liver, skin, central nervous system, muscle, and mammary gland. Stem cells vary in their capacity to undergo tissue specific differentiation, and these progenitors are therefore subdivided according to their developmental potency.

Embryonic stem cells are derived from the inner cell mass of the developing blastomere. An embryonic stem cells cell is self-renewing, totipotent or pluripotent (can become all but extra-embryonic tissues), and theoretically immortal. Pluripotent stem cells offer the

possibility of an infinitely renewable source of replacement cells (Polak and Bishop, 2006).

1.3.3 Tissue engineering scaffolds

Scaffolds are often used in TE to carry cells from the lab to the patient. Additionally, when implanted, these scaffolds fulfil a passive role, in maintaining a physical space in which tissue repair or regeneration can take place, in replacing the structural loss of tissue integrity, in concentrating cells or drugs at the site of interest, protecting them against shear force, degradation and inflammation (Drury and Mooney, 2003). They also serve an active role in providing a physiological environment essential for the survival of anchorage dependent cells and their expression of a biologically relevant phenotype.

Independent of their specific application scaffolds used for TE purposes need to have certain characteristics (Thomson *et al.*, 1995; Hutmacher, 2000): (i) be highly porous with an interconnected pore network for cell growth and flow transport of nutrients and metabolic waste; (ii) be biocompatible and bioresorbable with controllable degradation and resorption rates to match tissue replacement; (iii) have suitable surface chemistry for cell attachment, proliferation, and differentiation; and (iv) have mechanical properties to match those of the tissues at the site of implantation.

1.3.3.1 Prefabricated scaffolds

A traditional TE strategy involves the seeding of cells onto prefabricated scaffolds. Four types of biomaterials generally used for this purpose are (Hutmacher, 2001; Yang and El Haj, 2006): (1) Naturally derived organic materials: collagen, fibrin, hyaluronic acid, chitosan, alginate (2) naturally derived inorganic materials: coralline hydroxyapatite, (3) synthetic organic: aliphatic polyesters, poly(ethylene) glycol; and (4) synthetic inorganic materials: tricalciumphosphate, plaster of Paris, glass ceramics.

The main advantage of using prefabricated scaffolds is that their physical and chemical properties can be tailored with great specificity using whatever harsh method as long as the final result is cell friendly. However, this strategy is time consuming as it requires cell activity to achieve a sufficient cell density and to produce the 3D ECM environment

generally within the pores of a porous support structures (Hollister, 2005) through migration, proliferation and deposition of ECM proteins (Cooper *et al.*, 1991; Chen *et al.*, 2005).

1.3.3.2 Cell encapsulating scaffolds

As opposed to cell seeding of prefabricated scaffolds, encapsulating cells during scaffold formation (Nicodemus and Bryant, 2008) afford the ability to provide the site of interest with an adequate number of cells in a relevant 3D environment within an instant. Cell encapsulation involves mixing a cell suspension with a liquid hydrogel precursor solution which is subsequently crosslinked into a network. Only a few materials, such as the collagen hydrogels described here, are suitable for cell encapsulation as the scaffold fabrication process needs to be cytocompatible and two main categories can be distinguished (Nicodemus and Bryant, 2008): (1) biopolymer hydrogels (*i.e.* collagen, fibrin, alginate) (Mansbridge *et al.*, 1998; Hunt and Grover, 2010) and (2) synthetic based hydrogels (*i.e.* purely synthetic, *i.e.* poly(ethylene glycol), with or without incorporated biological signals and derivatised biopolymers).

1.4 Collagen as a scaffolding material

Collagen type I is commonly used as a scaffold in TE (Vaissiere *et al.*, 2000; Glowacki and Mizuno, 2008) and collagen hydrogels were one of the first materials to be used for cell encapsulation (Elsdale and Bard, 1972; Bell *et al.*, 1979).

Collagen is naturally produced by fibroblasts, osteoblasts, and chondroblasts and is found in most connective tissues being most abundant in bone, cornea, dermis and tendon. For example about 60% of the total protein content comprises collagen in dermal tissue (Ahlfors and Billiar, 2007). The use of collagen as a scaffolding material to deliver cells (that generally reside in a collagen rich environment) to the site of interest is attractive as the material is biocompatible, has low immunogenicity (Furthmayr and Timpl, 1976), is conserved across species (Chu *et al.*, 1984), is naturally remodelled by cells, and contains critical binding moieties (Ruoslahti and Pierschbacher, 1987) essential for the survival of cells such as fibroblasts which are anchorage dependent.

Collagen type I is part of a superfamily of more than 20 genetically distinct collagens. These major structural proteins make up about a third of the total protein content in higher order animals (Bailey *et al.*, 1998).

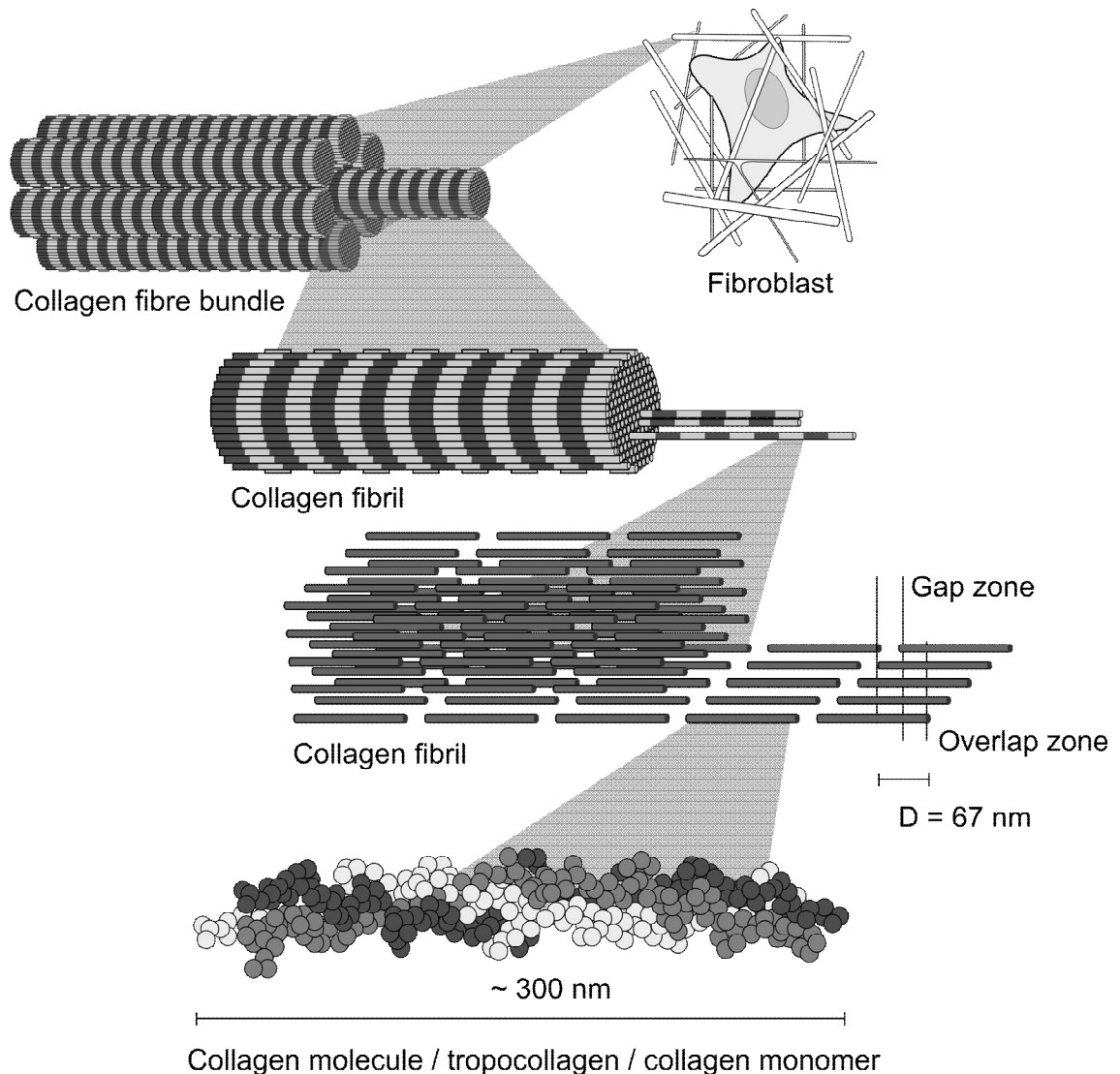


Figure 7 – A type I collagen fibre is composed of smaller collagen fibrils which themselves comprise of microfibrils. These in turn are assembled from tropocollagen molecules in a regular staggered array which give rise to their striated appearance when viewed under an electron microscope.

All collagens share the same triple helical conformation of three polypeptide chains each with glycine (Gly) typically as every third residue in the amino acid sequence (*i.e.* Gly-X-Y repeat) which further contains a high percentage of hydroxyproline and proline residues. Collagen type I, a heterotrimer composed of two $\alpha 1(\text{I})$ chains and one $\alpha 2(\text{I})$ chains, is classified as a fibrous collagen (comprising types I, II, III, V and XI)

which constitute a group of rod-like triple helical monomers (hetero- and homotrimers) which self-assemble in a parallel, quarter staggered arrangement into cross-striated (with an axial periodicity of 67 nm; Figure 7) fibrils (Van der Rest and Garrone, 1991). Fibrous collagen precursors are synthesised as soluble procollagens which are converted into collagens by cleavage of terminal propeptides by MMPs.

1.4.1 'In vitro' self-assembly of collagen fibrils

Collagen can be extracted from native tissues using weak organic acid solutions (Jordan-Lloyd and Marriott, 1935). It is interesting to note that the acid soluble collagen fraction decreases with age (BANFIELD, 1952) due to the increase in amount and changes in the type of (acid stable enzymic and non-enzymic) cross-links between collagen molecules and microfibrils (Bailey *et al.*, 1998).

The collagen used in this study is derived from rat tail tendon extracted in acetic acid (Wu *et al.*, 2005). By raising the ionic strength (by the addition of sodium chloride) or the pH of this acid solubilised monomeric collagen solution to physiological levels the collagen molecules self-assemble (*i.e.* precipitate and aggregate) *in vitro* (at room temperature) (Silver, 1981) within a matter of minutes into a non-crosslinked entangled network of polymer chains (*i.e.* collagen fibrils) with the same striated appearance as found *in vivo* (Francis *et al.*, 1942).

What results is a highly entangled network of collagen polymer chains and due to the volume of solutions used in the extraction, purification (by dialysis) and reconstitution process the resulting collagen polymer hydrogels contain a high degree of non-structural water.

1.4.2 Cell encapsulation in collagen hydrogels

It is interesting to note that the major driving force behind this self-assembly process is the increase in entropy associated with the loss of water bound to the monomer as the polymerisation occurs (Kadler *et al.*, 1987). The process is mild and allows for the encapsulation of cells during the hydrogel formation to form living tissues within the space of an hour (Bell *et al.*, 1979; Nakanishi *et al.*, 2003). It was noted early, however,

that the collagen hydrogels were unstable due to the high water content (Elsdale and Bard, 1972) making them difficult to handle.

1.4.2.1 Mechanical instability of collagen hydrogels

A decrease in the fluid content improves the mechanical properties by increasing the collagen density and the frequency and strength of inter-fibre, physical attractive (electrostatic) forces (Rosenblatt *et al.*, 1992).

1.4.2.2 Self-compaction

It is known that due to its mechanical instability a (unconfined) collagen hydrogel seated on a solid (non-porous) surface will over time and under its own weight spontaneously expel its interstitial fluid content (Elsdale and Bard, 1972) (syneresis or unconfined self-compression) through part of the gel surface (more than 50% in 2 hours (Brown *et al.*, 2005; Neel *et al.*, 2006).

1.4.2.3 Cell-mediated compaction

Additionally, encapsulated fibroblasts can expel the interstitial fluid and condense the collagen matrix through the generation of tractional forces from cell locomotion, elongation and spreading mediated by the expression of collagen binding integrins (mainly $\alpha2\beta1$) (Ehrlich and Rittenberg, 2000). Depending on the cell and collagen concentration the time it takes for a collagen hydrogel to achieve its maximum contraction can vary from several hours to several days (Dallon and Ehrlich, 2008).

1.4.2.4 Mechanical compaction

The fluid expulsion process can be accelerated by placing the gel on a porous (absorbent) substructure (Brown *et al.*, 2005; Neel *et al.*, 2006) which provides an additional driving force (a negative capillary pressure) and increases the total fluid leaving surface. The process could further be accelerated by increasing the gravitational stress (from the gel's mass) by the addition of a compressive load onto (the apical surface of) the hydrogel. This process has been termed plastic compression for the

plasticity of the deformation (Brown *et al.*, 2005), although at high strain levels an elastic recoil can be observed (Neel *et al.*, 2006).

Speed is the greatest advantage of the compression technique over cell contracted or self-compacted hydrogels. To illustrate this point it has previously been shown that the compression protocol established by this lab can increase in five minutes the break force of a (0.7 ml/cm²) collagen hydrogel to twice that of the same volume contracted by 2.0×10^5 fibroblasts/ml over a one week *in vitro* culture period (Hu *et al.*, 2010). Apart from skin tissue, the collagen hydrogel compression technique has been used to create bladder (Engelhardt *et al.*, 2010), corneal (Mi *et al.*, 2010), bone (Bitar *et al.*, 2007; Buxton *et al.*, 2008), and neural (East *et al.*, 2010) tissue equivalents.

Although the resulting compressed collagen sheets (Brown *et al.*, 2005) have the ultimate tensile properties approaching those of native tissues (Ahlfors and Billiar, 2007) they do not have the break strength required to hold a suture because of their slender thickness (100 μ m).

The break force of the compressed collagen sheets was previously improved by increasing the thickness through layering the material by rolling (along their long axis) the sheets into rod shaped constructs (Brown *et al.*, 2005; Neel *et al.*, 2006). Although, *in vivo*, adequate suture retention was found up to five weeks post-implantation (Mudera *et al.*, 2007), the fabrication and therefore the mechanical properties are subject to a certain degree of (intra- and inter-operator) variability.

Additionally, the rod shape and spiral structure are not ideal for the construction of large flat structures (for example to mimic epithelial tissues). It would be possible to produce a flat construct from a stack of multiple compressed collagen sheets. However, the resulting construct would be difficult to manage. It would be possible to improve the handling of such a construct by cell-mediated integration of the separate sheets into a unified material, but this would require an *in vitro* culture period (Marenzana *et al.*, 2007).

In the present study an alternative strategy was explored in which the thickness and the break strength of the compressed collagen sheets were improved by increasing the pre-compression volume of the collagen hydrogel.

1.5 Thesis overview

The purpose of this study was to test the utility of the collagen hydrogel compression process to rapidly fabricate a connective tissue equivalent which could be used as a suturable medical device for the delivery of living cells maintained in a physiological, or organotypic, organisation.

Two strategies were studied to increase the suturability of compressed collagen hydrogels: (1) by increasing of the collagen bulk material and (2) by the hybridisation with a suturable, degradable synthetic polymer mesh.

Having identified the inherent physical limitation of the compression of increased volume collagen hydrogels, the study focussed on the *in vitro* characterisation of the hybridisation process using a novel and an established, commercially available synthetic material.

The hybrid construct based on the commercially available material was seeded with keratinocytes and fibroblasts and tested for safety and efficacy *in vivo* in a lapine model of an acute full thickness skin defect. Skin equivalents implanted directly after fabrication were compared to those that were matured *in vitro* over a 2 week period.

1.5.1 Hypothesis under test

“The collagen hydrogel compression process can be used to rapidly engineer a living dermal equivalent for use in skin tissue engineering.”

“The suturability (measured as the break force) of a compressed collagen hydrogel can be improved by increasing the pre-compression volume provided that the post-compression strain level remains the same.”

“A suturable collagen construct can be fabricated by compressing a collagen hydrogel hybridised with a suturable synthetic degradable polymer mesh.”

1.5.2 Aims and objectives

The aim of this study was to explore *in vitro* and *in vivo* two strategies that could improve the suturability, or break force, of compressed collagen hydrogels by intrinsic and extrinsic means without significantly affecting cell viability and function.

The main objectives were as follows:

1. Quantify the percentage fluid loss over the collagen hydrogel compression process as a measure of hydraulic permeability in relation to the change in collagen density as indicated by embedded markers.
2. Quantify the mechanical break force of a collagen hydrogel with an increased pre-compression volume compressed to over 99% strain and compare this to that of a collagen hydrogel with the 'standard' pre-compression volume (Brown *et al.*, 2005) compressed to over 99% strain.
3. Test the feasibility of encapsulating a degradable synthetic polymer mesh during the polymerisation of a collagen hydrogel to construct a hybrid construct consisting of a mechanical synthetic polymer backbone and a collagen cell carrying component.
4. Determine post-compression viability of cells encapsulated and compressed in the presence of the synthetic polymer mesh, directly after compression and after a short *in vitro* culture period, to determine any negative effects of this method.
5. Spatially layer and culture *in vitro* different cell lines (*i.e.* epithelial and mesenchymal cells) on and inside the hybrid construct to test the feasibility of mimicking a complex tissue.
6. Test the safety and efficacy of this complex tissue equivalent *in vivo* in an animal wound model.

2. Materials and Methods

2.1 Collagen hydrogels

2.1.1 Formation

Note: the size of the collagen hydrogels in these experiments is expressed as the ratio of volume (in ml) to fluid leaving surface (FLS) area (in cm²) to allow for comparison between setups. For (5 ml; 0.7 ml/cm²) collagen hydrogels (Brown *et al.*, 2005), four volumes of sterile, acid-soluble (incubated at 4°C) rat tail derived (type I) monomeric collagen solution (2.16 mg/ml or 0.2% w/v protein in 0.6% acetic acid: First Link UK Ltd, West Midlands, UK) were mixed with one volume of 10-fold concentrated minimal essential medium (MEM; used as a pH indicator) and brought to neutral pH (pH 7.4) by titration with 1M sodium hydroxide (NaOH). The collagen solution was cast into one of the two pockets (each measuring 33x22x10 mm³) of a custom built stainless steel mould (weighing 120 grams) seated on a glass slide and left to polymerise undisturbed at room temperature in a laminar flow hood for a period of 30 minutes at room temperature (Figure 8a).

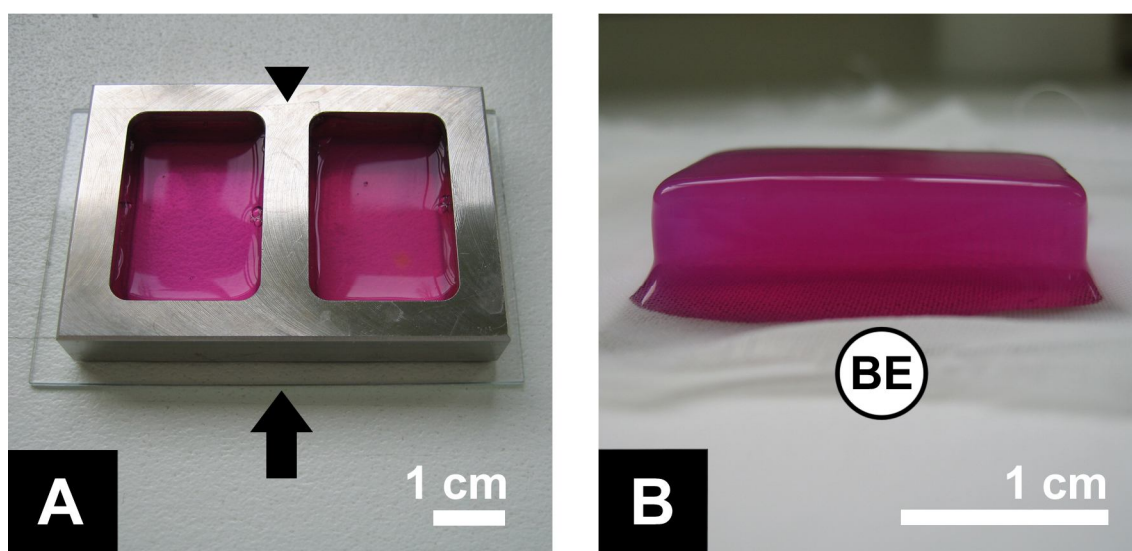


Figure 8 – (a) Neutralised collagen hydrogels (pink) cast in pockets of a stainless steel mould (arrow head) which is seated on a glass slide (arrow). (b) Collagen hydrogel after a 30 minute setting period transferred onto a standard setup of blotting elements (BE). Scale bars are shown at the bottom right corners.

2.1.2 Unconfined compression

When the collagen had polymerised after the 30 minute setting period, the resulting hydrogel was transferred onto a standardised assembly of blotting elements (Figure 8b), consisting of a layer of nylon mesh (mesh size $\sim 50 \mu\text{m}$) on top of a stainless steel mesh (mesh size $\sim 300 \mu\text{m}$) and three sheets of filter paper (Whatman, Grade 1, 240 mm diameter). A constant gravitational load (130 gram on a surface area of 7.4 cm^2 ; a stress equivalent of 1.8 kN/m^2) was immediately applied onto the top surface of the gel (in an unconfined configuration) for a period of 5 minutes to remove the interstitial fluid content (Figure 9a). After the compression, the resulting collagen sheet was placed into a (phosphate) buffered (saline) solution (PBS, catalogue number BR0014G, Oxoid, Hampshire, UK) to prevent further loss of fluid from evaporation.

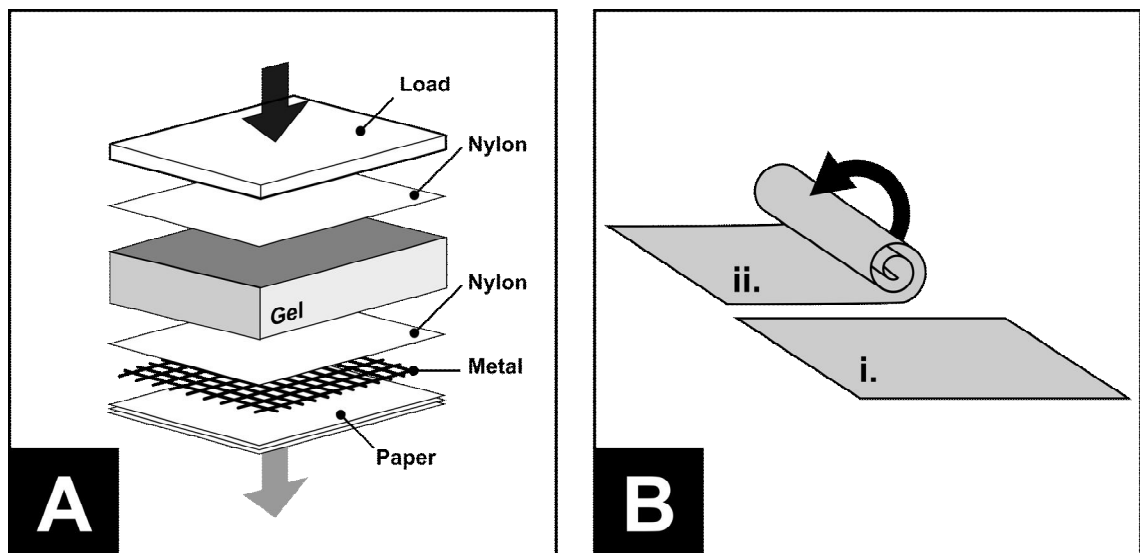


Figure 9 – (a) Illustration of the standard assembly in which the fluid content (grey arrow) of collagen hydrogels is removed through the basal surface by the negative capillary action exerted by a standard setup of blotting elements (three sheets of filtration paper, a metal and a nylon mesh) and the gravitational force from the application (in an unconfined configuration and in the direction of the black arrow) of a load on the apical surface. (b) The resulting (i) compressed collagen sheet (after a 5 minute compression) could be rolled along the long axis (ii) into spiralled constructs.

2.1.3 Confined compression

To study the compression of larger volume ($> 1.95 \text{ ml/cm}^2$) hydrogels, the collagen solutions were prepared and neutralised as described above and cast into a newly developed and custom built chamber (which laterally confined the gel preventing it from buckling during compression; measuring $7 \times 22 \times 60 \text{ mm}^3$) seated on a glass slide (Figure 10). The collagen solution was allowed to polymerise for 30 minutes after which time the glass was replaced by the standard setup of blotting elements (nylon and metal mesh, and filtration paper sheets; details described above) and a vertical load was applied by placing a free gliding (stainless steel) plunger (40 gram on a surface area of cm^2 ; a stress equivalent of 2.6 kN/m^2) onto the set gel within the compression chamber.

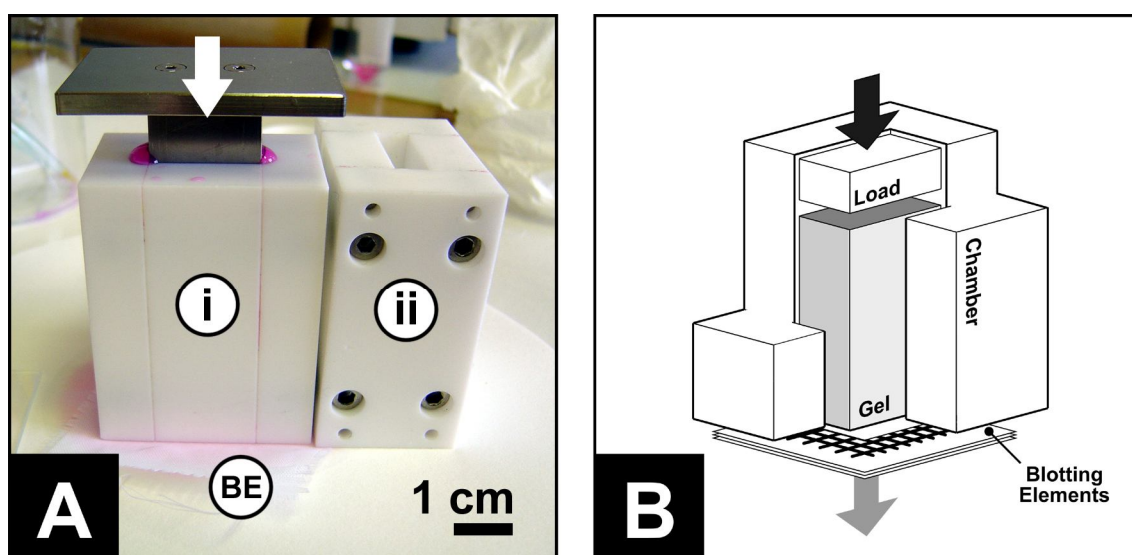


Figure 10 – (a) Photograph (scale bar shown at bottom right) and (b) cutaway illustration of the custom built compression chamber (i, front and, ii, side view) in which collagen hydrogels are compressed on the standard setup of blotting elements (BE) and through the application of a free gliding stainless steel plunger (white and black arrow).

Inference about the loss in fluid content over the compression process from these confined compressed collagen hydrogels was made by measuring the change in height of the plunger. The position of the plunger was recorded on video with a digital camera (12 megapixel, CANON IXUS 960 IS, Canon inc., Tokyo, Japan) and the change in height at each time point was measured in each video frame with the software program ImageJ (NIH, Bethesda, MD).

2.1.4 Compaction assay

To study the regional changes in collagen density over the compression of a collagen hydrogel, 10 mg of activated carbon (Aldrich, Cat. No. 16155-1) was mixed with a neutralised 5.7 ml/cm² collagen hydrogel to achieve an even distribution of carbon particles throughout the gel body. Immediately, the gel was cast in a transparent compression chamber and allowed to set for 30 minutes after which time the gel was placed on the standardised setup of blotting elements (described above) resulting in the (confined) compression of the gel driven by the gels own weight and the negative capillary pressure from the blotting elements. The compression was recorded on video by digital camera and inference of the change in collagen density was made from the change in the relative positions of the carbon particles within the gel body measured in each video frame.

2.1.5 Scanning Electron Microscopy

For high resolution images of the FLS the compressed collagen hydrogels were immediately immersed in liquid nitrogen for 1 minute, cut transversely, fixed overnight in 2.5% glutaraldehyde, freeze dehydrated overnight (Heto Drywinner, Birkerød, Denmark), sputter coated with gold palladium a Polaron E5 100 sputter coater (Quorum Technologies, East Sussex, UK) and viewed in a scanning electron microscope (SEM; JEOL JSM-5500LV, Japan) operated at 15 kV (Wollweber *et al.*, 1981).

2.1.6 Double fluid leaving surface compression

Based on the data obtained from the experiments described above, a regime for the compression of a 3.25 ml/cm² (5 ml) collagen hydrogel was decided on. This involved the compression of the gel on the basal FLS for 10 minutes and subsequently on the apical FLS for another 10 minutes (1.8 kN/m², standard setup of blotting elements).

2.1.6.1 Physical characterisation

The physical properties of the resulting thick compressed collagen constructs were compared to those of the previously described spiralled collagen gels (Brown *et al.*, 2005; Neel *et al.*, 2006). These constructs were prepared by the compression (1.8

kN/m²; 5 minutes on a standard setup of blotting elements) of a 0.7 ml/cm² (5 ml) collagen hydrogel and spiralling the resulting collagen sheets along their long axis (Figure 9b). Weight measurements were recorded using an analytical balance (BDH, UK) directly after fabrication of the constructs.

2.1.6.2 Dynamic mechanical analysis

Tensile mechanical analysis was used to compare the tensile mechanical properties of spiralled compressed collagen sheets with those of the thick compressed collagen construct. These were carried out using a Perkin-Elmer DMA-7e (Perkin Elmer Instruments, USA) at room temperature with constant sample hydration maintained by the application of PBS.

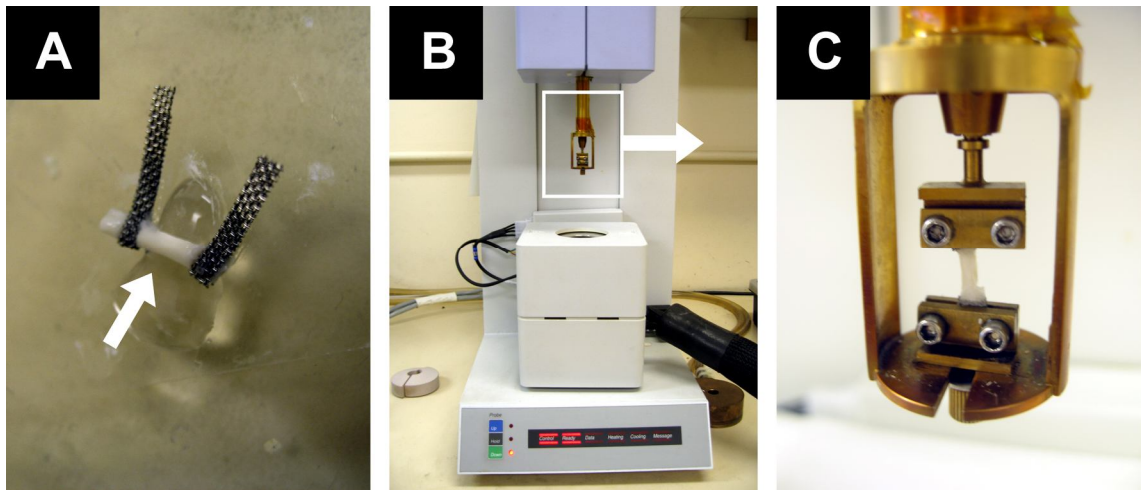


Figure 11 – (a) Photograph of spiralled, compressed collagen hydrogel clamped at either end with strips of metal mesh reinforced with super glue to facilitate gripping. (b) Specimen (insert, c) mounted in the tension clamps of a dynamic mechanical analyser.

Specimens were mounted in the tension clamps of the DMA system (Figure 11). The samples were clamped at each end using 2 mm strips of metal mesh reinforced by cyanoacrylate adhesive to facilitate gripping during testing. The dimensions of each specimen were measured with a travelling microscope. The initial applied load was 1 mN, and the specimen was tested in tension until failure at a loading rate of 200 mN/min. From the stress–strain curve (Figure 12), Young’s modulus, ultimate tensile

strength (UTS), and yield strain were calculated. Samples that did not break mid-substance were discarded from analysis.

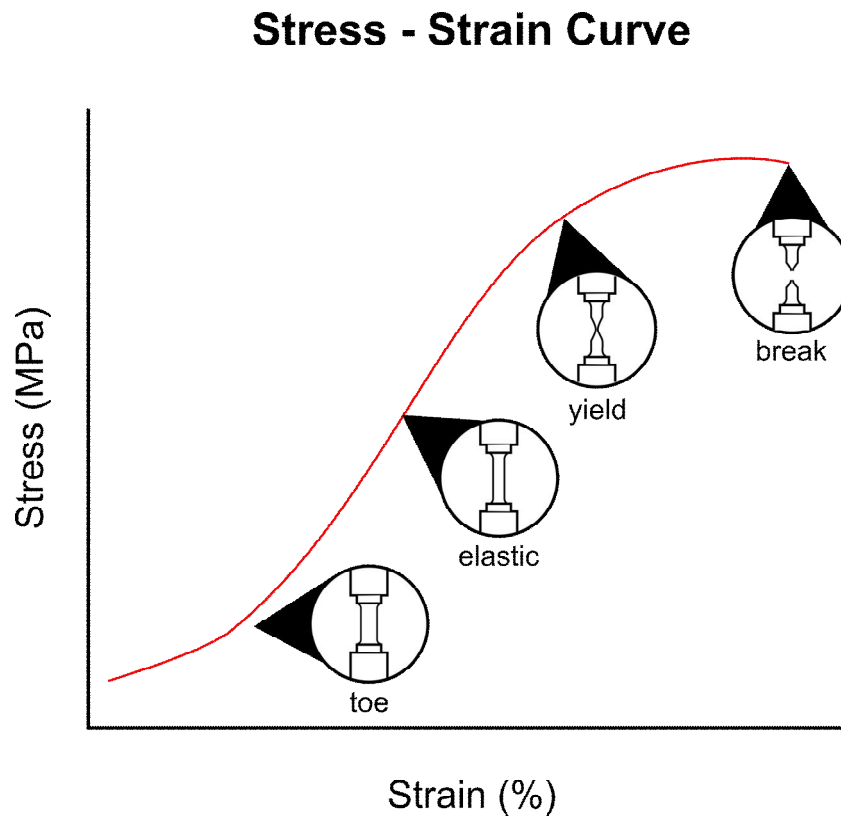


Figure 12 – Typical tensile test stress-strain curve showing the toe and elastic region, yield point and ultimate tensile (break) stress.

2.2 Hybrid constructs

A second strategy to improve mechanical properties was investigated by hybridising 1.4 ml/cm² (10 ml) collagen hydrogels with synthetic polymer meshes. Two different materials were tested: (1) a commercially available poly-[lactide-co-glycolide] (PLGA; Vicryl®, VM95, Ethicon) mesh and (2) a newly synthesised poly-[lactic acid-co-caprolactone] (PLACL) mesh.

2.2.1 PLACL mesh fabrication

Yarns were prepared from melt spun filaments (25 filaments each) (Figure 13a) with, a total finess of 165 dtex (decitex; grams per 10³ meter length), an individual filament

linear density of 6.6 dtex, an individual filament diameter of 28.4 μm , a tenacity (*i.e.* breaking load per unit linear density of the unstrained specimen) of $19.5 \pm 0.9 \text{ cN tex}^{-1}$ (centinewton per tex) and an elongation at break of $41.1 \pm 2.3\%$. The yarns were knitted into a mesh (Figure 13b) with a weft-pattern (Figure 13c). It should be noted that the PLACL co-polymer was synthesised in by Uppsala University (Uppsala, Sweden) and that the co-polymer was melt-spun and weft-knitted into a mesh by Aachen University (Aachen, Germany).

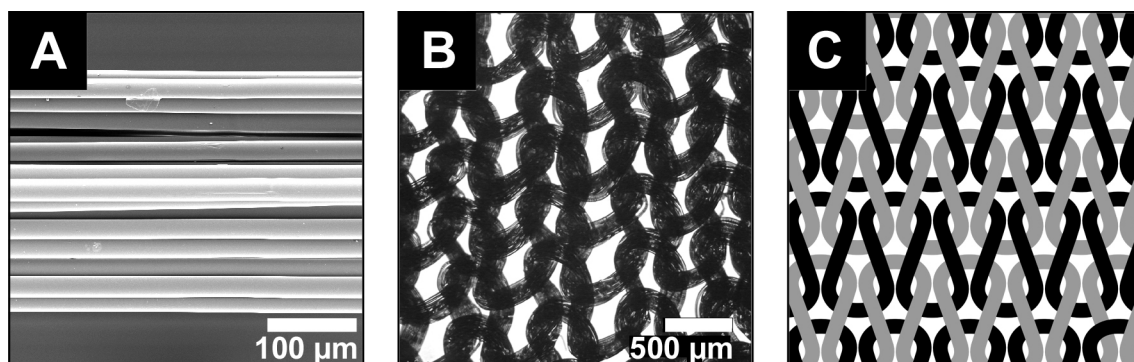


Figure 13 – (a) Scanning electron micrograph of the filament structure of the PLACL yarn (scale bar is shown at the bottom right corner). (b) Light micrograph of the PLACL mesh showing the weft-knit pattern (scale bar shown at bottom right). (c) Illustration of a weft knit pattern which consists of a single yarn looped horizontally to form a row with each row building on the previous one.

2.2.2 Hybridisation of collagen hydrogels

The PLACL-compressed collagen hydrogel hybrid (PLACL-CCHH) and PLGA-CCHH construct were prepared from two neutralised collagen solutions and either the PLACL or PLGA mesh. For acellular constructs, a 5 ml collagen solution was neutralised (as described above) and cast into a stainless steel mould ($33 \times 22 \times 20 \text{ mm}^3$) (Figure 14), the PLACL or PLGA mesh ($30 \times 20 \text{ mm}^2$) added on top, and a second (5 ml) neutralised collagen volume poured. After the 30 minute setting period, the resulting hybrid construct was compressed in the unconfined configuration as previously described (Ananta *et al.*, 2009) (Figure 14b).

2.2.3 Physical characterisation of compression

To evaluate their influence on the final collagen density of the collagen component of the PLGACL-CCHH construct the compression time and load were varied and weight measurements were recorded using an analytical balance directly after the compression to infer and compare the collagen density between compression regimes. The following conditions were tested on the standard set of blotting elements: compression times of 5 minutes and 10 minutes, with loads of 1.8 and 3.6 kN/m².

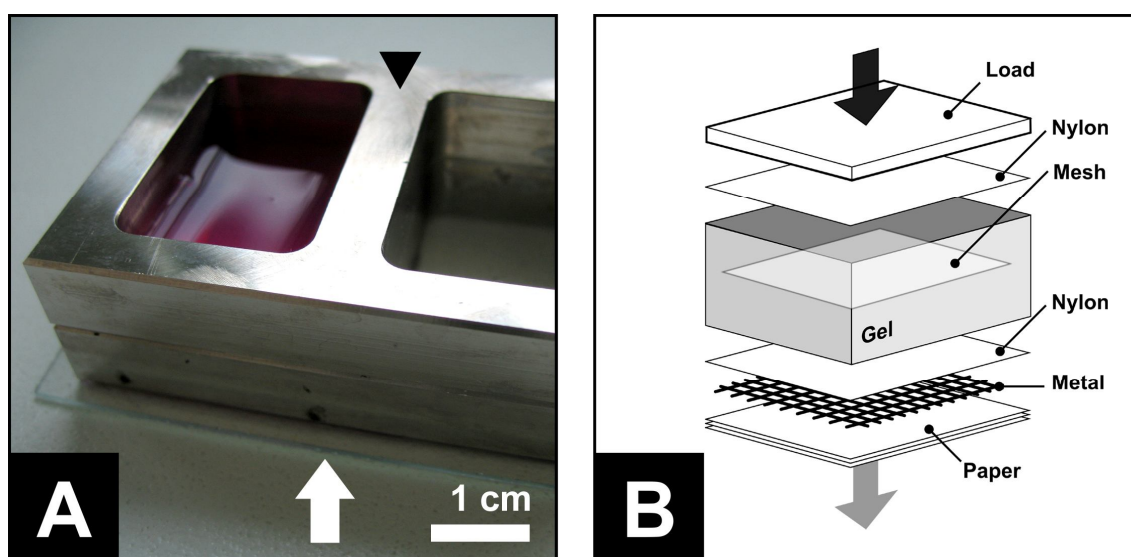


Figure 14 – (a) Photograph showing seated on a glass slide (white arrow) the stainless steel mould (arrow head) of increased height in which the two volumes (10 ml) of collagen are set around a synthetic degradable mesh. Scale bar shown at bottom right corner. (b) Illustration of the unconfined compression setup of the set collagen hydrogel with encapsulated synthetic degradable mesh.

2.2.4 Cell culture

2.2.4.1 Fibroblast maintenance

Human neonatal foreskin fibroblasts (hNNF) and rabbit dermal ear fibroblasts (rDEF) were maintained in a humidified atmosphere, in 5% CO₂ and at 37°C. The growth medium was prepared from Dulbecco's Modified Eagle Medium (DMEM; catalogue number D6429, SIGMA, Irvine, UK) supplemented with 10% (v/v) fetal calf serum (FCS; First Link, West Midlands, UK), 100 U/ml penicillin and 100 µg/ml streptomycin

(P/S; 500 µg mL⁻¹ and 500 units mL⁻¹ respectively; catalogue number 5140-122 Invitrogen/Gibco, UK). Cells were maintained in 35 ml of growth medium (changed twice a week) within T-225 (225 cm²) cell culture flasks (catalogue number 431082, Corning-Costar Corp., Corning, New York, USA) featuring gas-permeable caps.

2.2.4.2 Passaging of fibroblasts

The growth medium was removed from the culture flasks and the monolayer of cells was washed twice with 10 ml of PBS. The cells were then covered with 6 ml of a 0.05% (1x) trypsin solution and incubated at 37°C. The trypsinisation progress was monitored under an inverted microscope until approximately 90% of the cells were rounded up, generally occurring after 4 to 6 minutes. The cells were then released from the culture surface by hitting the side of the flask against the palm of the hand the cells were detached. If only a few cells would detach the flasks were left for an additional 60 seconds before further attempts were made. After the cells were released the trypsin was neutralised with 12 ml of DMEM/10%FCS solution. The cell suspension was then collected in a 10 ml universal tube and centrifuged at 2000 RPM for 5 minutes to pellet the cells. The supernatant was then decanted from the tube without disturbing the cell pellet and the cells were resuspended in DMEM.

Cells were then counted with the haemocytometer trypan blue dye exclusion method (Mishell *et al.*, 1980) as follows (Figure 15). A 10 µl aliquot of the single-cell suspension was diluted with a trypan blue solution in a 1:2 dilution ratio. A cover slip was placed over the counting surface of the haemocytometer (Figure 14) after which 10 µl of the cell suspension was introduced into both loading wells with a pasteur pipette. The stained (dead) and non-stained (viable) cells were counted in each of the four counting areas (1 mm²; volume 10⁻⁴ ml) of both chambers (side A and B) under a phase-contrast microscope (Leica) at 100x (10x objective) magnification. The cell number in the original suspension could be calculated with the following formula:

$$\text{Number of cells in suspension} = \frac{\text{total number of counted cells}}{8 (\text{counting areas})} \times \text{dilution} \times 10^4$$

Both hNNFs and rDEFs were plated at a density of 3 to 10 x10⁴ viable cells/25 cm² in a T-225 flask.

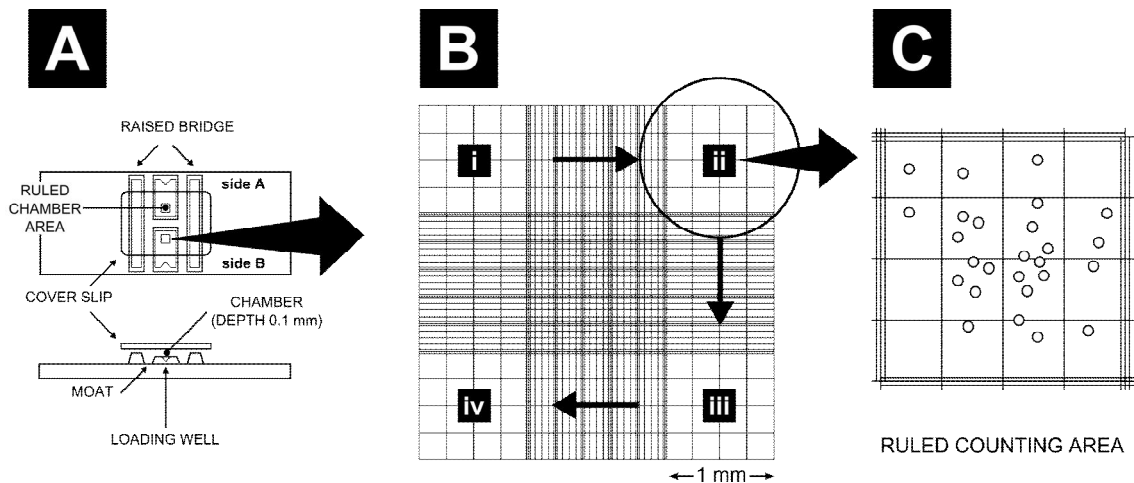


Figure 15 – (a) Illustration of a haemocytometer used to count cells suspended in a known volume trapped in two counting chambers (with a depth of 0.1 mm) underneath a cover slip and over ruled counting areas (b) Cells in either chamber were counted in four (i, - iv) ruled (1 mm²) counting areas (insert, c).

2.2.5 Fabrication of living dermal equivalents

For comparative purposes the previously established compression regime (unconfined, 1.8 kN/m² for 5 minutes on the standard setup of blotting elements) was used in the following experiments. For the creation of living dermal tissue equivalents the collagen component of the hybrid construct was cell seeded as follows. Eight volumes (4 ml) of collagen solution were mixed with one volume of MEM, neutralised (as described above), and mixed with one volume growth medium (see below for details) in which 2×10^5 cells were suspended. The cytocompatibility of the technique was tested with hNNFs (passage 4-6) and rDEFs (passage 2-5). hNNFs were kindly donated by the Institute of Orthopaedics and rDEFs were explanted from tissue biopsies obtained from rabbit ears (method described below under 'Fibroblast explant culture').

2.2.6 Morphometric measurements

The physical dimensions of the hybrid constructs were measured with a travelling microscope. Pore size and porosity were determined with ImageJ from digital photographs taken with a digital camera (Olympus, Camedia, C-2020 Zoom, Tokyo, Japan) attached to a light microscope (Olympus BH-2, Tokyo, Japan). For high

resolution images the constructs were viewed with SEM using the methods described above.

2.2.7 Alamar Blue reduction assay

The Alamar Blue (AB) reduction assay as an indirect measure for the number of viable cells (Nakayama *et al.*, 1997). The AB dye, the non-fluorescent resazurin, is reduced by metabolically active (viable) cells to the highly fluorescent and quantifiable dye resorufin (O'Brien *et al.*, 2000). To test cell survival after the compression of the PLACL- and PLGA-CCHH material the constructs were incubated, directly after fabrication, in a 10% AB dye solution in phenol red-free DMEM (Gibco, Paisley, UK) for four hours at 37°C and 5% CO₂ after which time the amount of fluorescence was measured (Fluoroskan Ascent Labsystems International, Helsinki, Finland; 510 nm excitation, 590 nm emission). hNMFs were tested with the PLACL-CCHH and rDEFs were tested with the PLGA-CCHH.

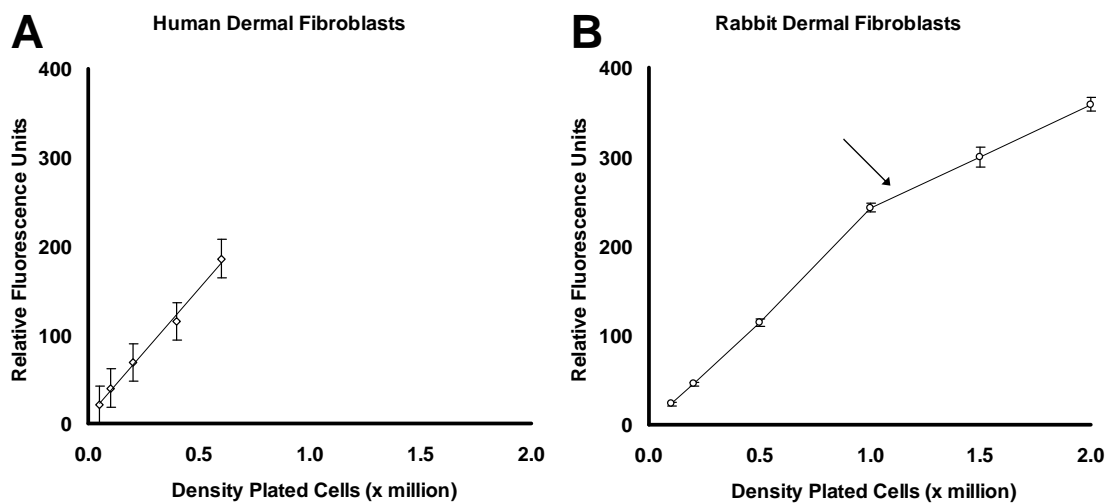


Figure 16 – AB reduction (expressed as relative fluorescent units, RFU) as a function of cell number. (a) Human fibroblasts and (b) rabbit fibroblasts were incubated on tissue culture plastic with AB as previously described. For both panels, values were deducted from the autofluorescence of AB without cells. For rabbit fibroblasts it was found that over 1 million cells the linear relationship between the RFU and cell number changed (arrow).

The fluorescence intensity was expressed as relative fluorescence units (RFU) and for each sample the obtained value was subtracted by the value representing the autofluorescence of the (non reduced, non-fluorescent) 10% AB solution. The AB reduction by collagen compressed cells was compared to that of (non-compressed) cells plated onto tissue culture plastic. The assay was repeated after 7 days in static *in vitro* culture after compression to evaluate cell proliferation. In this 7 day period constructs were maintained in growth medium (DMEM, 10% FCS, 1% P/S) under 5% CO₂ at 37°C, for 1 week, the culture medium was replaced every two days. To determine the relation between the number of cells and the intensity of fluorescence, standard curves were obtained for hNNFs and rDEFs (Figure 16) by quantifying the AB reduction over the four hour period by various cell densities plated onto tissue culture plastic (in 10% AB solution at 37°C and 5% CO₂).

2.2.8 Confocal microscopy

To test the short term biocompatibility of the PLACL mesh the distribution of live and dead cells was visualised after a 7 day culture period by confocal microscopy. Cell seeded (within the bottom collagen compartment), PLACL-CCHH constructs were cultured for 7 days (static culture conditions) and on the last day incubated for 45 minutes in 20 µM 5-chloromethylfluorescein diacetate (CMFDA, CellTracker Green, catalogue number C2925, Invitrogen, Paisley, UK) to stain for live cells, washed in PBS and incubated for 45 minutes in 2 mM ethidium homodimer-1 (EH-1, catalogue number E1169, Invitrogen, Paisley, UK) to stain for dead cells. On the same day serial images were taken throughout the entire thickness of the bottom collagen component at 15 µm intervals with a confocal microscope (40x objective). To evaluate the cell distribution the cell number in a 45 µm thick region most distal and most proximal to the PLACL mesh was manually counted from the obtained digital images. The number of cells (both viable and dead) in each region was expressed as a percentage of the total number of (viable and dead) cells counted in both regions. Cell viability in these two regions was determined by dividing the counted number of viable cells by the total number of dead and viable cells.

2.3 Skin equivalents

The following *in vitro* and *in vivo* experiments were carried out with the PLGA-CCHH constructs. To test the utility of a rapidly engineered stable dermal equivalent for the *in vitro* reconstruction of an epidermis, rabbit ear keratinocytes were seeded on the apical surface of an rDEF seeded PLGA-CCHH.

2.3.1 Cell culture

2.3.1.1 Keratinocyte isolation

RDKs were isolated (within 24 hours post-mortem) from tissue taken from the ventral side of adult male rabbit ear lobes (Figure 17). The top part of the ear lobe was harvested, closely shaven with electric animal clippers (Oster Corporation, model number A5-00, Milwaukee, Wisconsin, USA), washed in 70% Industrial Methylated Spirits (IMS; Genta Medical, York, UK) for 2 minutes and subsequently twice in sterile PBS containing 2% P/S for 5 minutes.

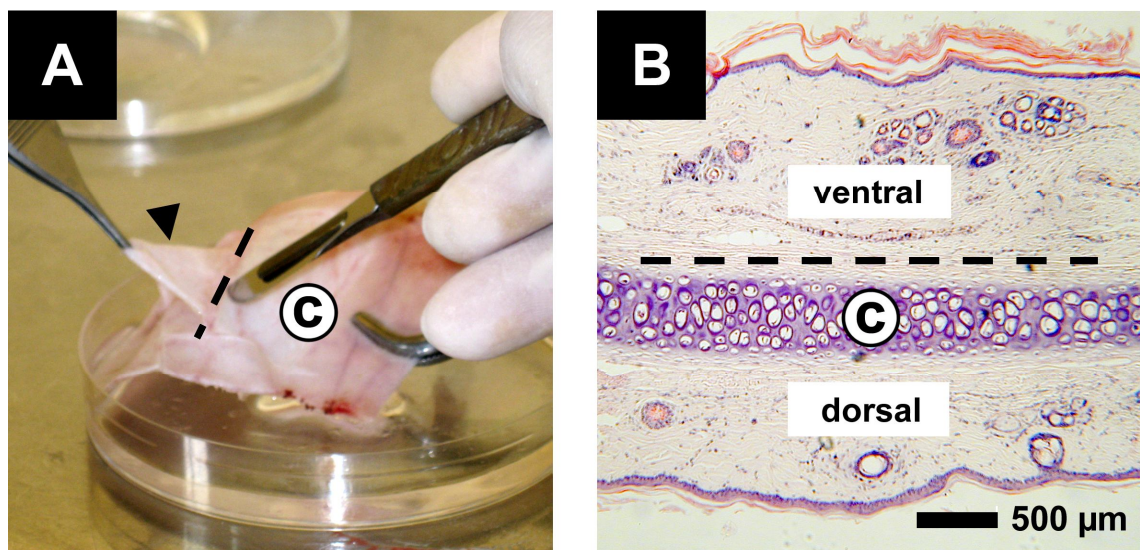


Figure 17 – (a) Photograph showing the harvest of skin (arrow head) from rabbit ear lobes ventral to the cartilage (C). (b) Histological section showing the difference in number of hair follicles between skin ventral and dorsal to the cartilage (dashed line shows the plane of dissection).

A skin graft ventral to the ear cartilage of approximately 10 to 15 cm² was taken. The graft was divided into smaller pieces of approximately 5x5 mm² which were then incubated in 0.25% (5x) trypsin-EDTA (catalogue number 15400-054, Invitrogen/Gibco) with 2% P/S for 90 minutes at 37° C. It should be mentioned that trypsin causes a separation of the epidermis above the basal lamina (Nielsen and Don, 1984) often leaving basal keratinocytes still attached to the dermal component.

After incubation, the epidermis and the dermis were separated with forceps in a sterile tissue culture dish with PBS+2% P/S solution to prevent dehydration. The epidermal surface of the dermal pieces was scraped with a scalpel blade to release any still adherent basal keratinocytes. The dermal fragments were kept in PBS+2% P/S solution at 4° C until further use and the scraped cell suspension was transferred from the dish to a 50 ml Falcon tube. DMEM containing 10% FCS was added to inactivate the trypsin. The solution was then filtered through a 70 µm cell strainer (BD Falcon, cat. no. 352350), centrifuged at 2000 revolutions per minute (RPM) for 5 minutes and resuspended in keratinocyte growth medium (KGM; CnT-07, CellNTec, Switzerland). The cell suspension was then stored at 4° C.

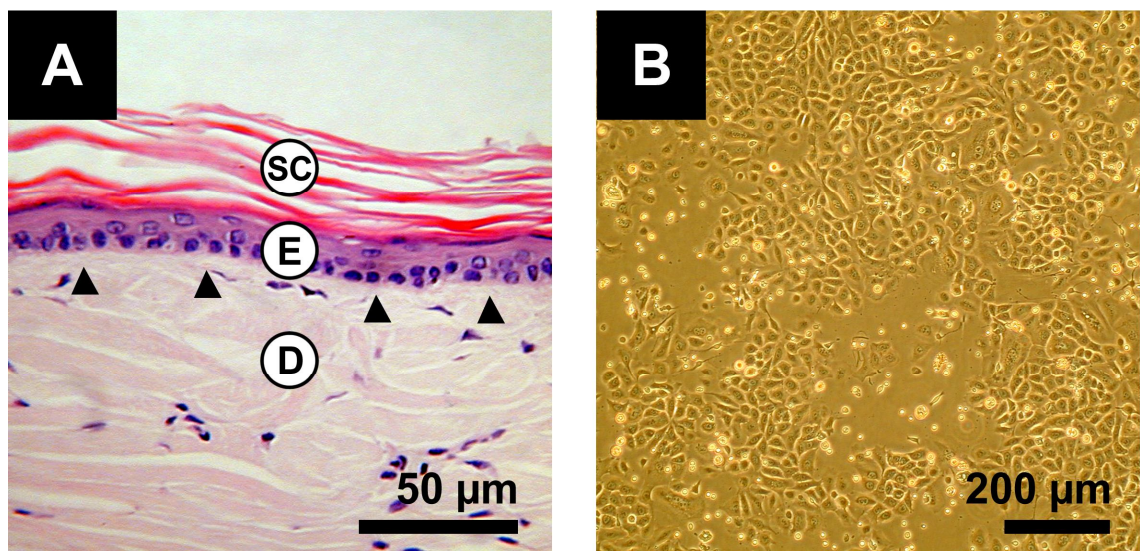


Figure 18 – (a) Histological section showing the basal keratinocytes (black arrow heads) in the epidermis (E) that were separated enzymatically from the dermis (D) and mechanically from the stratum corneum (SC). (b) Phase contrast micrograph showing the typical cobble stone morphology of basal keratinocytes. Scale bars are shown at the bottom right corner.

The epidermal fragments were transferred to a beaker with 0.25% trypsin + 2% P/S to which a magnetic stirring bar was added and the epidermal fragments were stirred at 100 RPM on a magnetic stirrer (Stuart, Bibby Sterilin Ltd., Stone, Staffordshire, UK) for 30 minutes at room temperature. DMEM/10%FCS was added to inactivate the trypsin. The epidermal pieces were rubbed against the wall of the beaker with the tip of a 25 ml serological pipette (catalogue number 4251, Corning-Costar Corp., Corning, New York, USA) to release any still adherent keratinocytes from the stratum corneum (Figure 18a).

The suspension was then filtered through a 70 µm cell strainer to remove the stratum corneum and then centrifuged at 2000 RPM for 5 minutes. The cells were resuspended in KGM. The cell fractions from the dermal and epidermal fragments were pooled to obtain a single keratinocyte suspension and counted with the haemocytometer and trypan blue dye exclusion assay and were then seeded in T-225 flasks at 0.5 to 1.0x10⁶ cells/25 cm². The medium was changed after the first two days to remove the debris and dead cells and three times weekly after that. The keratinocytes were passaged for expansion only once when the culture became 80% confluent and then used for seeding of the constructs when again 80% confluent (Figure 18b).

2.3.1.2 Keratinocyte passage

The growth medium was removed from the culture flasks and the monolayer of cells was washed twice with 10 ml of PBS. The cells were then covered with 10 ml of a 0.25% trypsin + 2% P/S solution. The trypsinisation progress was monitored under an inverted microscope until approximately 90% of the cells were rounded up, generally occurred after 4 to 6 minutes. The cells were then released from the culture surface by hitting the side of the flask against the palm of the hand until most of the cells were detached. If only a few cells would detach the flasks were left for an additional 30 seconds before further attempts were made. After the cells were released the trypsin was neutralised with 20 ml of DMEM/10%FCS solution. The cell suspension was then transferred to a 50 ml Falcon tube. The flasks were rinsed with 10 ml PBS to remove any remaining keratinocytes from the flask and this suspension was then transferred to the Falcon tube. The tube was then centrifuged at 2000 RPM for 5 minutes to pellet the cells. The supernatant was decanted from the tube without disturbing the cell pellet. The

cells were resuspended in KGM and counted with the haemocytometer and trypan blue dye exclusion assay.

2.3.1.3 Fibroblast explant culture

The dermal fragments, obtained after separating the epidermis from the dermis (see above), were cut into smaller (2x2 mm²) squares and transferred to 6-well plates. Ten to fifteen dermal pieces were placed in the centre of each 6-well plate and a glass cover slip (glass cover, 22x26 mm², catalogue number 631-0131, VWR Scientific, Media, Philadelphia, USA) was placed on top of them and weighed down with a 10 gram stainless steel weight to keep the samples physically attached to the well plate (Figure 19). Then 5 ml DMEM/10%FCS was added to each well and the plate was placed in a humidified 37° C, 5% CO₂ incubator. The growth medium was changed twice weekly. Upon confluence the cells were passaged at a density of 3 to 10 x10⁴ cells/25 cm² for expansion.

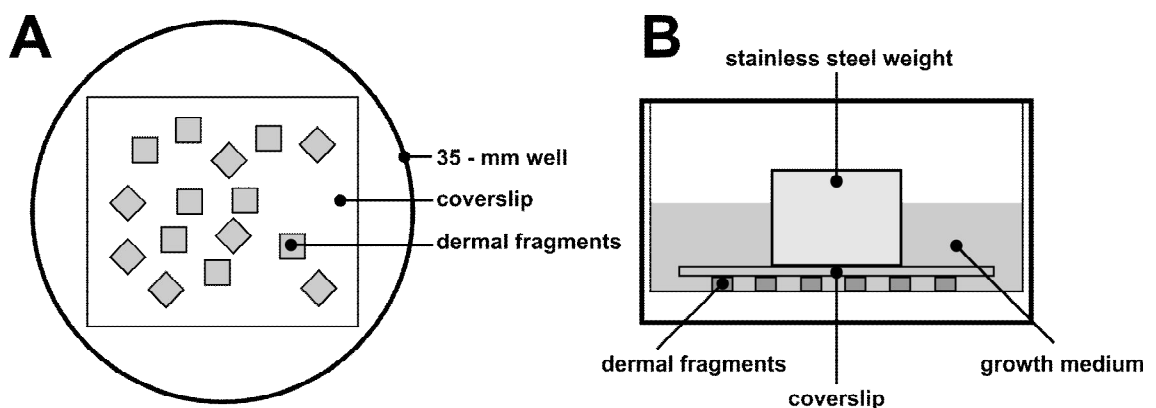


Figure 19 – (a) Illustration of the top view of a skin explant culture showing a glass cover slip placed over dermal fragments in a 6-well plate. (b) Side view of skin explant culture showing a stainless steel weight on top of the cover slip to physically attach the dermal fragments to the plate to allow for the outgrowth of fibroblasts.

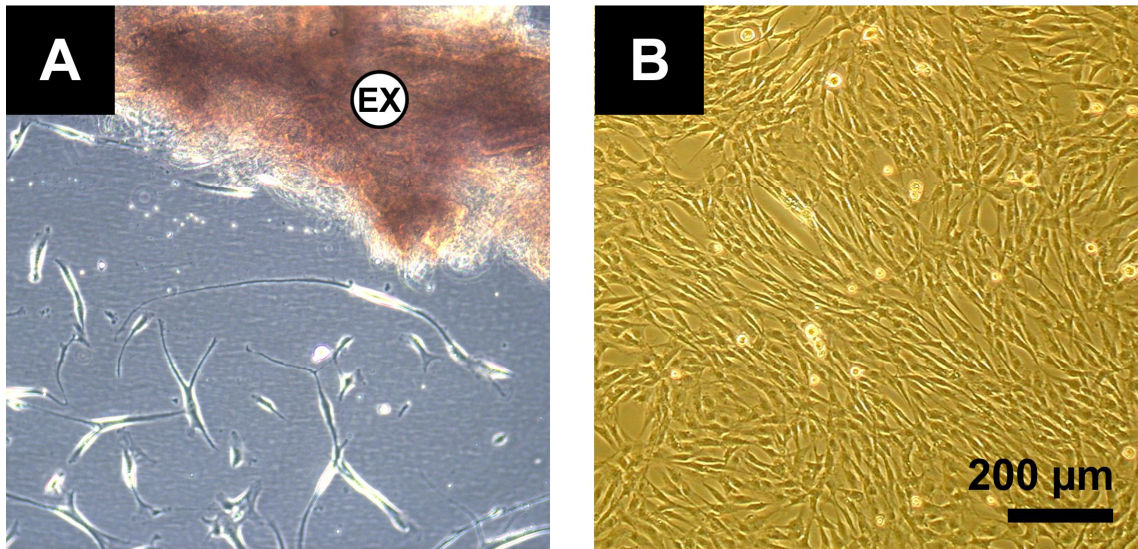


Figure 20 – (a) Micrograph showing a fibroblast explant culture, day 5, established from a dermal fragment (EX) using the skin explant culture system described in Figure 19. (b) Fibroblast explant culture, at day 14. Scale bar shown at bottom right corner.

2.3.2 Fabrication of living skin equivalents

Fibroblast seeded PLACL-CCHH constructs (dermal equivalents) were fabricated (as described above), placed onto metal grids in a well of a 6-well plate and submerged in KGM (CnT-07; ~7 ml). 2.3 to 2.6 x10⁶ cells were brought into a 500 μl of KGM and this suspension (inoculum) was added to the apical surface of the dermal equivalents (Figure 21a) to form a subconfluent monolayer epithelium (Figure 21c). The keratinocytes were allowed to attach for 4 hours after which the KGM was topped up to 8 ml.

The cell seeding efficiency was determined by counting the number of cells that had not attached to the dermal equivalents. The KGM with dead, non-adherent keratinocytes) was aspirated, the wells (collecting attached, viable keratinocytes) were trypsinised, and both cell fractions were pooled in a single cell suspension. Cells from this suspension were counted with the haemocytometer and trypan blue dye exclusion assay (Figure 15). The seeding efficiency was calculated by dividing the number of cells that had adhered to the hybrid construct (the number of cells in the inoculum minus the number of cells found in the well) by the number of cells in the inoculum.

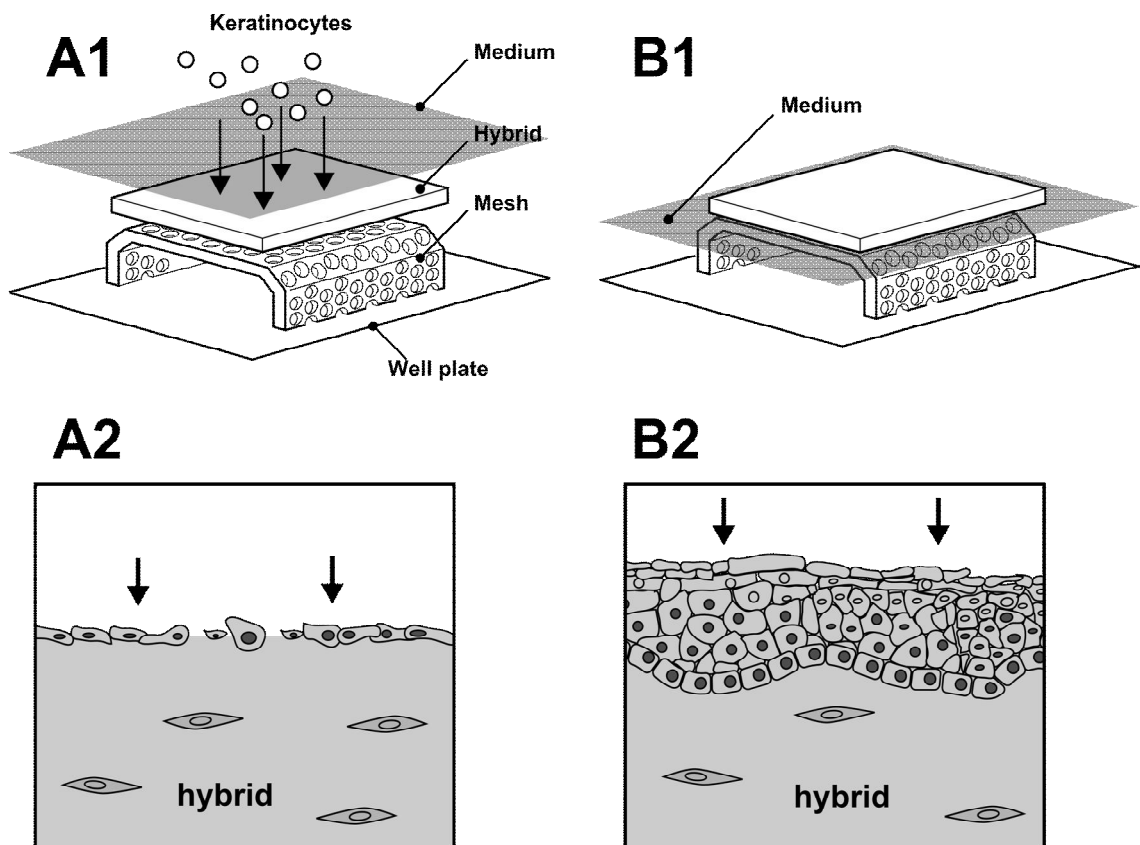


Figure 21 – Illustration of the keratinocyte / fibroblast co-culture setup. (a) Keratinocytes were statically seeded on the apical surface of living dermal equivalents (*i.e.* fibroblast seeded PLGA-compressed collagen hybrid constructs) (a1) placed on stainless steel meshes in 6-well plates. (a2) The subconfluent epidermis was cultured to confluence submerged in growth medium. (b1) At confluence the skin equivalents were raised to the air-liquid interface by lowering the volume of growth medium to allow for the formation of a (b2) stratified epidermis.

The co-culture constructs were kept submerged in KGM for 3 to 5 days to allow the keratinocytes to achieve a confluent monolayer. The medium was then diminished so that the constructs on the metal grids were located at the air-liquid interface (Figure 21b). The constructs were cultured for an additional day on KGM and subsequently for twelve days on keratinocyte differentiation medium (CnT-02-3D, CellnTec, Switzerland) to form a differentiated and stratified epidermis (Figure 21d).

2.4 Implantation study

2.4.1 Study design

All experiments were approved by a local ethical review committee and carried out under Home Office Project Licence PPL 80/2200 according to the Animals Scientific Procedures Act (1986). Fifteen female New Zealand rabbits (kg) with an initial weight of 2.9 - 3.5 kg were purchased from B&K Universal (Grimston, Aldbrough, Hull, East Yorkshire, UK) and housed in an approved animal facility. On arrival, rabbits were placed into individual cages and allowed to acclimatise to their new surroundings for 7 days before initiation of experiments. Rabbit chow and water were available *ad libitum*.

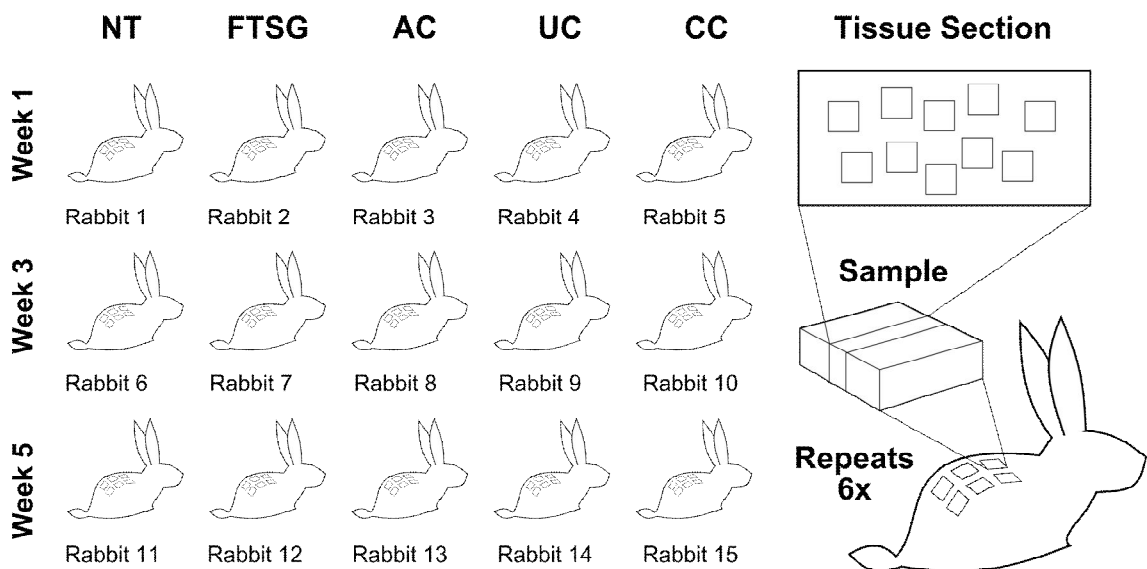


Figure 22 – Schematic diagram of the experimental design. Six full thickness skin defects were created on the dorsum of rabbits which were either left untreated (NT) or treated with full thickness skin grafts (FTSG), acellular constructs (AC), uncultured (UC) and cultured (CC) cell seeded constructs. Wound healing was evaluated in histological sections 1, 3 and 5 weeks after injury.

PLGA-CCHH constructs were tested in standardised full thickness skin defects on the dorsum of female adult New Zealand rabbits (see Figure 22 for an overview of the experimental design). Healing of wounds treated with two of the following constructs was compared. The first group of (male derived, allogeneic) keratinocyte and fibroblast

seeded hybrid constructs were fabricated and directly implanted without an *in vitro* culture period (uncultured constructs; UCs).

The second group of constructs were fabricated and cultured *in vitro* (for 2-3 week) to allow the keratinocytes to differentiate into a stratified epithelium (cultured constructs; CCs). The controls were wounds treated with acellular constructs (AC), wounds treated with the rabbits own skin or autologous full thickness skin grafts (FTSG) and wounds that were left open (no treatment, NT). Wounds were analysed after 1, 3 and 5 weeks after implantation. In each rabbit, six wounds were created and all six wounds were given one of the five treatments so that each of the 15 rabbits represented one out of five treatments and one of three time points.

2.4.2 Preparation

On the day of surgery, the rabbits were weighed and pre-medicated by intramuscular injection of Hypnorm 0.3 ml/kg (0.095 mg/kg fentanyl citrate and 3 mg/kg fluanisone) into the caudal thigh muscle. A period of 5-10 minutes was allowed for the animal to become sedated after which the animal was immobilised for intravenous cannulation by wrapping the body in a blanket sparing the head. The area over a marginal ear vein was depilated and wiped with 70% ethanol after which the vein was cannulated with a 23-Gauge butterfly cannula which was fixed with tape to the ear and flushed with 0.9% normal saline.

The rabbits were anaesthetised with Diazepam (5 mg/ml, 0.1 ml/kg, i.v.) after which the fur on the dorsal area between the scapulae and the iliac crests was shaved with small animal clippers (Oster, Model A5, Milwaukee, USA) (Figure 23a).

To be able to identify individual rabbits a three character code was tattooed inside the ear (Figure 23b). An outline of the areas to be excised was measured out with a ruler, drawn with a skin-marking pen and subsequently tattooed (Figure 23a). The rabbit was then transferred in the supine position onto a synthetic sheepskin rug to prevent excessive heat loss and given oxygen at a gas flow rate of 1 L/min through a face mask with a rebreathing bag (Figure 23c,d). Supplemental doses of Hypnorm 0.05-0.1 ml/kg were given every 20-30 minutes to maintain anaesthesia (Figure 23d). Intra-operative fluid loss was compensated with a continuous infusion of 0.9% saline at 10ml/kg of

body weight per hour. Heart rate and peripheral oxygen saturation were monitored continuously with a pulse oximeter. The rate of respiration was monitored by observing the movement of the chest. The surgical anaesthesia was continuously monitored for adequate depth and considered sufficient in the absence of an ear pinch reflex and pedal withdrawal reflex (pinch on the rear fifth ray distal phalanx). The skin was then disinfected with a 70% alcohol solution containing 0.6% chlorhexidine and the surrounding areas were covered with sterile surgical drapes.

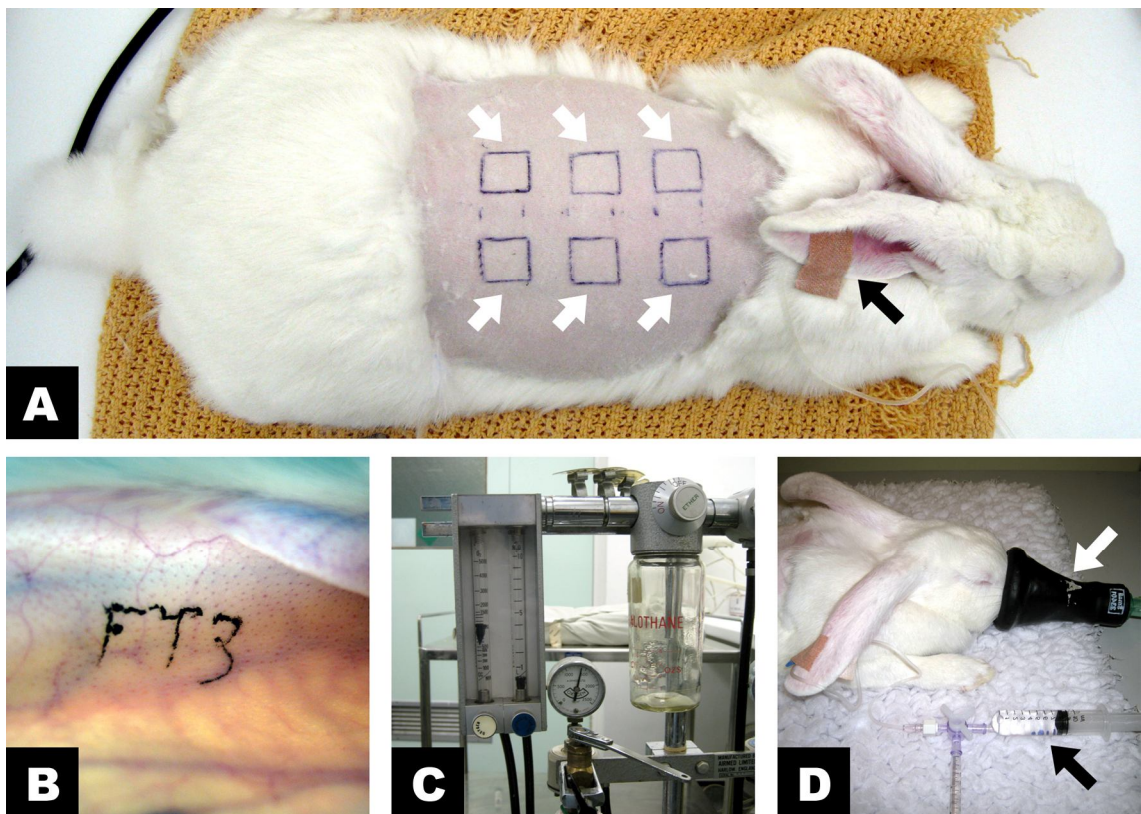


Figure 23 – (a) Pre-operative preparation of a rabbit subject. Anaesthetics and fluids were administered peri-operatively through a cannula inserted in a marginal ear vein (black arrow). The dorsum between the scapulae and the iliac crests was depilated and squares of 2x2 cm² (white arrows) were marked out with indelible ink and tattooed. (b) A three character code was tattooed inside the ear to identify the individual animals. (c) Oxygen was supplied during surgery at a flow rate of 1 L/min through a face mask (white arrow, d) and supplemental doses of anaesthetic (black arrow) were administered throughout the operation.

2.4.3 Surgical procedure

Three 2x2 cm² (Figure 24a) standardised full thickness skin defects (down to, but not including the panniculus carnosus; Figure 24b,c,d) spaced 2 cm's apart were created on both sides of the spine (Figure 23).

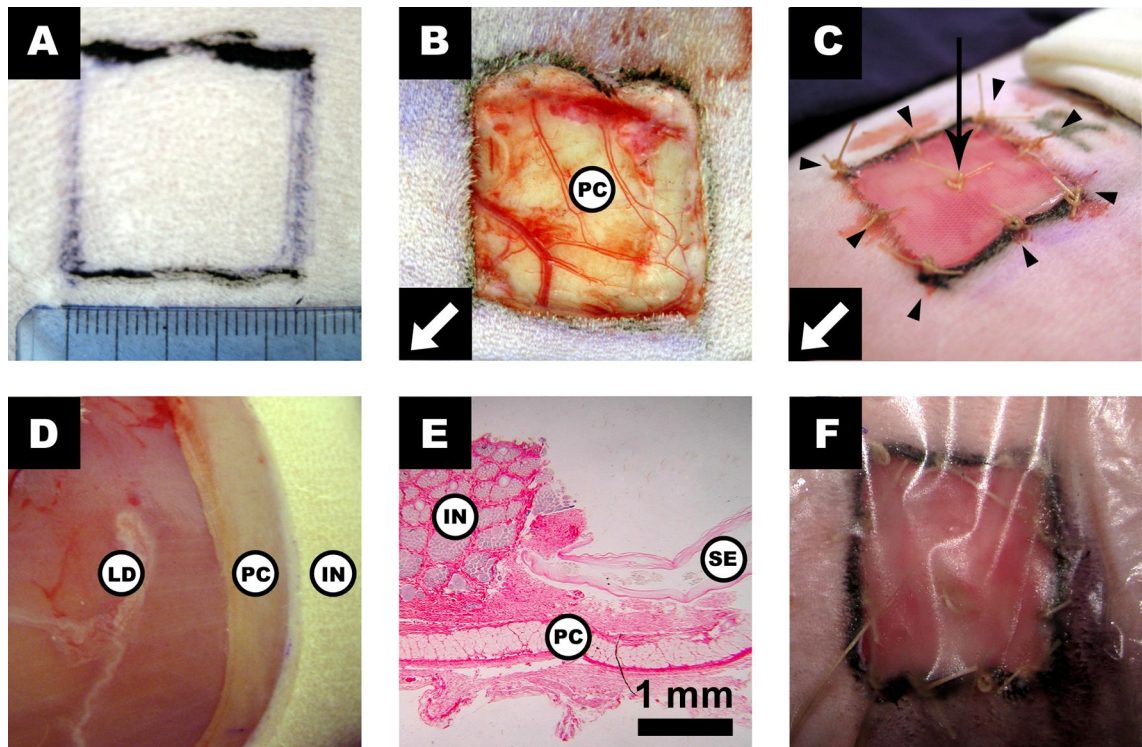


Figure 24 – Detailed photograph of the surgical procedure. (a) A 2x2 cm² square was tattooed and (b) a full thickness defect was created along the inner margins of the outline. (c) Constructs were implanted into the defect by the placement of corner and midway sutures (arrow heads) and a single central quilting suture (arrow). (d) Photograph showing the anatomy of the relevant tissue layers: integument (IN), panniculus carnosus (PC) and latissimus dorsi muscle (LD). (e) Histological transverse cross-section showing the intact integument (IN) and the skin equivalent (SE) implanted in the defect over the panniculus carnosus (PC). (f) After implantation the wounds were covered with an adhesive occlusive dressing.

Haemostasis of the exposed wound bed was obtained with a disposable cautery pen to avoid bleeding under the hybrid construct. Constructs were washed in 0.9% saline to remove cell culture media components that might cause an adverse antigenic response. The hybrid construct was placed on the wound bed and air pockets were expelled before it was fixed into place with eight interrupted sutures (3-0 Vicryl, W9507T, Ethicon)

along the edges (four in the corners and four midway along the sides) and one central quilting suture (through the panniculus carnosus) (Figure 24c). The hybrid constructs were kept humid using 0.9% normal saline throughout the surgery.

The operating time did not exceed 3 hours. Postoperative analgesia was provided by two subcutaneous injections of 2.2mg/kg Rimadyl (carprofen, Pfiser Ltd., Sandwich, UK) once every 12 hours in the scruff of the neck. The wounds were covered with semipermeable adhesive film (Op-Site, Smith and Nephew, Largo; Figure 24f) which was secured around the four edges with surgical tape. Rabbits were individually caged (Figure 25a) and plastic cone collars were required for the entire length of the study for all rabbits to prevent the wounds from being disturbed during grooming (Figure 25b). Animals and wounds were inspected daily to ensure that the dressings were intact. Dressings were only left on for two days after which they were removed because of the collection of moisture to prevent maceration.

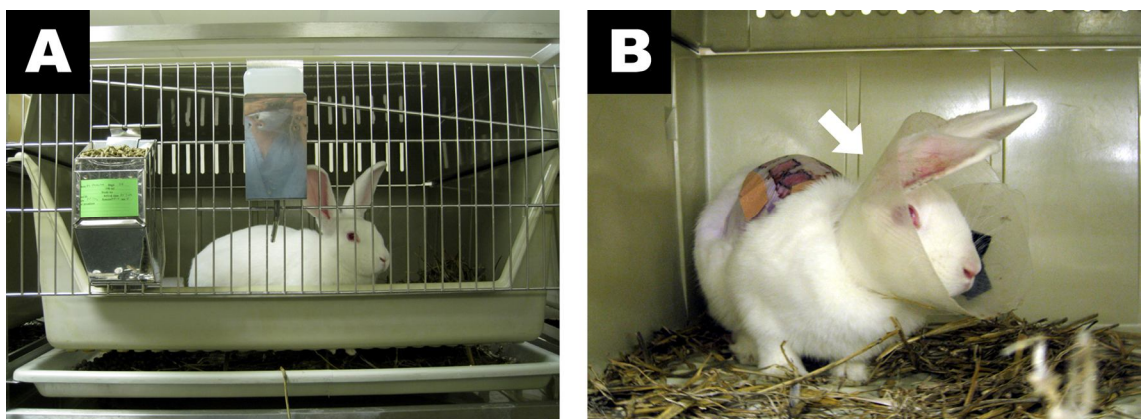


Figure 25 – (a) Rabbits were individually caged and had free access to water and food. (b) Post-surgery rabbits were fitted with a plastic cone collar (arrow) for the further duration of the study to prevent interference of the wounds by grooming.

2.4.4 Tissue harvest and handling

At the end of the study period, the animals were sedated, immobilised, and euthanised with an overdose of sodium pentobarbitone (Lethabarb, 2.5 ml, 324 mg/ml, Arnolds, Reading, UK) administered intravenously through a marginal ear vein. The wounds were excised with a margin of normal skin and the samples were immediately fixed in 10% (v/v) neutral-buffered formol saline (Genta Medical, York, UK) for 12-24 hours.

The fixed tissue was bisected, one half kept for storage for future analysis, and the other half again cut in two. The two resulting samples were placed into cassettes processed overnight by a routine automated procedure and embedded in paraffin wax.

2.4.5 Histology

2.4.5.1 Hematoxylin & eosin

Five-micrometer tissue sections were cut and mounted on SuperFrost/Plus slides, air dried for 10 minutes and heated in an oven at 60 °C for 30 to 60 minutes. The sections were deparaffinised in through three changes of Xylene (for 3 minutes each) and rehydrated with 3 minute incubations in a series of decreasing concentrations of IMS solutions (100%, 100%, and 70%) and finally tap water. The sections were stained for 6-8 minutes in Harris' haematoxylin (nuclear stain), washed in running tap water for 5 minutes, decolourised/differentiated for 3 seconds in 1% acid IMS, washed in running tap water (5 minutes), stained in eosin (ECM stain) for 2-5 minutes, washed in running tap water (5 minutes). Sections were then dehydrated through increasing concentrations of IMS solutions (70%, 100%, and 100%) and cleared through three changes of Xylene, each change for 10 seconds. Cover slips were mounted onto the slides over the tissue sections with Depex mounting media.

2.4.5.1.1 Epidermal regeneration

The epidermis has an important function in preventing infection and dehydration, so the effect of the various treatment methods on epidermal regeneration was tested. The percentage wound coverage by newly formed epithelium was determined by the extent of the new epithelial layer divided by the length of the wound, as measured from the H&E stained tissue sections. Because of the depth of the wound, no hair growth occurred in the newly laid down tissue and thus the wound length was measured as the distance between hair follicles (Figure 26).

2.4.5.1.2 Wound contraction

To study the influence of the hybrid material on wound contraction the distance between the hair follicles in the healed tissue was measured and divided by the original wound length (Figure 26).

2.4.5.1.3 Wound composition

The changes in cross sectional area and thickness of newly deposited connective tissue, the original wound bed and panniculus carnosus were determined from H&E stained sections (Figure 26).

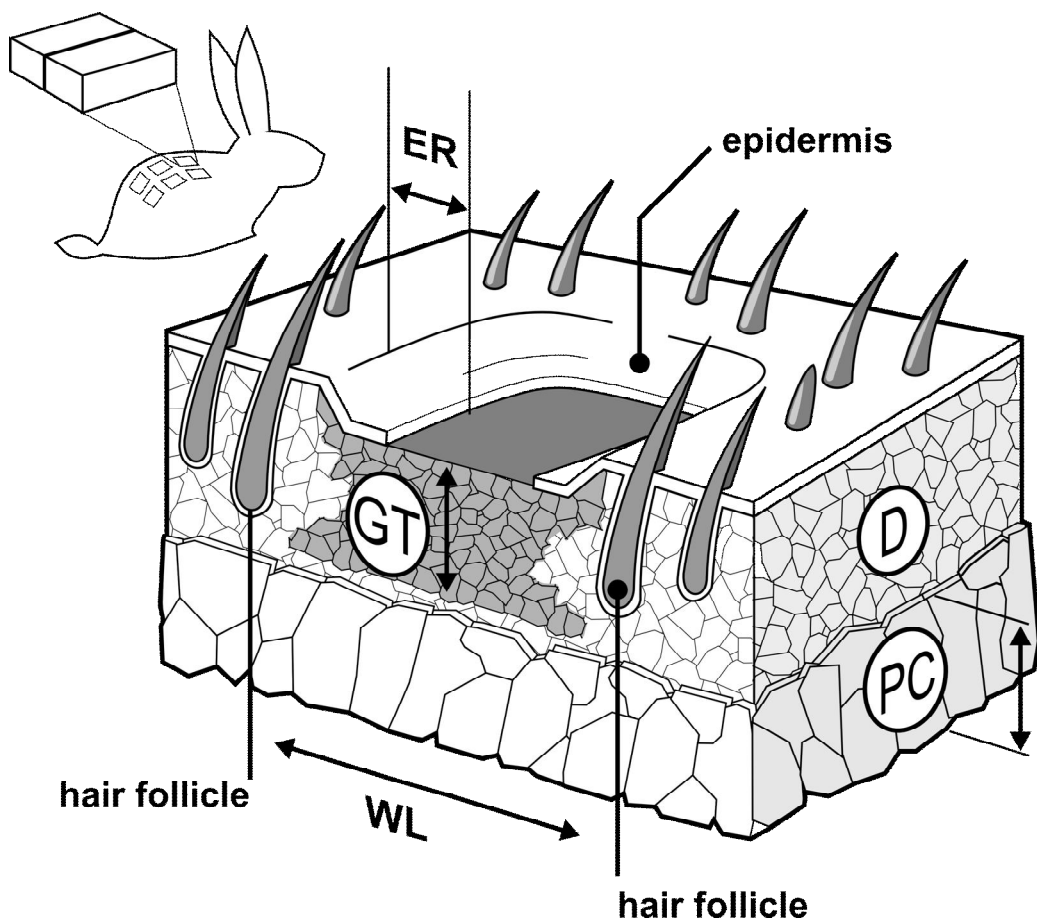


Figure 26 – Illustration of the histomorphometric evaluation of the excised wound. See text for details (D, dermis; WL, wound length; GT, granulation tissue; PC, panniculus carnosus; ER, epidermal regenerate).

The outline of each tissue was traced with the in-built function in ImageJ and number of pixels representing the cross sectional area was determined by the measure function. This value could then be converted to a metric scale using a calibrated image featuring a scale bar and taken at the same magnification as the sample image. The thickness of each tissue was determined by dividing the cross sectional area by the length of the measured area.

2.4.5.2 Collagen birefringence

Collagen maturation is important for the strength of the wound so to study this, the change in birefringence of the collagen content was visualised and quantified as it matures by picrosirius red staining, polarised light microscopy and image analysis. Various types (I, II and III, etc.) of collagen have a natural birefringence which can be enhanced by Sirius red staining when viewed in a polarised light microscope. Sirius Red, a strong anionic dye, stains collagen by reacting, via its sulphonic acid groups, with basic groups present in the collagen molecule. The elongated dye molecules are attached to the collagen fibre in such a way that their long axes are parallel. This parallel relationship between dye and collagen results in a 5-6 times increase in optical retardations (birefringence) of the collagen bundles.

2.4.5.2.1 Picrosirius red staining

A 0.1% Sirius red F3B in saturated aqueous solution of picric acid was made by firstly adding approximately 15 gram of wet picric acid to 500 ml distilled water. The solution was stirred overnight with a magnetic stirrer. To ensure saturation picric acid was added until no more crystals could be dissolved. The final picrosirius red solution was made by dissolving 0.5 gram of Sirius red F3B (C.I. 35782) in the saturated picric acid solution.

Five-micrometer tissue sections were cut and mounted, deparaffinised and rehydrated to water as described above. The tissue sections were then incubated in the picrosirius red solution for one hour at room temperature, washed in two changes of acidified water (0.5% acetic acid in distilled water), for three minutes each, washed for 5 minutes in running tap water, counterstained with Harris's haematoxylin for 1 minute,

differentiated in 1% acid ethanol for 3 seconds and washed in water for another 5 minutes. Sections were dehydrated, cleared and mounted as described above.

2.4.5.2.2 Polarised light microscopy

After picosirius red staining the birefringence of the collagen in the tissue sections were visualised under a polarising microscope equipped with two polarisers (Figure 27). A linear polarising filter (polariser; Olympus, Tokyo, Japan) was placed on the microscope's field iris diaphragm ring, below the sample, to provide for the linearly polarised illumination of the samples. The analyser (also a linear polarising filter) was fitted above the sample (within the intermediate module). The transmission axis of the (lower) polariser was rotated such that it was at right angles with that of the analyser. This could be determined when the linearly polarised light was completely extinguished resulting in a blackout of the field of view.

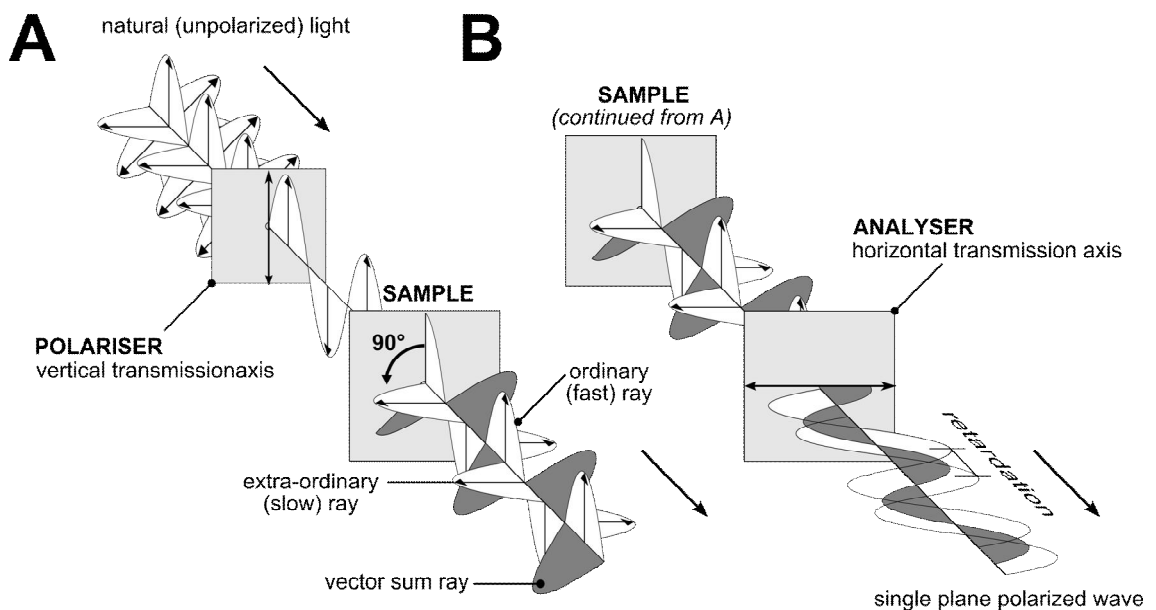


Figure 27 – Illustration of the principal behind polarised light microscopy. (a) Natural light is polarised by a linearly polarising filter (*i.e.* polariser) parallel to the transmission axis. (b) This linearly polarised light beam is then transmitted through the specimen (Sirius red stained collagen) and is refracted in an ordinary and an extra-ordinary ray which move out of phase depending on the degree of birefringence and the thickness of the specimen. As they pass through the second polariser (*i.e.* analyser) they interfere either destructively or constructively

depending on the phase difference and an image is created resulting from the unequal transmission of the components of the polychromatic light.

To enable an objective quantitative assessment, slides were captured with a digital camera (2.11 megapixel, 1600x1200-pixel, Olympus C-2020 Zoom, Japan) mounted on the microscope. Up to ten fields were captured from each slide under 20x objective, and all slides were photographed on the same day to avoid any variability associated with the light source.

2.4.5.2.3 Image analysis

Picrosirius red stained collagen fibres viewed under polarised light show different polarisation colours (or hues) depending on the thickness and packing of the collagen fibrils. As the fibre thickness increases, the colour changes from green to yellow to orange to red. To evaluate collagen maturation in tissue samples, their interference colour patterns were recorded as 24-bit digital RGB (red, green, and blue) photographs. These images were converted to the an 8-bit colour space using the build in “HSB Stack” command in the image analysis tool ImageJ (NIH, USA). This command transforms the image into a stack of 3 channels, each channel representing one of the three perceptual colour attributes: hue, saturation and brightness (HSB).

The analyses were performed on the hue channel as this contained the pure colour information and the latter two channels were discarded. The transformation from the RGB to the HSB colour space reduces the colour palette from 16.7 million (24-bit) to 256 (8-bit) values (Figure 28a). Using the threshold function in ImageJ the minimum and maximum values of each colour range of interest still perceive as that particular colour were defined (Figure 28a): 2-9 and 230-256 for red, 10-38 for orange, 39-51 for yellow and 52-128 for green. The hue ranges 1-2 and 129-229 consisted of non-birefringent tissue elements.

The number of pixels within each colour range was determined by the in-built measure function (Figure 28b-d). The red and orange hues represent the thicker collagen fibrils whereas the yellow and green hues represent the thinner collagen fibrils. Collagen maturation was expressed as the ratio between the amounts of thick fibrils to thin fibrils.

The collagen content was determined by the total number of pixels representing an interference colour divided by the total number of pixels in the image.

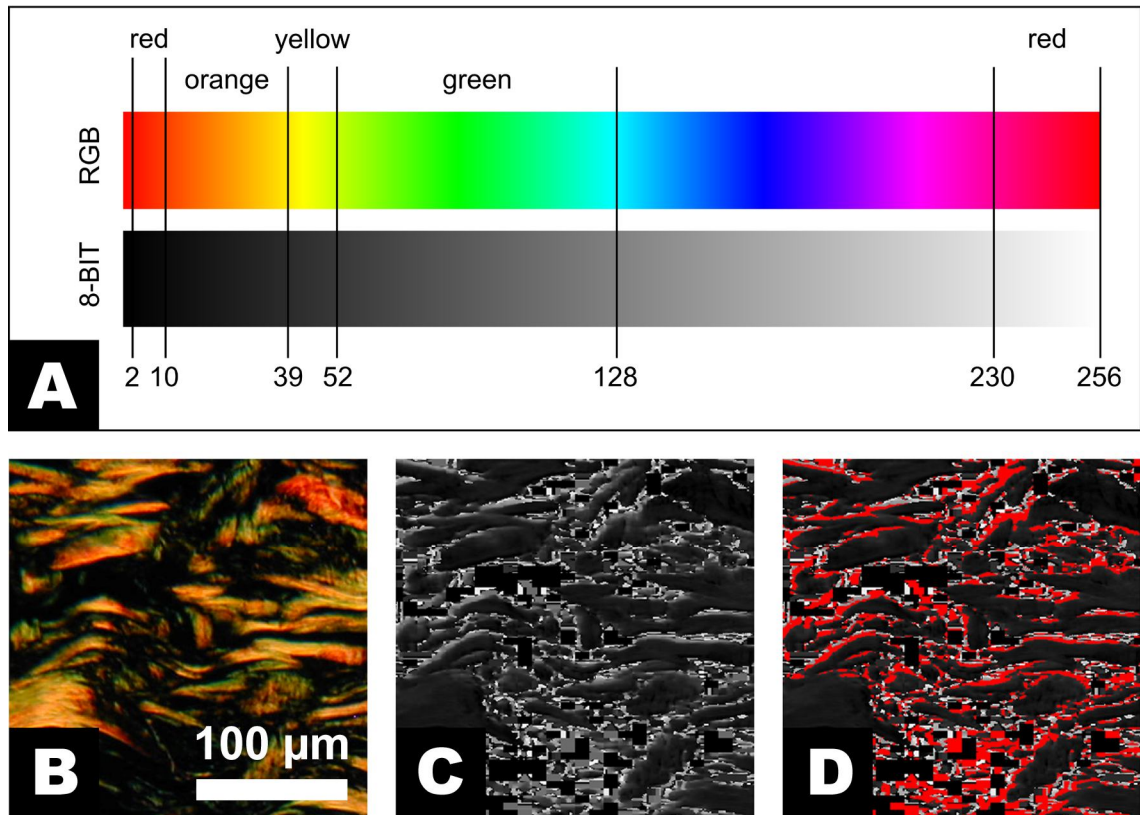


Figure 28 – Analysis of birefringence within tissue samples using image analysis software. (a, b) The RGB (red, green, and blue) colour space (16.7 million colours) in which the micrographs were photographed was converted into a (a, c) HSB (hue, saturation and brightness) colour space (8-bit; 256 colours). The (birefringent) colours of interest (*i.e.* red, orange, green and yellow) were numerically defined (see ‘a’) and measured in the HSB channel (d, an example is given for the colour green).

2.4.6 Immunostaining

2.4.6.1 Immunofluorescence

Tissue sections were stained with a mixture of mouse monoclonal anti-human (with cross reactivity to rabbit antigens) (catalogue number NB120-11213, Novus Biologicals, Cambridge, UK) antibodies (immunoglobulin G, IgG) directed against cytokeratins (1, 4, 5, 6, 8, 10, 13, 18, and 19) expressed in the cytoplasm of epithelial

cells. The labelling of antigens by the antibodies was visualised with a polyclonal goat anti-mouse IgG conjugated to the fluorescent marker fluorescein isothiocyanate (FITC) (catalogue number F-4018, Sigma-Aldrich Co. Ltd., Dorset, UK). See Figure 29 for an overview of the immunofluorescence technique.

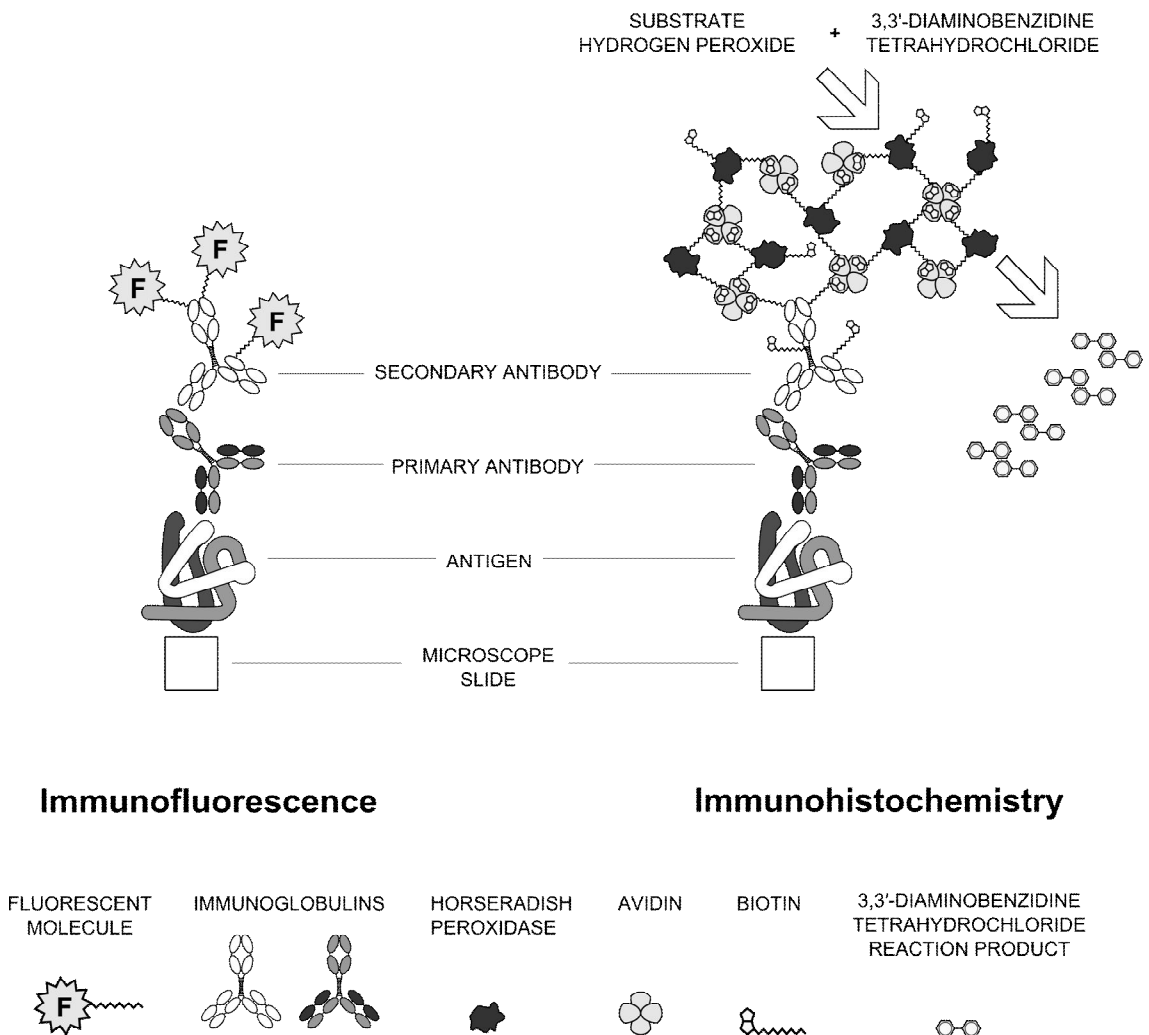


Figure 29 – Illustration showing the main principle behind immunofluorescence (IF) and immunohistochemistry (IHC). In both IF and IHC a primary antibody (monoclonal) attaches to an antigen of interest after which a secondary antibody (polyclonal) conjugated with a visualising system is attached to the primary antibody to visualise the location of the antigen. In IF the secondary antibody is conjugated to a fluorescent molecule whereas in IHC it is conjugated with biotin which binds to a preformed biotinylated avidin-horseradish peroxidase (HRP) complex which converts the colourless substrate into a coloured reaction product. As avidin binds to four biotin molecules the reaction is enhanced by the localised complex of an accumulated ‘cloud’ of HRP enzyme.

Five-micrometer tissue sections were cut and mounted, deparaffinised and rehydrated to water as described above. To prevent non-specific binding of the antibodies non-target proteins on the samples were blocked by incubation at room temperature for 30 minutes in 1.5% normal goat serum diluted in washing buffer (*i.e.* PBS) after which time the sections were washed with PBS three times. The samples were incubated with primary antibody diluted in washing buffer (100 µl) at a concentration of 1:100 (v/v) for 30 minutes at room temperature. Samples were then washed and incubated with the FITC conjugated secondary antibody at a concentration of 1:200 for 30 minutes at room temperature in the dark followed by a further three washes in PBS. The specimens were then mounted using Vectashield® with 4',6-diamidino-2-phenylindole (DAPI, catalogue number H-1500, Vector Laboratories, Peterborough, UK). Rabbit skin was used as a positive control and rabbit skin with the primary antibody omitted was used as a negative control. Specimens were stored in the dark prior to examination using a fluorescence microscope (Olympus). Images at 200x magnification (20x objective; FITC filter) were captured using a digital camera attached to the microscope.

2.4.6.2 Immunohistochemistry

Tissue sections were stained with a mouse monoclonal anti-rabbit CD31 (Abcam, catalogue number ab9498, Cambridge, UK) antibody (IgG) directed against the platelet endothelial cell adhesion molecule (PECAM-1) expressed on the surface of endothelial cells, and with a mouse monoclonal anti-rabbit CD45 (catalogue number MCA808G, Serotec, Oxford, UK) antibody (IgG) directed against the pan leukocyte marker protein tyrosine phosphatase, receptor type, C expressed on the surface of all hematopoietic cells (except for erythrocytes and platelets). The labelling of antigens by the antibodies was visualised with the VECTASTAIN Elite ABC Kit (catalogue number PK-6102, Vector Laboratories, Peterborough, UK). See Figure 29 for an overview of the immunohistochemistry technique.

Five-micrometer tissue sections were cut and mounted, deparaffinised and rehydrated to water as described above. It was then necessary to perform an antigen retrieval step for both antibodies. This was achieved by incubating the specimens in a sodium citrate buffer (0.01M Sodium Citrate, 0.05% Tween-20, pH 6.0) in a steamer; 40 and 20 minutes for CD31 and CD45 respectively. The samples were allowed to cool in the antigen retrieval solution for 10 minutes by removing the steaming to room temperature

after which samples were washed for 5 minutes in Tris-buffered saline (TBS) with Tween (50 mM Tris Base, 150 mM NaCl, 0.05% Tween-20, pH 7.6) with constant agitation.

To prevent non-specific binding of the antibodies non-target proteins on the samples were blocked by incubation at room temperature in 1.5% normal horse serum (Vector Laboratories, Peterborough, UK) diluted in washing buffer. Samples were washed in TBS for 5 minutes with constant agitation. The samples were incubated overnight at 4°C in primary antibody diluted in washing buffer (100 µl) at a concentration of 1:25 (v/v) for CD31 and 1:75 (v/v) for CD45. Samples were washed and incubated in 3% hydrogen peroxide for 30 minutes at room temperature in the dark to block the endogenous peroxidase activity. Samples were washed and incubated for 30 minutes at room temperature with a horse anti-mouse polyclonal, biotinylated secondary antibody (diluted 1:200 in washing buffer) according to the specifications of the manufacturer. Samples were washed and then incubated for 30 minutes with the avidin/biotin complex (ABC Reagent, Vector Laboratories, Peterborough, UK). Samples were washed and incubated for 10 minutes in the dark at room temperature in 3,3'-diaminobenzidine (DAB peroxidase substrate solution, catalogue number PK-4105, Vector Laboratories, Peterborough, UK).

Samples were washed and incubated for 6 minutes in a 0.5% (w/v) copper sulphate ($\text{CuSO}_4 \cdot 5\text{H}_2\text{O}$) in 0.9% (w/v) NaCl to enhance the colour of the DAB-horseradish peroxidase reaction product to a dark brown. Samples followed by washing in running tap water and counterstained with Harris's haematoxylin for 1 minute, wash in 1% acid ethanol for 3 seconds and wash well with water. Sections were then dehydrated, cleared and mounted, as previously described.

Positive and negative controls were included in all staining runs. Negative controls constituted samples where the primary antibody incubation step was omitted (and replaced with washing buffer) and positive controls were tissue samples where the targeted antigen was present; spleen and liver for CD45 and CD31 respectively.

2.4.6.3 Image Analysis

2.4.6.3.1 Angiogenic response

ImageJ was used to determine the average number and the size of vessel cross sections in each image (20x objective; Figure 30a). The in-built ‘colour deconvolution’ function allowed us to separate the brown of the DAB reaction product and the blue of the haematoxylin counterstain into separate channels. The DAB channel was then selected and automatically thresholded using the “Make Binary” command which uses an iterative procedure based on the iso-data algorithm to divide the image into objects and background (Figure 30b). These black and white images were visually compared with the original RGB images from the digital camera to detect nonspecific selection. The lumina of the cross sections were filled using the “fill holes” command and the number of cross sections and the average cross sectional area (*i.e.* luminal area and endothelial cell area) per image were determined (Figure 30c).



Figure 30 –Tissue sections stained for CD31 positive endothelial cells (with DAB) were (a) photographed and, using image analysis software, the staining was converted, in three steps (see text for details), into (b) black areas representing blood vessel cross sections comprising an endothelial cell mass and (when present) a lumen. (c) The number and the total area of the blood vessel cross sections per area were then calculated.

2.4.6.3.2 Inflammatory response

To quantify the inflammatory response the number of nuclei per image and the number of DAB stained cells (*i.e.* CD45 positive leukocytes) were counted using the “cell

counter” plugin in ImageJ (Figure 31). The percentage of leukocytes was determined by dividing the number of DAB positive cells by the total number of nuclei (*i.e.* cells).

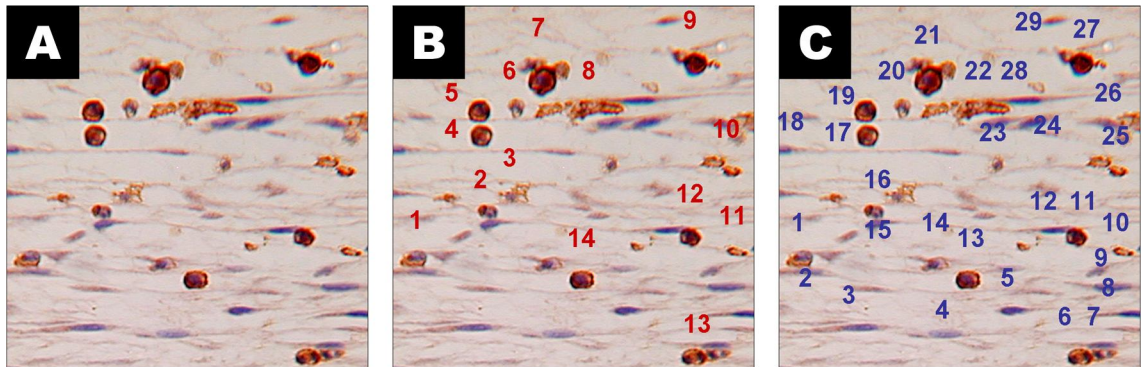


Figure 31 - Figure 30 – (a) Immuno-histochemical detection of CD45-positive leukocytes using DAB visualisation. (b) Visual output of the ‘cell counter’ plugin showing the stained cells that were manually marked for inclusion in the total count. (c) The visual output for haematoxylin stained nuclei.

2.5 Statistical analysis

The data were analyzed using the Statistical Package for the Social Sciences software program (SPSS, version 13.0, Chicago, IL, US). For all analyses, statistical significance was set at the 0.05 level.

A normal (or *t*) distribution (with a particular mean and variance) was assumed of the (*in vitro*) variables of interest and parametric tests were used to test the difference between two (*t*-test for independent samples) or more means (analysis of variance; ANOVA). When performing the *t*-test, the Levene's test was used to test the assumption of equal variances (or homogeneity of variance) and to correct for and if unequal variances were detected. If differences were detected by ANOVA analysis, a Tukey-HSD (Honestly Significant Difference) or a Bonferroni *post hoc* test was applied to identify those differences.

For the *in vivo* experiments six repeats of one condition at one time point were tested in a single rabbit and, therefore, a two-way (treatment modality and time) multilevel repeated measures ANOVA (RM-ANOVA) was used to analyse the data. Significant multilevel main effects were followed up with a Bonferroni *post hoc* test. Significant

interaction effects were followed up by testing the simple main effects (*i.e.* one-way ANOVAs for each factor, treatment modality and time, conducted separately at each level of the other factor).

3. Results

3.1 Collagen hydrogel compression

3.1.1 Compression of large volume hydrogels

Collagen (type I) monomers can be extracted from non-cross-linked fractions of collagenous tissues (Bailey *et al.*, 1998) (such as is abundant in the tendon found in tails of young rats) by dissolution in dilute acid (such as acetic acid) and reconstituted into fibrils (with a structure similar to those found in native tissue) by neutralisation of the acid solubilised monomeric collagen solution with sodium hydroxide (Francis *et al.*, 1942).

This spontaneous fibrillogenesis that occurs at neutral pH results in a collagen hydrogel consisting of a loose lattice network of collagen fibrils (held together by non-covalent fibril-fibril interactions (Rosenblatt *et al.*, 1994) and physical entanglement) surrounded by a high-volume of non-structural water (as a result of the extraction and reconstitution process). The interstitial fluid has an inhibitory effect on the formation of these inter-fibrillar attractive forces resulting in poor mechanical properties of the gel. It has been shown that mechanical loading of the collagen hydrogels (Brown *et al.*, 2005) can expel the interstitial fluid content thereby, increasing the collagen fibril packing density, raising the frequency and strength of inter-fibrillar interactions, and producing mechanically strong collagen hydrogels in a matter of minutes.

This technique involves the application of a gravitational load (of 1.8 kN/m²) for a predetermined time period (of 5 minutes) on the apical surface of a rectangular, unconstrained (not confined at the sides) collagen hydrogel seated on top of (porous) blotting elements (a standard setup of nylon and metal mesh, and filtration paper sheets). The dual action of the compressive load and the negative capillary pressure (exerted by the blotting elements) produces a phase separation that involves the outflow of the fluid content (mainly) through the basal surface of the hydrogel (referred to as the FLS) and concomitant retention and increase in concentration of collagen fibrils. The technique has only been tested on collagen hydrogels with a 3-ml volume and an FLS

area of 4.3 cm² (or 0.7 ml per cm² FLS area) which after the compression have a thickness of approximately 30 μm.

A preliminary study in (an *ex vivo* rabbit model of) a full thickness skin defect (measuring 3 x 2 cm²) to test the feasibility of the use of the compressed collagen sheet as a skin implant showed that the fragile material was easily cut by running a suture (a 4/0 prolene suture) through and that after implantation the collagen sheet easily pulled away from the stitches when only a small strain (of approximately 20%) was applied to the wound (Figure 32). Therefore, although the material strength (determined by the material breaking load per material cross sectional area) of these compressed collagen sheets approaches that of native tissues, they are, because of their thickness, fragile and difficult to handle.

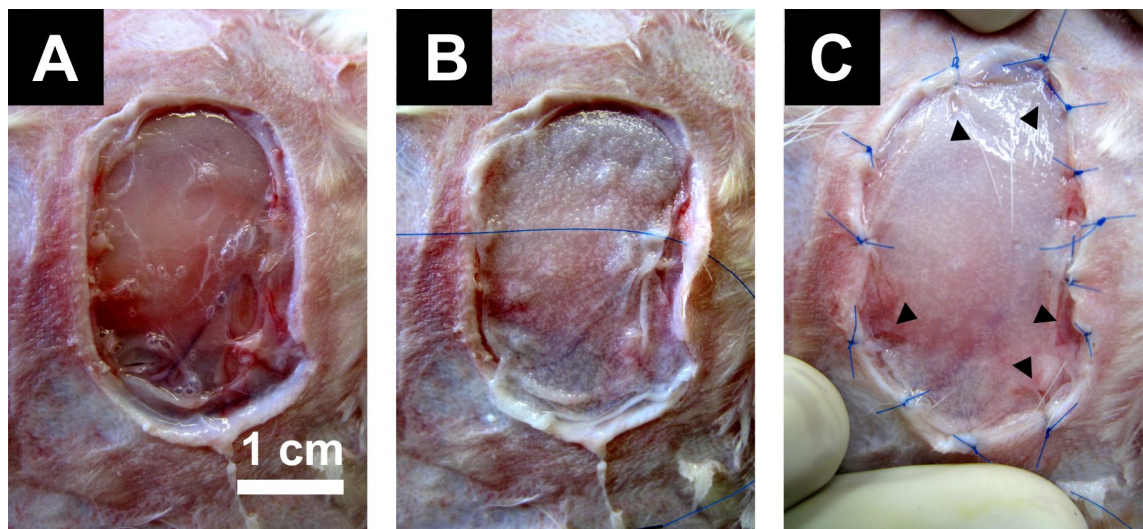


Figure 32 – (a) Rabbit model of a full thickness skin defect. (b) Compressed collagen sheet placed onto the defect and sutured in place. (c) Manually applied strain of 20% tears the collagen sheet away from the stitches (arrow heads).

From the basic rules of physics, the suture holding capacity or material breaking load can be improved, provided that the UTS (determined here by the collagen fibril density) remain constant, by simply increasing the thickness (or cross sectional area) of the compressed collagen gels, as $F_{\text{break}} = \text{UTS} \times (\text{material cross sectional}) \text{ Area}$. The increase in thickness has previously been achieved for the (0.7 ml/cm²) compressed collagen gel by rolling the collagen sheets (along their short axis) into rods (Brown *et al.*, 2005) allowing the collagen material to be sutured and implanted *in vivo* (Mudera *et*

al., 2007). The rolling of the sheets, however, is not conducive to the creation of epithelial like structures.

Now, the hypothesis under test is that the break strength can be improved, provided that the UTS (or collagen fibril density) remains constant, by increasing the thickness of the compressed collagen sheets through the increase of the pre-compression volume per FLS area.

3.1.2 Non-linear relationship of hydrogel volume to fluid loss

The hypothesis under test is that the thickness and therefore break strength of a compressed collagen hydrogel can be improved by increasing the pre-compression volume per FLS area provided that the UTS remain constant. It has previously been shown that the UTS of the compressed collagen gel is determined by the collagen fibril density which is inversely related to the percentage fluid expulsion (Neel *et al.*, 2006). Therefore the time that a constant, gravitational load is applied for on the hydrogel (which determines the percentage fluid loss) is an important parameter to control when changing the pre-compression volume. To ask the question if a fold increase in the pre-compression collagen volume requires the same fold increase in compression time to result in a pre-determined percentage fluid loss, the compression (under a constant load of 1.8 kN/m²) of three incremental volumes (1.95, 2.60 and 3.25 ml/cm²; a fixed increment of 0.65 ml/cm²) was studied (over a 25 minute compression period).

In the previously established regime the collagen gels were compressed in an unconstrained configuration (Figure 9a). This assumes minimal loss of fluid through the very low surface area of the vertical edge surfaces. However, due to the height to base ratio of the tested volumes the collagen hydrogels had to be laterally confined over the compression process in a custom built chamber to prevent the gel body from buckling (Figure 10b). The vertical load was applied by a free gliding plunger while the gels were seated on the standard setup of blotting elements (nylon and metal mesh, and filtration paper sheets). The vertical displacement (or height loss) of the plunger was used as an indirect measure of the percentage (of the initial volume) fluid loss and recorded over time.

A graphical representation of the percentage fluid loss of the three increased volume collagen hydrogels is given in Figure 33. It shows that it required a disproportionately larger unit increase in time for every unit increase in collagen volume to result in a set percentage of fluid removal. An example of 75% fluid loss is given in Figure 33; increasing the volume from 1.95 (by 0.65) to 2.60 ml/cm² increases the compression time required for a 75% loss in volume by 55%. An additional increase in volume by 0.65 ml/cm² (to 3.25 ml/cm²) increases this time by 270%; a 5-fold increase. Additionally, a logarithmic relationship was found between the percentage fluid loss and compression time. The slope of the curves represents the respective rates (*i.e.* change in percentage fluid loss divided by the time in which this change occurred) at which fluid leaves the three hydrogels and it can be observed that every unit volume fluid outflow from the collagen hydrogels is accompanied by a unit decrease in the rate of this outflow.

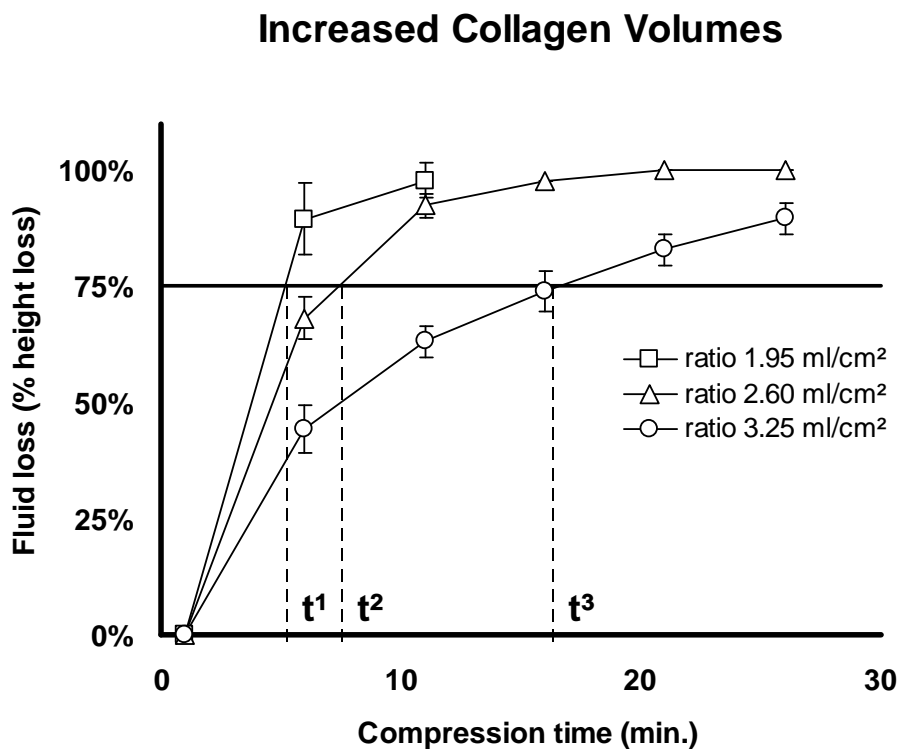


Figure 33 – A non-linear increase of compression time (t^{1-3}) of collagen hydrogels is required for every unit (here 0.65 ml/cm²) increase in collagen volume (per fluid leaving surface area; ml/cm²) to achieve the same percentage (*e.g.* 75%) fluid loss. Values are means \pm SD for 3 hydrogels for each volume.

The expulsion of the fluid content from a compressed collagen hydrogel can be described by the physical concept of volumetric flux (or fluid expulsion rate) which is defined as the amount of volume that flows through a unit area (in this case the size of the FLS) per unit time; $\text{flux} = \text{volume} / \text{time} / \text{area}$. This model suggests that at a constant flux and constant (FLS) area every fold increase in volume requires the same fold increase in time to allow for this volume to be expelled. The results here show, however, that as the compression progressed the rate of fluid expulsion (or flux) reduced and every unit increase in pre-compression volume required a disproportionately larger unit increase in compression time to obtain a set percentage of fluid removal. The fluid expulsion (flux) from a collagen hydrogel can be modelled with Darcy's law for flow through porous media ($\text{flux} = \text{permeability} \times \text{pressure} / \text{viscosity}$). From this model it can be appreciated that the decreasing fluid expulsion rate over the compression process could be the results of a mass-transfer dependent decrease in permeability (of the FLS) or pressure (driving fluid expulsion) and/or of a mass-transfer dependent increase in viscosity (of the fluid expelled).

3.1.3 Fluid saturation of blotting elements and fluid outflow

From Darcy's law it follows that the mass-transfer dependent decrease in fluid expulsion from collagen hydrogels could be caused by a decreasing operating pressure. The pressure driving fluid expulsion is generated by the gravitational load (which is constant, 1.8 kN/m^2) and the negative capillary action exerted by the absorbent components of the blotting elements (nylon mesh and filtration paper sheets). The gravitational load is constant over the compression process, but fluid saturation of the absorbent components could, result in a mass transfer dependent reduction in capillary pressure leading to the declining fluid expulsion rate. To ask the question if fluid saturation of the absorbent components causes the mass transfer dependent decrease in the fluid expulsion rate, the confined compression (1.8 kN/m^2) was studied and compared to collagen hydrogels (2.67 ml/cm^2) seated on; (a) the standard setup of nylon and metal mesh and three filtration paper sheets, and (b) a modified setup (as the standard setup but without the absorbent components); *i.e.* only metal mesh. The vertical displacement (or height loss) of the plunger (load) was used as an indirect measure of the percentage (of the initial volume) fluid loss and recorded over time.

A graphical representation of the results (Figure 34) show that when the support on which the hydrogels were compressed did not feature the absorbent elements the relationship between fluid loss and time shifted to the left- and upward but remained logarithmic and did not become linear. The slope of the curves represents the fluid expulsion rate (flux) from the collagen hydrogels and the shift indicated a higher flux from gels compressed on the modified support than on the standard setup of blotting elements. An example is given in Figure 34, showing (a 50%) reduction in the required time to achieve a 75% fluid loss when the absorbent components were removed. It was noted that in the two studied setups the direct interface through which fluid is expelled from the gel was more porous for the modified (metal mesh) than the standard setup (nylon mesh); average pore size of 300 vs. 50 μm . It is assumed that this difference accounted for the faster removal of fluid in the modified setup.

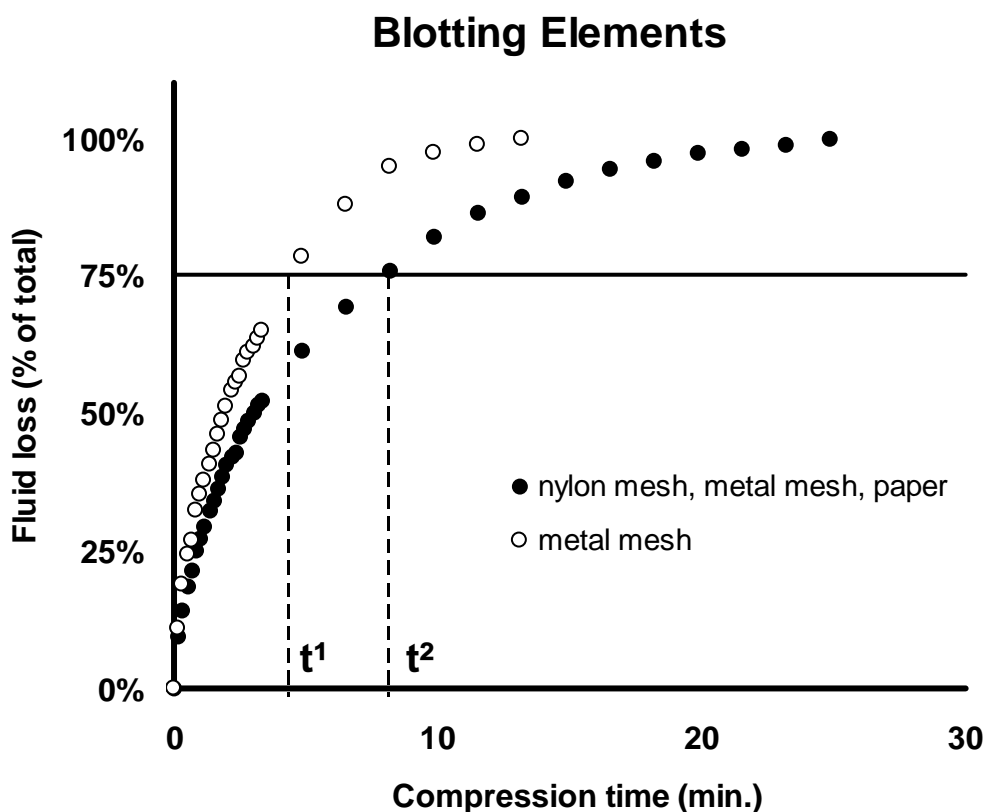


Figure 34 – Representative plots of fluid expulsion from collagen hydrogels under confined compression on two different types of blotting elements. Fluid saturation of the blotting elements does not influence the logarithmic relationship between fluid loss and time.

These results suggest that the supporting blotting elements do influence (by their porosity) the outflow of fluid, but this influence appears to be constant (mass transfer independent) over the compression as the removal of these components does not prevent the change in the fluid expulsion rate over the compression process excluding fluid saturation (and concomitant decrease in capillary pressure) of the blotting elements as a cause for this phenomenon.

3.1.4 Anisotropic collagen compaction

Following from Darcy's law (flux = permeability x pressure / viscosity) the decreasing rate in fluid expulsion over the compression process could result from a mass transfer dependent decrease in permeability (of the FLS). It is possible that the increase in collagen density at the FLS resulting from the expulsion of fluid impedes further fluid outflow.

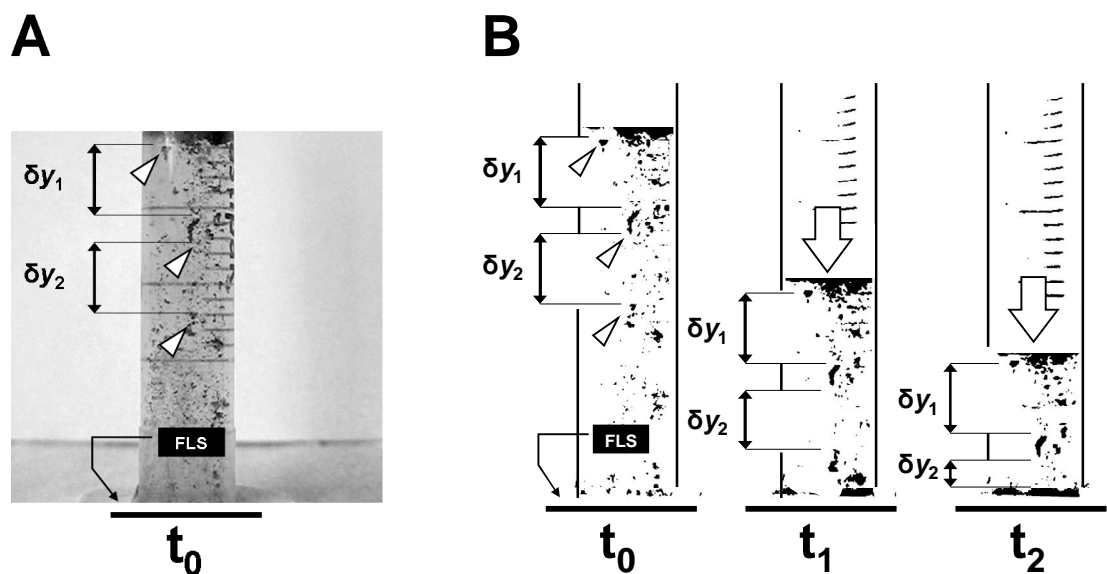


Figure 35 – (a) Photograph of a collagen hydrogel marked with charcoal particles (white arrow heads) (FLS, fluid leaving surface) (b) Binarised photographs showing the change in distance ($\delta y_{1,2}$) between markers trapped inside a collagen gel at various time points of confined compression (white arrows show the direction of compression).

To determine in a quantitative manner the changes in collagen density over the compression process markers (charcoal particles) were incorporated (during the

polymerisation process) in a (3.25 ml/cm²) collagen hydrogel cast in a transparent (cylindrical) chamber (Figure 35a) and tracked over the confined compression process (driven by the gels own weight and the negative capillary pressure from the blotting elements) (Hadjipanayi and Ananta, *et al.*, 2010).

A subset of the markers would float to the surface of the gel within the first few minutes of the polymerisation process but after the standard 30 minute incubation period no spontaneous displacement could be observed suggesting that the markers were fixed into the collagen network. Figure 35a shows that at the start of the compression (t_0) the markers were randomly distributed throughout the gel body. As the compression progresses the densification of collagen in and fluid loss from various regions could be determined from the decrease in the vertical distance (δy) between arbitrarily chosen markers (Figure 35b).

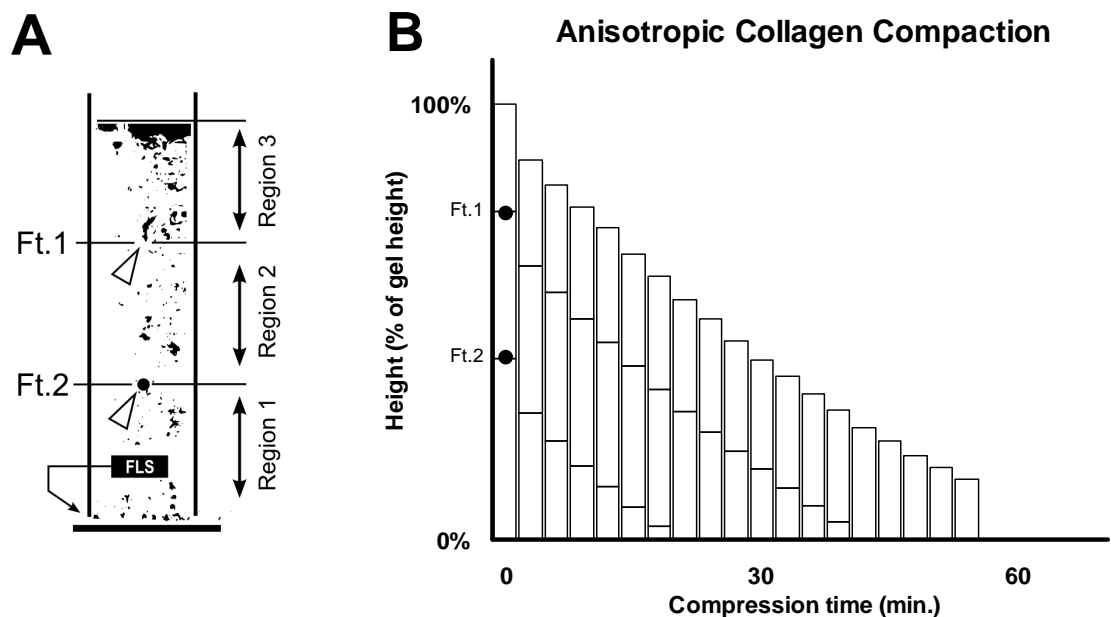


Figure 36 – (a) A vertical bar graph. Each bar represents the height of a collagen hydrogel at different times during confined compression. The two horizontal lines with the bars represent the position of two arbitrarily selected markers within the gel. Collagen above these markers does not compact until the markers reach the basal fluid leaving surface.

Figure 36a illustrates the example of how two arbitrarily chosen divide the collagen hydrogel into three regions and Figure 36b shows that these three regions decreased in

height not in parallel to each other but in sequence, contributing sequentially to the total amount of fluid loss. For instance, it is not until the bottom region (region 1) has reached its maximum compression level that the second region (region 2) will begin to decrease in volume. All the while the top region (region 3) remained at its original volume until also the second region (region 2) had been completely compacted.

From the change in the pattern of marker positions over the compression process, it was found that fluid loss did not occur homogeneously throughout the entire height of the collagen and two distinct regions with different macroscopic responses could be distinguished; the bulk region and a small boundary region at the FLS. The bulk region was characterised by its tendency to retain its original height with no change in the relative distances between the markers (suggesting little or no compaction occurring in this region). In contrast, the FLS region showed a continuous accumulation of markers, suggesting that collagen compaction in a compressed collagen gel is highly localised at the FLS and that only fluid in direct contact with the FLS is available for expulsion.

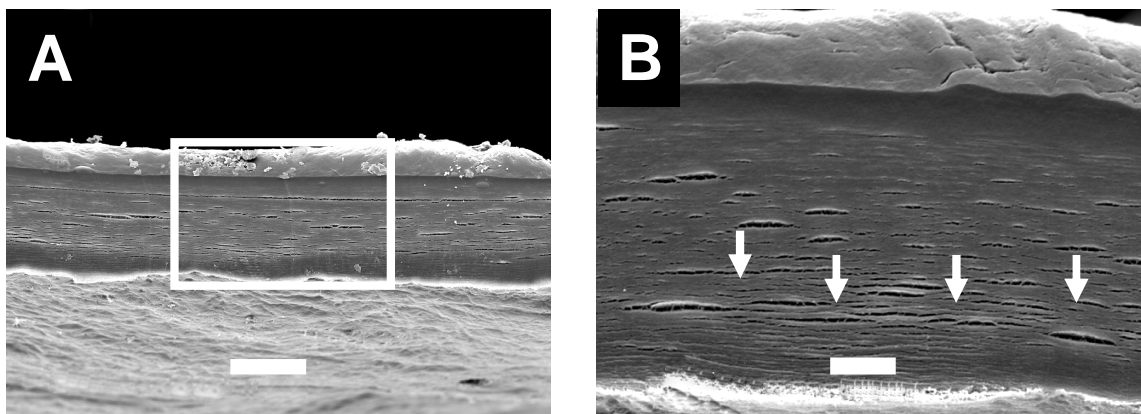


Figure 37 – (a) Scanning electron micrograph of a transverse cross-section of a 3.25 ml/cm² collagen hydrogel sequentially compressed on its basal and apical horizontal surface to achieve a near 100% strain level. Scale bar measures 50 μ m. (b) At higher magnification the lamellar structure formed by the compression process can be observed within the hydrogel. Scale bar measures 10 μ m.

The material structure in cross sections of compressed (3.25 ml/cm²) collagen hydrogels was visualised by SEM to test if indeed a dense boundary collagen layer had formed at the FLS. Figure 37a shows that in cross section two distinct regions could be distinguished. In the largest region (compressed region), located at the FLS, lamellar

structures were visible throughout while furthest away from the FLS a more amorphous (uncompressed) region could be seen. At higher magnification (Figure 37b) the lamellae could be seen becoming denser in the direction of the compression with the densest layers forming at the FLS.

It is concluded that the compression of collagen hydrogels does not result in a global compaction of the collagen matrix but is localised to the FLS. Only a fraction of the total volume is available for flow. And it is proposed that with every unit fluid expelled a unit decrease in hydraulic permeability and fluid outflow rate occurs due to the local accumulation of collagen at the basal FLS.

3.1.5 Sequential fluid expulsion through two fluid leaving surfaces

It was found increasing the pre-compression collagen hydrogel volumes extends the required compression time under a constant load in a non-linear fashion due to the decrease in hydraulic permeability of the FLS caused by the accumulation of collagen at this surface. This could set limitations to the maximum volume that could be compressed without applying a load that exceeds the maximum stress that for instance cells embedded in the hydrogel could tolerate. As it is not technically possible to prevent the formation of the collagen barrier at the FLS, short from not performing the compression, increasing the total FLS could prove beneficial to shorten the compression time and double the maximum hydrogel volume that can be maximally compressed by a given load.

From the previous experiment (Figure 33) it can be seen that for a (laterally confined) 3.25 ml/cm² collagen hydrogel compressed with a constant load of 1.8 kN/m² it required towards 30 minutes to achieve the near complete removal of the fluid content through its basal surface, but towards only 10 minutes for the removal of half the content. Therefore the hypothesis under test is that it would require only 20 minutes for the near complete removal of the fluid content of a 3.33 ml/cm² collagen hydrogel through two FLSs as opposed to the 30 minutes in a single FLS configuration. To test this, a constant load was applied for exactly 10 minutes on the gel to remove the first half of the fluid content through the basal FLS and then turned the gel on its apical surface and

continued the compression for an additional 10 minutes to remove the second half. This regime resulted in a $98.9 \pm (SD) 0.5\%$ weight (fluid) loss (values derived from 20 samples).

It was found that the time required to achieve a set percentage fluid loss through a single FLS of a collagen hydrogel compressed under a constant load was shortened when the FLS area was increased by the utilisation of a second FLS. This strategy has important practical implications with regards to up-scaling the technique as it would theoretically double the maximum volume that could be fully compressed under a given load. Additionally, the findings add to the evidence that the decrease in hydraulic permeability of the FLS was mass transfer dependent.

3.1.6 Characterisation of compressed large volume hydrogels

The hypothesis under test is that the break force of compressed collagen hydrogels can be increased by improving the size properties of compressed collagen hydrogels by way of raising the pre-compression volume. As the UTS is determined by the break force (F_{break}) per cross sectional area, an increase in break force ($F_{break} = UTS \times Area$) can only be obtained if the cross sectional area can be increased without significantly reducing the UTS of the material.

To test this hypothesis 3.33 ml/cm² collagen hydrogels was compressed using the regime described above (1.8 kN/m² applied for 10 minutes on the basal and then apical FLS) and compared the mechanical properties of the resulting sheets to those of 0.7 ml/cm² gels that were compressed with the previously established protocol (1.8 kN/m² applied for 5 minutes on the basal FLS). The 5-fold increase in pre-compression volume resulted in an equal fold increase in thickness of the resulting collagen sheet [$489 \pm (SD) 160 \mu\text{m}$ vs. $95 \pm 15 \mu\text{m}$, $t(8.9) = 9.48$, $p < 0.001$].

The ‘thin’ (0.7 ml/cm²) collagen constructs were fragile, difficult to handle and had to be spiralled to facilitate comparison of the tensile properties by DMA with the ‘thick’ (3.33 ml/cm²) constructs which were more robust. The ‘thin’ collagen constructs (Figure 38a) had a higher UTS compared to the ‘thick’ constructs (Figure 38b) as measured by

the ultimate strength [1.28 ± 0.42 vs. 0.54 ± 0.06 MPa); $t(10) = 3.91, p = 0.003$] and yield strength [1.08 ± 0.32 vs. 0.45 ± 0.04 MPa); $t(6.2) = 5.04, p = 0.002$] (Figure 38c).

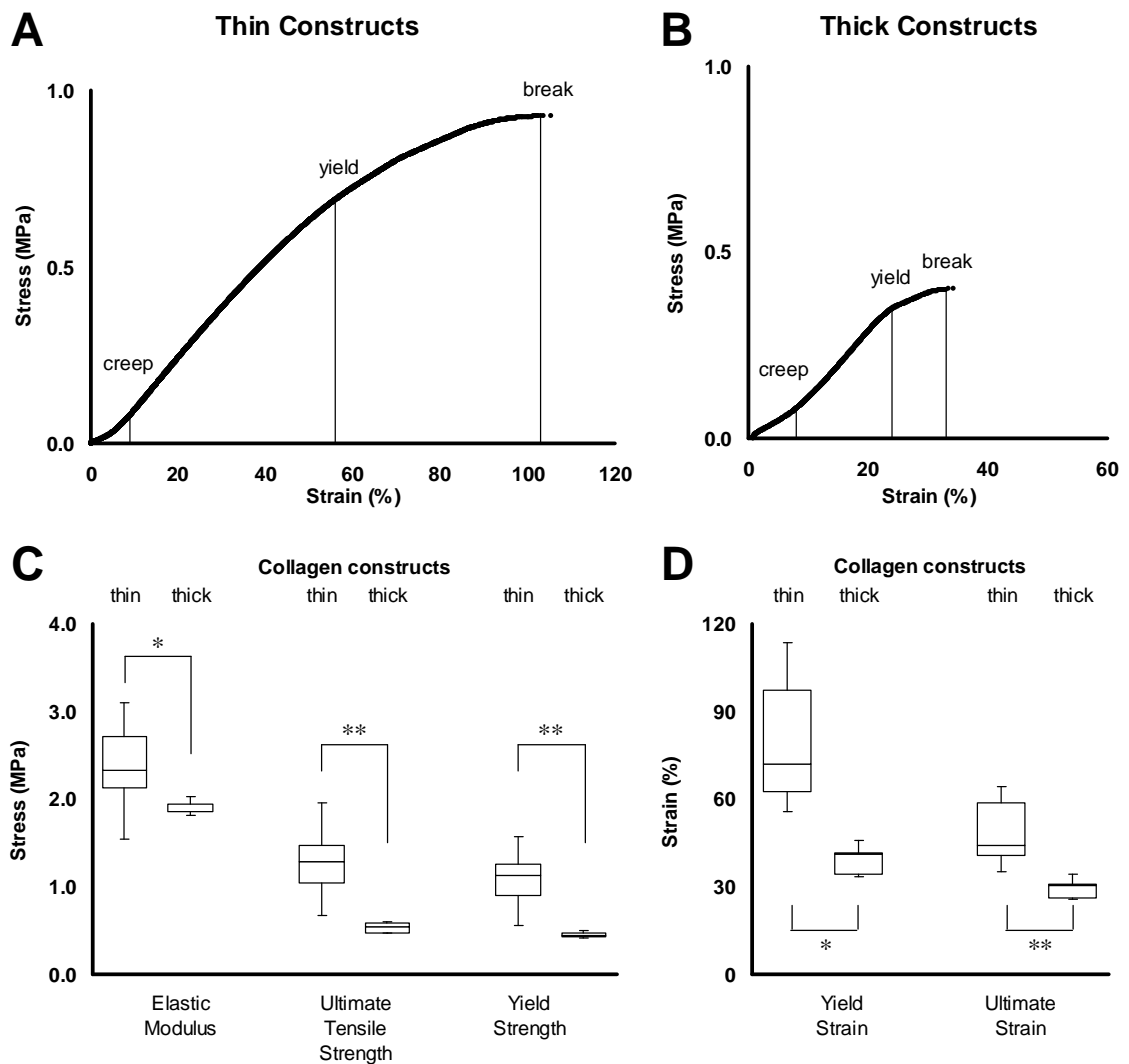


Figure 38 – Representative stress-strain curves for (a) compressed 0.7 ml/cm² (spiralled) and (b) 3.33 ml/cm² (thick) collagen hydrogel showing the toe region, the yield and break point. (c, d) Box and whisker plots showing the spiralled collagen gels had better mechanical tensile properties than thick collagen constructs. The boxes indicate the 75th and 25th percentiles, the whiskers indicate the minimum and maximum values, the lines show the median values. Values are derived from 7 samples for spiralled constructs and 5 samples for thick constructs. Asterisks above graphs indicate significance level (*, $p < 0.05$; **, $p < 0.01$).

Additionally, the ‘thin’ constructs had greater stiffness (resistance to deformation; Figure 38c) than ‘thick’ constructs [2.38 ± 0.51 vs. 1.90 ± 0.08 MPa); $t(6.5) = 2.42, p =$

0.049]. The ductility (amount of deformation before failure; Figure 38d) of the ‘thin’ constructs was also found to be higher, as measured by ultimate strain [68.9 ± 14.1 % vs. 39.3 ± 5.3 %]; $t(8) = 4.39, p = 0.002$] and the yield strain [47.9 ± 11.5 % vs. 29.6 ± 3.5 %]; $t(4.7) = 3.39, p = 0.021$]. Although the rolled ‘thin’ collagen constructs showed superior mechanical properties over the ‘thick’ collagen constructs the latter showed smaller variations in these properties.

These differences in mechanical properties could be attributed to the difference in collagen density. It was found that although the (absolute) pre-compression volumes of both ‘thin’ and ‘thick’ constructs were the same [5.15 ± 0.16 ml vs. 5.04 ± 0.44 ml, $t(23.7) = 1.29, p = 0.21$], the percentage fluid loss was higher for the ‘thin’ constructs [99.30 ± 0.22 % vs. 98.91 ± 0.52 %, $t(25.9) = 3.09, p = 0.005$] resulting in a lower post-compression weight [43 ± 13 mg vs. 33 ± 5 mg, $t(12) = 2.69, p = 0.02$] suggesting that the ‘thin’ construct had a higher average collagen density.

Summarising, the thickness of compressed collagen gels were increased 5.1-fold by raising the pre-compression volume. Although the mechanical strength of these thicker collagen constructs was 2.4-fold lower than the ‘thin’ collagen constructs (following from $F_{\text{break}} = \text{UTS} \times \text{Area}$) the implied break force was 2.2-fold higher than the ‘thin’ collagen constructs.

The break force of compressed collagen hydrogels were increased by improving the size properties of compressed collagen hydrogels by way of raising the pre-compression volume. The data underlines the relationship between strength and collagen density and the importance of precise control over the percentage fluid removal.

3.2 Hybrid constructs

3.2.1 Hybridisation of compressed collagen hydrogels

Fabricating sutureable collagen constructs by way of mechanically compressing large volume collagen hydrogels has certain technical limitations. A second strategy was therefore investigated that involved the incorporation of degradable synthetic organic polymer meshes in compressed collagen hydrogels. The hypothesis under test is that synthetic polymer meshes can be embedded in collagen hydrogels and the resulting hybrid material can be mechanically compressed to produce constructs that can be sutured and implanted.

3.2.2 Fluid removal from a PLACL-CCHH

Initially a mesh produced from a newly developed, slow degrading PLACL co-polymer was used to test the hypothesis. The co-polymer was made from 3% L-lactide and 97% ϵ -caprolactone, degrades by simple hydrolysis, and based on its composition the expected time for it to completely degrade is between 6 to 12 months.

A brief description of the textiles and the fabrication of the mesh is given here. The PLACL co-polymer was melt spun into yarns consisting of 25 filaments each. Each filament had a linear density of 6.6 dtex (decitex; grams per 10^3 meter length), a diameter of 28.4 μm , and each yarn had, a total fineness of 165 dtex, a tenacity (*i.e.* breaking load per unit linear density of the unstrained specimen) of $19.5 \pm (SD) 0.9$ cN/tex (centinewton per tex), and an elongation at break of $41.1 \pm 2.3\%$. The multifilament yarns were processed into meshes [thickness $0.63 \pm (SD) 0.02$ mm] with a weft-knit. It should be noted that the PLACL co-polymer was synthesised in by Uppsala University (Uppsala, Sweden) and that the co-polymer was melt-spun and weft-knitted into the mesh by Aachen University (Aachen, Germany).

The following protocol was used to test for the feasibility of forming a PLACL-CCHH material using the compression technique. A 0.7 ml/cm² collagen hydrogel was cast, a PLACL mesh was placed on top, and a second 0.7 ml/cm² collagen volume was cast. After a 30 minute incubation period the resulting hybrid materials were subjected (in an

unconfined configuration) to a 1.8 kN/m² load for 5 minutes to remove the fluid content of the collagen components. What resulted was a PLACL-CCHH consisting of the mesh coated on both surface with compressed collagen hydrogels (further characterisation described below).

Although the collagen density with the incorporation of a synthetic backbone is no longer critical for the sutureability of the construct the control of this parameter still has important implications with regards for instance to the induction of stiffness specific cell phenotypes and the integration strength between collagen and mesh.

Previously it was shown for a collagen hydrogel compressed on blotting elements that an increase in compressive load increased the rate of weight loss (Neel *et al.*, 2006). To test if the presence of the PLACL mesh prevented the expulsion of fluid and compaction of collagen, possibly through some sort of splinting action preventing the transmission of the mechanical load onto the hydrogel at high levels of compaction, the compression was compared of PLACL-collagen hybrid constructs loaded with a constant load of 1.8 and 3.6 kN/m² for a time period of 5 and 10 minutes.

The percentage weight (fluid) loss was recorded and the results were subjected to a two-way ANOVA having two levels of load (1.8 and 3.6 kN/m²) and two levels of time (5 and 10 minutes). All effects were statistically significant at the .05 significance level. The main effect of time on the post compression weight yielded an *F* ratio (probability information provided by ANOVA) of $F(1, 8) = 120, p < 0.001$ (Figure 39), such that the average percentage weight loss was significantly higher when the construct was loaded for 10 minutes (mean, $M = 98.9\%$; standard deviation, $SD = 0.1\%$) then for 5 minutes ($M = 98.3\%$, $SD = 0.1\%$). There was no significant main effect of load on the final weight, $F(1, 8) = 0.3, p = 0.580$. Additionally, no significant interaction effects were found between load and time, $F(1, 8) = 0.00, p = 1.00$.

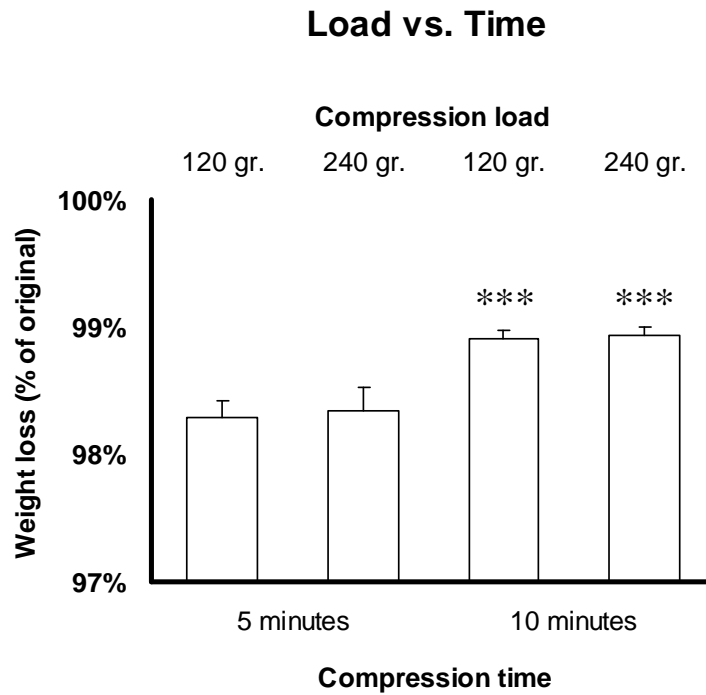


Figure 39 – Bar graphs showing the amount of fluid removed from PLACL hybridised collagen gels (1.4 ml/cm²) expressed as the percentage weight loss resulting from an unconfined compression with a gravitational load of 1.8 or 3.6 kN/m² for 5 or 10 minutes. Values are means \pm SD for 3 samples. Asterisks show a significant main effect of time on weight loss (*, $p < 0.001$).

The data suggested that at a near maximum compaction level of the collagen component in the PLACL-CCHH the previously described load dependent removal of the fluid content appeared to be inhibited; increasing the load did not result in a higher percentage fluid loss unless the compression time was increased. This suggested that this level of compaction fluid outflow was governed by the capillary action of the blotting elements and no longer by mechanical loading; the compaction had become time dependent.

It is concluded that at high levels of collagen compaction (> 98%) fluid loss from the gel component of the PLACL-CCHH was not dependent on the size of the compression load (in the range of 1.8 and 3.6 kN/m²) but on the compression duration relying on negative capillary pressure rather than mechanical loading to achieve a high collagen density.

3.2.3 Physical characterisation of PLACL- and PLGA-CCHHs

Compressed collagen hydrogels were also hybridised with a PLGA (Vicryl) co-polymer knitted mesh to form a PLGA-CCHH construct to allow for a comparison of the suitability of the newly developed PLACL mesh for TE purposes with this well characterised and commercially available PLGA mesh.

The PLACL mesh (Table 1, Figure 40a) had a lower porosity (defined as the ratio of the area of the voids and the total area) [16 ± 1 (*SD*) % vs. 46 ± 1 %, $t(9) = 62.0$, $p < 0.001$] and a smaller average pore size [0.55 ± 0.03 mm² vs. 0.04 ± 0.02 mm², $t(54) = 112.0$, $p < 0.001$] and a lower thickness [0.63 ± 0.02 mm vs. 0.15 ± 0.01 mm, $t(54) = 112.0$, $p < 0.001$] than the PLGA mesh (Figure 40b).

Mesh properties	PLACL	PLGA
Pattern	Tricot knit	Tricot knit
Yarn diameter (μ m)	270	100
Pore size (mm ²) ***	0.04 ± 0.02	0.55 ± 0.03
Porosity (%) ***	0.16 ± 0.01	0.46 ± 0.01
Mesh thickness (mm) ***	0.63 ± 0.02	0.15 ± 0.01
Compressed collagen dimensions	PLACL-hybrid	PLGA-hybrid
Thickness apical compartment (mm)	0.09 ± 0.01	0.10 ± 0.02
Thickness basal compartment (mm) *	0.07 ± 0.01	0.09 ± 0.02

Table 1 - Poly-[lactic acid-co-caprolactone] (PACL) and poly-[lactide-co-glycolide] (PLGA) meshes and compressed collagen components in respective hybrid constructs. Values are means \pm *SD* for 6 samples (*, $p < 0.05$; *, $p < 0.001$).**

In a transverse cross section of the PLGA- and PLACL-CCHHs flat collagen sheets could be observed on either side of the mesh (Figure 40c, d). As expected from the previously observed anisotropic compaction profile of compressed collagen hydrogels, the basal collagen sheet, featuring the FLS, was thinner than the apical sheet in both constructs, although the difference was only marginally significant in the PLGA-CCHH [PLACL, 0.07 ± 0.01 mm vs. 0.09 ± 0.01 mm, $t(10) = 2.31$, $p = 0.044$; PLGA, 0.09 ± 0.02 mm vs. 0.10 ± 0.02 mm, $t(12) = 1.97$, $p = 0.073$].

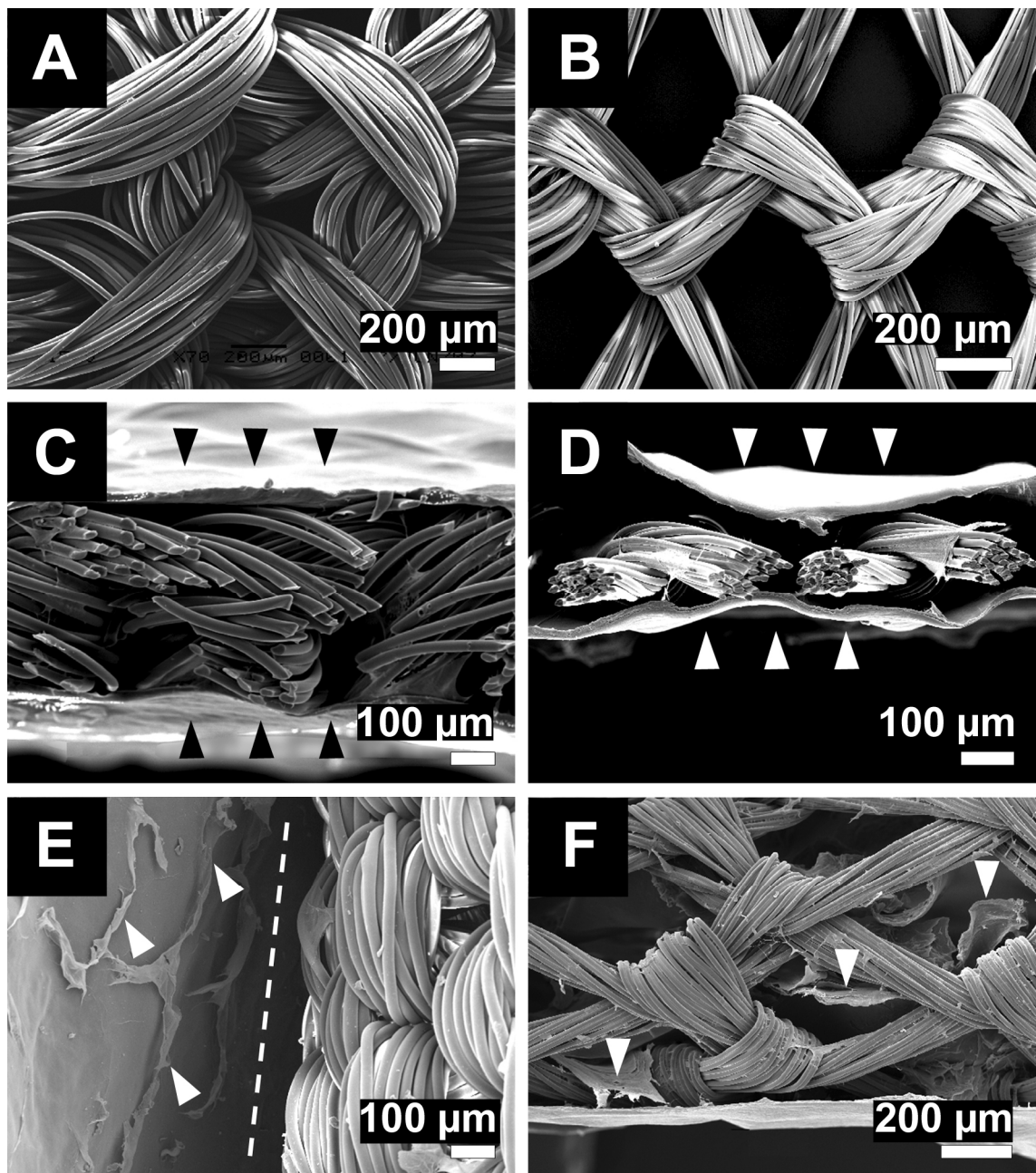


Figure 40 – Scanning electron micrographs of meshes made of (a, c, e) poly-[lactic acid-co-caprolactone] (PLACL) and (b, d, f) poly-[lactide-co-glycolide] (PLGA): (a, b) Mesh structure. (c, d) Transverse cross sections of collagen hydrogels hybridised with either of the meshes. The compressed collagen component (arrow heads) can be seen as flat sheets above and below the mesh. (e) In PLACL-collagen hybrid constructs the collagen (left from dotted line) does not extend deeply into the pores (right from dotted line) and superficial shreds (arrow heads) can be seen at the interface with the mesh, suggesting that there is no physical contact between the apical and basal collagen components. (f) The collagen in the PLGA-collagen gel hybrid construct can be seen protruding through the pores and extending towards the other side (arrow heads). Scale bars are shown in the bottom right corners.

Between constructs only the basal collagen sheet differed in thickness, being thinner in the PLACL-CCHH [apical collagen sheet, 0.09 ± 0.02 mm vs. 0.09 ± 0.01 mm, $t(11) = 0.204$, $p = 0.842$; 0.09 ± 0.02 mm vs. 0.07 ± 0.02 mm, $t(11) = 2.67$, $p = 0.022$]. This could possibly be due to the relatively denser structure of the PLACL mesh.

SEM analysis of the interface between the knitted mesh and the collagen gel showed that the top and bottom collagen layer did not physically contact each other through the dense structure of the PLACL mesh, but the collagen was able to traverse the larger pores of the PLGA mesh (Figure 40e, f).

Collagen hydrogels incorporated with two different degradable synthetic polymer meshes were compressed to form integrated material structures consisting of a synthetic, degradable polymer mesh coated with compressed collagen sheets. The findings showed the potential of the technique to combine compressed collagen hydrogels with different types of mesh materials.

3.2.4 Post-compression cell viability and proliferation

Previously the compression of a cell seeded 0.7 ml/cm² collagen hydrogel with a 1.4 kN/m² static load resulted in an 14% reduction in cell viability (determined by fluorescence microscopy) (Brown *et al.*, 2005). To study the effects of, an increased volume collagen hydrogel (1.4 ml/cm²), the embedding of a mesh, and the mesh structure on post-compression cell viability (5×10^5) fibroblasts were seeded within the bottom collagen component of both the PLACL- and PLGA-CCHHs and these constructs were then subjected to the standard compression regime (application of a 1.8 kN/m² static load on the standard setup of blotting elements in an unconfined configuration).

The AB reduction assay was used to assess the number of viable cells after the compression process. The assay measures the reduction of AB into the highly fluorescent dye by (metabolically active) viable cells. As the reagent is non-toxic it was possible to monitor cell number on the same samples at different time points.

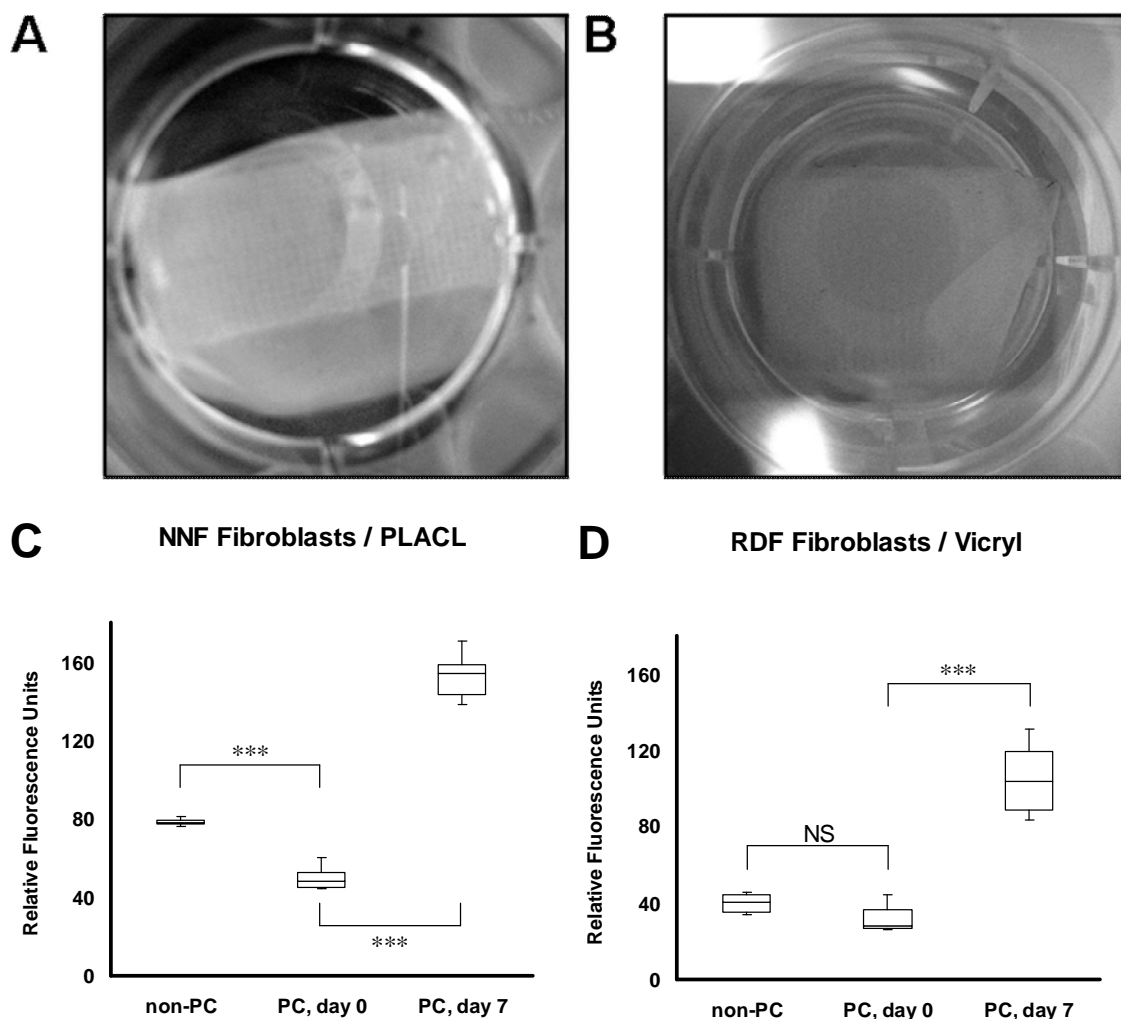


Figure 41 – Photographs of the cell-seeded (a) PLACL- and (b) PLGA-collagen hybrid construct after 7 days of static culture. (c) Box-and-whisker plots showing the amount of fluorescence (from the Alamar Blue reduction assay expressed as relative fluorescence units) produced by $5 \cdot 10^5$ cells (human and rabbit dermal fibroblasts) not exposed to the compression process (non-PC; plated on tissue culture plastic) and by the same number of cells directly (PC, day 0) and seven days (PC, day 7) after being exposed to the compression process while seeded inside the (d) PLACL- and (b) PLGA-collagen hybrid constructs (NS, not significant; Tukey's HSD *post hoc* analysis; *, $p < 0.001$; values are for 6 samples).**

Cell viability was measured directly after compression to determine cell survival and after a seven day culture period to evaluate if the construct could support cell growth. To determine the percentage cell survival the AB reduction of the cell inoculum introduced and compressed in the hybrid construct was divided by the reduction of a

same size inoculum added to tissue culture plastic. Cells from two different sources were used to test the hybrid constructs; human dermal (foreskin) fibroblasts with the PLACL-CCHH and rabbit dermal (ear) fibroblasts with the PLGA-CCHH.

Over the seven day culture period no deformation of either of the hybrid constructs could be observed (Figure 41a, b). Further, it can be noted from the standard curve (fluorescence from AB reduction versus viable cell number; Figure 16) and the data that the fold increase in cell number can directly be derived from the fold increase in fluorescence (expressed as RFU).

A one-way ANOVA was used to test differences in viable cell number among the three different time points; before, directly after and 7 days after compression. For both the PLACL- and PLGA-CCHH the viable cell number differed significantly across the three time points; PLACL-CCHH, $F(2, 17) = 269.5, p < 0.001$; PLGA-CCHH, $F(2, 17) = 47.7, p < 0.001$ (Figure 41c, d).

Tukey HSD *post hoc* comparisons of the three time points showed a reduction in viable cell number after compression of 36% for the PLACL-CCHH [from 78.3 ± 2.0 (SD) RFU to 49.9 ± 6.1 RFU, $p < 0.001$] and 8% (not significant) for the PLGA-CCHH [from 39.4 ± 6.3 RFU to 31.7 ± 8.0 RFU, $p = 0.630$]. At day 7, post compression, the number of cells cultured inside the compressed hybrid constructs had increased 3-fold for both the PLACL ($M = 152.6, SD = 12.1, p < 0.001$) and PLGA-CCHH ($M = 105.2, SD = 22.6, p < 0.001$).

A cell inoculum introduced and compressed within the basal collagen compartment of the PLACL- and PLGA-CCHH, to create living dermal equivalents, showed a reduction in cell viability, as measured with the AB reduction assay, which was not significant for the PLGA based dermal equivalent (8%) but significant for the PLACL based dermal equivalents (36%). In light of the previously found 14% reduction in cell viability for non-hybridised compressed collagen hydrogels (Brown et al., 2005) the incorporation of dense mesh structure seemed to negatively affect post-compression cell survival with a more open mesh structure showing better cell viability retention. Additionally, it was found that the decrease in cell number was recovered after a static culture period showing the ability of the hybrid constructs to support cell growth

3.2.5 In vitro analysis of short term biocompatibility of PLACL

The PLGA (Vicryl) material has previously been well characterised. The characteristics of the newly PLACL-material on the other hand are mainly derived from predictions made from its polymer composition. PLACL degrades through simple hydrolysis and intermediate degradation products are caproic and lactic acid (Pitt *et al.*, 1981) which negatively effect cell viability through lowering of the surrounding pH (Sung *et al.*, 2004). Although the release of these degradation products was expected to be low based on the predicted degradation profile, the question was asked if any cytotoxic effects (on cell viability and migration) from the mesh embedded within the PLACL based dermal equivalent were present and obscured by a larger, compensatory increase in cell number described above.

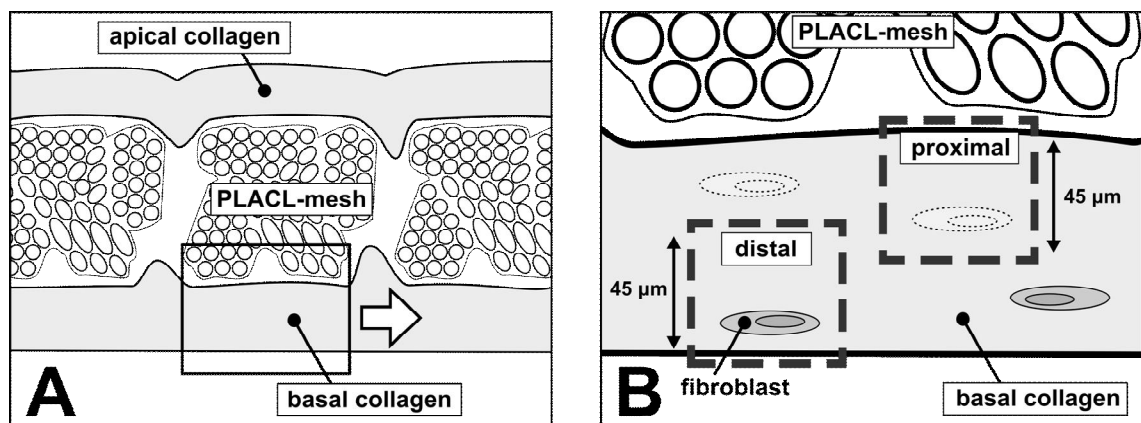


Figure 42 – (a) Illustration of a transverse cross section through the PLACL based dermal equivalent showing the apical and basal collagen component and the PLACL-mesh in between. (b) Detailed illustration of the box shows the proposed direction of the release of degradation products (DP). To study possible cytotoxic effects regions (45 m thick) proximal and distal to the mesh were studied for differences in percentage viable cells and in cell number to establish if cells died with the proximal region or moved out of this region.

To test this, live and dead fibroblasts within the basal collagen compartment of the PLACL based dermal equivalents were visualised post-compression, after a seven day static culture period, with a cytoplasmic fluorescent dye (CMFDA; specific for live cells) and counterstained with a nuclear dye (EH-1; specific for dead cells). The percentage of viable cells and the total number of cells (live and dead) were determined

in two overlapping regions (each 45 μm thick) within the 70- μm thick basal collagen compartment; a proximal (closest to the collagen-PLACL interface) and distal (free interface) region (Figure 42). Possible cytotoxic effects of degradation products released by the PLACL material were expected to result in an increase in cell death and/or a decrease in total cell number (migration) in the proximal compared to the distal region.

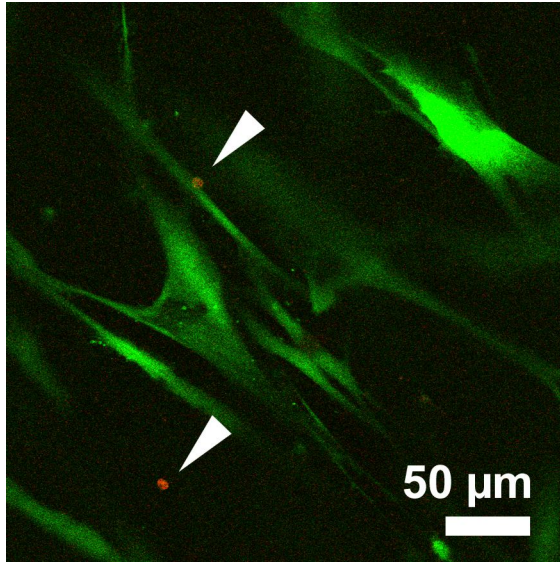


Figure 43 - Confocal fluorescence micrograph of CMFDA (live cells staining in green) and EH-1 (dead cell staining in red; white arrow heads) stained human dermal (foreskin) fibroblasts seeded within the bottom collagen component of a PLACL-based dermal equivalent. Image obtained 7 days after fabrication and static culture. Scale bar is shown at bottom right.

It was found that throughout the collagen gel fibroblasts with a bipolar spindle morphology characteristic for cultivation on stiff substrates were found (Figure 43). The percentage viable cells did not differ between collagen regions proximal and distal to the mesh (Figure 42b) suggesting that there were no (preferential) cytotoxic effects of (degradation products from) the PLACL mesh on cells over the 7 day culture period [90.0 ± 1.6 (SD) % vs. 90.0 ± 3.4 %, $t(10) = 0.209$, $p = 0.839$] (Figure 44a). The increase in the percentage of viable cells from 64% (direct post-compression; see above) to 90% (after a 7-day culture period) suggests that cells had proliferated. This is in line with the AB viability data (described above).

The distal and proximal region studied were 45 μm thick and partially overlapped each other (the basal collagen component was 70 μm thick). Therefore to assess the cell distribution, the number of live and dead cells in the proximal and distal region was standardised by dividing this number by the total combined number of cells counted in both regions. It was found that the standardised number of cells in the proximal region did not differ significantly from the distal region [48 ± 6.8 % vs. 52 ± 6.8 %, $t(10) = 1.069$, $p = 0.310$] (Figure 44b). This demonstrates that in the time period tested the cells

did not migrate away from the PLACL mesh due to toxic effects of the material or due to limitations in diffusion of nutrients through the collagen matrix to the cells.

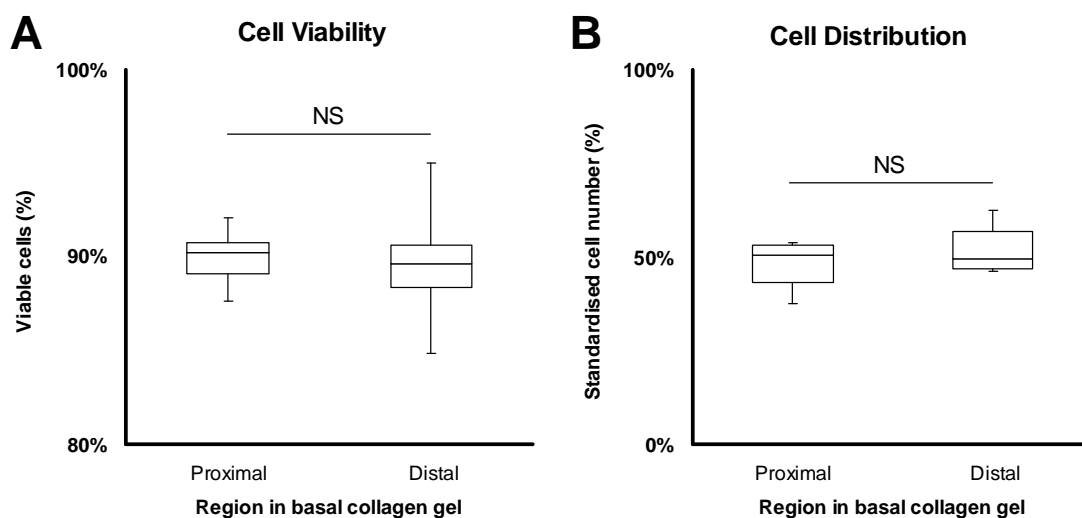


Figure 44 – Box-and-whisker plots. PLACL-collagen hybrid constructs, after seven days of static culture, showed no differences in (a) cell viability and (b) cell distribution between the collagen region at the collagen-PLACL interface (proximal) and the collagen region at the free interface (distal) (NS, not significant; values are for 6 samples).

The cell-seeded basal collagen component of a PLACL based dermal equivalent after a 7-day static culture period showed a uniform distribution of cells (both viable and dead) throughout the collagen demonstrating that no (significant levels of) toxic degradation products had formed and that the diffusion of nutrients was not impaired during the study period.

3.2.6 Effect of an aqueous medium on the PLACL and PLGA mesh

When statically culturing the cell seeded dermal equivalents in standard growth medium, it was observed that a subset (~40%) of the PLACL based constructs rolled up (Figure 45). Similar observations have previously been made with cell seeded PLGA

(Vicryl) meshes (Cooper *et al.*, 1991), but a similar experience was not found in the current series of experiments.

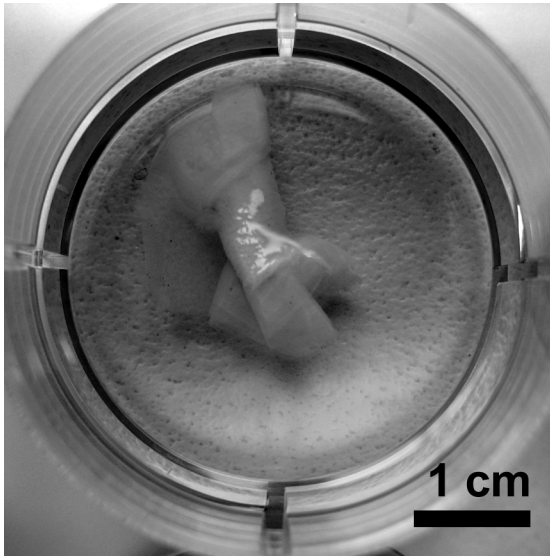


Figure 45 – Photograph. Contraction and rolling of the cell-seeded PLACL-compressed collagen hybrid construct under static *in vitro* culture conditions. Scale bar is shown at the bottom right corner.

To test if the deformation was the result of cell activity, the PLACL material (without the cell seeded collagen component) was incubated in a PBS buffer solution for 3 hours (at 37°C and neutral pH). As was found with the cultured cell seeded, collagen embedded meshes the PLACL material curled up (Figure 46a, b) demonstrating that this was a cell-independent, aqueous solution mediated effect.

The structure of the PLACL and PLGA material is useful for TE purposes. Its porous architecture allows for the diffusion of nutrients from the wound bed to the upper surface (before vascularisation occurs). A low porosity can impede diffusion but also accelerate polymer degradation (through autocatalytic processes) (Athanasίου *et al.*, 2007). Also the mesh structure is conducive to the prevention of wound contraction. Size retention over its implantation period is therefore essential.

To test if the aqueous solution mediated structural changes involved the size and porosity properties of the PLACL- and PLGA-material, measurements and imaging (digital photography, light microscopy, SEM; see Figure 46) were performed before and after incubation of PLACL and PLGA meshes in a PBS buffer solution for 3 hours (at 37°C and neutral pH).

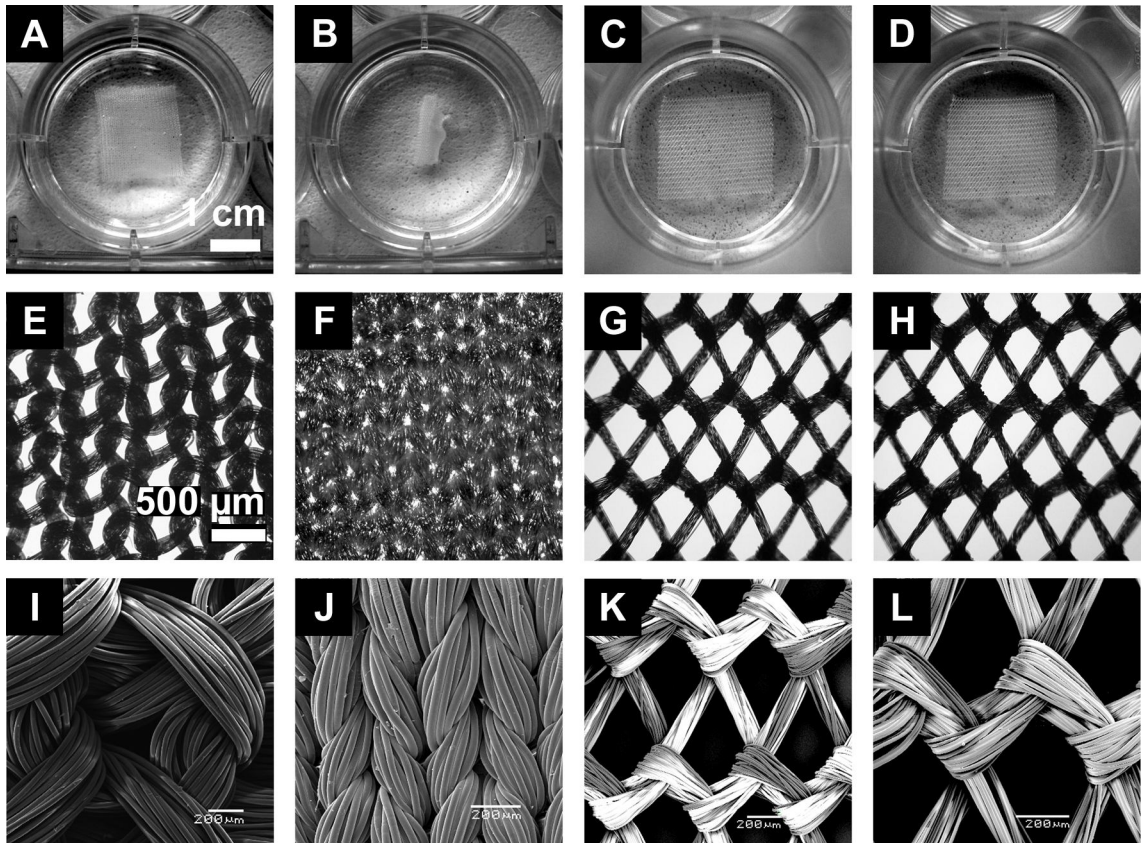


Figure 46 – (a-d) Photographs, (e-h) light micrographs, and (i-l) scanning electron micrographs showing the PLACL mesh before (a, e, i, c, g, k) and after (b, f, j, d, h, l) 3 hours of incubation in a buffer solution at 37 °C and neutral pH.

Macroscopically (a, b) contraction and deformation (curling) was observed, and at a microscopic level (e, f) a decrease in pore size and a tightening of the fibres was found (i, j).

Light microscopy (Figure 46e - h) revealed a 70% decrease in porosity for the PLACL mesh (defined as the ratio of the area of the voids and the total area) [from 15.8 ± 1.0 to 5.3 ± 0.8 (SD) %, $t(10) = 20.3$, $p < 0.001$] and no statistically significant difference for the PLGA mesh [$t(10) = 1.70$, $p = 0.119$] (Figure 47a). SEM analysis revealed a longitudinal shrinkage of the filaments in the PLACL mesh (Figure 46i, j) but no structural changes for the PLGA mesh (Figure 46k, l). Image analysis of photographs taken of the meshes revealed a 60% decrease in mesh surface area for the PLACL material [from 2.7 ± 0.2 to 1.1 ± 0.2 (SD) %, $t(10) = 14.4$, $p < 0.001$] and none for the PLGA mesh [$t(10) = 1.97$, $p = 0.077$] (Figure 47b).

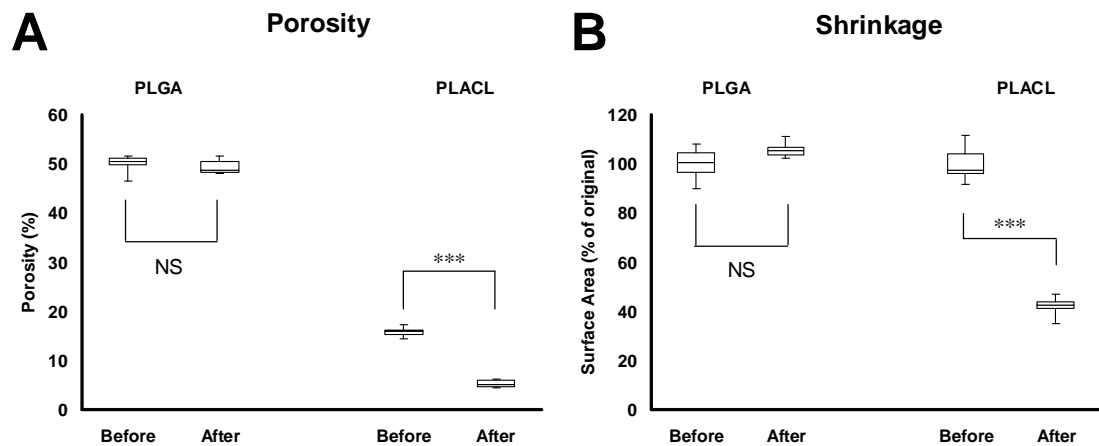


Figure 47 – Box-and-whisker plots. (a) The decrease in porosity and (b) mesh size of the PLACL mesh after exposure to an aqueous medium (NS, not significant; *, $p < 0.001$; values are for 6 samples).**

Under acellular and static conditions, aqueous media caused a longitudinal shortening of the yarns in the dense knit pattern of the PLACL-mesh resulting in rolling of the mesh and a 60% decrease in surface area and a 60% decrease in porosity. No significant structural changes of the PLGA-mesh were measured in the studied time period.

3.2.7 Keratinocyte-fibroblast co-culture in PLGA-CCHHs

To test if the PLGA-CCHH construct could be utilised for the fabrication of skin substitutes, rabbit derived keratinocytes and dermal fibroblasts were spatially layered on the surface and in the collagen component, respectively (Figure 21).

It was previously shown that (proliferating) keratinocytes positively influence epidermal regeneration in a dose dependent manner (Svensjo *et al.*, 2001). The aim was therefore to achieve the maximum density of cells on the available surface space in the shortest amount of time. The hypothesis under test was that a supernumerary number of cells could be seeded to achieve a confluent keratinocytes monolayer. It was previously established that it would require approximately 3 to 5 x 10⁵ keratinocytes per cm² to achieve confluence (Szabo *et al.*, /20).

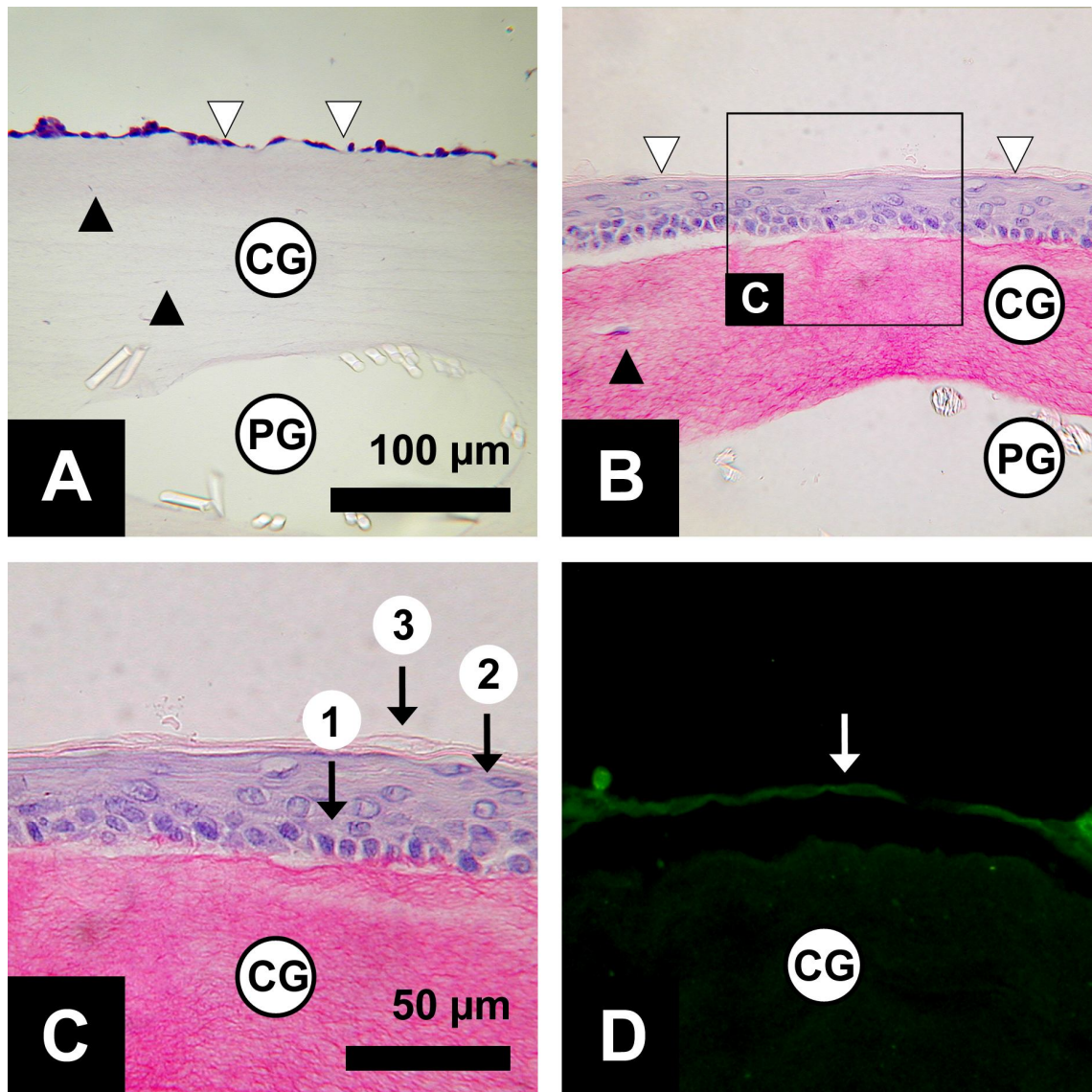


Figure 48 - Micrographs of haematoxylin-eosin stained reconstructed skin showing the PLGA-compressed collagen gel hybrid constructs with rabbit keratinocytes (white arrow heads) seeded on the surface of the apical collagen component (CG) (a) directly after cell seeding and (b) after 2 weeks of culture (PG, poly(lactide-co-glycolide) mesh). The region in the box is magnified (x2) in (c) showing that the rabbit dermal keratinocytes form a continuous and stratified epidermis with (1) cuboidal basal cells attached to the apical collagen component, (2) flattened suprabasal cells and (3) a stratum corneum. (d) Immunofluorescent staining of cytokeratins showing the epithelial origin of the formed epidermal tissue (arrow points to the stratum corneum).

Therefore an inoculum of 2.6×10^6 cells in 1 ml was statically seeded onto the surface of the top collagen compartment of the PLGA-based dermal equivalent (prepared as described above). After a 2-hour incubation period, it was determined from the Trypan Blue exclusion assay that 82 ± 7 (SD) % of the keratinocytes (values are for 18 samples) had attached to the collagen surface. This implied that keratinocytes were seeded at a density of 5 ± 0.4 (SD) $\times 10^5$ cells/cm² and histological observation revealed a near confluent distribution (Figure 48a).

To test if the PLGA dermal equivalent (n = 18 constructs) was suitable for maintenance and differentiation of keratinocytes at the air liquid interface, the keratinocyte seeded constructs were cultured for an additional 2-3 days submerged in growth medium (under static conditions) to achieve confluence (Figure 21a). The confluent keratinocyte monolayer was then raised to the air liquid interface to stratify the epidermis over a 2 week period (Figure 21b). The histological appearance of the reconstructed epidermis showed cuboidal basal cells attached to the apical collagen component, flattened suprabasal cells and a stratum corneum (Figure 48b, c). Cytokeratins expression could be detected in the epidermis layers by immunohistochemical staining showing the epithelial origin of the epidermal tissue formed (Figure 48d).

It was possible to achieve a (near) confluent monolayer of keratinocytes by static seeding of a supernumerary number of cells allowing for the creation of a living skin equivalent with a near confluent epidermal monolayer within three hours and with a stratified epidermis within three weeks. The latter finding proved that PLGA-CCHH was porous and thin enough to allow nutrient flow through the thickness of the construct from the basal to the apical surface.

3.3 Implantation study

The safety and efficacy of the skin equivalent (*i.e.* cell-seeded and acellular PLGA-CCHH) were tested in (a rabbit model of) an acute (excisional) full thickness (dorsal) skin defect.

To test if the wound healing benefit (in terms of improved outcome parameters) of a stratified (differentiated) epidermis over a monolayer epidermis warranted the extended (2 weeks) *in vitro* culture period of the skin equivalent, two conditions were tested: the skin equivalents were either implanted directly after fabrication without an *in vitro* culture period (*i.e.* UCs) or after 2 weeks of (*in vitro*) culture in which period the keratinocytes were allowed to differentiate to form a stratified epidermis (*i.e.* CCs).

Wound healing with the cell seeded skin equivalents was compared with that with ACs (PLGA-CCHH without cells) to differentiate between effects that result from the physical properties of the scaffold and those from the keratinocytes and fibroblast co-culture. Wounds that were left untreated (open defects) represented spontaneous wound healing and were used as (negative) controls. Lastly, FTSGs, the current gold standard for the treatment of full thickness defects, were used as (positive) controls.

The full thickness skin defects were created by excision of the dorsal skin (epidermis and dermis) of the rabbit up to (not including) the underlying panniculus carnosus muscle and the grafts were sutured in place by interrupted stitches and a single central quilting suture (Davenport *et al.*, 1988). The skin equivalents were easy to handle and suture; no delamination of the collagen from the PLGA mesh was observed during suturing.

It should be noted that (post-operatively) the grafts were covered with an occlusive dressing (Opsite) for the first period of implantation (Figure 24f) and that as fluid collected over the grafts underneath the Opsite, the dressings were removed after the first 3 days post-surgery. Animals were sacrificed and the wounds excised 1, 3 and 5 weeks after implantation of the skin equivalents.

Wounds were evaluated for the following outcome parameters: wound contraction, graft take, rate of epithelialisation, angiogenesis, adverse reactions directed against implanted

material (*i.e.* inflammation), and dermal scarring (or collagen maturation). Female rabbits were used as subjects into which male cell seeded skin equivalents were implanted to allow the differentiation of host cells from donor cells in tissue specimens. Additionally, in the clinical setting the use of allogeneic cells is attractive over autologous cells as it prevents a delay in treatment that would otherwise result from an *in vitro* culture period to achieve the necessary cell numbers required for a therapeutic effect.

3.3.1 Engraftment

Graft take is important if the skin equivalents are to have an extended effect on the wound healing process and is usually determined by (i) adherence of the graft to the wound bed, (ii) vascularisation and (iii) viability of the graft.

The FTSGs showed 'graft take', persisting inside the wound defect over the study period with adequate size retention of wounds (Figure 49). The FTSGs, post-implantation, showed a normal skin colour indicating adequate blood perfusion of the graft. Additionally, hair growth on the FTSGs was observed, indicating the hair follicles had survived the transplantation process. These findings show that the panniculus carnosus muscle provides an adequate wound bed for 'graft take' and permanent engraftment.

Untreated wounds showed progressive closure of the wound primarily by contraction resulting in a scar significantly smaller than the original defects size. No hair growth was noted with the newly formed connective tissue (Figure 49).

The skin equivalents showed progressive desiccation over time (Figure 49). Of the skin equivalents all the ACs remained *in situ* over the course of the experiment, whereas most of the cell seeded constructs were lost by the end of the experiment; this occurred faster with the cultured than with the UCs. Table 2 gives an overview of the number of grafts that were found *in situ* at each time point for each graft type.

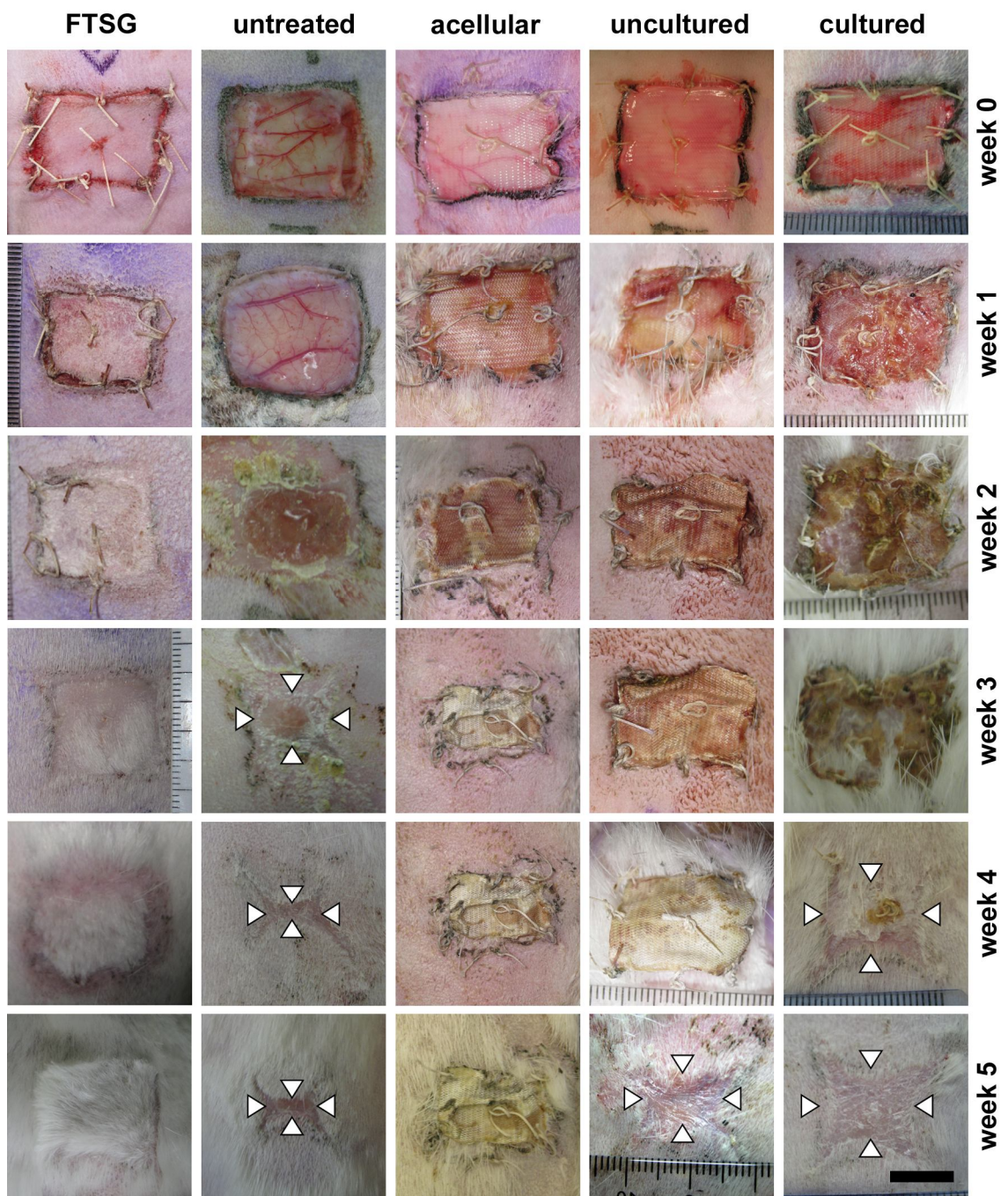


Figure 49 – Weekly, post-operative photographs of full thickness wound defects on the dorsum of a rabbit treated with full thickness skin grafts (FTSG), untreated, treated with acellular skin equivalents and uncultured and (2 week) cultured (cell seeded) skin equivalents (white arrow heads indicate the margins of the closed wound).

	week 1	week 2	week 3	week 4	week 5
FTSG	18/18	12/12	12/12	6/6	6/6
Acellular	18/18	12/12	12/12	6/6	6/6
Uncultured	18/18	12/12	12/12	6/6	1/6
Cultured	18/18	11/12	6/12	1/6	0/6

Table 2 - Number of grafts out of the initial number of grafts that were still found *in situ* at each time point (post-operatively). (FTSG, full thickness skin graft; acellular skin equivalents and cell-seeded uncultured and cultured skin equivalents).

Microscopic evaluation at low magnification of the H&E stained tissue cross-sections (Figure 50) revealed that after one week of implantation the skin equivalents could be seen in contact with the newly formed, underlying granulation tissue. At week 3 the construct was undermined by the complete regeneration of the epidermis resulting in the ejection of the skin equivalents from the wound bed.

At higher magnification (Figure 51) various degrees of integration with the underlying granulation could be seen for ACs in the first week after implantation. Minimal areas of take were observed in wounds treated with ACs showing incorporation of the basal collagen component (Figure 51a) and some instances of the mesh into the underlying granulation tissue (Figure 51b) with little inflammatory infiltration (of polymorphonuclear leukocytes) was observed. The cell seeded skin equivalents, however, showed a more marked inflammatory infiltration with no incorporation of the collagen or the mesh into the underlying wound (Figure 51b, c).

Therefore, in the first week there was partial take of the ACs, but all skin equivalents showed progressive desiccation with ultimately no permanent engraftment of either the AC or cell-seeded skin equivalents. By week 3, grafts were invariably undermined by epidermal regeneration ejecting the constructs from the wounds.

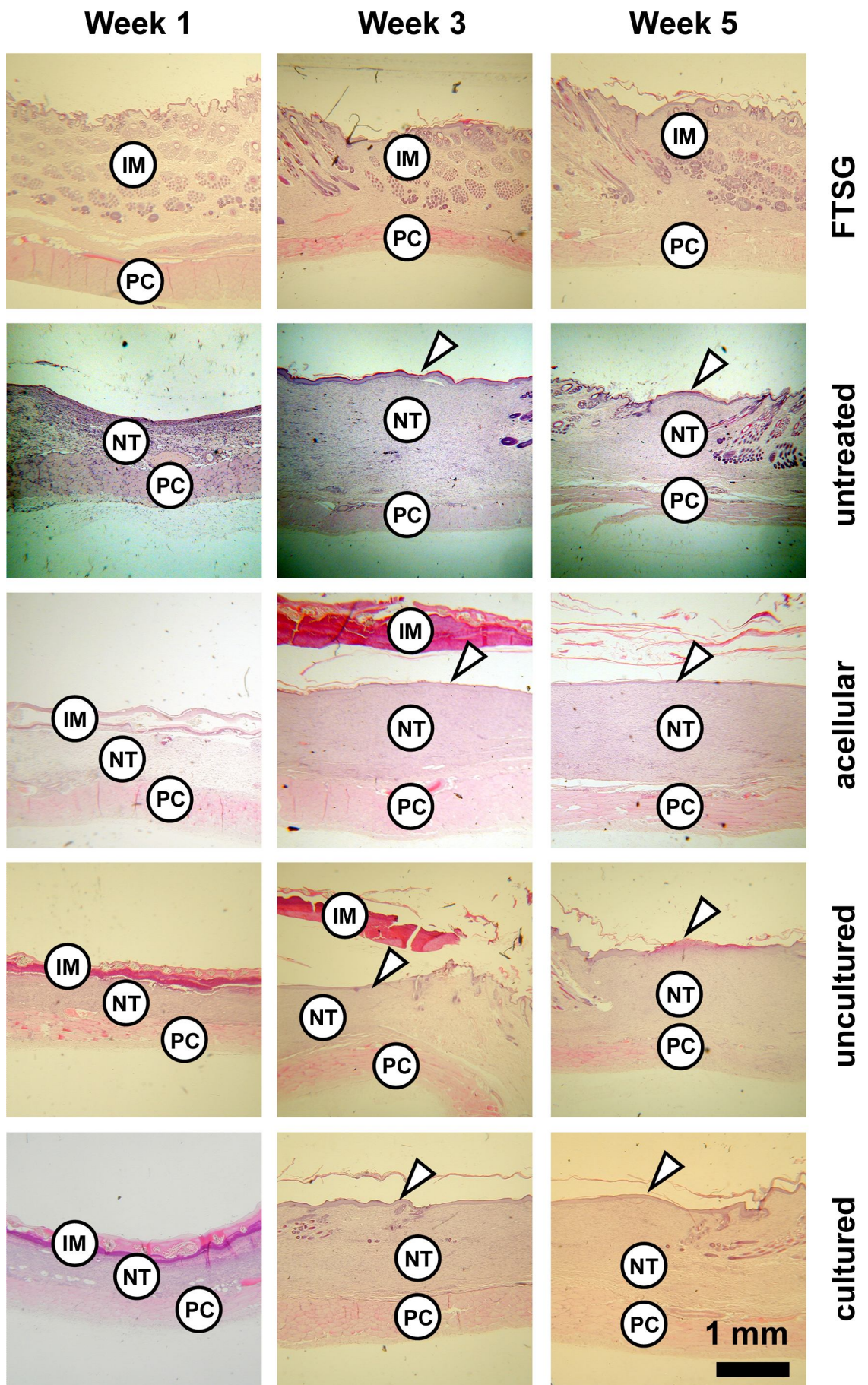


Figure 50 – Micrographs (magnification bar measures 1 mm) of haematoxylin and eosin stained tissue cross sections of rabbit, dorsal, full thickness wounds (1, 3 and 5 week post-injury) treated with full thickness skin grafts (FTSG), untreated, treated with acellular skin equivalents and uncultured and (2 week) cultured (cell seeded) skin equivalents (IM, implant; PC, panniculus carnosus muscle; NT, newly formed connective tissue; white arrow head shows epidermal regeneration).

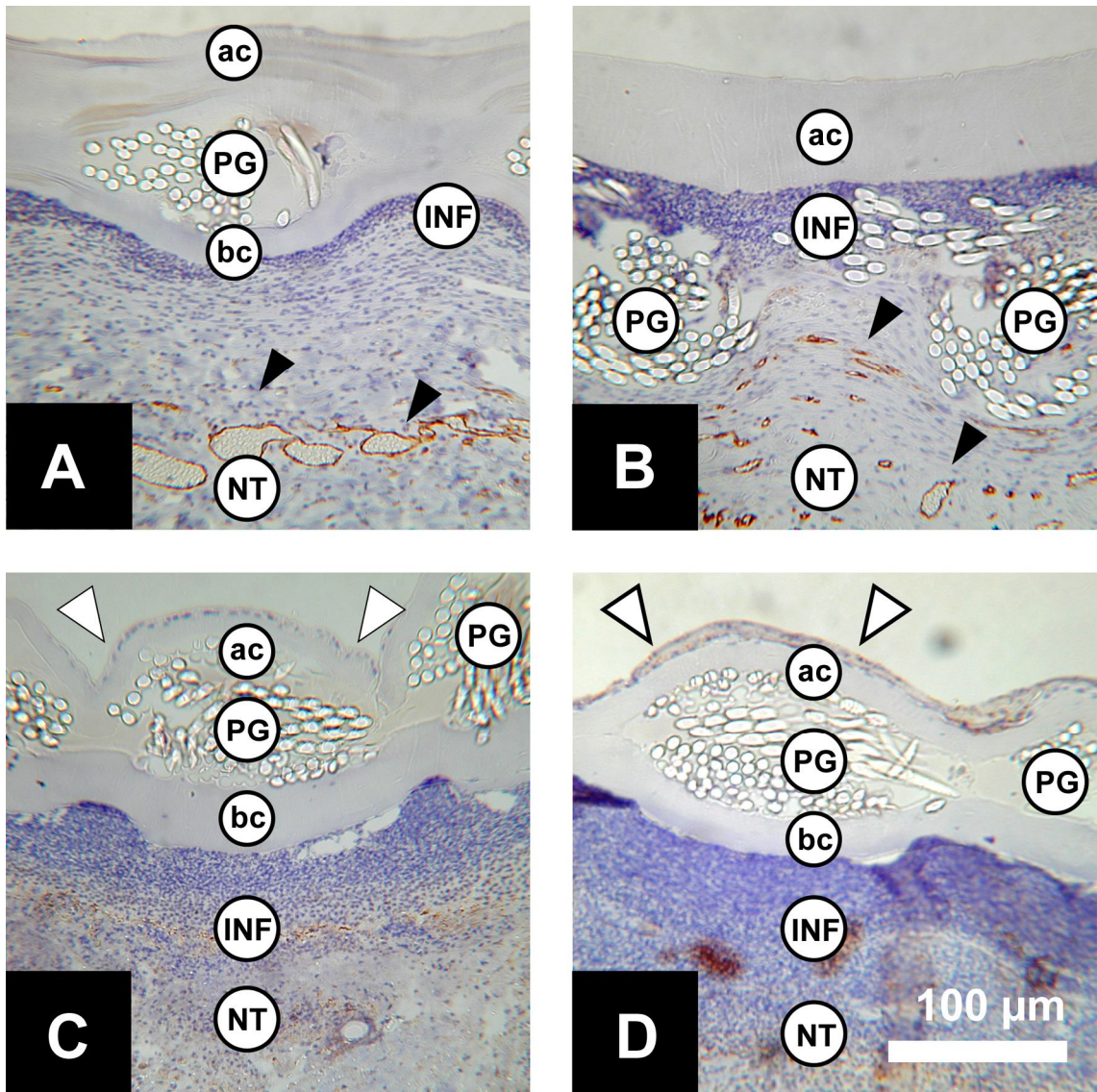


Figure 51 – Micrographs of the interface between the implant and the wound bed in full thickness skin defects one week after implantation (staining with CD31 antibody for endothelial cells and haematoxylin counterstaining). Full thickness defect treated with acellular skin equivalents show partial integration of (a) the basal collagen component (bc) and (b) PLGA-mesh (PG) (of the PLGA-compressed collagen hybrid material) into the underlying granulation tissue. The

inflammatory infiltration (INF) was more marked in wounds treated with (c) uncultured and (d) cultured (cell seeded) skin equivalents than in wounds treated with the acellular constructs (ac, apical collagen component; black arrow heads point to CD31+ blood vessels; white arrow heads point to the *in vitro* formed epidermal layer on top of the apical collagen component of the skin equivalent).

3.3.2 Wound contraction

Although the skin equivalents showed no permanent engraftment the size of the wounds at inspection appeared to be larger than of those that were left untreated (Figure 49).

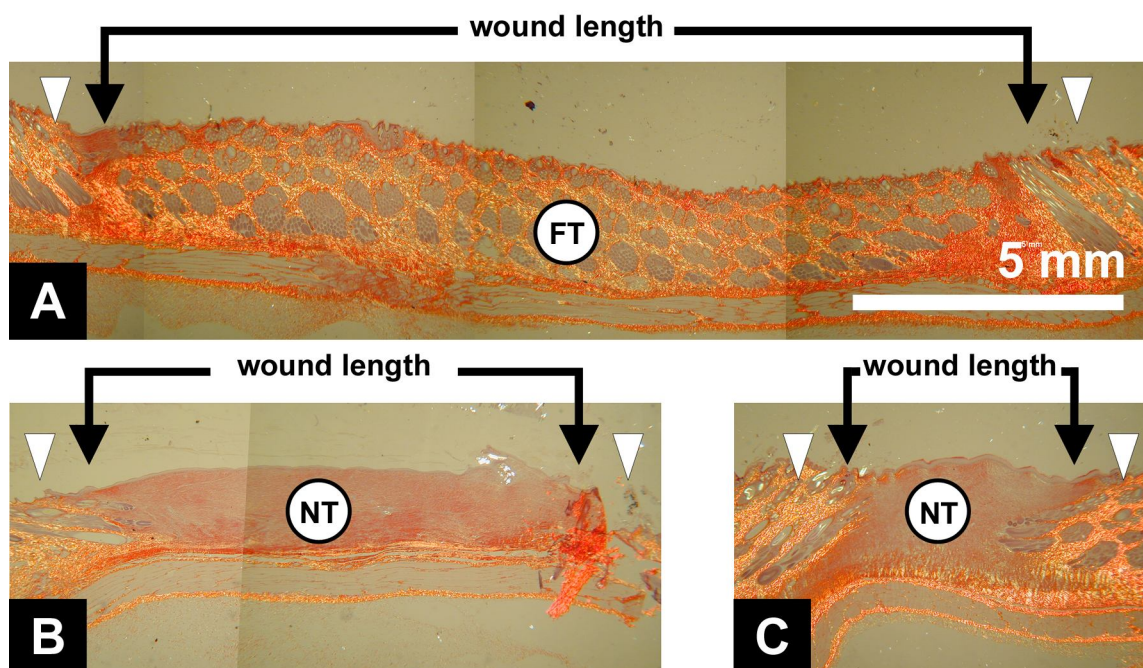


Figure 52 – Polarised light micrographs of picrosirius stained tissue sections showing the wound length of full thickness skin defects at five weeks after implantation of (a) full thickness skin graft (FT; scale bar is shown at the bottom right corner), and (b) a skin equivalent (here no longer *in situ*) and after (c) no treatment (white arrow heads point to unwounded skin; NT, newly formed connective tissue).

To test if the skin equivalents indeed prevented wound contraction the length of the wounds were measured in samples harvested 1, 3 and 5 weeks after implantation and compared to the original wound length (measured on the day of surgery). Measurements

were taken from histological transverse cross sections as over the experiment the wound margins moved underneath the skin equivalents, preventing the direct measurement of the wound area.

The percentage size retention of the wound area was determined, as a measure of the prevention of wound contraction, by dividing the wound length, measured in tissue sections from the wound samples obtained at each time point (Figure 52) by the original wound length (obtained directly after implantation on the day of surgery).

The wound length was measured as the distance between hair follicles as no hair growth occurred in the newly formed connective tissue. Results were compared to wounds treated with FTSGs, the gold standard, and to wounds left untreated.

A two-way RM-ANOVA was conducted on the percentage retention of wound area. The data for the three skin equivalents (AC, UC, and CC) did not differ between them and the data were therefore pooled into a single 'hybrid construct' group and compared to the FTSG and 'no treatment' group. The independent variables therefore included two between-groups factors, treatment, three levels ('hybrid construct', FTSG, NT) and time with three levels (1, 3 and 5 weeks).

A significant main effect of graft type on the postoperative wound size was observed, $F(2, 6) = 9.3, p = 0.014$. *Post hoc* (Tukey HSD) simple effects analysis revealed that wounds treated with FTSGs ($M = 95.6\%$, $SD = 13.8\%$) were on average significantly larger in size than NT wounds ($M = 50.8\%$, $SD = 37.1\%$) showing better retention of the wound area. Wounds treated with the skin equivalents ($M = 72.0\%$, $SD = 30.0\%$) showed a marginally significant greater size retention than NT wounds; ($p = 0.071$) (Figure 53). Further, a significant main effect of time on the postoperative wound size was found, $F(2, 6) = 18, p = 0.003$, such that the wound size decreased over time for all groups. Simple effects analysis revealed that only the decrease between week 1 ($M = 105.2\%$, $SD = 9.0\%$) and week 3 ($M = 64.2\%$, $SD = 24.1\%$) was statistically significant ($p = 0.005$). No significant interaction effects were found between treatment and time, $F(4, 6) = 2.4, p = 0.164$.

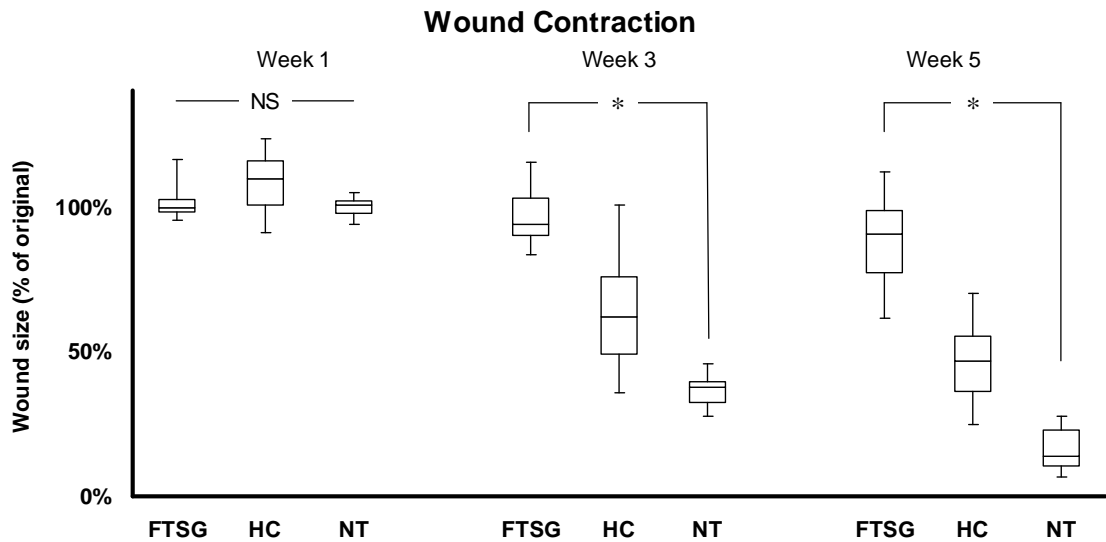


Figure 53 – Box and whisker plots showing the effect of full thickness skin grafts (FTSG), (acellular and cell seeded) hybrid constructs (HC) and ‘no treatment’ (NT) on post-operative wound size after 1, 3 and 5 weeks (NS, not significant; *, $p < 0.05$).

The gold standard the FTSG results show that wounds contracted despite treatment with FTSGs and the PLGA-CCHs and that FTSGs were able to delay contraction. Although there was no permanent engraftment of the skin equivalents the treated wounds showed after five weeks 55% wound contraction compared to the 84% of untreated wounds and to the 12% of FTSGs grafted wounds.

3.3.3 Inflammatory response to allogeneic cell therapy

In the clinical setting, the main advantage of allogeneic over autologous cell therapy is that a sufficient number of cells can be made available without delaying treatment. However, a disadvantage is that an increased inflammatory response could result, leading to graft rejection, although it has previously been shown that allogeneic cells lose their immunogenicity following serial passages (Theobald *et al.*, 1993).

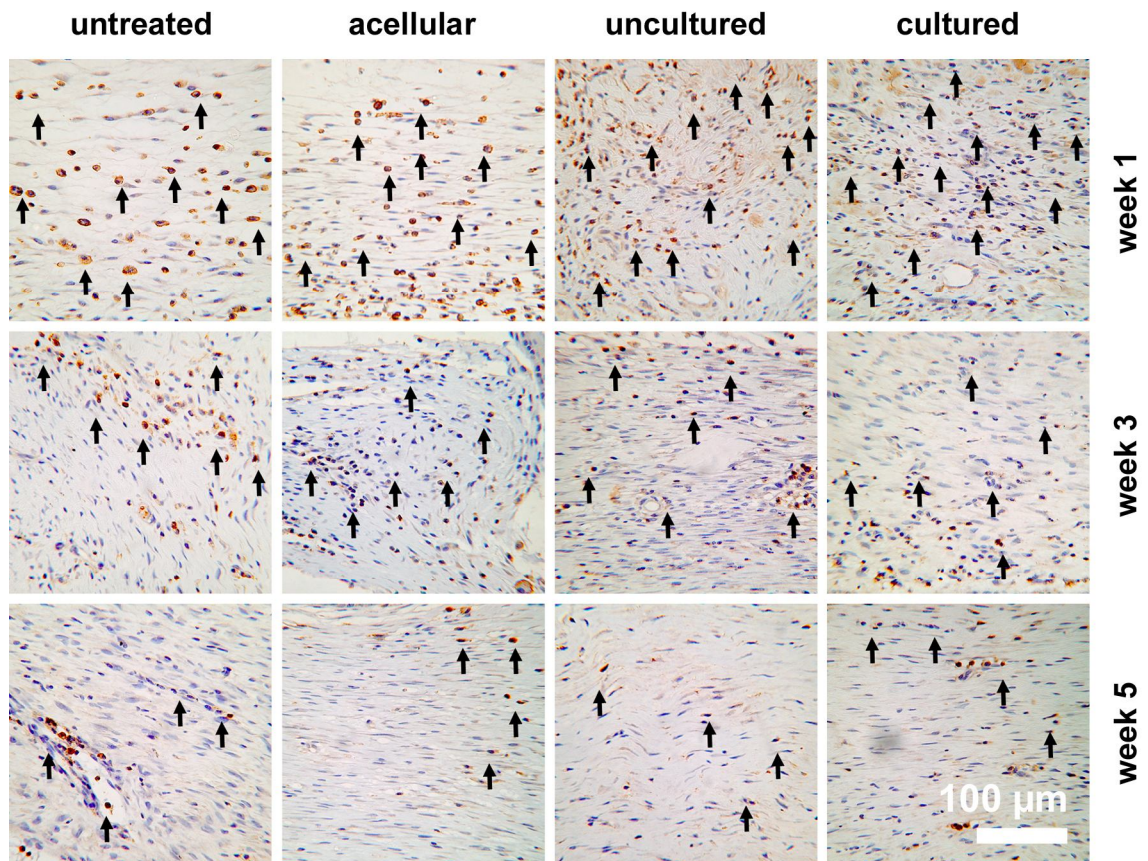


Figure 54 – Immunohistochemical detection of CD45+ cells (black arrows) within the newly formed connective tissue for the different treatment groups at weeks 1, 3 and 5 (DAB visualisation and haematoxylin counterstain; magnification bar measures 100 μm).

In the first week, an apparently larger inflammatory infiltration was found in wounds treated with ACs than in wounds treated with allogeneic cell-seeded skin equivalents. This could in part explain that ACs showed integration into the underlying wound bed, whereas the cell seeded constructs did not (Figure 51). To quantify the inflammatory response to the allogeneic cell-seeded skin equivalents the percentage CD45+ cells (*i.e.*

leukocytes) of the total number of (nucleus containing) cells within the wound bed was determined by CD45 antibody staining and haematoxylin (nuclear stain) counterstaining (Figure 54). The inflammatory response was determined in tissue sections from wound samples taken 1, 3 and 5 weeks after implantation and the results were compared to wounds in which no cells were introduced (*i.e.* NT and AC group).

For the interpretation of the results it should be noted that adult male rabbit keratinocytes (second passage) and dermal fibroblasts (third to fifth passage) were used and that the skin equivalents were cultured in serum free growth medium and were washed (with 0.9% saline) before implantation.

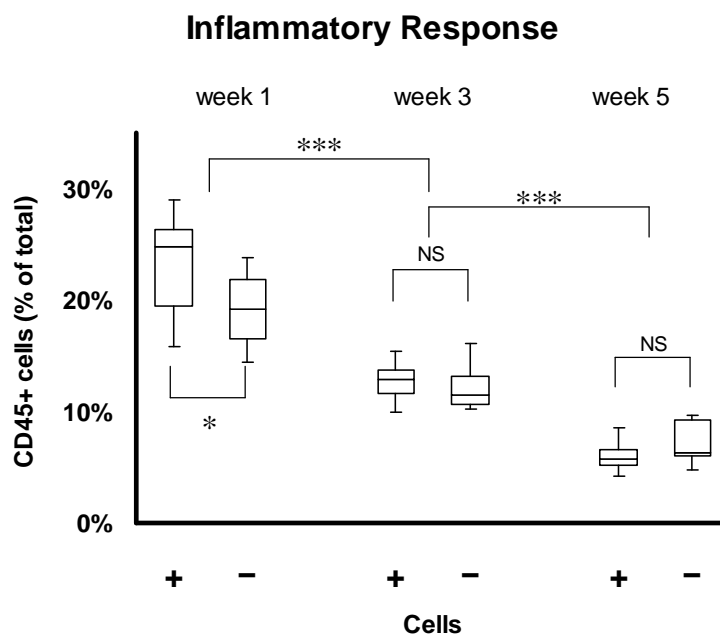


Figure 55 - Box and whisker plots for the percentage CD45+ cells at each time point for each treatment condition. (c) Box and whisker plots for the percentage CD45+ cells comparing the effect of the presence (+) or absence (-) of (allogeneic) cells in the defects at each time point (*, $p < 0.001$; *, $p < 0.05$; NS, not significant).**

An RM-ANOVA was conducted on the determined percentage CD45+ cells. As there was no difference between the UC and CC group and between the AC and NT group the data were pooled into a cellular (UC, CC) and 'no cells' group (AC, NT). The

independent variables therefore included two between-groups variables, treatment, with two levels (cells, no cells) and time with three levels (1, 3 and 5 weeks).

A significant main effect of treatment was found, $F(1, 6) = 8.0, p = 0.03$ such that the average leukocyte count was higher in allogeneic cell treated wounds ($M = 14.1\%$, $SD = 8\%$) than in wounds where no cells were introduced ($M = 12.8\%$, $SD = 5\%$; Figure 55). There was a significant main effect of time, $F(2, 6) = 75.8, p < 0.001$; for both groups the percentage of leukocytes decreased with time. A Tukey HSD *post hoc* simple effects analysis of time revealed that the average percentage of CD45+ cells at week 1 ($M = 21\%$, $SD = 4.4\%$) was significantly greater than week 3 ($M = 13\%$, $SD = 1.8\%$; $p < 0.001$) and at week 3 significantly greater than week 5 ($M = 7\%$, $SD = 1.7\%$; $p < 0.001$). Additionally, a significant interaction effect was found between allogeneic cell therapy and time, $F(2, 6) = 14.2, p = 0.005$, showing that the allogeneic cell-induced increased immune response was time depended. Simple effects analyses showed that only the difference in inflammatory response in the first week between wounds treated with allogeneic cells ($M = 23\%$, $SD = 4\%$) and 'no cells' ($M = 19\%$, $SD = 4\%$) was significant, $F(1, 2) = 24.1, p = 0.039$.

Wounds treated with the allogeneic cell seeded PLGA based skin equivalents showed a higher immunologic reaction in the acute healing phase (week 1) compared to untreated defects or treated with ACs.

3.3.4 New connective tissue formation

The formation of new connective tissue is important to replace lost tissue and to close the wound. The formation of an inadequate amount may result in incomplete wound closure or at later stages in wound dehiscence (Irvin and Hunt, 1974). An overabundance of granulation tissue on the other hand could give rise to hypertrophic scars and scar contracture (Rockwell *et al.*, 1989). To study the effects of the skin equivalents on the formation of new connective tissue in the full thickness skin defects, the thickness and the cross sectional area of the newly formed connective tissue was measured in H&E stained sections (Figure 26) of wound samples obtained 1, 3 and 5 weeks after implantation of the skin equivalents.

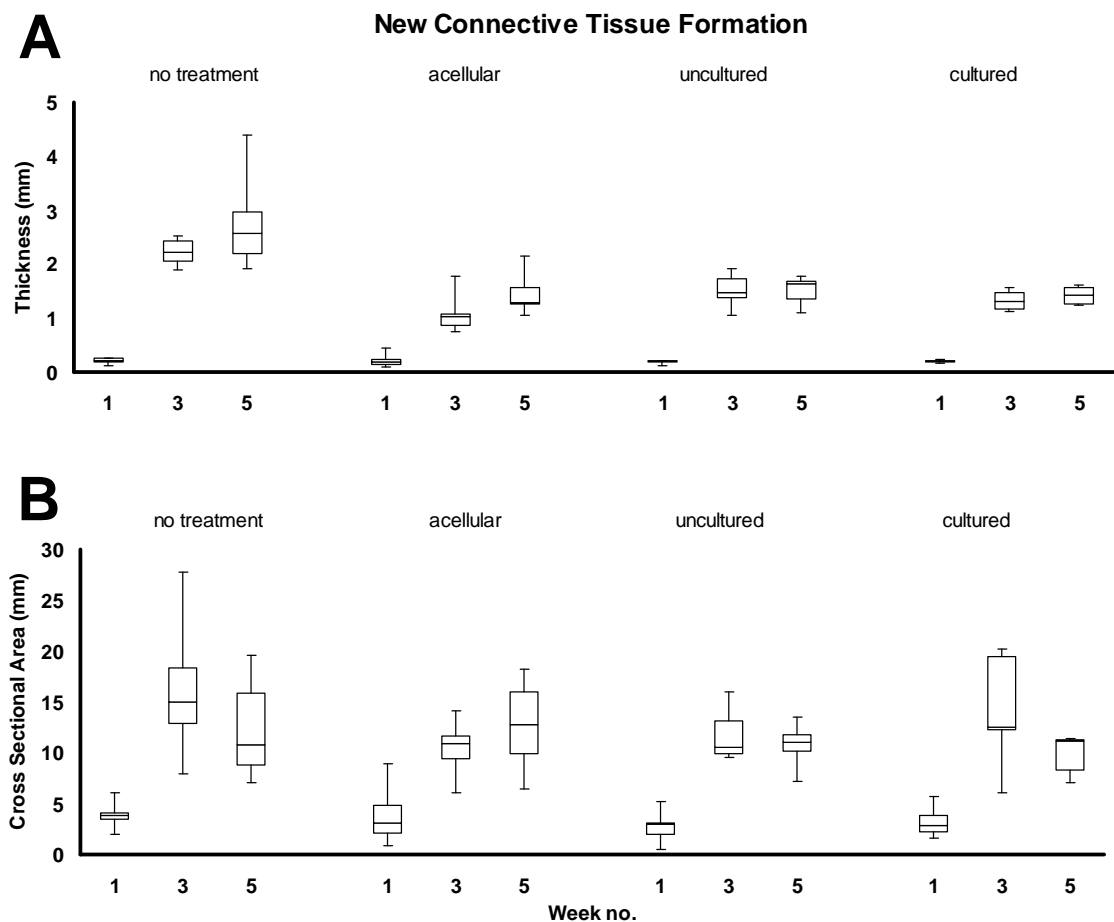


Figure 56 – Box and whisker plots for the average thickness of newly formed connective tissue in full thickness wounds untreated (open defects, ‘no treatment’) and treated with acellular and uncultured and cultured cell seeded skin equivalents for three time points post-wounding.

A two-way RM-ANOVA was conducted on the average thickness of the newly formed connective tissue. The thickness did not differ between the three skin equivalents (Figure 56) and the data were therefore pooled into a single ‘skin equivalent’ group and compared to the ‘no treatment’ group (Figure 57). The independent variables therefore included two between-groups factors, treatment with two levels (no treatment, skin equivalents) and time with three levels (1, 3 and 5 weeks).

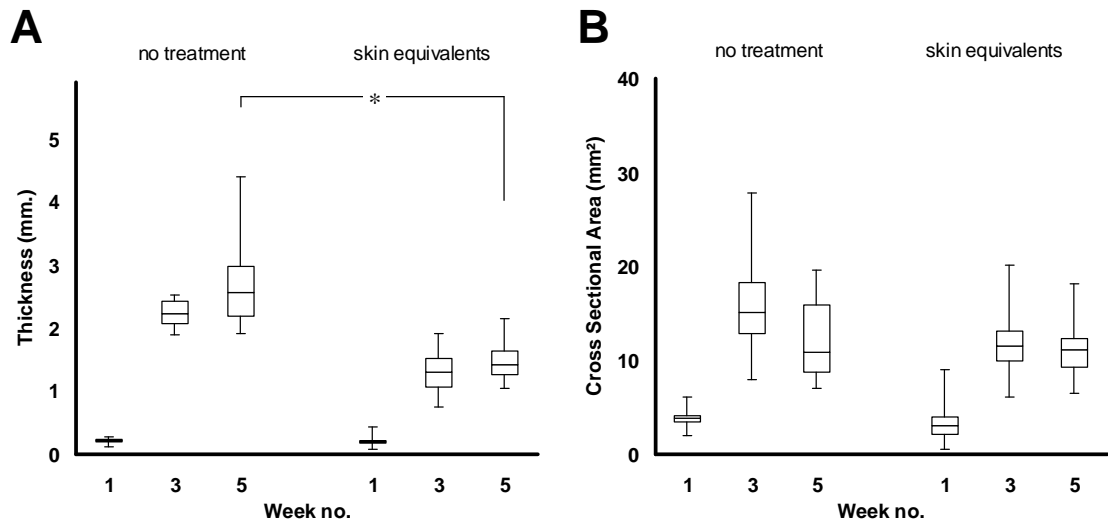


Figure 57 – The effect of wound grafting of full thickness skin defects with the PLGA-collagen hybrid construct on (a) the cross sectional area and (b) thickness of the newly formed connective tissue compared to open defects or no treatment (*, $p < 0.05$).

A significant main effect of treatment on the average thickness of the newly formed connective tissue was found, $F(1, 6) = 77, p < 0.001$, such that the connective tissue was thicker in wounds in the ‘no treatment’ group ($M = 1.74, SD = 1.24$ mm) than in wounds treated with the skin equivalents ($M = 0.99, SD = 0.62$ mm) ($p < 0.001$). A significant main effect of time on the average thickness was observed, $F(2, 6) = 188, p < 0.001$; the connective tissue increased in thickness with time in all groups. Both the increase in thickness from week 1 ($M = 0.2, SD = 0.07$ mm) to week 3 ($M = 1.8, SD = 0.62$ mm) ($p < 0.001$) and from week 3 to week 5 ($M = 2.1, SD = 0.62$ mm) ($p < 0.001$) were statistically significant. Additionally, a significant interaction effect was found between grafting and time, $F(2, 6) = 20.2, p = 0.002$, indicating that the effect of treatment on connective tissue thickness increased with time. Simple effects analyses revealed that the thickness of the connective tissue in untreated wounds ($M = 2.77, SD =$

0.90 mm) was (47%) larger than grafted wounds in week 5 ($M = 1.46$, $SD = 0.28$ mm) respectively, $F(1, 2) = 476$, $p = 0.002$ (Figure 57a). The difference between ungrafted (NT; $M = 2.23$, $SD = 0.25$ mm) and grafted ($M = 1.30$, $SD = 0.33$ mm) wounds in week 3 was only marginally significant, $F(1, 2) = 13.8$, $p = 0.065$.

A two-way RM-ANOVA was conducted on the cross sectional area of the newly formed connective tissue. The three skin equivalents were again pooled into a single 'skin equivalent' group and compared to the 'no treatment' group. The independent variables therefore included two between-groups factors, treatment with two levels (skin equivalents, no treatment) and time with three levels (1, 3 and 5 weeks).

No significant main effect of treatment on the total cross sectional area of the newly formed connective tissue was found, $F(1, 6) = 0.251$, $p = 0.635$, indicating that there was no difference in the amount of connective tissue formed in construct treated and untreated wounds. No significant main effect of time on the cross sectional area was observed, $F(2, 6) = 1.082$, $p = 0.397$. Additionally, no significant interaction effect was found between grafting and time, $F(2, 6) = 1.118$, $p = 0.387$ (Figure 57b).

Although the initial thickness data suggested that less connective tissue was formed in construct treated than in untreated wounds the measurements of the cross-sectional area showed that this was not the case. The apparent difference seems to be the result of the same amount of granulation tissue spread over a different wound length in treated wounds and untreated wounds (Figure 52).

The connective tissue formed within full thickness wounds not only fills the wound defect but is also a source of force generation that helps to approximate the wound margins, decreasing the wound area requiring to be reepithelialised. To test the relationship between the amount of connective tissue and the wound size in this study a correlational analysis was conducted on the thickness of the newly formed connective tissue and the wound length (determined in tissue samples obtained at 1, 3 and 5 weeks after surgery) of untreated defects and defects treated with the skin equivalents.

It was found that the amount of newly formed connective tissue was significantly related to the wound size. The thickness of the newly formed connective tissue showed

a strong negative correlation (Pearson correlation coefficient (r) = -0.67, $p < 0.001$) with the size of the wound (Figure 58), such that as the amount of newly formed connective increases the wound size decreases. Of the variation in wound size 45% (0.67^2) could be explained by the amount of connective tissue formed.

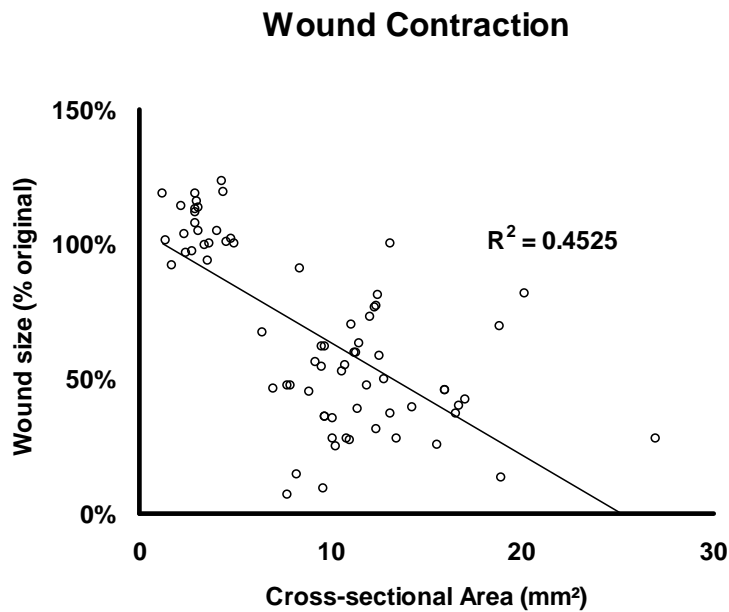


Figure 58 – Correlation between cross sectional area of the connective tissue newly formed in full-thickness skin defects and the wound size (*, $p < 0.002$).

There is therefore a significant relationship between the wound size and the amount of granulation tissue formation. This data suggest that the reduction in wound size is (at least in part) brought about by granulation tissue formation.

3.3.5 Collagen content of the newly formed connective tissue

The ECM of the newly formed connective tissue consists of collagens, proteoglycans and glycoproteins. It is primarily believed that the collagen content is directly responsible for the wound's UTS (Doillon *et al.*, 1985a) and a disturbance to the balance between collagen deposition, degradation and remodelling may result in defective wound healing. To study the maturation of collagen within newly formed connective tissue polarised light microscopy was used to analyse the birefringence of collagen fibrils stained with picrosirius red.

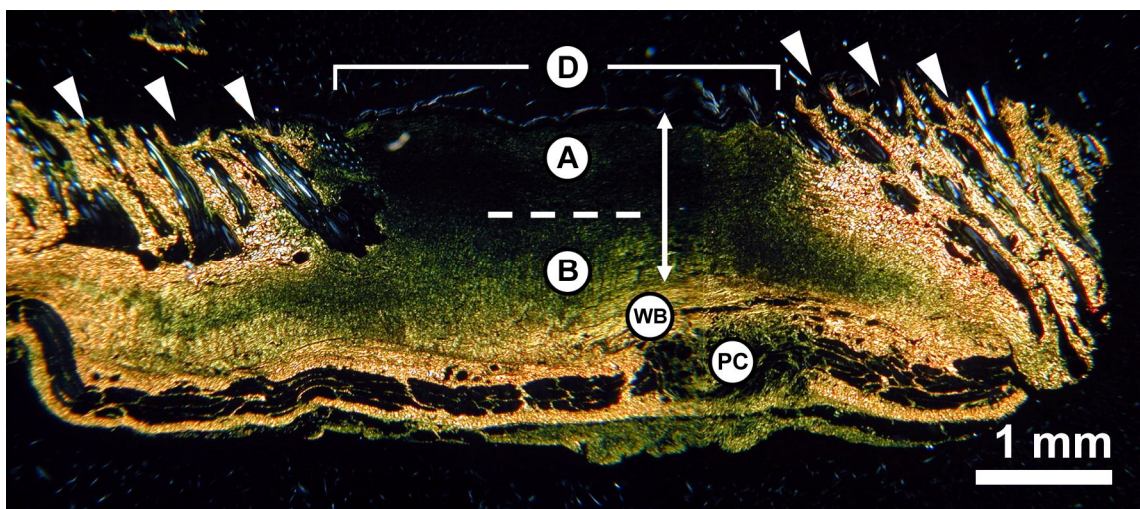


Figure 59 – Micrograph visualising the birefringence of a picrosirius stained tissue section of a full thickness skin defect 3 weeks after injury. Central, the full thickness defect (d) can be seen bordered by hair follicles (white arrow heads) and extending from the epidermis to the original wound bed (wb) (between white arrows). Within the defect a new connective tissue has been deposited in which two distinct regions can be seen; an apical region (a) and a basal region (b). (pc, panniculus carnosus muscle).

Birefringence is the capacity of a material to change the polarisation state of light. This can be visualised as the appearance (state change) and change in colour (determined by the induced phase retardation and interference) of polychromatic light transmitted through the specimen seated between two polarising filters that have their transmission axes set at right angles to each other. It has been found that during wound remodelling the birefringence of collagenous tissues changes and this is mainly attributed to a closer

packing of the collagen fibrils (Doillon *et al.*, 1985b). To test if the skin equivalents had a promoting effect on the increase in collagen content in the connective tissue newly formed within the full thickness defects the change in birefringence was quantified in picrosirius stained tissue sections.

Tissue sections from 1, 3 and 5 week old wounds were stained with picrosirius red to enhance the natural birefringence of the collagen molecules. At microscopic inspection a gradient in the amount and in the hues of the birefringent material could be observed within the newly formed connective tissue and two distinct regions could be distinguished; an apical and a basal region (Figure 59).

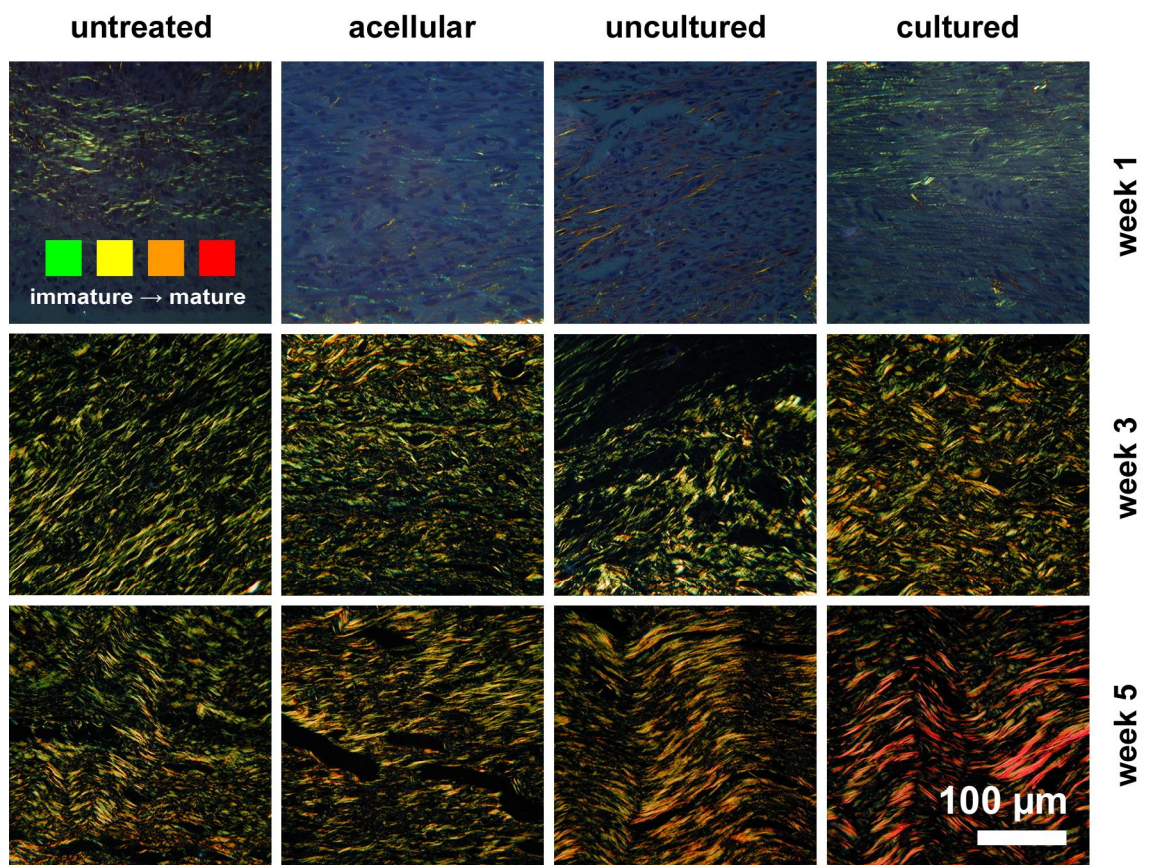


Figure 60 – Picrosirius red stained, newly formed connective tissue in full thickness wounds viewed under a linearly polarising light microscope showing the change in amount of collagen and their interference colours over time and between treatment groups. The colour chart indicates the hues for immature to mature collagen fibrils, scale bar is shown at the bottom right corner.

Per tissue section the amount of birefringent material (as a percentage of the total measured tissue area) was quantified in up to ten photographed fields of view (polarised light microscope; 20x objective) of randomly selected areas in the apical and basal regions of the newly formed connective tissue. To quantify the percentage amount of birefringent material within the digital photographs the number of pixels with the (wave lengths or) hues associated (Rich and Whittaker, 2005) with birefringence (green, yellow, orange and red; Figure 28) were counted and divided by the number of pixels of the total tissue area.

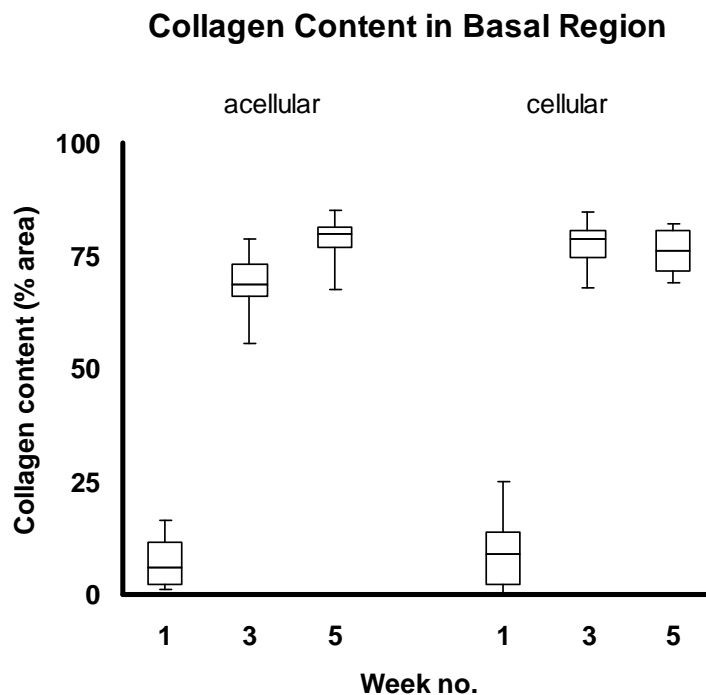


Figure 61 - Box and whisker plot for the collagen content (from the percentage birefringent material per tissue area) in the basal region of the newly formed connective tissue showing the effect of cell therapy on the amount of collagen in the apical regions of the newly formed tissue.

No differences were found in the percentage birefringent material per tissue area between UC and CC group and between AC and NT group the data were pooled in 'acellular' (AC, NT) and 'cellular' (UC, CC) treatment groups (Figure 60).

A two-way RM-ANOVA was conducted on the percentage birefringent material per tissue area in the apical and basal regions of the newly formed connective tissue. The

independent variables included two between-groups factors, treatment, two levels ('acellular' and 'cellular' groups) and time with three levels (1, 3 and 5 weeks).

In the basal region of the newly formed connective tissue no significant main effect of treatment on the amount of birefringent material was found, $F(1, 6) = 1.5, p = 0.266$; indicating that there were no differences in the collagen content between cellular and acellular treatments. There was a significant main effect of time on the amount of birefringent material in the newly formed connective tissue, $F(2, 6) = 414, p < 0.001$; the collagen content increased over time for both groups. The collagen content increased 9-fold from week 1 ($M = 8.3\%, SD = 6.4\%$) to week 3 ($M = 73.3\%, SD = 7.4\%$) ($p < 0.001$) and did not change from week 3 to week 5 ($M = 77.2\%, SD = 4.9\%$) ($p = 0.569$). Additionally, no significant interaction effect between treatment and time was observed, $F(2, 6) = 2.37, p = 0.174$ (Figure 61).

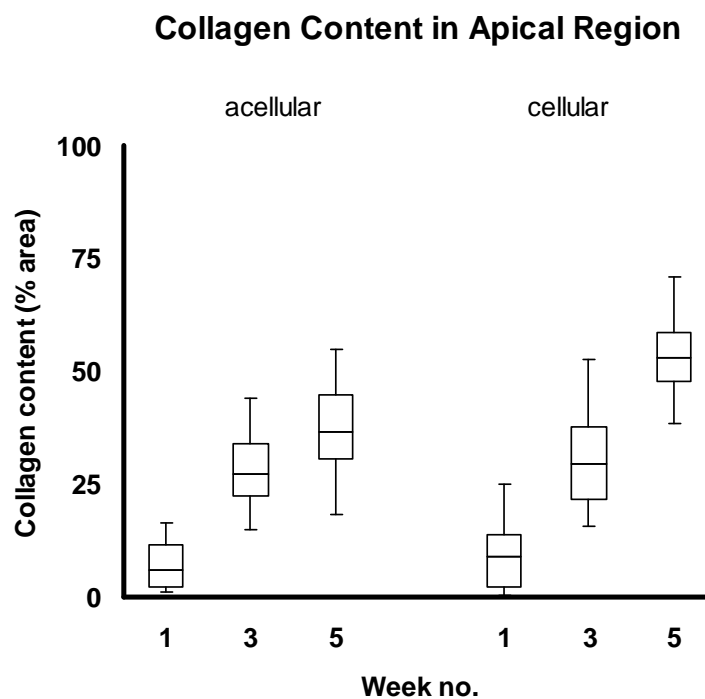


Figure 62 - Box and whisker plot for the collagen content (measured by the percentage increase of birefringent material per field of view) showing the effect of cell therapy on the amount of collagen in the apical regions of the newly formed tissue.

In the apical region of the newly formed connective tissue a marginally significant main effect of treatment on the amount of birefringent material was found, $F(1, 6) = 4.9$, $p = 0.069$; the collagen content of wounds was higher in the cellular ($M = 31.3\%$, $SD = 20.9\%$) than in the acellular treatment group ($M = 24.7\%$, $SD = 15.6\%$). There was a significant main effect of time on the amount of birefringent material in the newly formed connective tissue, $F(2, 6) = 54.0$, $p < 0.001$. The collagen content increased over time for both groups. The collagen content increased 4-fold from week 1 ($M = 8.3\%$, $SD = 6.4\%$) to week 3 ($M = 29.9\%$, $SD = 10.6\%$) ($p = 0.003$) and 1.5-fold from week 3 to week 5 ($M = 45.7\%$, $SD = 13.3\%$) ($p = 0.014$) were statistically significant. Additionally, no significant interaction effect between treatment and time was observed, $F(2, 6) = 2.73$, $p = 0.144$ (Figure 62).

Regardless of the wound treatment the birefringent material content as a measure of collagen content in the newly formed connective tissue in the skin defects increased more rapidly in the (deeper) basal regions where it reached an apparent maximum three weeks post-injury whereas the collagen content in the (more superficial) apical regions continued to increase up to five weeks (post-injury) at which time it still had not yet reached the level measured in the basal regions at week 3. Only a late (week 5) and marginally significant increase in collagen content could be found in the apical region of wounds treated with UCs and CCs. That this effect occurred only after 5 weeks could be due to the apparent lag in the increase in collagen content between the apical and basal regions. Also any possible effects of the skin equivalents on the collagen content in the basal regions could have been obscured as an apparent maximum had been reached by week 3.

3.3.6 Collagen maturation

Not only the increase in collagen content but also the increase in fibril diameter that occurs with collagen maturation is important for the UTS of the wound (Doillon *et al.*, 1985a). Collagen maturation can be detected by picosirius red staining and observation under polarised light microscopy. Due to the birefringent properties of the collagen molecule, a light beam passing through a collagen fibril will give rise to specific interference colours (or hues) depending on the diameter of the fibril (Doillon *et al.*, 1985b). Thinner (more immature collagen) fibrils will light up in green and yellow hues whereas thicker (more mature collagen) fibrils will show orange and red hues (Figure 60).

It has previously been shown that transplanted autologous fibroblasts improve collagen maturation in a dose dependent manner (Lamme *et al.*, 2000). To test if the skin equivalents had a promoting effect on collagen maturation in the newly formed connective tissue of the full thickness skin defects, the ratio of thick to thin collagen fibres was determined in picosirius red stained tissue sections viewed in a polarised light microscope. An increase in the thick to thin ratio would suggest an increase in collagen maturation. Per tissue section the area of the individual interference colours (as a percentage of the total measured tissue area) was quantified in up to ten photographed fields of view (20x objective) of randomly selected areas in the apical and basal regions of the newly formed connective tissue. To determine the ratio of thick to thin fibres the percentage area taken up by the interference colours (hues) associated with thick fibres (orange, red) was divided by the percentage area of the interference colours associated with thin fibres (yellow, green).

A two-way RM-ANOVA was conducted on the ratio of thick collagen fibres in the apical and basal regions of the newly formed connective tissue. There was no difference between the AC and NT group and the data were therefore pooled into one ('no cells') group. The independent variables included two between-groups factors, treatment, three levels ('no cells', UCs and CCs) and time with three levels (1, 3 and 5 weeks).

In the basal region of the newly formed connective tissue (Figure 63) a significant main effect of treatment on the ratio of thick to thin collagen fibres was found, $F(2, 3) = 165.3$, $p = 0.001$, such that the ratio in wounds treated with UCs ($M = 0.74$, $SD = 0.60$)

was 2-fold higher than after treatment with no cells ($M = 0.37$, $SD = 0.29$) and 3.5-fold higher in wounds treated with the CCs ($M = 1.31$, $SD = 1.01$) compared to acellular treatments. A significant main effect of time on the ratio of thick to thin collagen fibres was found, $F(2, 3) = 286.7$, $p < 0.001$; the ratio increased with time for all groups. The thick to thin fibre ratio increased 4-fold from week 1 ($M = 0.18$, $SD = 0.12$) to week 3 ($M = 0.66$, $SD = 0.46$) ($p = 0.017$) followed by a 2-fold increase from week 3 to week 5 ($M = 1.28$, $SD = 0.86$) ($p = 0.007$). Additionally, a significant interaction was observed between treatment and time on the ratio of thick to thin collagen fibres, $F(4, 3) = 39.4$, $p = 0.006$; the effect of the treatment time on the ratio increased with time. Simple effects analyses revealed a significant main effect of treatment in the fifth week, $F(2, 1) = 860.4$, $p = 0.024$, such that the thick to thin fibre ratio was 3-fold higher in wounds treated with CCs ($M = 2.42$, $SE = 0.73$) than wounds in the ‘no cells’ group ($M = 0.68$, $SE = 0.22$) ($p = 0.046$).

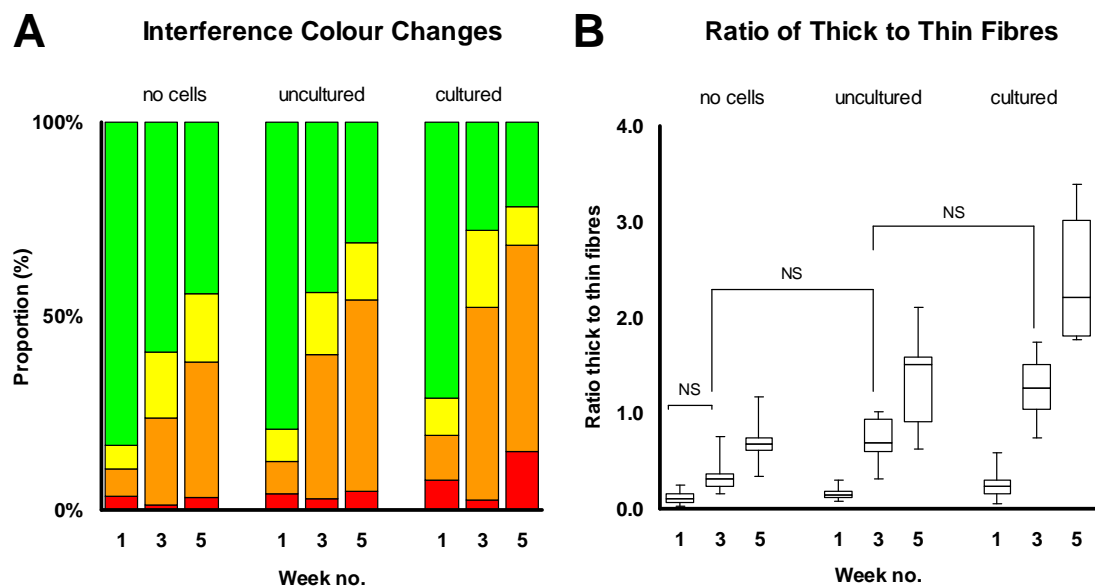


Figure 63 – Collagen maturation in the basal regions of the newly formed connective tissue. (a) Post-injury changes (at three time points) in proportion of birefringence interference colours of collagen fibres in full thickness wounds treated without cells (no cells; groups consist of untreated wounds and those treated with acellular skin equivalents) and with uncultured and cultured (cell seeded) skin equivalents. (b) Box and whisker plot of the ratio in the proportion of thick (represented by red and orange colours) to thin (represented by green and yellow colours) collagen fibres as presented in (a).

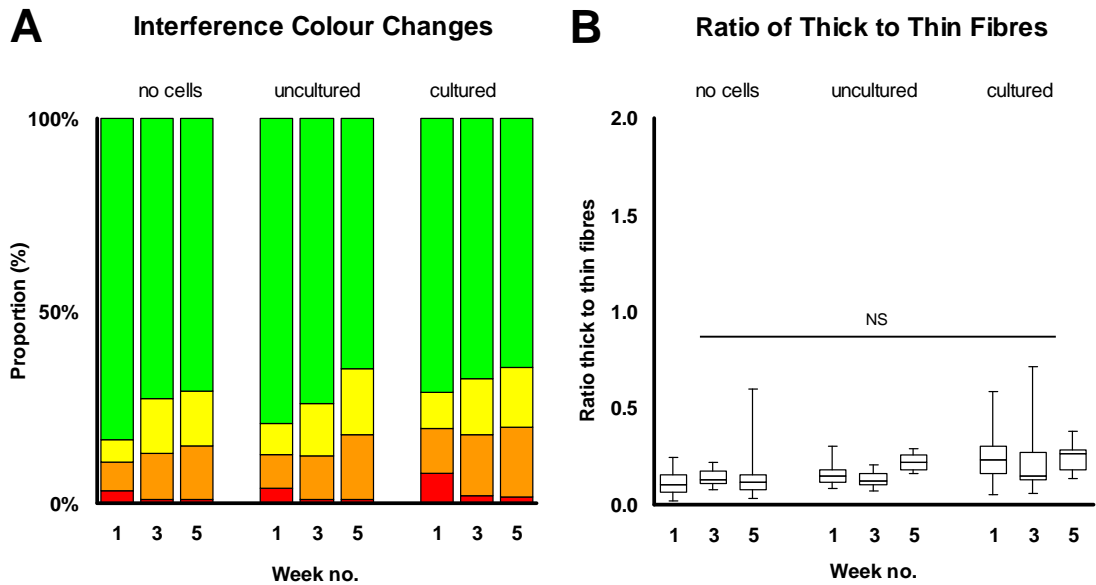


Figure 64 – Collagen maturation in the apical regions of the newly formed connective tissue. (a) Post-injury changes (at three time points) in proportion of birefringence interference colours of collagen fibres in full thickness wounds treated without cells (no cells; groups consist of untreated wounds and those treated with acellular skin equivalents) and with un cultured and cultured (cell seeded) skin equivalents. (b) Box and whisker plot of the ratio in the proportion of thick (represented by red and orange colours) to thin (represented by green and yellow colours) collagen fibres as presented in (a) (NS, not significant).

In the apical region of the newly formed connective tissue (Figure 64), a marginally significant main effect of treatment on the ratio of thick to thin collagen fibres was found, $F(2, 3) = 6.46, p = 0.082$, such that the ratio was 80% higher in wounds treated with the CCs ($M = 0.25, SD = 0.17$) and 20% higher in wounds treated with the UCs ($M = 0.17, SD = 0.07$) than after treatment with no cells ($M = 0.14, SD = 0.10$). No significant effect of time on the ratio of thick to thin collagen fibres was found, $F(2, 3) = 0.77, p = 0.537$. Additionally, no significant interaction between treatment and time could be observed, $F(4, 3) = 0.45, p = 0.77$.

Although after three weeks the constructs had been ejected from the wounds, at week 5 collagen maturation (thick to thin fibre ratio) was 3.5-fold higher for wounds treated with the CCs and 2-fold higher for wounds treated with UCs than when no cells were introduced in the wounds.

3.3.7 Panniculus carnosus

The physiology of wound healing in the dorsal skin of rabbits is different from humans and this has been attributed to the presence of the subcutaneous panniculus carnosus muscle, which enables wounds to heal primarily by contraction relying less on new connective tissue formation. The precise role of this muscle in the wound contraction process is, however, not yet certain. The relationship between the size of the panniculus carnosus muscle and the size of the wound was therefore investigated in this study.

Correlational analysis revealed that the thickness of the underlying panniculus carnosus muscle was significantly related to the wound size. However, the size of the underlying panniculus carnosus muscle showed only a weak negative correlation ($r = -0.37$, $p = 0.002$) with wound size (Figure 65). Of the variation in wound size only 13% (0.37^2) could be explained by the size of the panniculus carnosus muscle.

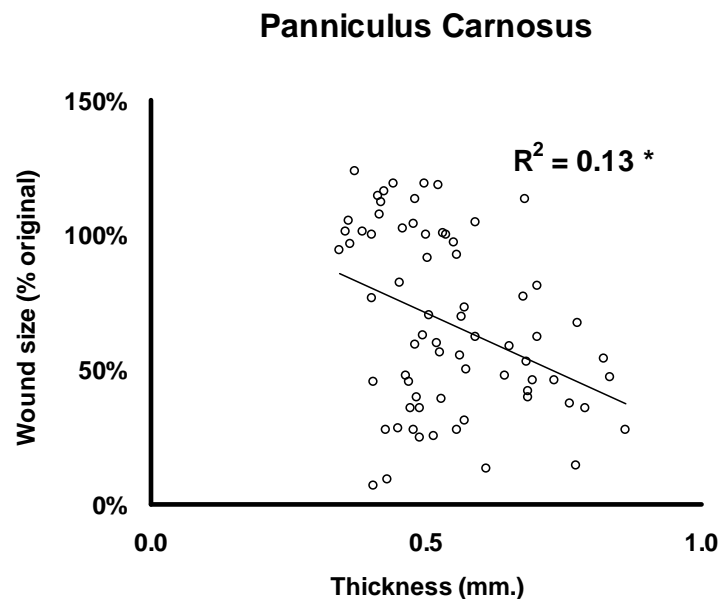


Figure 65 – Correlation between the thickness of the panniculus carnosus muscle and the wound length (*, $p < 0.002$).

To test if splinting the wound with the skin equivalents or the treatment with cells had an effect on the size of the panniculus carnosus muscle the cross sectional area of the

muscle was measured in H&E stained sections and divided by the wound length to yield an average muscle thickness (Figure 66).

A two-way RM-ANOVA was conducted on the average thickness of the panniculus carnosus muscle. The independent variables included two between-groups factors, grafting, four levels (NT, AC, UC, CC) and time with three levels (1, 3 and 5 weeks) (Figure 66).

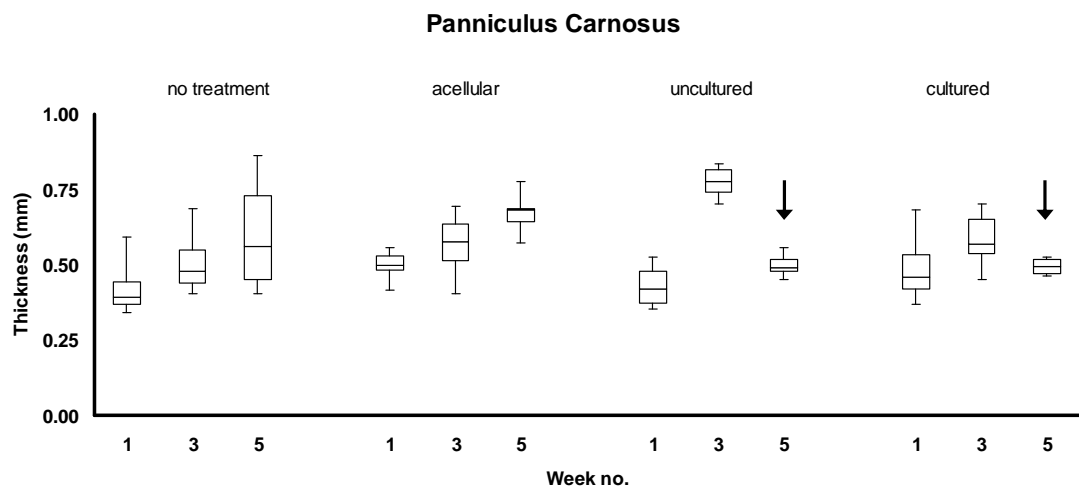


Figure 66 - Box and whisker plots for the average thickness of the subcutaneous panniculus carnosus muscle in full thickness wounds untreated ('no treatment') and treated with acellular and uncultured and cultured cell seeded skin equivalents for three time points post-wounding.

No significant main effect of the treatment was found, $F(3, 5) = 0.198, p = 0.893$. No significant main effect of time on the thickness of the panniculus carnosus was found, $F(2, 5) = 2.3, p = 0.191$. It should be noted that in the UC and CC group the rabbits for the 5 week time point were younger than those in the other groups. This possibly accounts for the increase in thickness of the muscle over time in all except these two groups. Additionally, no significant interaction was found between treatment and time. Over the five week period the average thickness of the panniculus carnosus muscle increased 10% [95% CI = 4% to 16%] in size but the power of this study was too low to detect this.

Neither the implantation of the skin equivalents or the treatment with cells had a significant effect on the size of the panniculus carnosus muscle. The increase in thickness over time was most probably due to the growth of the animals, as the thickness decreased with the use of younger animals. Additionally, only a weak, yet significant, correlation with the wound size was found. Both findings suggest that the panniculus carnosus muscle most likely only plays a passive role in wound contraction.

3.3.8 Epidermal regeneration

The epidermis has the capacity to regenerate after injury and the rate of epidermal wound closure and the rate at which it does so can be increased by transplantation of cultured keratinocytes and fibroblasts reducing the risk of infection and dehydration. To compare the effects of the UCs and CCs on epidermal wound closure the percentage wound coverage by epidermal regeneration was determined. The percentage wound coverage was determined by measuring the length of the epidermal regenerate divided by the length of the wound (Figure 67).

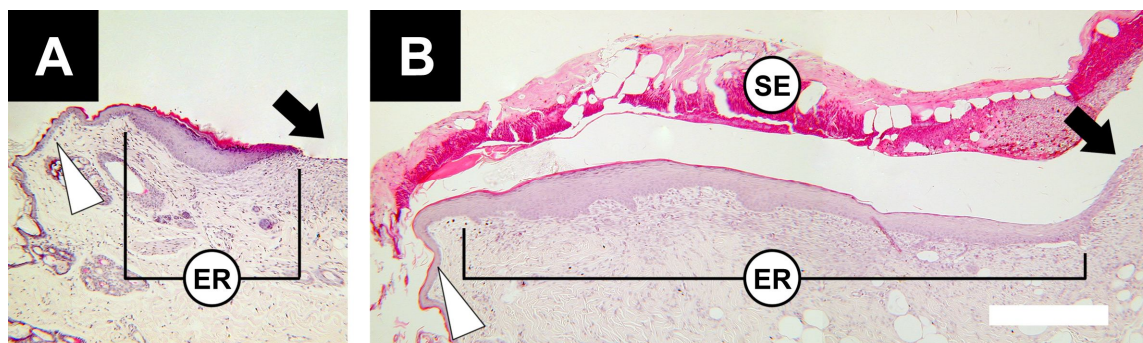


Figure 67 – Micrographs of wound edges, one week after injury, showing the difference in the length of epidermal regenerates (ER) in full-thickness skin defects receiving (A) no treatment or (B) treatment with cultured (cell seeded) skin equivalents (SE). Black arrows indicate the wound bed and white arrow heads point to the normal epidermis. Scale bar at the bottom right measures 1 mm.

A two-way RM-ANOVA was conducted on the percentage wound closure by epidermal regeneration. There was no difference between the AC and NT group and the data were therefore pooled into one ('no cells') group. The independent variables included two

between-groups factors, treatment, three levels ('no cells', UC, CC) and time with three levels (1, 3 and 5 weeks).

There was a significant main effect of treatment on the percentage wound closure by epidermal regeneration, $F(2, 3) = 39.3, p = 0.007$. Simple effects analysis revealed that compared to treatment without cells ($M = 70\%, SD = 42.6\%$) epidermal wound closure was higher in wounds treated with the cultured cell seeded skin equivalents ($M = 81\%, SD = 27.8\%$) ($p = 0.009$). As expected, there was a significant main effect of time on the percentage wound closure by epidermal regeneration, $F(2, 3) = 2246.3, p < 0.001$, such that the percentage wound closure increased from the first week ($M = 24.2\%, SD = 15.0\%$) to the third week ($M = 100\%$) ($p < 0.001$). In addition a significant interaction between treatment and time was found, $F(4, 3) = 39.3, p = 0.006$. No significant simple effects were observed, suggesting that overall, the epidermal wound closure increased with time in wounds treated with the skin equivalents (Figure 68a).

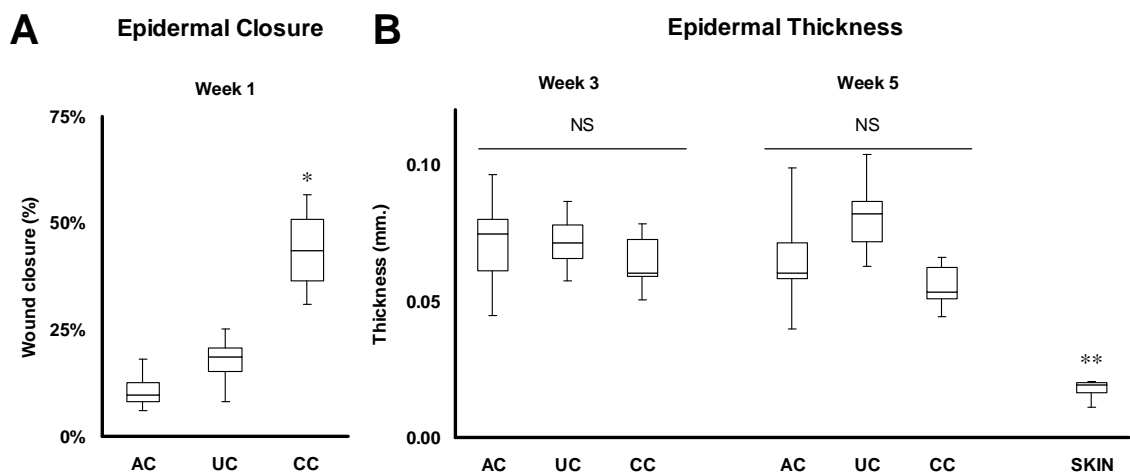


Figure 68 – (a) Box and whisker plots for percentage wound coverage of full-thickness skin defects by epidermal regeneration at week 1 showing that the percentage closure increased with the number of cells used to treat the wound. (b) The epidermis had completely regenerated in all wounds at weeks 3 and 5 and the regenerated epidermis was 4 times thicker than that of normal (unwounded) skin (, $p < 0.01$).**

Analysis revealed that the thickness of the regenerated epidermis ($M = 68, SD = 15 \mu\text{m}$) was almost 4-fold greater than in unwounded skin ($M = 18, SD = 4 \mu\text{m}$), $t(33.4) = 19.21, p < 0.001$. To test if the treatment type had an effect on the thickness of the

regenerated epidermis a two-way RM-ANOVA was conducted. The independent variables included two between-groups factors, treatment, three levels (no cells, UCs, CCs) and time with two levels (3 and 5 weeks).

No significant main effect of treatment, $F(2, 2) = 0.174$, $p = 0.851$, and no significant main effect of time on the thickness of the epidermal regenerate was found, $F(2, 2) = 6.143$, $p = 0.140$ (Figure 68b). Additionally, no significant interaction was observed between treatment and time, $F(2, 2) = 1.183$, $p = 0.458$.

The percentage wound closure in the first week by newly formed epithelium was 4 times higher in wounds treated with cultured equivalents compared to acellular treatment. UCs increased epidermal regeneration 1.5 fold, but this effect was not statistically significant. At weeks 3 and 5 the wounds in all groups were closed and at both time points the newly formed epidermis was almost 4-fold thicker than that of normal skin.

3.3.9 Angiogenic response

The formation of new blood vessels from endothelial cells from pre-existing vessels (or angiogenesis) is essential to wound healing. Angiogenesis stimulating factors are released by host cells (inflammatory cells, keratinocytes, endothelial cells and dermal fibroblasts) in response to the inflammatory wound healing response induced by the surgical procedure. Additionally, cells (keratinocytes, fibroblasts) seeded within an implant can stimulate the endogenous release of angiogenic growth factors.

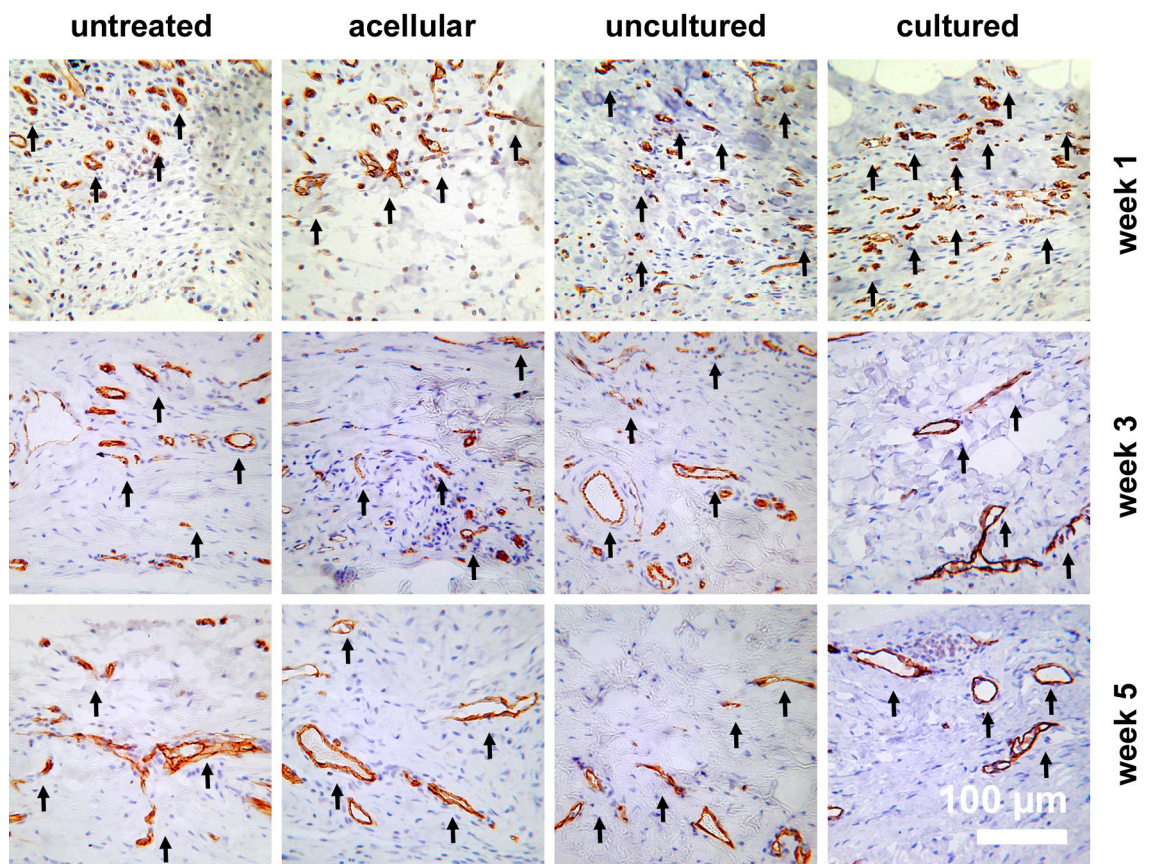


Figure 69 – Immunohistochemical detection of CD31+ endothelial cells visualising angiogenesis at three points in the connective tissue newly formed in healing full thickness skin defects, untreated, treated with acellular, uncultured and cultured skin equivalents (DAB chromogen, haematoxylin counterstain; scale bar is shown at the bottom right corner).

No vascularisation of the dense collagen components (of the skin equivalents) could be observed. To test if the UCs and CCs were able to stimulate angiogenesis in the wounds the number of blood vessels within the granulation tissue was quantified in histological

sections and compared to the acellular (AC, NT) treatments. Tissue sections were stained for CD31+ endothelial cells and counter stained with haematoxylin (Figure 69). Per tissue section two parameters were measured in up to ten fields of view (light microscope; 20x objective) of randomly selected areas throughout the newly formed connective tissue: (i) the number of blood vessel cross sections per field of vision and (ii) the total area of the blood vessel cross sections (representing endothelial cell and luminal area) expressed as percentage of the tissue area (in the field of view).

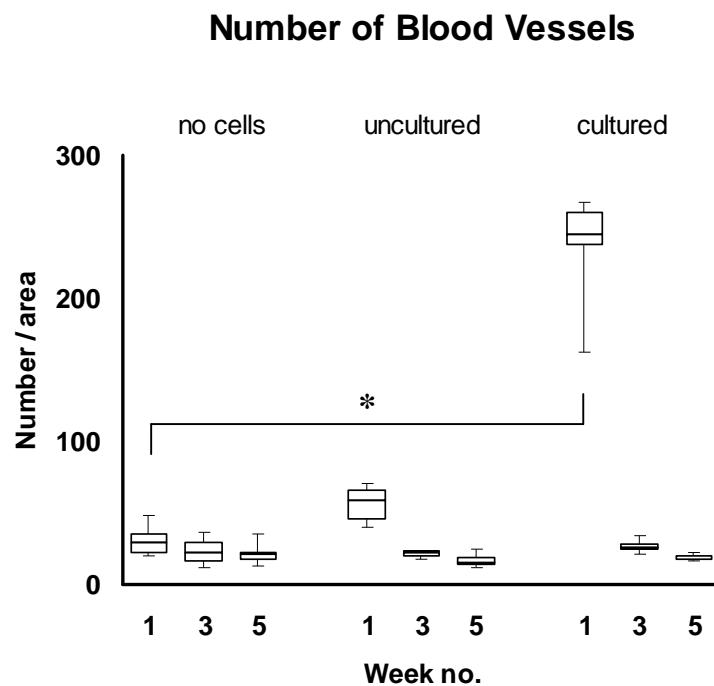


Figure 70 - Box and whisker plots for the number of CD31+ blood vessel cross sections per area newly formed connective tissue in wounds treated without cells (no cells; groups consist of untreated wounds and those treated with acellular skin equivalents) and with uncultured and cultured (cell seeded) skin equivalents for three time points post-surgery (*, $p < 0.05$; *post hoc* analysis for the interaction between treatment and time). Values are for 6 samples, except 'no cells' = 12 samples.

Firstly, a two-way RM-ANOVA was conducted on the number of blood vessel cross sections per tissue area. There was no difference between the AC and NT group and the data were therefore pooled into one ('no cells') group. The independent variables

included two between-groups factors, treatment, three levels (no cells, UCs, CCs) and time with three levels (1, 3 and 5 weeks).

There was a significant main effect of the treatment on the number of blood vessel cross sections in the granulation tissue, $F(2, 3) = 220, p = 0.001$, such that a significantly greater number of blood vessels was present in wounds treated with the CCs ($M = 94.4, SD = 105.7$) than in wounds treated without cells ($M = 24.8, SD = 8.2$) ($p = 0.001$). A significant main effect for time was found, $F(2, 3) = 384, p = 0.001$; for all groups the number of blood vessel cross sections decreased over time. A *post hoc* (Tukey HSD) simple effects analysis of time revealed that only the difference in blood vessels number between the first week ($M = 88.3, SD = 90.3$) and third week ($M = 23.4, SD = 6.1$) was significant ($p = 0.001$). In addition, a significant interaction effect between treatment and time was observed, $F(4, 3) = 208, p < 0.001$. Main effects analysis revealed a significant main of the number of blood vessels in the granulation tissue in the first week for wounds treated with the CCs, $F(2, 1) = 438.4, p = 0.034$. *Post hoc* (LSD) analysis revealed a significant difference between CCs ($M = 236.6, SD = 38.3$) and treatments without cells ($M = 24.8, SD = 8.2$) ($p = 0.022$) (Figure 70).

Additionally, a two-way RM-ANOVA was conducted on the percentage tissue area occupied by the blood vessel cross sections (luminal and endothelial cell area) (Figure 30). Again no difference between the AC and NT group was found and the data were pooled into one ('no cells') group. The independent variables included two between-groups factors, treatment, three levels ('no cells', UCs, CCs) and time with three levels (1, 3 and 5 weeks).

A significant main effect of treatment on the total size of the blood vessel cross sectional area was found, $F(2, 3) = 24, p = 0.014$, such that the vascularity was significantly higher in wounds treated with the CCs ($M = 5.5\%, SD = 4.7\%$) than in wounds where no cells were introduced ($M = 2.7\%, SD = 1.2\%$) ($p = 0.13$). The difference between UCs ($M = 3.1\%, SD = 1.8\%$) and treatment without cells ($M = 2.7\%, SD = 1.2\%$) was not statistically significant ($p = 0.633$).

Vessel Cross Sectional Area

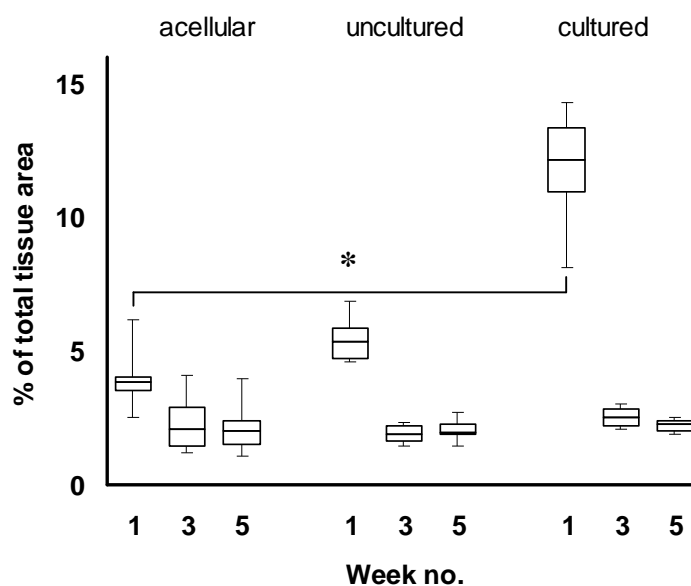


Figure 71 - Box and whisker plots for the size percentage of the blood vessel cross sectional area per area newly formed connective tissue in wounds treated without cells (no cells; groups consist of untreated wounds and those treated with acellular skin equivalents) and with uncultured and cultured (cell seeded) skin equivalents for three time points post-surgery (*, $p < 0.05$; *post hoc* analysis for the interaction between treatment and time). Values are for 6 samples, except ‘no cells’ = 12 samples.

A significant main effect of time was found, $F(2, 3) = 84.3$, $p = 0.002$, indicating that the total size of the blood vessel cross sectional area decreased over time for all groups. A Tukey HSD *post hoc* analysis revealed that the total size of the blood vessel cross sectional area was significantly greater in the first week ($M = 7.1\%$, $SD = 3.6\%$) than in the third week ($M = 2.2\%$, $SD = 0.8\%$) ($p < 0.004$); the difference between the third and fifth week was not statistically significant ($p = 0.916$). Additionally a significant interaction between treatment and time was found, $F(4, 3) = 19.8$, $p = 0.017$. A significant main effect of treatment was found in the first week, $F(2, 1) = 756.0$, $p = 0.026$; the effect of treatment on the size of the total blood vessel cross sectional area was time dependent. Simple effects *post hoc* (Bonferroni) analysis showed that in the first week there was only a significant difference in the total blood vessel cross sectional

area between CCs ($M = 11.8\%$, $SD = 2.2\%$) and treatment without cells ($M = 3.8\%$, $SD = 0.9\%$) ($p = 0.05$) (Figure 71).

Immunohistological staining for CD31+ cells showed that there was no vascularisation of the skin equivalents, however, a positive angiogenic effect (inferred from the number and total cross sectional area of blood vessels) of the CCs on the granulation tissue in acute full thickness skin wounds could be found in the acute phase of wound healing (first week post-implantation). In the first week wounds treated with the CCs showed a statistically significant 8-fold higher number of blood vessels and a (significant) 3-fold greater blood vessel cross sectional area than wounds that were not treated with cell seeded implants. UCs, in the first week, showed, respectively, a 2-fold and a 1.4-fold greater effect over treatments without cells for these two parameters. The power of this study, however, was too small to detect these effect sizes. In weeks 3 and 5 no differences between cellular and acellular therapies could be detected and in all groups both the number of vessels and the total size of the vessel cross sectional area had decreased below the levels that were found in the first week for the acellular treatment group.

4. Discussion

4.1 Collagen hydrogel compression

In the present study an alternative strategy was explored in which the thickness and the break strength of the compressed collagen sheets were improved by increasing the pre-compression volume (Figure 10) of the collagen hydrogel. The handling properties of the compressed collagen sheets have previously been improved through layering of the material by rolling (along their long axis; Figure 9b) the sheets into rod shaped structures (Brown *et al.*, 2005). Although, *in vivo*, an adequate suture retention was found up to five weeks post-implantation (Mudera *et al.*, 2007), the fabrication and therefore the mechanical properties are subject to a certain degree of (intra- and inter-operator) variability (Figure 38). Additionally, the shape and structure are not ideal for the construction of thicker, stronger flat structures. It would be possible to stack multiple compressed collagen sheets. However, an additional culture period would be required to produce an integrated structure (Marenzana *et al.*, 2007). Compressing increased collagen hydrogel volumes to increase the thickness and the break strength of the resulting sheets was therefore explored in the present study.

It was found that, improving the mechanical properties of large volume collagen hydrogels by the expulsion of the interstitial fluid (*i.e.* hydraulic permeability) through the gel membrane is hampered by the anisotropic and mass transfer dependent increase in collagen fibril density at the FLS.

A collagen hydrogel can be described as a poro-elastic, biphasic material consisting of a (phase separated) highly entangled network of collagen polymer chains (fibrils; solid phase) with a typical pore volume fraction of more than 0.9 which is saturated with (an incompressible) fluid (liquid phase). Qualitative analysis showed that in the solid phase, away from the FLS, fluid flow and network collapse (or collagen compaction) during compression is prevented by the incompressibility of the interstitial fluid (Figure 36), whereas at the FLS fluid flow is allowed to occur, and it is here that the collagen network previously supported by expelled fluid volume collapses into dense collagen lamellae (Figure 37).

This anisotropic change of collagen density in a collagen hydrogel compressed to 50% strain in a confined configuration has previously been demonstrated with the use of entrapped markers, similar to the charcoal assay (Figure 35) described here (Girton *et al.*, 2002; Chandran and Barocas, 2004). The compression induced anisotropy was also demonstrated with polarised light microscopy in collagen hydrogels compressed in an unconfined configuration up to 99% strain (Brown *et al.*, 2005). To my knowledge, however, the present study is the first to consider the physical implications of these compression-induced structural changes for the creation of thicker collagen constructs through the compression of larger volume collagen hydrogels.

The condensation of the normal ECM architecture with concomitant decrease in hydraulic permeability through the application of an external load, has previously been described for biological tissues such as glomerular basement membrane (Robinson and Walton, 1989), articular cartilage (Oloyede and Broom, 1994) and collateral ligament (Weiss and Maakestad, 2006). The relationship between compression and hydraulic permeability found in glomerular basement membranes (Leung and Robinson, 1990) has previously modelled with poly(glyceryl methacrylate) hydrogels showing that the permeability could be accurately predicted by mathematically representing the hydrogel and the basement membrane as a continuum-like distribution of fibres.

To elaborate, this continuum theory regards the randomly arrayed fibres as elements within the fluid that cannot be displaced and that hinder an otherwise straight outflow of fluid. This process is described by the Carman-Kozeny equation which mathematically relates permeability to specific network properties such as fractional void volume (*i.e.* porosity, the fractional volume of the matrix not occupied by solid components), mean hydraulic radius of the pores, pore size (determined by fibre spacing and diameter) (Swartz and Fleury, 2007). A modification of this equation known as the Happel model (John, 1959) also accounts for the contribution of fibrillar orientation to flow resistance (with perpendicular oriented fibres providing larger resistance to fluid flow than parallel fibres), making it more suitable for highly porous (fibrous) media (with a porosity greater than 0.5), such as collagen hydrogels (typical porosity of more than 0.9).

Present and previous experimental findings indeed validate that the predicted mechanism of change in hydraulic permeability in the compressed collagen hydrogel system is contributed by changes in porosity (Figure 36), (presumably) average

effective pore size, and fibril orientation relative to flow (Girton *et al.*, 2002; Chandran and Barocas, 2004; Brown *et al.*, 2005). The last has been quantified with polarised light microscopy measuring increased retardation values as the collagen fibrils closer to the FLS change from a random to an orientation perpendicular to the direction of fluid flow (Girton *et al.*, 2002).

It is proposed here that collagen hydrogel compaction is a self-limiting process due to the mass transfer dependent decrease in hydraulic permeability whether through, the application of a gravitational load (Figure 33) or negative capillary action (Figure 36). It could be speculated that given enough time a collagen hydrogel could through cell contraction obtain a mechanical strength superior to that of a compressed collagen hydrogel, however, cell mediated gel contraction has also been shown to be limited as a direct function of collagen fibrillar density (Serpooshan *et al.*, 2010). Additionally, it is speculated here that mechanical compression can introduce a collagen density that lies passed the physiological range that can be obtained through cell mediated contraction.

Referring back to D'Arcy's equation, the implication for the mechanical compression of collagen hydrogels is that when the hydraulic permeability has sufficiently decreased to match the driving force (*i.e.* gravitational load) fluid flow will cease and further removal of the fluid content can then be established by introducing a second (uncompressed) FLS (Section 2.1.6) or by increasing the gravitational load (Bitar *et al.*, 2007; Cheema, Ananta *et al.*, 2010). The first strategy in effect doubles the volume that can be expelled from a hydrogel under a set load. Further compaction could be achieved by increasing this load, however, it has previously been shown that increased stress levels have both immediate and long-term negative effects on viability of encapsulated cells (Bitar *et al.*, 2007; Cheema, Ananta *et al.*, 2010). Therefore the compression of collagen hydrogels is limited both by physical and biological effects.

It should be noted that the mechanical strength of normal collagen rich connective tissues is not only dependent on fibril density, but also fibril diameter (Cheema *et al.*, 2007), fibril orientation, and the presence of other ECM proteins (*i.e.* fibronectin, elastin, proteoglycans). And relying solely on improving the mechanical properties by increasing the collagen density not only has implications for cell viability, mass transfer of nutrients, but also for other aspects that could influence the performance of a TE scaffold. For instance cell behaviour can be influenced through the transduction of

mechanical signals from surface receptors through the cytoskeleton to the nucleus (Wang *et al.*, 2009). It has been shown for instance that proliferation in collagen hydrogels increase with higher mechanical stiffness of the substrate (Hadjipanayi *et al.*, 2009). Additionally, invasion of an tissue engineered implant by endothelial cells can be greatly reduced with decreasing pore size (Sahota *et al.*, 2003) with significant implications for vascularisation and integration of the implant into the underlying wound bed. Lastly, the *in vivo* degradation rate of a collagen hydrogel has previously been shown to decrease with collagen density (Helary *et al.*, 2010) with compressed collagen sheets persisting up to 5 weeks (Mudera *et al.*, 2007). This is important as it would determine the biological activity of an implant as the integrity of the cell carrying component determines how long cells will remain at the site of interest.

The previously promising advantages of using collagen hydrogels in combination with the compression technique involved the ability to rapidly provide cells with a 3D context, creating living tissue equivalents with good cell viability retention and with tensile properties approaching those of native tissues in the space of an hour (Brown *et al.*, 2005). It is now concluded that there are limitations to the thickness and break force of compressed collagen hydrogels that can be achieved by this technique imposed by physical as well as biological considerations. The question is then asked how the compression technique on collagen hydrogels compares to other rapid strategies for the creation of tissue equivalents with appropriate handling properties that allow for *in vivo* application.

Other, cell-independent means, to improve the mechanical stiffness of the non-crosslinked, tightly entangled fiber network of collagen hydrogels involve introducing inter- and intrafibrillar crosslinks through, exposure to aldehydes (*e.g.* glutaraldehyde (Cheung *et al.*, 1985) or aldehyde sugars), enzymatic treatment (*e.g.* lysyl oxidase (Kagan and Li, 2003) and transglutaminase (Piacentini *et al.*, 2000)), non-enzymatic glycation (*e.g.* by reducing sugars such as glucose and ribose (Girton *et al.*, 1999)) and photo-polymerisation using UVA light either alone (Weadock *et al.*, 2004) or with riboflavin (which induced by UVA forms free crosslinking radicals) (Ahearne *et al.*, 2008).

Although these methods are effective in increasing mechanical stiffness, some approaches are either too cytotoxic (glutaraldehyde, UVA (Weadock *et al.*, 2004), and

free radicals released from UVA / riboflavin (Ahearne *et al.*, 2008)), too time-consuming (30 mM ribose requires a 3-week incubation period for a 2-fold increase in ultimate stress (Girton *et al.*, 1999)), or too costly and impractical for bulk changes in mechanical properties (*e.g.* lysyl oxidase and transglutaminase). Recently, genipin (derived from the fruit of *Gardenia Jasminoides*) has been described to crosslink collagen hydrogels (Shreiber *et al.*, 2005) with little cytotoxicity at concentrations less than 1 mM, showing a 2-fold increase in storage modulus in 4 hours time. The speed of cross-linking can be increased with higher concentrations but above 5 mM a significant reduction in cell viability is observed.

As opposed to fabricating and seeding scaffolds in sequence, encapsulating cells during scaffold formation (Nicodemus and Bryant, 2008) afford the ability to provide the site of interest with an adequate number of cells in a relevant 3D environment within an instant. The importance of a 3D cell environment was previously illustrated by the finding that a 3D substrate directly affects the distribution of anchored ECM receptors over the cell membrane thereby not only influencing cell morphology (Beningo *et al.*, 2004) but also cell activity. The latter is further illustrated by the finding that in fibroblasts in 3D culture VEGF mRNA expression was 22-fold higher than when cultured in a monolayer (Pinney *et al.*, 2000).

Cell encapsulation in hydrogels involves mixing a cell suspension with a liquid hydrogel precursor solution which is subsequently crosslinked into a network. Only a few materials are suitable for cell encapsulation as the scaffold fabrication process needs to be cytocompatible. Two main categories can be distinguished (Nicodemus and Bryant, 2008): (1) biopolymer hydrogels (*i.e.* collagen, fibrin, alginate) and (2) synthetic based hydrogels (*i.e.* purely synthetic, *i.e.* poly(ethylene glycol), with or without incorporated biological signals and derivatised biopolymers).

Collagen hydrogels were one of the first materials used for cell encapsulation (Elsdale and Bard, 1972; Bell *et al.*, 1979). Other natural materials suitable for cell encapsulation are fibrin (Rowe *et al.*, 2007), alginate (Bent *et al.*, 2001) and chitosan. Fibrin hydrogels are prepared by mixing fibrinogen with thrombin. The latter catalyses the release of fibrinopeptides (A and B) and the subsequent self-assembly of the fibrin hydrogel (Blombäck and Bark, 2004). Alginate hydrogels are prepared by ionic crosslinking of precursors with calcium sulphate (CaSO₄) (Bent *et al.*, 2001). Chitosan, a natural

polysaccharide obtained by deacetylation of chitin, is water soluble under dilute acid conditions ($\text{pH} < 6$) and forms a physically crosslinked hydrogel at a pH exceeding 6.2 (Chenite *et al.*, 2000).

As opposed to alginate and chitosan, collagen and fibrin naturally contain essential cell recognition sites (*i.e.* the integrin ligand RGD tripeptide) important for cell attachment, survival, and function (Ruoslahti and Pierschbacher, 1987). Fibrin, however, has the disadvantage that it is rapidly degraded by plasminogen and MMPs which may be secreted by the cells they contain (Ahmed *et al.*, 2007). Alginate is biocompatible and non-immunogenic (Alsberg *et al.*, 2001) but cannot be degraded enzymatically in mammals (Lansdown and Payne, 1994) and slowly dissolves *in vivo* at neutral pH as the divalent crosslinking cations are lost. Lastly, chitosan lacks mechanical strength and also has a tendency to dissolve.

It is apparent that the mechanical and chemical properties of natural materials are difficult to control and are subject to biological variation. Currently synthetic based hydrogels are explored to address these issues. These hydrogels are formed by (1) radical chain polymerisation, (2) step-growth polymerisation, or (3) mixed-mode polymerisation.

Radical chain polymerisation occurs in the order of seconds to several minutes. An initiator is decomposed into free radicals (possibly by an initiating signal) in the presence of monomers (synthetic, *e.g.* poly(ethylene glycol); or natural, *e.g.* fibrinogen (Almany and Seliktar, 2005), chitosan (Ono *et al.*, 1999; Hong *et al.*, 2006), alginate (Yeh *et al.*, 2006), hyaluronic acid (Yeh *et al.*, 2006; Kim *et al.*, 2007), chondroitin sulphate (Li *et al.*, 2003b)) which generally have been modified to contain two or more functional (*i.e.* crosslinkable) groups (*i.e.* methacrylate (Li *et al.*, 2003b; Yeh *et al.*, 2006), azide (Ono *et al.*, 1999)). A free radical will bind a monomer forming a new radical which will then bind another monomer resulting in the generation of a polymer chain. The initiation of the chain polymerisation can be brought about by thermal (Temenoff *et al.*, 2004), redox (Hong *et al.*, 2006), or photo-initiating (Ono *et al.*, 1999; Li *et al.*, 2003b; Yeh *et al.*, 2006) systems.

Radical polymerisation allows for greater control of the mechanical properties and degradation of the resulting hydrogels by modifying the number of functional groups,

the duration of the initiating signal (*e.g.* UV-exposure) (Ahearne *et al.*, 2008), and the concentration of the initiator (Hong *et al.*, 2007) and precursors (Burdick *et al.*, 2005). However, greater mechanical stiffness is generally accompanied with higher cytotoxicity from UV-exposure (Yeh *et al.*, 2006), toxic by-products (Li *et al.*, 2003b) and free radicals (Hong *et al.*, 2007) reduce cell survival in a dose dependent manner.

A second strategy for encapsulating cells, one which does not require (potentially cytotoxic) initiators involves step-polymerization and crosslinking of water-soluble multifunctional nucleophilic (*i.e.* electron rich) precursors. An example is hyaluronic acid which has been conjugated with (crosslinkable) thiol groups. The air oxidation of these thiols to disulfides allows for the formation of HA-based hydrogels under physiological conditions (Shu *et al.*, 2002). This process which can take minutes to hours can be accelerated by the use of Michael-type addition reaction (Metters and Hubbell, 2005) which involves the reaction between multifunctional unsaturated (or electrophilic, *i.e.* electron deficient) precursors (*e.g.* acrylated poly(ethylene glycol)) and multifunctional nucleophile precursors (*e.g.* thiolates).

A third strategy for the fabrication of synthetic hydrogels is the mixed-mode polymerisation (Rydholm *et al.*, 2005) which involves both radical chain and step-growth polymerisation reactions of multifunctional, acrylated and thiolated precursors. The step-growth reaction involves the linkage between an acrylate and a thiol group and the chain polymerisation involves the reaction between two acrylates.

The use of biological precursors such as collagen or fibrin has the advantage over the use of purely synthetic precursors in that these biological materials have cell adhesion motifs (Ruoslahti and Pierschbacher, 1987) and confer to the hydrogel a cell-mediated degradability (Rowe *et al.*, 2007). Synthetic hydrogels, however, suffer from the disadvantage that the resorption rate does not necessarily match the rate of matrix deposition by the cells and the materials are not always degraded by the cells' natural mechanisms as they generally degrade by simple hydrolysis (Nicodemus and Bryant, 2008). To make synthetic hydrogels more biomimetic cell binding moieties can be introduced by the hybridisation with fibrinogen (Almany and Seliktar, 2005) and collagen (Doillon *et al.*, 1995) precursor molecules or grafting of the synthetic precursors with cell binding motifs (Burdick and Anseth, 2002). These techniques have already resulted in transparent, biomimetic synthetic scaffolds with sufficient suture

retention strength that they could be sutured into corneal defects (Rafat *et al.*, 2008; Deng *et al.*, 2010). These experimental constructs have, however, not yet been tested for their suitability for cell encapsulation and long term support of embedded cells.

An emerging cell encapsulation strategy involves natural or synthetic peptides or proteins that self-assemble into hydrogels made of complex nano-scale structures (Rajagopal and Schneider, 2004; Williams *et al.*, 2010). Depending on the hydrophobicity, hydrophilicity and charge of the side groups of the amino acid sequence the peptides or proteins assemble into various nano-structures (*e.g.* β -sheets and β -hairpins) through a great number and a variety of weak non-covalent interactions (*e.g.* hydrogen bonding, electrostatic interactions, hydrophobic interactions and van der Waals interactions). Although these hydrogels are stable they are mechanically weak and require cells to strengthen the matrix through the deposition of ECM (Kisiday *et al.*, 2002).

4.2 Hybrid constructs

The combination of cell encapsulating hydrogels with prefabricated scaffolds, such as presented here, is an attractive one, as the strategy prevents considerations of mechanical strength compromising those concerning cytocompatibility. In the present study thin sheets of living, suturable dermal-like tissue were created in the space of an hour by polymerising and cell seeding a monomeric collagen solution (after inoculation with dermal fibroblasts) around a synthetic, degradable polymer mesh and mechanically compressing (in an unconfined configuration; Figure 14) the resulting hybrid material to improve the integration between the collagen hydrogel and the mesh (Ananta *et al.*, 2009). This technique was tested with two different slow degrading polyester meshes: (1) a weft knitted mesh made of a newly developed PLACL (a 97:3 copolymer of poly-L-lactic acid and ϵ -caprolactone; Figure 13) (Ananta *et al.*, 2009) and (2) a commercially available warp knitted mesh made of Vicryl (a 90:10 copolymer of glycolic acid and lactic acid, polyglycolic acid, PLGA; Figure 40b).

The hybrid construct in the present study was designed as a permanent tissue substitute which is why was chosen for a degradable material to act as the mechanical backbone. Biodegradable synthetic polymers offer a number of advantages as scaffolding material over naturally derived materials. As they are chemically synthesized, they can be

reproducibly manufactured on a large-scale and it is possible to control their mechanical and physical properties over a wide range using harsh solvents and/or reactants as long as the final product is cell friendly. For instance, the degradation rate and UTS of synthetic polymers can be tailored by varying the molecular weight or by co-polymerisation with other synthetic polymers (Holland *et al.*, 1987).

Synthetic polymers can be separated in two main groups, namely plastics and elastomers (McKeen, 2008). Plastics are categorised into two main groups depending on their response to heat: thermosetting polymers (or thermosets) and thermosoftening plastics (or thermoplastics). A thermosetting polymer is a prepolymer in a soft solid or viscous state that changes irreversibly into an infusible, insoluble polymer network by curing (i.e. hardening of the material through the introduction of covalent crosslinks by heat, chemical reactions or irradiation). A thermoplastic polymer in contrast is in a liquid state at its melting temperature and changes reversibly into a solid below this temperature. Elastomers (or elastic polymers) can elastically deform up to 200% strain and can also be prepared as thermosets and thermoplastics.

The biodegradable synthetic polymers most studied are thermoplastic and the main classes are, polyesters (*e.g.* poly(α -hydroxy acids), polyorthoesters, polyanhydrides, polyphosphazenes, polyurethanes, poly (propylene fumarate), and poly (anhydrides) (Gunatillake and Adhikari, 2003; Yang and El Haj, 2006).

Synthetic polymers are generally fabricated into porous three-dimensional shapes (*i.e.* sponges/foams) by the removal of pre-dispersed compounds (*e.g.* gas, water, salts) from a solidifying polymeric solution (Tateishi *et al.*, 2002), such as solvent casting and porogen (or particulate) leaching (Mikos *et al.*, 1994), liquid-liquid phase separation (*i.e.* phase separation of a polymer solution with subsequent removal of the solvent phase) (Schugens *et al.*, 1996), emulsification/freeze-drying (*i.e.* water is used as the porogen) (Whang *et al.*, 1995), and gas foaming (*i.e.* gas is used as the porogen) (Mooney *et al.*, 1996). These scaffold fabrication techniques are labour intensive, use potentially cytotoxic porogens or conditions, and require extended culture time or dynamic cell seeding techniques (Godbey *et al.*, 2004) to achieve a homogeneous cell distribution.

For the purpose of this study a textile mesh was chosen as the porous and flat scaffold-architecture would accommodate the collagen compression technique. The fibres of

textiles are generally manufactured by one of four main techniques: (1) melt spinning (Ananta *et al.*, 2009), (2) dry spinning, (3) wet spinning (Ellis and Chaudhuri, 2007), and (4) electrospinning (Scott *et al.*, 2007). The first three methods are essentially the same where fibres are drawn out from a polymer solution (or from a polymer melt) extruded through a spinneret (Tuzlakoglu and Reis, 2009). Electrospinning uses an electric field to draw fibres from a polymer melt or solution allowing for the creation of thin nano-structures (Scott *et al.*, 2007). A draw-back of melt spinning is that the heat reduces the molecular weight of the polymer and thereby increases the degradation rate.

Regardless of their manufacture, the fibres can be processed into 3D mesh like structures with either knitted, woven or nonwoven patterns (Tuzlakoglu and Reis, 2009). The main advantage of knitted and nonwoven over woven structures is that they do not unravel when cut. An added disadvantage of the woven structure is that it makes meshes more prone to rolling (Cooper *et al.*, 1991) leading to difficulty in handling.

The PLACL mesh tested in the present study is a newly developed synthetic material which is expected to degrade over a period of 6 to 12 months through simple hydrolysis into caproic and lactic acid (Pitt *et al.*, 1981) which depending on the degradation rate could negatively affect cell viability through lowering of the surrounding pH (Sung *et al.*, 2004). Qualitative findings in the present study indicate that after a 7-day *in vitro* culture period no significant levels of toxic degradation products had formed as cells embedded in the basal collagen component did not appear to move away from the mesh and no increased reduction in cell viability was found in regions close to the PLACL material (Figure 44).

In the *in vitro* testing phase a subset of the PLACL-CCHH were found to macroscopically contract in size and roll up when exposed to aqueous media at 37°C and did so even when not coated with cell seeded compressed collagen hydrogels (Figure 46). The cell independent mechanism behind this is unclear but from a study on another synthetic polyester poly(ethylene terephthalate) (PET) (Knox *et al.*, 1981) a cause can be proposed. PET like PLACL and other thermoplastics, is semicrystalline, because it does not crystallise easily upon cooling as the polymer chains have to form highly ordered structures from their entangled state in order to become crystalline. What generally occurs is some crystallisation in certain regions of the polymers resulting in polymers with crystalline regions and amorphous regions, thus termed semicrystalline

polymers. It is speculated here that an aqueous medium induces a relaxation of stretched amorphous polymer chains in the melt spun filaments resulting in a longitudinal (rather than transverse, Figure 46i, j) shrinkage of the yarns (with a decrease in porosity, Figure 47a) and an increase in crystallisation (resulting in an apparent increase in stiffness). One of the main functions of a TE scaffold is to maintain a functional space in which tissue regeneration can take place. Because of its inability to retain its shape and size dimensions the PLACL-mesh was considered unsuitable for *in vivo* applications.

The second material tested with the hybridisation technique was the PLGA (Vicryl) mesh which is well characterised. The PLGA material is commonly used as a resorbable suture and the mesh form is found particularly useful for hernia repair (Luijendijk *et al.*, 2000). It degrades through non-enzymatic hydrolysis (Gorham *et al.*, 1987) into lactic acid and glycolic acid which are ultimately eliminated from the body in the form of CO₂ and H₂O (Yooa *et al.*, 2005). *In vivo* testing (Conn Jr *et al.*, 1974) showed that the material is completely degraded and absorbed after 60 days with minimal acute or chronic inflammatory reaction. Cells seeded directly onto the material showed more than 90% viability retention after a 4-day *in vitro* culture period (Vacanti *et al.*, 1988) and cells have over a 5-day *in vitro* culture period been shown to proliferate on the material (Chen *et al.*, 2005). Previous studies have reported that PLGA (Vicryl) meshes would roll up in culture when (unilaterally) seeded with cells (Cooper *et al.*, 1991). This, however, was not found in the present study, possibly due to the stabilising effects of the compressed collagen sheets.

Vicryl meshes have previously been used to improve the suturability of tissue engineered constructs. For instance air dried collagen membranes (25 µm thick) prepared from shredded limed bovine hide (Gorham *et al.*, 1984) were previously enhanced by the incorporation with this mesh (Gorham *et al.*, 1987) extending *in vitro* break strength retention of the mesh possibly due to the retardation of hydrolysis by the collagen coating. These constructs were able to successfully seal full thickness bladder defects in a lapine model (Monsour *et al.*, 1987) and full thickness oesophageal defects in a porcine model (Carachi *et al.*, 1989). These hybrid constructs were in both studies eventually replaced by epithelialised, new connective tissue. As opposed to the present technique, this strategy does not allow for cell encapsulation.

A commercially available biological dressing Dermagraft (Advanced Tissue Sciences, CA, USA) is created by seeding human neonatal fibroblasts onto the Vicryl mesh which

is then cultured for 2 to 3 weeks to achieve confluence of cells and ECM within the pores of the mesh (Cooper *et al.*, 1991). As previously mentioned the strategy of cell seeding on a prefabricated scaffold is time consuming as it relies on cell activity to achieve sufficient cell numbers and to provide a relevant 3D context. This problem is compounded by the small surface area available for cell attachment (Mansbridge *et al.*, 1998) and the fact that synthetic degradable polymers, such as PLGA, commonly have a hydrophobic surface chemistry which does not facilitate cell attachment (Ng *et al.*, 2001; Chen *et al.*, 2005; Vaquette *et al.*, 2008).

To address this issue, collagen micro-sponges were introduced within the interstices of the Vicryl mesh through freeze-drying of an acidic collagen solution followed by a cross-linking step with glutaraldehyde vapour (Chen *et al.*, 2000). This extended the surface area with a more suitable substrate for cell attachment. These PLGA-collagen sponge hybrid constructs were 200 μm thick and could be used to create tissues up to 8 mm thick by way of lamination or rolling (Chen *et al.*, 2003a). This hybrid material has been used for 3D *in vitro* cultures of chondrocytes (Chen *et al.*, 2003b), smooth muscle cells and urothelial cells (Nakanishi *et al.*, 2003), fibroblasts (Chen *et al.*, 2005), pancreatic b-cells (Kawazoe *et al.*, 2009) for the engineering of cartilage, skin and pancreatic like tissues.

These studies suggest that the PLGA-CCHH constructs presented here could be used for similar applications but with significantly shorter culture periods. Even though the introduction of micro-sponges resulted in a 5-fold increase in cell seeding efficiency and a 3-fold increase in proliferation (Chen *et al.*, 2005), the hybrid constructs still required 2 weeks of *in vitro* culture before use *in vivo*. In contrast, the cell encapsulation technique allows for seeding of a large number of cells with optimal efficiency and with 95% retention of pre-compression (Brown *et al.*, 2005) and 92% retention of post-compression cell viability (Figure 41).

Decreasing or removing a pre-implantation *in vitro* culture period has significant implications, as the PLGA biodegradable polymeric material degrades in a humid environment (Gorham *et al.*, 1987). A lengthy *in vitro* incubation period shortens the time that the polymeric support will remain structurally functional *in vivo* and it has been shown that the *in vivo* persistence of these PLGA-cell derived matrix hybrid sheets was shortened from 4-8 weeks (MacDonald *et al.*, 1992; Meddings *et al.*, 1993) to 2-4

weeks (Chen *et al.*, 2005). It is shown here that using encapsulation in a collagen hydrogel of both cells and mesh addresses this issue and results in a suturable living connective tissue within the space of an hour as opposed to weeks.

Encapsulation of a synthetic degradable mesh in cell seeded collagen hydrogel has previously been tested with polyglycolic acid (PGA) (Miki *et al.*, 1999) and PLGA (Vicryl) (Nakanishi *et al.*, 2003) to reconstruct oesophageal and bladder tissue respectively. In both studies the collagen hydrogels were not compacted, either by embedded cells or through mechanical loading, which in the first study (Miki *et al.*, 1999) resulted in a partial delamination of the collagen hydrogel from the mesh and in the second study (Nakanishi *et al.*, 2003) in the failure of the formation of a urothelium by subsequently seeded urothelial cells. Although comparison is difficult, the present findings suggest that the collagen hydrogel compression technique prevents delamination (Figure 41) and the formation of a substrate sufficiently stiff to support the formation of an epithelium (Figure 48).

4.3 Implantation study

In the present study a co-culture of allogeneic keratinocytes and fibroblasts maintained on the PLGA-CCHH were transplanted into a rabbit model of an acute full thickness skin defect. Fibroblast seeded compressed collagen sheets have previously been tested for this purpose (Hu *et al.*, 2010), however, the handling properties of the resulting skin equivalents were considered inadequate for *in vivo* implantation. The present findings show that the addition of the PLGA mesh improved handling with the retention of the ability to form a stratified epidermis by keratinocytes grown on the apical surface of the PLGA-CCHH. This indicated that the diffusion of nutrients from the basal surface to the apical surface of the construct was not impaired during culture at the air-liquid interface. This is also of importance *in vivo* as the construct features no vasculature.

Constructs that featured a near confluent epithelial monolayer (fabrication time 5 hours) and those that featured a stratified epithelium (fabrication time 3 weeks) were compared to test if the wound healing benefit (in terms of improved outcome parameters) warranted an extended *in vitro* culture period. No permanent engraftment of the implants was found, but in the first week post-wounding the co-culture constructs with a stratified epidermis did show a 4-fold higher percentage wound closure (Figure 68) and

an 8-fold higher number of blood vessels in the wound bed compared to untreated wounds (Figure 70). The constructs with a monolayer epidermis showed similar trends, but these were not statistically significant.

4.3.1 Epidermal closure

The cultured PLGA-CCHs carrying a differentiated and stratified keratinocytes stimulated epidermal closure (Figure 68). It has previously been shown that the application of keratinocytes directly to the wound can aid in epidermal closure (McAree *et al.*, 1993) with allogeneic keratinocytes performing equally well to autologous keratinocytes in burn and ulcer patients (Hefton *et al.*, 1983; Phillips *et al.*, 1990). They increase the rate of epithelialisation in a dose dependent manner (Butler *et al.*, 1999) by the release of growth factors and by physically contributing to the epidermal regenerate.

Commercially available cell therapies (Epicel, Epidex, Myskin) (Bottcher-Haberzeth *et al.*, 2010; Brusselaers *et al.*, 2010) generally involve the harvest of autologous keratinocytes from patients which are grown into confluent stratified sheets (cultured epidermal autografts; CEA) in the presence of murine fibroblasts before they are transplanted. Disadvantages associated with their use are their slow preparation time, variable engraftment rate, inefficiency against wound contraction, poor handling properties due to their fragile nature, and high production costs.

The addition of a dermal component (Horch *et al.*, 2000; Jones *et al.*, 2003), such as the one presented here, as a transport vehicle for these keratinocyte sheets addresses a large number of these issues, as epidermal sheets can be transplanted before they are confluent which would shorten the *in vitro* production time, and the presence of a dermal equivalent has shown to prevent wound contraction and improve the take of keratinocyte sheets.

Although a dermal component allows the transplantation of subconfluent keratinocytes, the findings show that the skin equivalents cultured for two weeks at the air/liquid interface to form a confluent, stratified epidermis showed a higher percentage wound closure than the UCs (featuring a subconfluent monolayer epidermis). It has previously been shown in a porcine (autologous) model of a full-thickness skin defect that the rate of epidermal regeneration and the thickness of the epidermal regenerate is directly

related to the number of transplanted dividing keratinocytes (Butler *et al.*, 1999) suggesting that differentiated keratinocytes do not contribute significantly. In addition, fibroblasts are also able to promote the proliferation and differentiation of keratinocytes in a dose dependent manner (Coulomb *et al.*, 1989; el-Ghalbzouri *et al.*, 2002) and show a synergistic effect on epidermal regeneration when transplanted together with keratinocytes (Svensjo *et al.*, 2002). These reports suggest that the increase in wound closure by epidermal regeneration between UCs and CCs could primarily be the result of the increase in fibroblast and keratinocyte number and not by the differentiation of the keratinocytes. It is therefore speculated that a skin equivalent equally effective as the cultured construct here can be prepared without an *in vitro* culture period by increasing the density of fibroblasts and (basal) keratinocytes. Although the number of fibroblasts that could potentially be encapsulated in a collagen hydrogel volume of fibroblasts is virtually unlimited the number of keratinocytes that can be seeded is limited by the surface area of the dermal equivalent. Fibrin encapsulation of keratinocytes is an already established technique for the delivery of growth factors (Acevedo *et al.*, 2010). Therefore, as a suggestion for future work, it would be interesting to test if a dermal equivalent with an increased number of fibroblasts and keratinocytes encapsulated in the collagen component would produce similar results as those described here for the CCs.

4.3.2 Inflammatory response

In adult mammals injury is inevitably followed by an inflammatory response which helps to remove any factors (*i.e.* microbial contamination and necrotic tissue) that delay wound healing (tissue formation and remodelling) and helps induce tissue formation (fibroplasia and angiogenesis) (Szpaderska and DiPietro, 2005; Eming *et al.*, 2007). Despite its positive effects on wound repair prolongation of inflammation can cause a delay in healing and excessive scarring.

The advantage of the use of allogeneic cells over autologous cells in TE is that they are readily available and prevent additional operative procedures for subjects receiving the cells. However, in contrast to autologous cells, allogeneic cells increase inflammation in a dose dependent manner (Figure 55), prolonging the presence of myofibroblasts and delaying collagen maturation (Lamme *et al.*, 2002). It has, however, been shown that serial passages (Theobald *et al.*, 1993) results in the loss of HLA-DR antigens and

major histocompatibility (MHC) class II antigen presenting cells, such as Langerhans cells allowing allogeneic cell lines to be transplanted across major histocompatibility barriers.

Similar concerns with regards to immunogenicity can be raised against the use of xenogeneic (rat tail) collagen. Although the conservation of the triple helical region of collagen across species (Fietzek and Kuhn, 1976) has often been used as an argument for the safety of exogenous (allogeneic, xenogeneic) collagen (Lynn *et al.*, 2004) previous studies have shown that rabbits can produce (both low and high) titer, species-specific antibodies against acid solubilised rat (tail, skin) collagen (WATSON *et al.*, 1954; Michaeli *et al.*, 1969). In the present study, however, no differences in leukocyte response were found between untreated wounds and those treated with ACs. These findings are agreement with those of a study in which compressed rat-tail collagen constructs were implanted in rabbits (Mudera *et al.*, 2007) suggesting that in this model antigenicity against the material is not a concern.

4.3.3 Angiogenesis

In the first week wounds treated with the CCs showed a statistically significant 8-fold higher number of blood vessels and a (significant) 3-fold greater blood vessel cross sectional area than wounds that were not treated with cell seeded implants.

The formation of new blood vessels (sprouting) from preexisting vessels (*i.e.* angiogenesis) is essential for wound healing (Tonnesen *et al.*, 2000). The importance of this has previously been underlined by clinical studies with Dermagraft showing that the application of higher cell numbers are correlated with an increased therapeutic effect (Mansbridge *et al.*, 1998) and that increased wound closure is mediated, in part, through the stimulation of blood vessel formation within the wound (Krishnamoorthy *et al.*, 2003). The transplantation of keratinocytes and fibroblast can directly stimulate angiogenesis by the production of VEGF (Brown *et al.*, 1992; Mansbridge *et al.*, 1998; Cheema *et al.*, 2008). Previous work from our lab has shown that the angiogenic potential of compressed collagen hydrogels can be simply and rapidly improved by increasing the seeding density of fibroblasts. At sufficient levels the cells will create a consumption driven hypoxic environment which induces vascular endothelial growth factor (VEGF) gene (Cheema *et al.*, 2008), and protein expression (Hadjipanayi *et al.*,

2010) which has shown to stimulate blood vessel formation both *in vitro* and *in vivo*. This illustrates the relative ease and flexibility with which the therapeutic effect can be tailored in this system.

4.3.4 Wound contraction

Although there was no permanent engraftment of the skin equivalents the treated wounds showed 55% wound contraction compared to the 84% of untreated wounds and to the 12% of FTSGs grafted wounds, 5 weeks post-injury (Figure 52).

The physiology of wound healing in animals such as rabbits and guinea pigs is different from humans as their skin, where it overlies the panniculus carnosus, is mobile in relation to the underlying tissue (BILLINGHAM and MEDAWAR, 1955). In the early phases of wound healing, defects in these regions largely and spontaneously close (Watts *et al.*, 1958) due to the migratory action of fibroblasts (Grinnell *et al.*, 2006) moving out from the wound margins pulling them inward over the underlying wound bed. Continuous undercutting of the margins from the wound bed inhibits this process (Watts *et al.*, 1958) allowing new connective tissue to be formed more extensively. This appears to mimic the human condition where the panniculus carnosus is mostly absent and the skin is less mobile.

A previous study in pigs suggests that in humans as in animals with mobile skin, granulation tissue formation in the early phases of wound healing does not significantly contribute to wound contraction (Gross *et al.*, 1995). At later stages, however, if the defect persists and a sufficient amount of granulation tissue has been allowed to form a further reduction of the wound size will occur through myofibroblast mediated contraction of the matrix under mechanical stimulation (Grinnell, 2000). *In vitro* studies suggest that the mechanical stress appears to be crucial for maintaining this late contraction process as apoptosis is initiated upon stress removal (Grinnell *et al.*, 1999; Hadjipanayi *et al.*, 2009). These findings were confirmed *in vivo* experiments in which the granulation tissue was released from the wound margins (Carlson *et al.*, 2003) or the wound was splinted (Carlson and Thompson, 2004).

Mechanical stress is an important modulator of granulation tissue proliferation and scar contracture could therefore very well be the end result of unfavourable mechanical

effects working on the site of injury which in the immobile skin can result in major body deformation and loss of joint motion. Although the present constructs appear to have an influence on early spontaneous contraction their ejection from the wound makes it unlikely that they will have an effect on scar contracture.

4.3.5 Engraftment

Therefore, in the first week there was partial take of the ACs, but all skin equivalents showed progressive desiccation with ultimately no permanent engraftment of either the AC or cell-seeded skin equivalents. By week 3, grafts were invariably undermined by epidermal regeneration ejecting the constructs from the wounds.

In the early phases the immobilisation of the construct within the wound bed is essential for engraftment and is provided by the (PLGA/Vicryl) sutures and the structural integrity of the (PLGA/Vicryl) mesh. As PLGA degrades in a humid environment (Gorham *et al.*, 1987) a pre-implantation *in vitro* culture period decreases *in vivo* persistence with reports showing a decrease in persistence from 4-8 weeks (MacDonald *et al.*, 1992; Meddings *et al.*, 1993) to 2-4 weeks (Chen *et al.*, 2005). Similar to previous reports about Dermagraft which is also a PLGA-collagen hybrid cultured for a 2-week period (Hansbrough *et al.*, 1992) the CCs in the present study showed no tearing during suturing, although over the implantation period the loss of CCs was greater and occurred earlier than UCs (Table 2).

Vascularisation is in part driven by the release of angiogenic factors from the transplanted cells (Cheema *et al.*, 2008) and their survival is therefore important to carry out this function. Although an increased angiogenic response was found in the wound bed (Figure 70) it fell short of involving the implant (Figure 51). It is considered here that the progressive desiccation of the constructs after the removal of the dressing (at day 3) could have resulted in the premature cessation in the release of angiogenic factors. Compressed collagen hydrogels (0.7 ml/cm²) have been shown to be susceptible to dehydration with complete loss of viability after only 60 seconds (Brown *et al.*, 2005). In addition, the failure of the implant to vascularise could in part be the result of the high fibril density of the compressed collagen component which could have further increased due the compacting effect of dehydration. It has previously been shown that

the pore size is an important determinant of how readily endothelial cells can invade an implant (Sahota *et al.*, 2003).

Now although the CCs featured a differentiated stratified epidermis with a stratum corneum (the functional barrier layer) this did not prevent the skin equivalents from dehydration. It has previously shown that even though an *in vitro* reconstructed epidermis structurally mimics native tissue it does not do so functionally (Fartasch and Ponc, 1994). One commercially available skin substitute, Integra, addresses this by featuring a silicone elastomer cured to the underlying dermal component (Yannas *et al.*, 1981). A second stage surgical intervention, however, is required to reconstruct the epidermis after the dermal component is vascularised.

Another factor that could have contributed to the failure of these skin equivalents to engraft is the inflammatory response to the embedded allogeneic cells. As opposed to the present study performed in an immunocompetent animal model, vascularisation of PLGA-(cell derived) collagen hybrids in full thickness skin defects has been shown in immune compromised animals (Cooper *et al.*, 1991; Chen *et al.*, 2005). It was found here that ACs, which did not increase inflammation, showed partial vascularisation and integration into the underlying wound bed (Figure 51). The point is further illustrated by Apligraf, a collagen based construct seeded with allogeneic (human) cells (Bell *et al.*, 1979; Wilkins *et al.*, 2004), which showed integration (and reduced wound contraction) in wounds of immune deficient (rat) subjects (Bell *et al.*, 1981a) but not in immune competent (human) subjects (Griffiths *et al.*, 2004).

Therefore, equal to current (allogeneic) cell seeded products (*i.e.* Apligraf and Dermagraft) which exert a therapeutic effect through multiple applications, the current cell-seeded experimental skin equivalents do not show integration into the wound bed of an immunocompetent recipient.

4.3.6 Granulation tissue formation

In the first 48 hours after injury the migration from adjacent fascia and dermis contribute primarily to the population of fibroblasts responsible for the production and remodelling of collagen within the granulation tissue after which time local proliferation becomes more important (Spyrou *et al.*, 1998). Transplanted autologous fibroblasts (in a

porcine model) have previously been shown to improve collagen maturation in full thickness skin defects in a dose dependent manner (Lamme *et al.*, 2000). Additionally, in a rabbit model it was found that the transplantation of a (non-autologous) fibroblast suspension accelerated the increase in wound strength (Sandulache *et al.*, 2003) compared to no treatment. Compared to autologous fibroblast treatment collagen maturation is slower with allogeneic cells (Lamme *et al.*, 2002) possibly due to the associated inflammatory response. In the present study, however, wounds treated with (allogeneic) cells resulted in increase in collagen maturation compared to wounds left untreated or treated with ACs (Figure 63).

It should be noted the present findings were obtained using linearly polarised light microscopy on picosirius red stained tissue sections. And although picosirius red (the method used here) has been used in various studies to quantify collagen in various studies (Pickering and Boughner, 1991; Rich and Whittaker, 2005; Cuttle *et al.*, 2005), there is evidence to suggest that the electrostatic binding of Sirius red to collagen is not stoichiometric (Puchtler *et al.*, 1988), implying that the enhancing properties are not proportionate to the actual amount of collagen present. Also questions have been raised about the specificity of the dye (Kiraly *et al.*, 1997) and the evaluation of unstained sections using polarised light microscopy in combination with digital imaging has been advocated. Finally, it has been shown that it is difficult to visualise all of the collagen at each instance when linearly polarised light is used (Whittaker *et al.*, 1994) because (parts of) collagen fibres aligned parallel to the transmission axis of either the polariser or analyser (Figure 27) appear dark leading to an underestimation of the actual collagen content. In contrast, circularly polarised light allows the visualisation of every portion of every fibre. It can be argued that all tissue sections were processed, visualised and analysed according to the same protocol and under constant conditions which would permit inter-sample comparison, but further analysis is required to confirm this. Therefore the validity of the finding that CCs improve collagen maturation has to be questioned at present.

4.3.7 Comparison with commercially available skin equivalents

The dermal equivalent in the present study (*i.e.* the compressed collagen hydrogel hybridised with Vicryl) is similar in composition to Dermagraft (Cooper *et al.*, 1991) which is fabricated by seeding and maintaining fibroblasts on a Vicryl mesh. The main

difference is that the extracellular matrix in Dermagraft is not exogenously provided but produced by the seeded cells necessitating a 2 to 3 week *in vitro* culture period to achieve sufficient tissue formation for a therapeutic effect (Cooper *et al.*, 1991). The product is currently FDA approved for the treatment of venous (Krishnamoorthy *et al.*, 2003; Omar *et al.*, 2004), neuropathic and diabetic ulcers (Marston *et al.*, 2003).

Although Dermagraft does not contain keratinocytes it is more effective than conventional treatments of chronic (persisting longer than 6 months) venous (Krishnamoorthy *et al.*, 2003; Omar *et al.*, 2004), neuropathic and diabetic ulcers (Marston *et al.*, 2003) and the product is FDA-approved for these applications. The material 'takes' in (immune-compromised) animal wounds, but integration in human (immuno-competent) subjects has not been reported and Dermagraft requires multiple applications to achieve a clinical effect. Dermagraft with a monolayer epidermis has been tested in athymic mice (Hansbrough *et al.*, 1993). Take was significantly reduced as grafts were prone to mechanical dislodgement, possibly due to the hydrolytic degradation of the PLGA material over the extended culture time that was required to form the epidermis (of 4-6 days over the 2-3 week). Although this is less of a concern for biological dressings, Dermagraft is currently still only applied clinically without an epidermis.

It should be mentioned that Dermagraft is not to be confused with Dermagraft-TC (Dermagraft Transient Cover, currently marketed as TransCyte) which is fabricated by culturing allogeneic human neonatal fibroblasts 17 days on Biobrane (Bertek Pharmaceuticals Inc., WV, USA) a semi-permeable polymer (silicone) membrane with partially embedded woven monofilament nylon mesh onto which porcine collagen peptides are chemically bound to form a hydrophilic surface (Hansbrough *et al.*, 1994). The product is devitalised by freezing and the cell produced ECM contains fibronectin, type I collagen, proteoglycans and growth factors. The product is a temporary cover for partial thickness burns and is spontaneously ejected by healing wounds. It has shown to, decrease hospital stay compared to conventional treatment (silvazine) (Amani *et al.*, 2006), prevent frequent and painful dressing changes, autografting, and decreases the time to wound closure compared to alternative treatments (Biobrane alone, silvazine) (Kumar *et al.*, 2004)

Other dermal substitutes worth mentioning are Alloderm (Lifecell Corporation, NJ, USA) and Integra (Integra Life Sciences Corp, NJ, USA). Both these acellular products permanently engraft in clinical acute wounds unlike the presented experimental skin equivalents and currently available cell-seeded TE dressings (*i.e.* Apligraf, Dermagraft, OrCel).

Alloderm is produced from human cadaver skin by the tonic removal of epidermis with NaCl and decellularisation with sodium dodecyl sulphate (a detergent) of the dermal component. Clinical studies have shown it to be useful as a dermal substitute in full thickness burns without signs of rejection, showing revascularisation, cellular repopulation, incorporation into the wound and cosmetic results similar to intermediate thickness skin grafts (Wainwright *et al.*, 1996).

Integra (Yannas *et al.*, 1981) is the first FDA-approved skin substitute (acellular) consisting of a suturable, semi-permeable silicone elastomer (polysiloxane, Dow Corning Liquid Silastic Medical Adhesive Type A) cured to an underlying dermal component made of a degradable crosslinked (vacuum dehydration and gluteraldehyde) coprecipitation of bovine collagen and (8%) chondroitin 6-sulfate (a shark cartilage derived glycosaminoglycan). Integra is used to reconstruct the skin in a two stage procedure in surgically excised burn injuries (Burke *et al.*, 1981; Heimbach *et al.*, 2003) or in excised benign or malignant lesions (Prystowsky *et al.*, 2000). After it has integrated, generally 2-3 weeks after implantation the silicone membrane is removed and the neodermis is grafted with a split thickness skin graft. Histologically the dermal matrix disappears after one month (Stern *et al.*, 1990) and only elicits a small transient immune response (Michaeli and McPherson, 1990). Graft take is similar to allografts, worse than autografts, but cosmetically superior over meshed autografts (Heimbach *et al.*, 1988) and the reconstructed skin has elastic properties matching that of normal skin (Nguyen *et al.*, 2010).

The cultured skin equivalent featuring a stratified epidermis (*i.e.* CCs) histologically mimics Apligraf (Organogenesis Inc., MA and Novartis Pharmaceutical Corp., NJ, US) (Wilkins *et al.*, 2004). This commercially available skin equivalent consists of a bovine collagen (type I) hydrogel seeded with allogeneic human neonatal foreskin fibroblasts (Bell *et al.*, 1979) and keratinocytes (Bell *et al.*, 1981a). The mechanical properties of the dermal component are improved by allowing collagen to contract for 6 days after

which keratinocytes are seeded and cultured for 4 days under submerged conditions and terminally differentiated into a stratified epidermis for an additional 7 days at the air/liquid interface. Apligraf is currently FDA approved for the treatment of venous leg (Falanga *et al.*, 1998) and diabetic foot ulcers (Veves *et al.*, 2001).

Apligraf is more effective than conventional treatment (*i.e.* compression therapy and saline-moistened gauze, respectively) in achieving wound closure in chronic (lasting longer than 6 months) non-healing venous leg (Falanga *et al.*, 1998) and diabetic foot ulcers (Veves *et al.*, 2001) and is FDA-approved for the treatment of these conditions. As previously mentioned, Apligraf does not persist in human acute full thickness skin defects (cells remain in the wound up to 4 weeks) (Griffiths *et al.*, 2004) and requires multiple applications for it to be effective. It is noteworthy that Organogenesis is currently in late stage development of a next generation allogeneic skin equivalent, VCTO1, which similar to Apligraf with the only difference being that the dermal matrix will be human fibroblast derived making its components all human.

The skin equivalent featuring a monolayer epidermis is histologically similar to OrCel (Forticell Bioscience, Inc., formerly Ortec International, Inc., NY, US) (Eisenberg and Llewelyn, 1998), which is currently under investigation for the treatment of chronic wounds. The product is currently FDA-approved for the treatment of split-thickness skin graft donor sites (Still *et al.*, 2003) and for use in the surgical release of hand syndactyly secondary to epidermolysis bullosa (Eisenberg and Llewelyn, 1998). This commercially available skin equivalent is fabricated by seeding allogeneic fibroblasts into a preformed lyophilised bovine collagen (type I) sponge which is cultured for 2 days, inverted and seeded with keratinocytes on its non-porous side and cultured for an additional 7-14 days (Bell *et al.*, 1981b) to form a confluent monolayer epidermis.

Compared to current techniques, the compression of fibroblast seeded collagen hydrogels with an encapsulated synthetic degradable mesh can significantly shorten the culture period required to fabricate a living dermal or skin equivalent with adequate handling and wound healing properties. As set out in Table 3 the time advantage of almost one week is quite significant when the UCs with a monolayer epidermis and the cultured skin equivalent with a stratified epidermis are compared to their commercially available equivalents (Dermagraft, OrCel and Apligraf). Additionally, the method is independent of cell activity and is therefore amenable to automation. These two

characteristics could result in the fabrication of biological dressings more reproducible and cost-effective than currently available products.

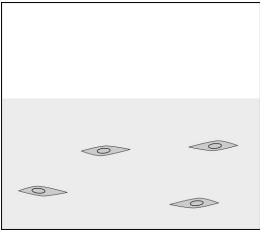
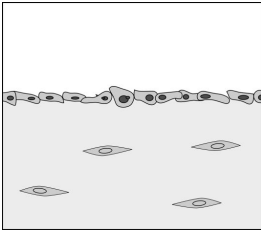
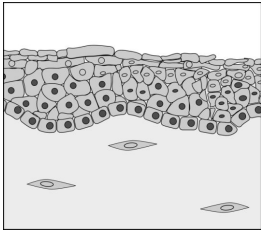
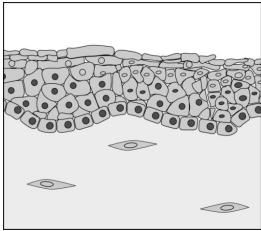
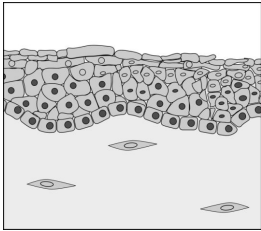
Histology					
	Dermagraft®	OrCel®	UC	Apligraf®	CC
Epidermal	n/a	7 days	4 hours	14 days	14 days
Dermal	2 - 3 weeks	2 days	1 hours	6 days	1 hour
Total	2 - 3 weeks	9 days	5 hours	20 days	14 days

Table 3 – Comparison of the fabrication times for the experimental skin equivalents (UC, uncultured constructs; CC, cultured constructs) and currently, commercially available, living, biological dressings (Dermagraft, OrCel, Apligraf).

5. Conclusions and future work

5.1 Conclusions

1. The expulsion of the interstitial fluid from a collagen hydrogel mechanically compressed under a constant force results in a mass transfer dependent and anisotropic increase in collagen fibril density in the direction of fluid flow and with a maximum at the hydrogel surface through which fluid leaves. This increase directly and negatively affects the hydraulic permeability of this FLS, progressively resisting the outflow of the fluid content.
2. The break strength (or suturability) of a fully (*i.e.* strained to over 98%) compressed collagen hydrogel can be improved by increasing the pre-compression volume. It is hypothesised, however, that the mass transfer dependent decrease in hydraulic permeability poses a physical limitation on the maximum volume (per unit area) of collagen hydrogel that can be adequately compacted and therefore on the maximum break strength that can be achieved by this method without significantly affecting cell viability.
3. The compression (to over 98% strain) of a fibroblast seeded collagen hydrogel (1.4 ml/cm²) with an encapsulated synthetic degradable polymer mesh results in the creation of a suturable, living dermal equivalent without significantly compromising cell survival. The 1 hour fabrication time is significantly less than the 2-3 weeks required to produce Dermagraft®, a commercially available biological dressing equivalent to the experimental dermal equivalent and currently FDA approved for the treatment of diabetic foot ulcers.
4. The experimental dermal equivalent could be used as a substrate for the formation of a monolayer and stratified epidermis for the production of skin equivalents. These findings results show that the fabricated dressings stimulate wound closure and the generation of blood vessels suggesting their potential utility in the treatment of lower limb ulcerations. As such it compares favourably with regards to the culture time of substrates used for the fabrication of currently commercially available skin equivalents (*i.e.* OrCel® and Apligraf®) which take 2 to 6 days. This implies a 20 to

40% reduction in overall fabrication time which could help reduce the high costs associated with the use of this type of tissue engineered dressing.

5.2 Future work

An interesting question to answer is why in clinical practice none of the currently available tissue engineered, living skin equivalents integrate or persist within the wound bed. At present, products as these only act as delivery devices of growth factors, cytokines and ECM to the site of injury and do not act as tissue substitutes. The present experimental skin equivalents could be used as a model with the data presented here as a basis for further research.

From a tissue engineering perspective the compression induced structural heterogeneity described here, could be useful for the creation of a skin substitute featuring an integrated and stiff, water-impermeable epidermal component (the compacted FLS) and an uncompacted dermal component in which different cell lines (*e.g.* fibroblasts, endothelial cells) could be embedded with high cell viability retention. It is proposed that the epidermal component at a certain collagen density could prevent desiccation of both the graft and the wound by decreasing the transfer of water. The physical properties of the largely uncompacted dermal component would allow for, higher interfacial contact with the wound bed, high permeability to oxygen and nutrients, and for an increased invasion of host cells into the graft.

6. References

- Acevedo C.A., Somoza R.A., Weinstein-Opppenheimer C., Brown D.I., Young M.E. Growth factor production from fibrin-encapsulated human keratinocytes. *Biotechnol. Lett.* 2010;**32**(7):1011-1017.
- Ahearne M., Yang Y., Then K.Y., Liu K.K. Non-destructive mechanical characterisation of UVA/riboflavin crosslinked collagen hydrogels. *British Journal of Ophthalmology* 2008;**92**(2):268.
- Ahlfors J.E., Billiar K.L. Biomechanical and biochemical characteristics of a human fibroblast-produced and remodeled matrix. *Biomaterials* 2007;**28**(13):2183-2191.
- Ahmed T.A.E., Griffith M., Hincke M. Characterization and inhibition of fibrin hydrogel-degrading enzymes during development of tissue engineering scaffolds. *Tissue Engineering* 2007;**13**(7):1469-1477.
- Almany L., Seliktar D. Biosynthetic hydrogel scaffolds made from fibrinogen and polyethylene glycol for 3D cell cultures. *Biomaterials* 2005;**26**(15):2467-2477.
- Alsberg E., Anderson K.W., Albeiruti A., Franceschi R.T., Mooney D.J. Cell-interactive alginate hydrogels for bone tissue engineering. *Journal of Dental Research* 2001;**80**(11):2025.
- Amani H., Dougherty W.R., Blome-Eberwein S. Use of Transcyte® and dermabrasion to treat burns reduces length of stay in burns of all size and etiology. *Burns* 2006;**32**(7):828-832.
- Ananta M., Aulin C.E., Hilborn J., Aibibu D., Houis S., Brown R.A., Mudera V. A poly(lactic acid-co-caprolactone)-collagen hybrid for tissue engineering applications. *Tissue Eng Part A* 2009;**15**(7):1667-1675.
- Athanasίου K.A., Schmitz J.P., Agrawal C.M. The Effects of Porosity on in Vitro Degradation of Polylactic Acid-Polyglycolic Acid Implants Used in Repair of Articular Cartilage. *Tissue Engineering* 2007;**4**(1):53-63.
- Bailey A.J., Paul R.G., Knott L. Mechanisms of maturation and ageing of collagen. *Mech. Ageing Dev.* 1998;**106**(1-2):1-56.
- BANFIELD W.G. [The solubility and swelling of collagen in dilute acid with age variations in man.]. *Anat. Rec.* 1952;**114**(2):157-171.
- Barrientos S., Stojadinovic O., Golinko M.S., Brem H., Tomic-Canic M. Growth factors and cytokines in wound healing. *Wound Repair Regen.* 2008;**16**(5):585-601.

Bell E., Ehrlich H.P., Buttle D.J., Nakatsuji T. Living tissue formed in vitro and accepted as skin-equivalent tissue of full thickness. *Science* 1981a;**211**(4486):1052-1054.

Bell E., Ehrlich H.P., Sher S., Merrill C., Sarber R., Hull B., Nakatsuji T., Church D., Buttle D.J. Development and use of a living skin equivalent. *Plast. Reconstr. Surg.* 1981b;**67**(3):386-392.

Bell E., Ivarsson B., Merrill C. Production of a tissue-like structure by contraction of collagen lattices by human fibroblasts of different proliferative potential in vitro. *Proc. Natl. Acad. Sci. U. S. A* 1979;**76**(3):1274-1278.

Beningo K.A., Dembo M., Wang Y. Responses of fibroblasts to anchorage of dorsal extracellular matrix receptors. *Proceedings of the National Academy of Sciences of the United States of America* 2004;**101**(52):18024.

Bent A.E., Tutrone R.T., McLennan M.T., Lloyd K., Kennelly M.J., Badlani G. Treatment of intrinsic sphincter deficiency using autologous ear chondrocytes as a bulking agent. *Neurourology and urodynamics* 2001;**20**(2):157-165.

Bergan J.J., Schmid-Schonbein G.W., Smith P.D., Nicolaides A.N., Boisseau M.R., Eklof B. Chronic venous disease. *N. Engl. J. Med.* 2006;**355**(5):488-498.

BILLINGHAM R.E., MEDAWAR P.B. Contracture and intussusceptive growth in the healing of extensive wounds in mammalian skin. *J. Anat.* 1955;**89**(1):114-123.

Bitar M., Salih V., Brown R.A., Nazhat S.N. Effect of multiple unconfined compression on cellular dense collagen scaffolds for bone tissue engineering. *Journal of Materials Science: Materials in Medicine* 2007;**18**(2):237-244.

Bleiziffer O., Eriksson E., Yao F., Horch R.E., Kneser U. Gene transfer strategies in tissue engineering. *J. Cell Mol Med.* 2007;**11**(2):206-223.

Blombäck B., Bark N. Fibrinopeptides and fibrin gel structure. *Biophysical chemistry* 2004;**112**(2-3):147-151.

Bottcher-Haberzeth S., Biedermann T., Reichmann E. Tissue engineering of skin. *Burns* 2010;**36**(4):450-460.

Brissett A.E., Sherris D.A. Scar contractures, hypertrophic scars, and keloids. *Facial. Plast. Surg* 2001;**17**(4):263-272.

Brown L.F., Yeo K.T., Berse B., Yeo T.K., Senger D.R., Dvorak H.F., Van De Water L. Expression of vascular permeability factor (vascular endothelial growth factor) by epidermal keratinocytes during wound healing. *Journal of Experimental Medicine* 1992;**176**(5):1375.

- Brown R.A., Wisema M., Chuo C.B., Cheema U., Nazhat S.N. Ultrarapid Engineering of Biomimetic Materials and Tissues: Fabrication of Nano- and Microstructures by Plastic Compression. *Advanced Functional Materials* 2005;**15**(11):1762-1770.
- Brusselaers N., Pirayesh A., Hoeksema H., Richters C.D., Verbelen J., Beele H., Blot S.I., Monstrey S. Skin replacement in burn wounds. *J. Trauma* 2010;**68**(2):490-501.
- Burdick J.A., Chung C., Jia X., Randolph M.A., Langer R. Controlled degradation and mechanical behavior of photopolymerized hyaluronic acid networks. *Biomacromolecules* 2005;**6**(1):386.
- Burdick J.A., Anseth K.S. Photoencapsulation of osteoblasts in injectable RGD-modified PEG hydrogels for bone tissue engineering. *Biomaterials* 2002;**23**(22):4315-4323.
- Burke J.F., Yannas I.V., QUINBY Jr W.C., BONDOC C.C., JUNG W.K. Successful use of a physiologically acceptable artificial skin in the treatment of extensive burn injury. *Annals of surgery* 1981;**194**(4):413.
- Butler C.E., Yannas I.V., Compton C.C., Correia C.A., Orgill D.P. Comparison of cultured and uncultured keratinocytes seeded into a collagen-GAG matrix for skin replacements. *Br. J. Plast. Surg.* 1999;**52**(2):127-132.
- Buxton P.G., Bitar M., Gellynck K., Parkar M., Brown R.A., Young A.M., Knowles J.C., Nazhat S.N. Dense collagen matrix accelerates osteogenic differentiation and rescues the apoptotic response to MMP inhibition. *Bone* 2008;**43**(2):377-385.
- Carachi R., Azmy A., Gorham S., Reid J., French D.A. Use of a bioprosthesis to relieve tension in oesophageal anastomosis: an experimental study. *Br. J. Surg.* 1989;**76**(5):496-498.
- Carlson M.A., Longaker M.T., Thompson J.S. Wound splinting regulates granulation tissue survival. *J. Surg. Res.* 2003;**110**(1):304-309.
- Carlson M.A., Thompson J.S. Wound splinting modulates granulation tissue proliferation. *Matrix Biol.* 2004;**23**(4):243-250.
- Castella L.F., Buscemi L., Godbout C., Meister J.J., Hinz B. A new lock-step mechanism of matrix remodelling based on subcellular contractile events. *J. Cell Sci.* 2010;**123**(Pt 10):1751-1760.
- Caulfield R.H., Tyler M.P., Austyn J.M., Dziewulski P., McGrouther D.A. The relationship between protease/anti-protease profile, angiogenesis and re-epithelialisation in acute burn wounds. *Burns* 2008;**34**(4):474-486.
- Chandran P.L., Barocas V.H. Microstructural mechanics of collagen gels in confined compression: poroelasticity, viscoelasticity, and collapse. *Journal of biomechanical engineering* 2004;**126**:152.

- Cheema U., Brown R.A., Alp B., MacRobert A.J. Spatially defined oxygen gradients and vascular endothelial growth factor expression in an engineered 3D cell model. *Cellular and molecular life sciences* 2008;**65**(1):177-186.
- Cheema U., Chuo C.B., Sarathchandra P., Nazhat S.N., Brown R.A. Engineering functional collagen scaffolds: Cyclical loading increases material strength and fibril aggregation. *Advanced Functional Materials* 2007;**17**(14):2426-2431.
- Cheer K., Shearman C., Jude E.B. Managing complications of the diabetic foot. *BMJ* 2009;**339**b4905.
- Chen F.M., Zhang M., Wu Z.F. Toward delivery of multiple growth factors in tissue engineering. *Biomaterials* 2010;**31**(24):6279-6308.
- Chen G., Sato T., Ohgushi H., Ushida T., Tateishi T., Tanaka J. Culturing of skin fibroblasts in a thin PLGA-collagen hybrid mesh. *Biomaterials* 2005;**26**(15):2559-2566.
- Chen G., Sato T., Ushida T., Hirochika R., Shirasaki Y., Ochiai N., Tateishi T. The use of a novel PLGA fiber/collagen composite web as a scaffold for engineering of articular cartilage tissue with adjustable thickness. *J. Biomed. Mater. Res. A* 2003a;**67**(4):1170-1180.
- Chen G., Sato T., Ushida T., Hirochika R., Tateishi T. Redifferentiation of dedifferentiated bovine chondrocytes when cultured in vitro in a PLGA-collagen hybrid mesh. *FEBS Lett.* 2003b;**542**(1-3):95-99.
- Chen G., Ushida T., Tateishi T. A hybrid network of synthetic polymer mesh and collagen sponge. *Chemical Communications* 2000;(16):1505-1506.
- Chenite A., Chaput C., Wang D., Combes C., Buschmann M.D., Hoemann C.D., Leroux J.C., Atkinson B.L., Binette F., Selmani A. Novel injectable neutral solutions of chitosan form biodegradable gels in situ. *Biomaterials* 2000;**21**(21):2155-2161.
- Cheung D.T., Perelman N., Ko E.C., Nimni M. Mechanism of crosslinking of proteins by glutaraldehyde III. Reaction with collagen in tissues. *Connective Tissue Research* 1985;**13**(2):109-115.
- Choi M., Armstrong M.B., Panthaki Z.J. Pediatric hand burns: thermal, electrical, chemical. *J. Craniofac. Surg* 2009;**20**(4):1045-1048.
- Chu M.L., de W.W., Bernard M., Ding J.F., Morabito M., Myers J., Williams C., Ramirez F. Human pro alpha 1(I) collagen gene structure reveals evolutionary conservation of a pattern of introns and exons. *Nature* 1984;**310**(5975):337-340.
- Cima L.G., Vacanti J.P., Vacanti C., Ingber D., Mooney D., Langer R. Tissue engineering by cell transplantation using degradable polymer substrates. *J. Biomech. Eng* 1991;**113**(2):143-151.

- Conn Jr J., Oyasu R., Welsh M., Beal J.M. Vicryl (polyglactin 910) synthetic absorbable sutures. *The American Journal of Surgery* 1974;**128**(1):19-23.
- Cooper M.L., Hansbrough J.F., Spielvogel R.L., Cohen R., Bartel R.L., Naughton G. In vivo optimization of a living dermal substitute employing cultured human fibroblasts on a biodegradable polyglycolic acid or polyglactin mesh. *Biomaterials* 1991;**12**(2):243-248.
- Coulomb B., Lebreton C., Dubertret L. Influence of human dermal fibroblasts on epidermalization. *J. Invest Dermatol.* 1989;**92**(1):122-125.
- Coulombe P.A. Wound epithelialization: accelerating the pace of discovery. *J. Invest Dermatol.* 2003;**121**(2):219-230.
- Cuttle L., Nataatmadja M., Fraser J.F., Kempf M., Kimble R.M., Hayes M.T. Collagen in the scarless fetal skin wound: detection with picrosirius-polarization. *Wound Repair Regen.* 2005;**13**(2):198-204.
- Dallon J.C., Ehrlich H.P. A review of fibroblast-populated collagen lattices. *Wound Repair and Regeneration* 2008;**16**(4):472-479.
- Davenport M., Daly J., Harvey I., Griffiths R.W. The bolus tie-over "pressure" dressing in the management of full thickness skin grafts. Is it necessary? *Br. J. Plast. Surg.* 1988;**41**(1):28-32.
- Deng C., Li F., Hackett J.M., Chaudhry S.H., Toll F.N., Toye B., Hodge W., Griffith M. Collagen and glycopolymer based hydrogel for potential corneal application. *Acta Biomaterialia* 2010;**6**(1):187-194.
- Doillon C.J., Cote M.F., Pietrucha K., Laroche G. Porosity and biological properties of polyethylene glycol-conjugated collagen materials. *Journal of Biomaterials Science, Polymer Edition* 1995;**6**(8):715-728.
- Doillon C.J., Dunn M.G., Bender E., Silver F.H. Collagen fiber formation in repair tissue: development of strength and toughness. *Coll. Relat Res.* 1985a;**5**(6):481-492.
- Doillon C.J., Dunn M.G., Berg R.A., Silver F.H. Collagen deposition during wound repair. *Scan Electron Microsc.* 1985b;(Pt 2):897-903.
- Drury J.L., Mooney D.J. Hydrogels for tissue engineering: scaffold design variables and applications. *Biomaterials* 2003;**24**(24):4337-4351.
- East E., de Oliveira D.B., Golding J.P., Phillips J.B. Alignment of Astrocytes Increases Neuronal Growth in Three-Dimensional Collagen Gels and Is Maintained Following Plastic Compression to Form a Spinal Cord Repair Conduit. *Tissue Engineering Part A* 2010;**0**(0).

Ehrlich H.P., Rittenberg T. Differences in the mechanism for high-versus moderate-density fibroblast-populated collagen lattice contraction. *Journal of Cellular Physiology* 2000;**185**(3):432-439.

Eisenberg M., Llewelyn D. Surgical management of hands in children with recessive dystrophic epidermolysis bullosa: use of allogeneic composite cultured skin grafts. *British journal of plastic surgery* 1998;**51**(8):608-613.

el-Ghalbzouri A., Gibbs S., Lamme E., Van Blitterswijk C.A., Ponec M. Effect of fibroblasts on epidermal regeneration. *Br. J. Dermatol.* 2002;**147**(2):230-243.

Ellis M.J., Chaudhuri J.B. Poly(lactic-co-glycolic acid) hollow fibre membranes for use as a tissue engineering scaffold. *Biotechnol. Bioeng.* 2007;**96**(1):177-187.

Elsdale T., Bard J. Collagen substrata for studies on cell behavior. *J. Cell Biol.* 1972;**54**(3):626-637.

Eming S.A., Krieg T., Davidson J.M. Inflammation in wound repair: molecular and cellular mechanisms. *J. Invest Dermatol.* 2007;**127**(3):514-525.

Engelhardt E.M., Stegberg E., Brown R.A., Hubbell J.A., Wurm F.M., Adam M., Frey P. Compressed collagen gel: a novel scaffold for human bladder cells. *J. Tissue Eng Regen. Med.* 2010;**4**(2):123-130.

Falanga V. Wound healing and its impairment in the diabetic foot. *Lancet* 2005;**366**(9498):1736-1743.

Falanga V., Margolis D., Alvarez O., Auletta M., Maggiasco F., Altman M., Jensen J., Sabolinski M., Hardin-Young J. Rapid healing of venous ulcers and lack of clinical rejection with an allogeneic cultured human skin equivalent. *Archives of dermatology* 1998;**134**(3):293.

Fartasch M., Ponec M. Improved barrier structure formation in air-exposed human keratinocyte culture systems. *J. Invest Dermatol.* 1994;**102**(3):366-374.

Fietzek P.P., Kuhn K. The primary structure of collagen. *Int. Rev. Connect. Tissue Res.* 1976;**7**:1-60.

Fodor W.L. Tissue engineering and cell based therapies, from the bench to the clinic: the potential to replace, repair and regenerate. *Reprod. Biol Endocrinol.* 2003;**1**:102.

Frame J.D., Still J., Lakhel-LeCoadou A., Carstens M.H., Lorenz C., Orlet H., Spence R., Berger A.C., Dantzer E., Burd A. Use of dermal regeneration template in contracture release procedures: a multicenter evaluation. *Plast. Reconstr. Surg* 2004;**113**(5):1330-1338.

Francis O.S., Cecil E.Hall, Marie A.J. Electron microscope investigations of the structure of collagen. *Journal of Cellular and Comparative Physiology* 1942;**20**(1):11-33.

Furthmayr H., Timpl R. Immunochemistry of collagens and procollagens. *Int. Rev Connect. Tissue Res.* 1976;**7**:61-99.

Gabbiani G. The myofibroblast in wound healing and fibrocontractive diseases. *J. Pathol.* 2003;**200**(4):500-503.

Girton T.S., Barocas V.H., Tranquillo R.T. Confined compression of a tissue-equivalent: collagen fibril and cell alignment in response to anisotropic strain. *J. Biomech. Eng* 2002;**124**(5):568-575.

Girton T.S., Oegema T.R., Tranquillo R.T. Exploiting glycation to stiffen and strengthen tissue equivalents for tissue engineering. *Journal of Biomedical Materials Research Part A* 1999;**46**(1):87-92.

Glowacki J., Mizuno S. Collagen scaffolds for tissue engineering. *Biopolymers* 2008;**89**(5):338-344.

Godbey W.T., Stacey Hindy B.S., Sherman M.E., Atala A. A novel use of centrifugal force for cell seeding into porous scaffolds. *Biomaterials* 2004;**25**(14):2799-2805.

Goffin J.M., Pittet P., Csucs G., Lussi J.W., Meister J.J., Hinz B. Focal adhesion size controls tension-dependent recruitment of alpha-smooth muscle actin to stress fibers. *J. Cell Biol* 2006;**172**(2):259-268.

Gorham S., McCafferty I., Baraza R., Scott R. Preliminary development of a collagen membrane for use in urological surgery. *Urol. Res.* 1984;**12**(6):295-299.

Gorham S.D., Monsour M.J., Scott R. The in vitro assessment of a collagen/vicryl (polyglactin) composite film together with candidate suture materials for use in urinary tract surgery. I. Physical testing. *Urol. Res.* 1987;**15**(1):53-59.

Griffiths M., Ojeh N., Livingstone R., Price R., Navsaria H. Survival of Apligraf in acute human wounds. *Tissue Engineering* 2004;**10**(7-8):1180-1195.

Grinnell F. Fibroblast-collagen-matrix contraction: growth-factor signalling and mechanical loading. *Trends Cell Biol.* 2000;**10**(9):362-365.

Grinnell F., Rocha L.B., Iucu C., Rhee S., Jiang H. Nested collagen matrices: a new model to study migration of human fibroblast populations in three dimensions. *Exp. Cell Res.* 2006;**312**(1):86-94.

Grinnell F., Zhu M., Carlson M.A., Abrams J.M. Release of mechanical tension triggers apoptosis of human fibroblasts in a model of regressing granulation tissue. *Exp. Cell Res.* 1999;**248**(2):608-619.

- Gross J., Farinelli W., Sadow P., Anderson R., Bruns R. On the mechanism of skin wound "contraction": a granulation tissue "knockout" with a normal phenotype. *Proc. Natl. Acad. Sci. U. S. A* 1995;**92**(13):5982-5986.
- Gunatillake P.A., Adhikari R. Biodegradable synthetic polymers for tissue engineering. *Eur. Cell Mater.* 2003;**5**:1-16.
- Hadjipanayi E., Brown R.A., Mudera V., Deng D., Liu W., Cheema U. Controlling physiological angiogenesis by hypoxia-induced signaling. *Journal of Controlled Release* 2010;**In Press, Corrected Proof**.
- Hadjipanayi E., Mudera V., Brown R.A. Close dependence of fibroblast proliferation on collagen scaffold matrix stiffness. *J. Tissue Eng Regen. Med.* 2009;**3**(2):77-84.
- Hansbrough J.F., Dore C., Hansbrough W.B. Clinical trials of a living dermal tissue replacement placed beneath meshed, split-thickness skin grafts on excised burn wounds. *J. Burn Care Rehabil.* 1992;**13**(5):519-529.
- Hansbrough J.F., Morgan J., Greenleaf G., Underwood J. Development of a temporary living skin replacement composed of human neonatal fibroblasts cultured in Biobrane, a synthetic dressing material. *Surgery* 1994;**115**(5):633.
- Hansbrough J.F., Morgan J.L., Greenleaf G.E., Bartel R. Composite grafts of human keratinocytes grown on a polyglactin mesh-cultured fibroblast dermal substitute function as a bilayer skin replacement in full-thickness wounds on athymic mice. *J. Burn Care Rehabil.* 1993;**14**(5):485-494.
- Harding K.G., Moore K., Phillips T.J. Wound chronicity and fibroblast senescence--implications for treatment. *Int. Wound J.* 2005;**2**(4):364-368.
- Hefton J.M., Madden M.R., Finkelstein J.L., Shires G.T. Grafting of burn patients with allografts of cultured epidermal cells. *Lancet* 1983;**2**(8347):428-430.
- Heimbach D., Luterman A., Burke J., Cram A., Herndon D., Hunt J., Jordan M., McManus W., Solem L., Warden G. Artificial dermis for major burns. A multi-center randomized clinical trial. *Annals of surgery* 1988;**208**(3):313.
- Heimbach D.M., Warden G.D., Luterman A., Jordan M.H., Ozobia N., Ryan C.M., Voigt D.W., Hickerson W.L., Saffle J.R., DeClement F.A. Multicenter postapproval clinical trial of integra (r) dermal regeneration template for burn treatment. *Journal of Burn Care & Research* 2003;**24**(1):42.
- Helary C., Bataille I., Abed A., Illoul C., Anglo A., Louedec L., Letourneur D., Meddahi-Pelle A., Giraud-Guille M.M. Concentrated collagen hydrogels as dermal substitutes. *Biomaterials* 2010;**31**(3):481-490.
- Hinz B. Formation and function of the myofibroblast during tissue repair. *J. Invest Dermatol.* 2007;**127**(3):526-537.

Holland S.J., Jolly A.M., Yasin M., Tighe B.J. Polymers for biodegradable medical devices: II. Hydroxybutyrate-hydroxyvalerate copolymers: hydrolytic degradation studies. *Biomaterials* 1987;**8**(4):289-295.

Hollister S.J. Porous scaffold design for tissue engineering. *Nature materials* 2005;**4**(7):518-524.

Hong Y., Mao Z., Wang H., Gao C., Shen J. Covalently crosslinked chitosan hydrogel formed at neutral pH and body temperature. *Journal of Biomedical Materials Research Part A* 2006;**79**(4):913-922.

Hong Y., Song H., Gong Y., Mao Z., Gao C., Shen J. Covalently crosslinked chitosan hydrogel: Properties of in vitro degradation and chondrocyte encapsulation. *Acta Biomaterialia* 2007;**3**(1):23-31.

Horch R.E., Debus M., Wagner G., Stark G.B. Cultured human keratinocytes on type I collagen membranes to reconstitute the epidermis. *Tissue Engineering* 2000;**6**(1):53-67.

Hu K., Shi H., Zhu J., Deng D., Zhou G., Zhang W., Cao Y., Liu W. Compressed collagen gel as the scaffold for skin engineering. *Biomedical Microdevices* 2010;1-9.

Hunt N.C., Grover L.M. Cell encapsulation using biopolymer gels for regenerative medicine. *Biotechnol. Lett.* 2010;**32**(6):733-742.

Hutmacher D.W. Scaffolds in tissue engineering bone and cartilage. *Biomaterials* 2000;**21**(24):2529-2543.

Hutmacher D.W. Scaffold design and fabrication technologies for engineering tissues--state of the art and future perspectives. *J. Biomater. Sci. Polym. Ed* 2001;**12**(1):107-124.

Irvin T.T., Hunt T.K. The effect of trauma on colonic healing. *Br. J. Surg.* 1974;**61**(6):430-436.

Jankunas V., Bagdonas R., Samsanavicius D., Rimdeika R. An analysis of the effectiveness of skin grafting to treat chronic venous leg ulcers. *Wounds-A Compendium of Clinical Research and Practice* 2007;**19**(5):128-137.

John H. Viscous flow relative to arrays of cylinders. *AIChE Journal* 1959;**5**(2):174-177.

Jones I., James S.E., Rubin P., Martin R. Upward migration of cultured autologous keratinocytes in Integra™ artificial skin: a preliminary report. *Wound Repair and Regeneration* 2003;**11**(2):132-138.

Jordan-Lloyd D., Marriott R.H. The Swelling of Structured Proteins The Influence of the Reticular Tissue on the Swelling of Collagen in Water and Hydrochloric Acid. *Proceedings of the Royal Society of London. Series B - Biological Sciences* 1935;**118**(810):439-445.

Kadler K.E., Hojima Y., Prockop D.J. Assembly of collagen fibrils de novo by cleavage of the type I pC-collagen with procollagen C-proteinase. Assay of critical concentration demonstrates that collagen self-assembly is a classical example of an entropy-driven process. *J. Biol Chem.* 1987;**262**(32):15696-15701.

Kagan H.M., Li W. Lysyl oxidase: properties, specificity, and biological roles inside and outside of the cell. *J. Cell Biochem.* 2003;**88**(4):660-672.

Kawazoe N., Xiaoting L., Tateishi T., Guoping C. Three-dimensional Cultures of Rat Pancreatic RIN-5F Cells in Porous PLGA-collagen Hybrid Scaffolds. *Journal of Bioactive and Compatible Polymers* 2009;**24**(1):25-42.

Kim J., Kim I.S., Cho T.H., Lee K.B., Hwang S.J., Tae G., Noh I., Lee S.H., Park Y., Sun K. Bone regeneration using hyaluronic acid-based hydrogel with bone morphogenic protein-2 and human mesenchymal stem cells. *Biomaterials* 2007;**28**(10):1830-1837.

Kiraly K., Hyttinen M.M., Lapvetelainen T., Elo M., Kiviranta I., Dobai J., Modis L., Helminen H.J., Arokoski J.P. Specimen preparation and quantification of collagen birefringence in unstained sections of articular cartilage using image analysis and polarizing light microscopy. *Histochem. J.* 1997;**29**(4):317-327.

Kisiday J., Jin M., Kurz B., Hung H., Semino C., Zhang S., Grodzinsky A.J. Self-assembling peptide hydrogel fosters chondrocyte extracellular matrix production and cell division: implications for cartilage tissue repair. *Proceedings of the National Academy of Sciences of the United States of America* 2002;**99**(15):9996.

Knox B.H., Scott M.G., Weigmann H.D., Rebenfeld L. The Effects of an Aqueous Medium on the Structure and Physical Properties of a Polyester Yarn. *Textile Research Journal* 1981;**51**(8):549.

Kose O., Waseem A. Keloids and hypertrophic scars: are they two different sides of the same coin? *Dermatol. Surg* 2008;**34**(3):336-346.

Koupidis S.A., Paraskevas K.I., Stathopoulos V., Mikhailidis D.P. Impact of lower extremity venous ulcers due to chronic venous insufficiency on quality of life. *Open. Cardiovasc. Med. J.* 2008;**2**:105-109.

Krishnamoorthy L., Harding K., Griffiths D., Moore K., Leaper D., Poskitt K., Sibbald R.G., Brassard A., Dolynchuk K., Adams J. The clinical and histological effects of Dermagraft (R) in the healing of chronic venous leg ulcers. *Phlebology* 2003;**18**(1):12.

Kumar R.J., Kimble R.M., Boots R., Pegg S.P. Treatment of partial-thickness burns: a prospective, randomized trial using Transcyte™. *ANZ journal of surgery* 2004;**74**(8):622-626.

Lamme E.N., van Leeuwen R.T., Brandsma K., Van M.J., Middelkoop E. Higher numbers of autologous fibroblasts in an artificial dermal substitute improve tissue regeneration and modulate scar tissue formation. *J. Pathol.* 2000;**190**(5):595-603.

Lamme E.N., van Leeuwen R.T., Mekkes J.R., Middelkoop E. Allogeneic fibroblasts in dermal substitutes induce inflammation and scar formation. *Wound. Repair Regen.* 2002;**10**(3):152-160.

Langer R., Vacanti J.P. Tissue engineering. *Science* 1993;**260**(5110):920-926.

Lansdown A.B., Payne M.J. An evaluation of the local reaction and biodegradation of calcium sodium alginate (Kaltostat) following subcutaneous implantation in the rat. *JR Coll Surg Edinb* 1994;**39**(5):284-288.

Laurens N., Koolwijk P., de Maat M.P. Fibrin structure and wound healing. *J. Thromb. Haemost.* 2006;**4**(5):932-939.

Leung B.K.-O., Robinson G.B. Ultrafiltration properties of hydrogel analogues of basement membrane: a comparison of the pore theory and the fibre-matrix hypothesis. *Journal of Membrane Science* 1990;**51**(1-2):141-159.

Li J., Chen J., Kirsner R. Pathophysiology of acute wound healing. *Clin. Dermatol.* 2007;**25**(1):9-18.

Li J., Zhang Y.P., Kirsner R.S. Angiogenesis in wound repair: angiogenic growth factors and the extracellular matrix. *Microsc. Res. Tech.* 2003a;**60**(1):107-114.

Li Q., Williams C.G., Sun D.D.N., Wang J., Leong K., Elisseeff J.H. Photocrosslinkable polysaccharides based on chondroitin sulfate. *Journal of Biomedical Materials Research Part A* 2003b;**68**(1):28-33.

Luijendijk R.W., Hop W.C.J., van den Tol M.P., de Lange D.C.D., Braaksma M.M.J., IJzermans J.N.M., Boelhouwer R.U., de Vries B.C., Salu M.K.M., Wereldsma J.C.J. A comparison of suture repair with mesh repair for incisional hernia. *The New England journal of medicine* 2000;**343**(6):392.

Lynn A.K., Yannas I.V., Bonfield W. Antigenicity and immunogenicity of collagen. *J. Biomed. Mater. Res. B Appl. Biomater.* 2004;**71**(2):343-354.

MacDonald A., Carachi R., Gibson A. A new oesophageal tube: assessment of collagen/vicryl composite membrane. *J. Pediatr. Surg.* 1992;**27**(7):856-858.

Mahmoud S.M., Mohamed A.A., Mahdi S.E., Ahmed M.E. Split-skin graft in the management of diabetic foot ulcers. *J. Wound Care* 2008;**17**(7):303-306.

Maja M.S., Flavio M.C., Thierry O., Eliane M., Claudia v.T., Pamela J.J. Keratinocyte biology and pathology. *Veterinary Dermatology* 1997;**8**(2):67-100.

Mansbridge J., Liu K., Patch R., Symons K., Pinney E. Three-dimensional fibroblast culture implant for the treatment of diabetic foot ulcers: metabolic activity and therapeutic range. *Tissue Engineering* 1998;**4**(4):403-414.

Marenzana M., Kelly D.J., Prendergast P.J., Brown R.A. A collagen-based interface construct for the assessment of cell-dependent mechanical integration of tissue surfaces. *Cell Tissue Res.* 2007;**327**(2):293-300.

Marenzana M., Wilson-Jones N., Mudera V., Brown R.A. The origins and regulation of tissue tension: identification of collagen tension-fixation process in vitro. *Exp. Cell Res.* 2006;**312**(4):423-433.

Marston W.A., Hanft J., Norwood P., Pollak R. The efficacy and safety of Dermagraft in improving the healing of chronic diabetic foot ulcers: results of a prospective randomized trial. *Diabetes Care* 2003;**26**(6):1701.

Martin P. Wound healing--aiming for perfect skin regeneration. *Science* 1997;**276**(5309):75-81.

McAree K.G., Klein R.L., Boeckman C.R. The use of cultured epithelial autografts in the wound care of severely burned patients. *Journal of Pediatric Surgery* 1993;**28**(2):166-168.

McKeen LW: Introduction to Plastics and Elastomers: Effect of Temperature and other Factors on Plastics and Elastomers (2), pp 1-39 (William Andrew Publishing, Norwich, NY 2008).

Meddings R.N., Carachi R., Gorham S., French D.A. A new bioprosthesis in large abdominal wall defects. *J. Pediatr. Surg.* 1993;**28**(5):660-663.

Metters A., Hubbell J. Network formation and degradation behavior of hydrogels formed by Michael-type addition reactions. *Biomacromolecules* 2005;**6**(1):290-301.

Mi S., Chen B., Wright B., Connon C.J. Plastic compression of a collagen gel forms a much improved scaffold for ocular surface tissue engineering over conventional collagen gels. *J. Biomed. Mater. Res. A* 2010.

Michaeli D., Martin G.R., Kettman J., Benjamini E., Leung D.Y., Blatt B.A. Localization of antigenic determinants in the polypeptide chains of collagen. *Science* 1969;**166**(3912):1522-1524.

Michaeli D., McPherson M. Immunologic study of artificial skin used in the treatment of thermal injuries. *Journal of Burn Care & Research* 1990;**11**(1):21.

Miki H., Ando N., Ozawa S., Sato M., Hayashi K., Kitajima M. An artificial esophagus constructed of cultured human esophageal epithelial cells, fibroblasts, polyglycolic acid mesh, and collagen. *ASAIO J.* 1999;**45**(5):502-508.

Mikos A.G., Thorsen A.J., Czerwonka L.A., Bao Y., Langer R., Winslow D.N., Vacanti J.P. Preparation and characterization of poly(l-lactic acid) foams. *Polymer* 1994;**35**(5):1068-1077.

- Mishell B.B., Shiigi S.M., Henry C., Mishell R.I. Selected methods in cellular immunology.1980.
- Mitev V., Miteva L. Signal transduction in keratinocyte proliferation and differentiation. *Biomed Rev* 1997;**8**31-48.
- Monsour M.J., Mohammed R., Gorham S.D., French D.A., Scott R. An assessment of a collagen/vicryl composite membrane to repair defects of the urinary bladder in rabbits. *Urological Research* 1987;**15**(4):235-238.
- Monstrey S., Hoeksema H., Verbelen J., Pirayesh A., Blondeel P. Assessment of burn depth and burn wound healing potential. *Burns* 2008;**34**(6):761-769.
- Mooney D.J., Baldwin D.F., Suh N.P., Vacanti J.P., Langer R. Novel approach to fabricate porous sponges of poly(-lactic-co-glycolic acid) without the use of organic solvents. *Biomaterials* 1996;**17**(14):1417-1422.
- Morasso M.I., Tomic-Canic M. Epidermal stem cells: the cradle of epidermal determination, differentiation and wound healing. *Biol Cell* 2005;**97**(3):173-183.
- Mudera V., Morgan M., Cheema U., Nazhat S., Brown R. Ultra-rapid engineered collagen constructs tested in an in vivo nursery site. *J. Tissue Eng Regen. Med.* 2007;**1**(3):192-198.
- Mulder M, Small N, Botma Y, Ziady L, MacKenzie J: Basic principles of wound care. (Pearson South Africa, 2002).
- Nakanishi Y., Chen G., Komuro H., Ushida T., Kaneko S., Tateishi T., Kaneko M. Tissue-engineered urinary bladder wall using PLGA mesh-collagen hybrid scaffolds: a comparison study of collagen sponge and gel as a scaffold. *J. Pediatr. Surg.* 2003;**38**(12):1781-1784.
- Nakayama G.R., Caton M.C., Nova M.P., Parandoosh Z. Assessment of the Alamar Blue assay for cellular growth and viability in vitro. *J. Immunol. Methods* 1997;**204**(2):205-208.
- Neel E.A.A., Cheema U., Knowles J.C., Brown R.A., Nazhat S.N. Use of multiple unconfined compression for control of collagen gel scaffold density and mechanical properties. *Soft Matter* 2006;**2**(11):986-992.
- Ng K.W., Hutmacher D.W., Schantz J.T., Ng C.S., Too H.P., Lim T.C., Phan T.T., Teoh S.H. Evaluation of ultra-thin poly (-caprolactone) films for tissue-engineered skin. *Tissue Engineering* 2001;**7**(4):441-455.
- Nguyen D.Q.A., Potokar T.S., Price P. An objective long-term evaluation of Integra (a dermal skin substitute) and split thickness skin grafts, in acute burns and reconstructive surgery. *Burns* 2010;**36**(1):23-28.

- Nicodemus G.D., Bryant S.J. Cell encapsulation in biodegradable hydrogels for tissue engineering applications. *Tissue Engineering Part B: Reviews* 2008;**14**(2):149-165.
- Nielsen H.I., Don P. Culture of normal adult human melanocytes. *Br. J. Dermatol.* 1984;**110**(5):569-580.
- O'Brien J., Wilson I., Orton T., Pognan F. Investigation of the Alamar Blue (resazurin) fluorescent dye for the assessment of mammalian cell cytotoxicity. *Eur. J. Biochem.* 2000;**267**(17):5421-5426.
- Oloyede A., Broom N. The generalized consolidation of articular cartilage: an investigation of its near-physiological response to static load. *Connective Tissue Research* 1994;**31**(1):75-86.
- Omar A.A., Mavor A.I.D., Jones A.M., Homer-Vanniasinkam S. Treatment of Venous Leg Ulcers with Dermagraft® 1. *European journal of vascular and endovascular surgery* 2004;**27**(6):666-672.
- Ono K., Saito Y., Yura H., Ishikawa K., Kurita A., Akaike T., Ishihara M. Photocrosslinkable chitosan as a biological adhesive. *Journal of Biomedical Materials Research Part A* 1999;**49**(2):289-295.
- Phillips T.J., Bhawan J., Leigh I.M., Baum H.J., Gilchrest B.A. Cultured epidermal autografts and allografts: a study of differentiation and allograft survival. *J. Am. Acad. Dermatol.* 1990;**23**(2 Pt 1):189-198.
- Piacentini M., Rodolfo C., Farrace M.G., Autuori F. " Tissue" transglutaminase in animal development. *INTERNATIONAL JOURNAL OF DEVELOPMENTAL BIOLOGY* 2000;**44**(6):655-662.
- Pickering J.G., Boughner D.R. Quantitative assessment of the age of fibrotic lesions using polarized light microscopy and digital image analysis. *Am. J. Pathol.* 1991;**138**(5):1225-1231.
- Pinney E., Liu K., Sheeman B., Mansbridge J. Human three-dimensional fibroblast cultures express angiogenic activity. *J. Cell Physiol* 2000;**183**(1):74-82.
- Pitt C.G., Gratzl M.M., Kimmel G.L., Surlis J., Schindler A. Aliphatic polyesters II. The degradation of poly (DL-lactide), poly (epsilon-caprolactone), and their copolymers in vivo. *Biomaterials* 1981;**2**(4):215-220.
- Polak J.M., Bishop A.E. Stem cells and tissue engineering: past, present, and future. *Ann. N. Y. Acad. Sci.* 2006;**1068**:352-366.
- Prystowsky J.H., Nowygrod R., Marboe C.C., Benvenisty A.I., Ascherman J.A., Todd G.J. Artificial Skin (Integra® Dermal Regeneration Template) for Closure of Lower Extremity Wounds. *Vascular and Endovascular Surgery* 2000;**34**(6):557.

- Puchtler H., Meloan S.N., Waldrop F.S. Are picro-dye reactions for collagens quantitative? *Histochemistry and Cell Biology* 1988;**88**(3):243-256.
- Rafat M., Li F., Fagerholm P., Lagali N.S., Watsky M.A., Munger R., Matsuura T., Griffith M. PEG-stabilized carbodiimide crosslinked collagen-chitosan hydrogels for corneal tissue engineering. *Biomaterials* 2008;**29**(29):3960-3972.
- Raffetto J.D. Dermal pathology, cellular biology, and inflammation in chronic venous disease. *Thromb. Res.* 2009;**123 Suppl 4**S66-S71.
- Rajagopal K., Schneider J.P. Self-assembling peptides and proteins for nanotechnological applications. *Current Opinion in Structural Biology* 2004;**14**(4):480-486.
- Rayment E.A., Upton Z. Finding the culprit: a review of the influences of proteases on the chronic wound environment. *Int. J. Low Extrem. Wounds.* 2009;**8**(1):19-27.
- Rich L., Whittaker P. Collagen and picrosirius red staining: A polarized light assessment of fibrillar hue and spatial distribution. *Brazilian Journal of Morphological Sciences* 2005;**22**(2):97-104.
- Robinson G.B., Walton H.A. Glomerular basement membrane as a compressible ultrafilter. *Microvascular research* 1989;**38**(1):36-48.
- Rockwell W.B., Cohen I.K., Ehrlich H.P. Keloids and hypertrophic scars: A comprehensive review. *Plast Reconstr Surg* 1989;**84**(5):827-837.
- Rosenblatt J., Devereux B., Wallace D.G. Effect of electrostatic forces on the dynamic rheological properties of injectable collagen biomaterials. *Biomaterials* 1992;**13**(12):878-886.
- Rosenblatt J., Devereux B., Wallace D.G. Injectable collagen as a pH-sensitive hydrogel. *Biomaterials* 1994;**15**(12):985-995.
- Rowe S.L., Lee S.Y., Stegemann J.P. Influence of thrombin concentration on the mechanical and morphological properties of cell-seeded fibrin hydrogels. *Acta Biomaterialia* 2007;**3**(1):59-67.
- Ruoslahti E., Pierschbacher M.D. New perspectives in cell adhesion: RGD and integrins. *Science* 1987;**238**(4826):491.
- Rydholm A.E., Bowman C.N., Anseth K.S. Degradable thiol-acrylate photopolymers: polymerization and degradation behavior of an in situ forming biomaterial. *Biomaterials* 2005;**26**(22):4495-4506.
- Sahota P.S., Burn J.L., Heaton M., Freedlander E., Suvarna S.K., Brown N.J., Mac Neil S. Development of a reconstructed human skin model for angiogenesis. *Wound Repair and Regeneration* 2003;**11**(4):275-284.

Sandulache V.C., Zhou Z., Sherman A., Dohar J.E., Hebda P.A. Impact of transplanted fibroblasts on rabbit skin wounds. *Arch. Otolaryngol. Head Neck Surg.* 2003;**129**(3):345-350.

Schmid-Schonbein G.W., Takase S., Bergan J.J. New advances in the understanding of the pathophysiology of chronic venous insufficiency. *Angiology* 2001;**52 Suppl 1**S27-S34.

Schugens C., Maquet V., Grandfils C., Jerome R., Teyssie P. Biodegradable and macroporous polylactide implants for cell transplantation: 1. Preparation of macroporous polylactide supports by solid-liquid phase separation. *Polymer* 1996;**37**(6):1027-1038.

Scott S., Catherine B., Matthew S., Michael M., Parthasarathy M., Joshua G., Michael M., Gary B. Extracellular matrix regenerated: tissue engineering via electrospun biomimetic nanofibers. *Polymer International* 2007;**56**(11):1349-1360.

Serpooshan V., Julien M., Nguyen O., Wang H., Li A., Muja N., Henderson J.E., Nazhat S.N. Reduced hydraulic permeability of three-dimensional collagen scaffolds attenuates gel contraction and promotes the growth and differentiation of mesenchymal stem cells. *Acta Biomaterialia* 2010;**In Press, Corrected Proof**.

Shreiber D.I., Sundararaghavan H.G., Song M., Munikoti V., Uhrich K.E. Modifying the Properties of Collagen Scaffolds with Microfluidics. *Materials Research Society Fall Meeting* 2005.

Shu X.Z., Liu Y., Luo Y., Roberts M.C., Prestwich G.D. Disulfide cross-linked hyaluronan hydrogels. *Biomacromolecules* 2002;**3**(6):1304-1311.

Silver F.H. Type I collagen fibrillogenesis in vitro. Additional evidence for the assembly mechanism. *Journal of Biological Chemistry* 1981;**256**(10):4973-4977.

Simka M., Majewski E. The social and economic burden of venous leg ulcers: focus on the role of micronized purified flavonoid fraction adjuvant therapy. *Am. J. Clin. Dermatol.* 2003;**4**(8):573-581.

Sipe J.D. Tissue engineering and reparative medicine. *Ann. N. Y. Acad. Sci.* 2002;**961**-9.

Spyrou G.E., Watt D.A., Naylor I.L. The origin and mode of fibroblast migration and proliferation in granulation tissue. *Br. J. Plast. Surg.* 1998;**51**(6):455-461.

Stadelmann W.K., Digenis A.G., Tobin G.R. Physiology and healing dynamics of chronic cutaneous wounds. *Am. J. Surg* 1998;**176**(2A Suppl):26S-38S.

Stern R., McPherson M., Longaker M.T. Histologic study of artificial skin used in the treatment of full-thickness thermal injury. *Journal of Burn Care & Research* 1990;**11**(1):7.

- Still J., Glat P., Silverstein P., Griswold J., Mozingo D. The use of a collagen sponge/living cell composite material to treat donor sites in burn patients. *Burns* 2003;**29**(8):837-841.
- Suh H. Tissue restoration, tissue engineering and regenerative medicine. *Yonsei Med. J.* 2000;**41**(6):681-684.
- Sung H.J., Meredith C., Johnson C., Galis Z.S. The effect of scaffold degradation rate on three-dimensional cell growth and angiogenesis. *Biomaterials* 2004;**25**(26):5735-5742.
- Suter M.M., Schulze K., Bergman W., Welle M., Roosje P., Muller E.J. The keratinocyte in epidermal renewal and defence. *Vet. Dermatol.* 2009;**20**(5-6):515-532.
- Svensjo T., Yao F., Pomahac B., Eriksson E. Autologous keratinocyte suspensions accelerate epidermal wound healing in pigs. *J. Surg. Res.* 2001;**99**(2):211-221.
- Svensjo T., Yao F., Pomahac B., Winkler T., Eriksson E. Cultured autologous fibroblasts augment epidermal repair. *Transplantation* 2002;**73**(7):1033-1041.
- Swartz M.A., Fleury M.E. Interstitial flow and its effects in soft tissues. 2007.
- Szabo I., Wetzel M.A., Rogers T.J. - Cell-Density-Regulated Chemotactic Responsiveness of Keratinocytes In Vitro. /20;- **117**(- 5):-1090.
- Szpaderska A.M., DiPietro L.A. Inflammation in surgical wound healing: friend or foe? *Surgery* 2005;**137**(5):571-573.
- Tateishi T., Chen G., Ushida T. Biodegradable porous scaffolds for tissue engineering. *Journal of Artificial Organs* 2002;**5**(2):77-83.
- Temenoff J.S., Park H., Jabbari E., Conway D.E., Sheffield T.L., Ambrose C.G., Mikos A.G. Thermally cross-linked oligo(poly(ethylene glycol) fumarate) hydrogels support osteogenic differentiation of encapsulated marrow stromal cells in vitro. *Biomacromolecules* 2004;**5**(1):5-10.
- Theobald V.A., Lauer J.D., Kaplan F.A., Baker K.B., Rosenberg M. "Neutral allografts"--lack of allogeneic stimulation by cultured human cells expressing MHC class I and class II antigens. *Transplantation* 1993;**55**(1):128-133.
- Thomson R, Wake M, Yaszemski M, Mikos A: Biodegradable polymer scaffolds to regenerate organs, pp 245-274 1995).
- Tomasek J.J., Gabbiani G., Hinz B., Chaponnier C., Brown R.A. Myofibroblasts and mechano-regulation of connective tissue remodelling. *Nat Rev Mol Cell Biol* 2002;**3**(5):349-363.

Tonnesen MG, Feng X, Clark RAF: Angiogenesis in wound healing, 5 ed, pp 40-46 (Nature Publishing Group, 2000).

Tuzlakoglu K., Reis R.L. Biodegradable polymeric fiber structures in tissue engineering. *Tissue Eng Part B Rev* 2009;**15**(1):17-27.

Vacanti J.P., Morse M.A., Saltzman W.M., Domb A.J., Perez-Atayde A., Langer R. Selective cell transplantation using bioabsorbable artificial polymers as matrices*. *Journal of Pediatric Surgery* 1988;**23**(1):3-9.

Vaissiere G., Chevally B., Herbage D., Damour O. Comparative analysis of different collagen-based biomaterials as scaffolds for long-term culture of human fibroblasts. *Med. Biol Eng Comput.* 2000;**38**(2):205-210.

Valencia I.C., Falabella A.F., Eaglstein W.H. SKIN GRAFTING. *Dermatologic Clinics* 2000;**18**(3):521-532.

Van der Rest M., Garrone R. Collagen family of proteins. *FASEB J.* 1991;**5**(13):2814-2823.

Vaquette C., Frochot C., Rahouadj R., Muller S., Wang X., Vandoeuvre F. Mechanical and Biological characterization of A Porous Poly-L-Lactic Acid-Co- -Caprolactone scaffold for Tissue Engineering. *Soft Materials* 2008;**6**(1):25-33.

Veves A., Falanga V., Armstrong D.G., Sabolinski M.L. Graftskin, a human skin equivalent, is effective in the management of noninfected neuropathic diabetic foot ulcers. *Diabetes Care* 2001;**24**(2):290.

Wainwright D., Madden M., Luterman A., Hunt J., Monafu W., Heimbach D., Kagan R., Sittig K., Dimick A., Herndon D. Clinical evaluation of an acellular allograft dermal matrix in full-thickness burns. *Journal of Burn Care & Research* 1996;**17**(2):124.

Wang N., Tytell J.D., Ingber D.E. Mechanotransduction at a distance: mechanically coupling the extracellular matrix with the nucleus. *Nat Rev Mol Cell Biol* 2009;**10**(1):75-82.

WATSON R.F., ROTHBARD S., VANAMEE P. The antigenicity of rat collagen. *J. Exp. Med.* 1954;**99**(6):535-550.

Watts G.T., Grillo H.C., Gross J. Studies in Wound Healing: II. The Role of Granulation Tissue in Contraction. *Ann. Surg.* 1958;**148**(2):153-160.

Weadock K.S., Miller E.J., Bellincampi L.D., Zawadsky J.P., Dunn M.G. Physical crosslinking of collagen fibers: Comparison of ultraviolet irradiation and dehydrothermal treatment. *Journal of biomedical materials research* 2004;**29**(11):1373-1379.

Weiss J.A., Maakestad B.J. Permeability of human medial collateral ligament in compression transverse to the collagen fiber direction. *Journal of biomechanics* 2006;**39**(2):276-283.

Werner S., Krieg T., Smola H. Keratinocyte-fibroblast interactions in wound healing. *J. Invest Dermatol.* 2007;**127**(5):998-1008.

Whang K., Thomas C.H., Healy K.E., Nuber G. A novel method to fabricate bioabsorbable scaffolds. *Polymer* 1995;**36**(4):837-842.

Whittaker P., Kloner R.A., Boughner D.R., Pickering J.G. Quantitative assessment of myocardial collagen with picrosirius red staining and circularly polarized light. *Basic Res. Cardiol.* 1994;**89**(5):397-410.

Wild S., Roglic G., Green A., Sicree R., King H. Global prevalence of diabetes: estimates for the year 2000 and projections for 2030. *Diabetes Care* 2004;**27**(5):1047-1053.

Wilkins L.M., Watson S.R., Prosky S.J., Meunier S.F., Parenteau N.L. Development of a bilayered living skin construct for clinical applications. *Biotechnology and bioengineering* 2004;**43**(8):747-756.

Williams R.J., Mart R.J., Ulijn R.V. Exploiting biocatalysis in peptide self-assembly. *Peptide Science* 2010;**94**(1):107-117.

Wollweber L., Stracke R., Gothe U. The use of a simple method to avoid cell shrinkage during SEM preparation. *J. Microsc.* 1981;**121**(Pt 2):185-189.

Wu C.C., Ding S.J., Wang Y.H., Tang M.J., Chang H.C. Mechanical properties of collagen gels derived from rats of different ages. *J. Biomater. Sci. Polym. Ed* 2005;**16**(10):1261-1275.

Yang Y., El Haj A.J. Biodegradable scaffolds--delivery systems for cell therapies. *Expert. Opin. Biol Ther.* 2006;**6**(5):485-498.

Yannas I.V., Burke J.F., Warpehoski M., Stasikelis P., Skrabut E.M., Orgill D., Giard D.J. Prompt, long-term functional replacement of skin. *ASAIO Journal* 1981;**27**19.

Yeh J., Ling Y., Karp J.M., Gantz J., Chandawarkar A., Eng G., Blumling Iii J., Langer R., Khademhosseini A. Micromolding of shape-controlled, harvestable cell-laden hydrogels. *Biomaterials* 2006;**27**(31):5391-5398.

Yoo J.Y., Kima J.M., Seob K.S., Jeonga Y.K., Leec H.B., Khanga G. Characterization of degradation behavior for PLGA in various pH condition by simple liquid chromatography method. *Bio-Medical Materials and Engineering* 2005;**15**(4):279-288.

Young H.E., Duplaa C., Romero-Ramos M., Chesselet M.F., Vourc'h P., Yost M.J., Ericson K., Terracio L., Asahara T., Masuda H., Tamura-Ninomiya S., Detmer K., Bray

R.A., Steele T.A., Hixson D., el-Kalay M., Tobin B.W., Russ R.D., Horst M.N., Floyd J.A., Henson N.L., Hawkins K.C., Groom J., Parikh A., Blake L., Bland L.J., Thompson A.J., Kirincich A., Moreau C., Hudson J., Bowyer F.P., III, Lin T.J., Black A.C., Jr. Adult reserve stem cells and their potential for tissue engineering. *Cell Biochem. Biophys.* 2004;**40**(1):1-80.